National Library of Canada
Canadian Theses Service
Ottawa, Canada
K1A 0N4

Bibliothèque nationale du Canada
Service des thèses canadiennes

NOTICE

The quality of this microform is heavily dependent upon the quality of the original thesis submitted for microfilming. Every effort has been made to ensure the highest quality of reproduction possible.

If pages are missing, contact the university which granted the degree.

Some pages may have indistinct print especially if the original pages were typed with a poor typewriter ribbon or if the university sent us an inferior photocopy.

Reproduction in full or in part of this microform is governed by the Canadian Copyright Act, R.S.C. 1970, c. C-30, and subsequent amendments.

AVIS

La qualité de cette microforme dépend grandement de la qualité de la thèse soumise au microfilmage. Nous avons tout fait pour assurer une qualité supérieure de reproduction.

S'il manque des pages, veuillez communiquer avec l'université qui a conféré le grade.

La qualité d'impression de certaines pages peut laisser à désirer, surtout si les pages originales ont été dactylographiées à l'aide d'un ruban usé ou si l'université nous a fait parvenir une photocopie de qualité inférieure.

La reproduction, même partielle, de cette microforme est soumise à la Loi canadienne sur le droit d'auteur, SRC 1970, c. C-30, et ses amendements subséquents.

NL-339 (r. 88/04) c

Canada

UNIVERSITY OF ALBERTA

ADAPTIVE PREDICTIVE CONTROL IN INDUSTRY

BY

MARJAN FORTUNA

A THESIS

SUBMITTED TO THE FACULTY OF GRADUATE STUDIES AND RESEARCH
IN PARTIAL FULFILLMENT OF THE REQUIRMENTS FOR THE DEGREE
OF MASTER OF SCIENCE

IN

PROCESS CONTROL

DEPARTMENT OF CHEMICAL ENGINEERING

EDMONTON, ALBERTA

SPRING, 1991

National Library
of Canada

Bibliothèque nationale
du Canada

Canadian Theses Service

Service des thèses canadiennes

Ottawa, Canada
K1A 0N4

The author has granted an irrevocable non-exclusive licence allowing the National Library of Canada to reproduce, loan, distribute or sell copies of his/her thesis by any means and in any form or format, making this thesis available to interested persons.

The author retains ownership of the copyright in his/her thesis. Neither the thesis nor substantial extracts from it may be printed or otherwise reproduced without his/her permission.

L'auteur a accordé une licence irrévocable et non exclusive permettant à la Bibliothèque nationale du Canada de reproduire, prêter, distribuer ou vendre des copies de sa thèse de quelque manière et sous quelque forme que ce soit pour mettre des exemplaires de cette thèse à la disposition des personnes intéressées.

L'auteur conserve la propriété du droit d'auteur qui protège sa thèse. Ni la thèse ni des extraits substantiels de celle-ci ne doivent être imprimés ou autrement reproduits sans son autorisation.

ISBN 0-315-666[illegible]

Canada

UNIVERSITY OF ALBERTA

RELEASE FORM

NAME OF AUTHOR : MARJAN FORTUNA

TITLE OF THESIS : ADAPTIVE PREDICTIVE CONTROL IN INDUSTRY

DEGREE : MASTER OF SCIENCE

YEAR THIS DEGREE GRANTED : 1991

Permission is hereby granted to THE UNIVERSITY OF ALBERTA LIBRARY to reproduce single copies of this thesis and to lend or sell such copies for private, scholarly or scientific research purposes only.

The author reserves other publication rights, and neither the thesis nor extensive extracts from it may be printed or otherwise reproduced without the author's written permission.

(SIGNED) Marjan Fortuna

PERMANENT ADDRESS :

147 Barton Avenue
Toronto, Ontario
Canada
M6G 1R1

DATE : 25 December 1990

UNIVERSITY OF ALBERTA

FACULTY OF GRADUATE STUDIES AND RESEARCH

The undersigned certify that they have read, and recommend to the Faculty of Graduate Studies and Research, for acceptance, a thesis entitled ADAPTIVE PREDICTIVE CONTROL IN INDUSTRY submitted by MARJAN FORTUNA in partial fulfillment of the requirements for the degree of MASTER OF SCIENCE IN PROCESS CONTROL.

....
D.G. Fisher
University Supervisor

....
J.D. Brooks
Industrial Supervisor

....
Dr. R.K. Wood

....
K.E. Bollinger

Date : January 15, 1991

TO MOM AND DAD

ABSTRACT

This thesis is concerned with the industrial application of long range adaptive predictive controllers. It focuses on the multi-step adaptive predictive controller (MAPC) developed by Sripada,(1988) and Foley,(1988). MAPC uses a modified Kalman filter predictor in the feedback path to deal with noise and to predict future values of the process output, and therefore, was expected to perform well in the industrial application. The theory behind MAPC is briefly summarized and the implementation of the controller is discussed in some detail.

The results of 3 MAPC implementations are then presented. The continuous stirred tank heater (CSTH) was used for the first experiments. This provided a controlled environment which to evaluate the performance characteristics of the MAPC algorithm. Esso Chemical's higher olefins plant in Sarnia provided the industrial testing environment. The MAPC algorithm was successfully used to control the reactor bed outlet temperature and to control the hydrofiner total outlet poisons.

On-line estimation was performed using both step and PRBS tests. Early results confirmed that it was essential to use a $\Delta/T(z^{-1})$ filter in order to remove unwanted high frequency components which cause model parameter bias. In the industrial experiments, off-line analysis of step and PRBS test proved to be useful in establishing initial parameter estimates and appropriate tuning parameter values for the RLS estimator. The trace of the

estimation covariance matrix, *tr{P}*, was used to ensure that the model parameter responses were smooth. The CSTH results showed that fast parameter movements caused non-linear output responses. This was attributed to the coupling between the estimator and the time-varying Kalman filter predictor. The *tr{P}* effectively decoupled the MAPC Kalman filter predictor from the control algorithm. Finally, the use of a deadzone on the prediction error as an estimator on/off criterion was not very effective. An incorrect deadzone lead to oscillatory parameter responses.

The MAPC algorithm performed well during experimentation. It was easily tuned by fixing the prediction and control horizons, and adjusting the control weighting and the ratio of noise covariances. CSTH results showed the controller to be very robust during large time delay swings for both servo and regulatory modes, even when the estimator was turned off. The industrial experiments focused on the regulatory performance of the MAPC algorithm. Good regulatory response under a variety of unmodelled disturbances was demonstrated. Process operator response to the technology was enthusiastic. Little additional training was required due to the fact that the operator interface was made consistent with all existing control applications at the plant.

The overall conclusion was, that adaptive controllers such as MAPC can perform well in selected industrial applications, but that there are still problems that require further research.

ACKNOWLEDGMENT

I would like to express my thanks and gratitude to my two thesis supervisors. Dr. D.G. Fisher who provided the support during my university research and experimentation, and Mr. J.D. Brooks who provided the structured guidance and industrial resources to perform the industrial experimental work. Both supervisors were instrumental in coordinating and establishing a cooperative M.Sc program with Esso Chemical Canada. I thank both of them for allowing me the distinct privilege of participating in such a program. I would also like to thank the Esso Chemical operating personnel at the higher olefins plant in Sarnia for their assistance during the implementation and experimentation stages of this thesis. Their enthusiasm and trust truly made the industrial experiments a success.

I would like to thank my parents and friends for their constant support and encouragement, without whom this work would not have been possible.

Finally, financial support provided by the Department of Chemical Engineering at the University of Alberta and Esso Chemical Canada, a Division of Imperial Oil Limited, is gratefully acknowledged.

TABLE OF CONTENTS

Chapter Page

1.0 INTRODUCTION 1

2.0 THEORETICAL DEVELOPMENT OF MULTI-STEP ADAPTIVE PREDICTIVE CONTROLLER 3

2.1 THE PLANT MODEL 3

2.1.1 Transfer Function Models 3
2.1.2 State-Space Models 7

2.2 PLANT IDENTIFICATION 9

2.2.1 Basic Least Squares Algorithm 10
2.2.2 Recursive Least Squares Estimation For An Industrial Environment 14

2.3 MODIFIED KALMAN FILTER PREDICTOR 24

2.4 THE MULTI-STEP PREDICTIVE ALGORITHM 30

2.4.1 The Basic Algorithm 31
2.4.2 Feedforwared Variables 36
2.4.3 Innovations Analysis of MAPC 39

2.5 THE MULTI-STEP CONTROL LAW 42

2.5.1 LU Decomposition 44
2.5.2 Selection of Tuning Values for MAPC 44

3.0 ADAPTIVE CONTROLLER IMPLEMENTATION 49

3.1 CONSIDERATIONS IN PARAMETER ESTIMATION 51

3.1.1 A Priori Information 52
3.1.2 PRBS Generation and Plant Testing 55
3.1.3 Plant Identification 62

3.2 OFF-LINE ANALYSIS AND MODEL IDENTIFICATION 66

3.2.1 Model Structure Selection 66
3.2.2 Estimator Tuning 77
3.2.3 Analysis of Model Prediction Error 81

3.3 ANALOG AND DIGITAL DATA FILTERING 82

3.3.1 Analog Anti-Aliasing Filters 82
3.3.2 Digital Data Filtering 89

3.4 COMPUTER SYSTEM AND ADAPTIVE CONTROL SOFTWARE 94

3.4.1 Control System Architecture 95
3.4.2 Structure of Adaptive Control Software . 100
3.4.3 Practical Considerations 103

TABLE OF CONTENTS

Chapter Page

4.0 EXPERIMENTAL APPLICATION OF MULTI-STEP ADAPTIVE PREDICTIVE CONTROL IN THE ACADEMIC AND INDUSTRIAL ENVIRONMENTS 107

4.1 CONTINUOUS STIRRED TANK HEATER 108

4.1.1 Process Description 108
4.1.2 CSTH Experimental Results 112
4.1.3 RLS Open Loop Identification in a Noisy Environment 113
4.1.4 Interaction Between the Kalman Filter and RLS Algorithm 117
4.1.5 Servo Response of the MAP Controller 120
4.1.6 Regulatory Response of the MAP Controller 123
4.1.7 MAP Controller Behavior in Presence of Changing Deadtime Dynamics 125

4.2 REACTOR BED TEMPERATURE CONTROL 142

4.2.1 Process Description 142
4.2.2 Process Model Selection and Identification 146
4.2.3 Multi-Step Adaptive Predictive Control of Reactor Bed Outlet Temperature 152

4.2.3.1 Operator/Engineer Interface 152
4.2.3.2 Experimental Results 153

4.2.4 PID Control Of Reactor Bed Outlet Temperature 161

4.3 HYDROFINER TOTAL OUTLET POISONS CONTROL 181

4.3.1 Process Description 181
4.3.2 Process Model Selection and Identification 184
4.3.3 Multi-Step Adaptive Predictive Control of Hydrofiner Total Outlet Poisons 189
4.3.4 PID Feedback-Feedforward Control of Hydrofiner Total Outlet Poisons 201

5.0 CONCLUSIONS AND FUTURE WORK 223

5.1 Recursive Least Squares Estimator Conclusions 223

5.2 Multi-Step Adaptive Predictive Controller Conclusions 226

5.3 Future Work 229

6.0 REFERENCES 231

LIST OF TABLES

Table **Page**

4.1.1 CSTH Steady State Operating Conditions 110
4.1.2 CSTH Continuous Time Parameters 111
4.1.3 Summary of Estimated Discrete Time Model for TC#1 114
4.2.1 Summary of Reactor Step Tests 147

LIST OF FIGURES

Figure Page

2.3.1 Block Diagram of Kalman Filter Predictor 28
2.4.1 Block Diagram of Multi-Step Adaptive Predictive Controller 40

3.1.1 Binary Linear-Shift Feedback Register 56
3.1.2 Time Plot of PRBS Sequence with T_{sw} = 1 min. 59
3.1.3 Time Plot of PRBS Sequence with T_{sw} = 5 min. 59
3.1.4 Spectral Density Plot of PRBS Sequence with T_{sw} = 1 min. 60
3.1.5 Spectral Density Plot of PRBS Sequence with T_{sw} = 5 min. 60
3.1.6 Open and Closed Loop Identification Configurations 63

3.2.1 Identification of Continuous Time Parameters From a Step Response Test 68
3.2.2 Time Delay Analysis Using Cross-Correlations 71

3.3.1 Simple Electronic Realization of Analog Anti-Aliasing Filter 87

3.4.1 Process Control System Architecture at the Higher Olefins Plant in Sarnia 96
3.4.2 Task Structure of the MAP Controller Software 101

4.1.1 Process Diagram of Continuous Stirred Tank Heater. 109
4.1.2 Open Loop RLS Identification 130
TC#1 *tr(P)*=1 No Regressor Filter
4.1.3 Open Loop RLS Identification 131
TC#1 *tr(P)*=1 1st Order T Filter (T_p=0.8)
4.1.4 Open Loop RLS Identification 132
TC#1 *tr(P)*=1 2nd Order T Filter (T_p=0.8)

4.1.5 Multi-Step Adaptive Predictive Control of CSTH ... 133
N_1=1, N_2=10, N_u=1, λ=10, R_w/R_v=0.01,
RLS=ON, *tr(P)*=1

4.1.6 Multi-Step Adaptive Predictive Control of CSTH ... 134
N_1=1, N_2=10, N_u=1, λ=10, R_w/R_v=0.9,
RLS=ON, *tr(P)*=1

4.1.7 Multi-Step Adaptive Predictive Control of CSTH ... 135
N_1=1, N_2=10, N_u=1, λ=10, R_w/R_v=2.0, RLS=ON

LIST OF FIGURES (...cont)

Figure Page

4.1.8 Multi-Step Adaptive Predictive Control of CSTH ... 136
Servo Response
$N_1=1$, $N_2=10$, $N_u=1$, $\lambda=10$, $R_w/R_v=2.0$, RLS=OFF, TC#2

4.1.9 Multi-Step Adaptive Predictive Control of CSTH ... 136
Servo Response
$N_1=1$, $N_2=10$, $N_u=1$, $\lambda=10$, $R_w/R_v=2.0$, RLS=OFF, TC#2

4.1.10 Multi-Step Adaptive Predictive Control of CSTH ... 137
TC#2 Regulatory Response
$N_1=1$, $N_2=10$, $N_u=1$, $\lambda=10$, $R_w/R_v=0.9$, RLS=OFF

4.1.11 Multi-Step Adaptive Predictive Control of CSTH ... 137
TC#2 Regulatory Response
$N_1=1$, $N_2=10$, $N_u=1$, $\lambda=10$, $R_w/R_v=0.9$, RLS=OFF

4.1.12 Multi-Step Adaptive Predictive Control of CSTH ... 137
TC#2 Regulatory Response
$N_1=1$, $N_2=10$, $N_u=1$, $\lambda=10$, $R_w/R_v=0.01$, RLS=OFF

4.1.13 Multi-Step Adaptive Predictive Control of CSTH ... 138
Changing Deadtime Performance
$N_1=1$, $N_2=10$, $N_u=1$, $\lambda=0$, $R_w/R_v=0.05$, RLS=ON, TC#1

4.1.14 Multi-Step Adaptive Predictive Control of CSTH ... 139
Varying Deadtime Dynamics
$N_1=1$, $N_2=10$, $N_u=1$, $\lambda=10$, $R_w/R_v=0.01$, RLS=ON

4.1.15 Multi-Step Adaptive Predictive Control of CSTH ... 140
Varying Deadtime Dynamics
$N_1=1$, $N_2=10$, $N_u=1$, $\lambda=1$, $R_w/R_v=0.01$, RLS=OFF

4.1.16 PID Control of CSTH 141
Servo And Regulatory Behaviour With Varying Deadtime Dynamics
(a) $K_p=0.5$, $K_i=0.015$, $K_d=0.1$, TC#1
(b) $K_p=0.5$, $K_i=0.015$, $K_d=0.1$, TC#2
(c) $K_p=0.5$, $K_i=0.015$, $K_d=0.1$, TC#3

4.2.1 Process Diagram of Reactor Bed Temperature Control 143

4.2.2 Reactor 5th Bed Temperature Step Test 164
(a) 5th Bed Outlet Temperature
(b) Quench Valve Position
(c) 4th Bed Outlet Temperature

LIST OF FIGURES (...cont)

Figure Page

4.2.3 Reactor Closed Loop PRBS Test 165
- (a) 5th Bed Outlet Temperature
- (b) Quench Valve Position
- (c) Quench Temperature
- (d) 4th Bed Outlet Temperature

4.2.4 Off-line Analysis of Reactor PRBS Data 166
- (a) Cross-correlation of Valve VS 5 Bed Outlet Temp
- (b) Impulse Response
- (c) Step Response
- (d) Parameter Trajectories
- (e) Constant Trace Variable Forgetting Factor
- (f) Model Prediction Error
- (g) Residual Auto Correlation Sequence

4.2.5 Honeywell PMXIII Multi-Step Adaptive Predictive Controller Operator/Engineer Interface 168

4.2.6 Reactor MAP Controller 24 Hour Test 169
14 November 1988
- (a) 5^{TH} Bed Outlet Temperature Response
- (b) 5^{TH} Bed Quench Valve Position
- (c) Quench Temperature
- (d) 4^{TH} Bed Outlet Temperature Response

4.2.7 Reactor MAP Controller 24 Hour Test 170
15 November 1988
- (a) 5^{TH} Bed Outlet Temperature Response
- (b) 5^{TH} Bed Quench Valve Position
- (c) Quench Temperature
- (d) 4^{TH} Bed Outlet Temperature Response

4.2.8 Reactor MAP Controller 24 Hour Test 171
8 December 1988
- (a) 5^{TH} Bed Outlet Temperature Response
- (b) 5^{TH} Bed Quench Valve Position
- (c) Quench Temperature
- (d) 4^{TH} Bed Outlet Temperature Response
- (e) Model Prediction Error
- (f) Residual Auto-Correlation Sequence

LIST OF FIGURES (...cont)

Figure Page

4.2.9 Reactor MAP Controller 24 Hour Test 173
9 December 1988
- (a) 5^{TH} Bed Outlet Temperature Response
- (b) 5^{TH} Bed Quench Valve Position
- (c) Quench Temperature
- (d) 4^{TH} Bed Outlet Temperature Response
- (e) Model Parameter Trajectories
- (f) Trace of M
- (g) Model Prediction Error
- (h) Residual Auto-Correlation Sequence

4.2.10 Reactor MAP Controller 24 Hour Test 175
10 December 1988
- (a) 5^{TH} Bed Outlet Temperature Response
- (b) 5^{TH} Bed Quench Valve Position
- (c) Quench Temperature
- (d) 4^{TH} Bed Outlet Temperature Response
- (e) Model Prediction Error

4.2.11 Reactor MAP Controller 24 Hour Test 177
12 December 1988
- (a) 5^{TH} Bed Outlet Temperature Response
- (b) 5^{TH} Bed Quench Valve Position
- (c) Quench Temperature
- (d) 4^{TH} Bed Outlet Temperature Response

4.2.12 Reactor MAP Controller 24 Hour Test 178
5 January 1989
$N_1=4,\ N_2=10,\ N_u=2,\ \lambda=50,\ R_w/R_v=0.05$
- (a) 5^{TH} Bed Outlet Temperature Response
- (b) 5^{TH} Bed Quench Valve Position
- (c) Quench Temperature
- (d) 4^{TH} Bed Outlet Temperature Response
- (e) $\hat{a}$ Parameter Trajectory
- (f) $\hat{b}$ Parameter Trajectory
- (g) Model Prediction Error
- (h) Residual Auto-Correlation Sequence

LIST OF FIGURES (...cont)

Figure Page

4.2.13 24 Hour PID Controller Test 180
30 November 1988
K_o=15, K_1=2.2, K_2=0.05
(a) 5^{TH} Bed Outlet Temperature
(b) Quench Valve Position
(c) Quench Temperature
(d) 4^{TH} Bed Outlet Temperature

4.3.1 Process Diagram of Hydrofiner Control 182

4.3.2 Open Loop Hydrofiner Step Tests 203
1 December 1988
(a) Total Outlet Poisons
(b) Hydogen Flow
(c) Total Inlet Poisons
(d) Fresh Feed Flow

4.3.3 Open Loop Hydrofiner PRBS Test 204
2 December 1988
(a) Total Outlet Poisons
(b) Hydogen Flow
(c) Total Inlet Poisons
(d) Fresh Feed Flow

4.3.4 Hydrofiner Step Test On-line Identification 205
3 December 1988
Δ_d=0, $tr(\mathbf{P})$=0.1, RLS=ON
(a) Total Outlet Poisons
(b) Hydogen Flow
(c) Total Inlet Poisons
(d) Fresh Feed Flow

4.3.5 Hydrofiner Step Test On-line Identification 206
3 December 1988
Δ_d=0, $tr(\mathbf{P})$=0.1, RLS=ON
(a) a Parameter Trajectory
(b) b Parameter Trajectory
(c) Model Prediction Error
(d) Estimated Residual Auto-Correlation Sequence

4.3.6 Honeywell PMXIII Multi-Step Adaptive Predictive Controller Operator/Engineer Interface 207

LIST OF FIGURES (...cont)

Figure Page

4.3.7 Hydrofiner Open Loop PRBS Test 208
6 December 1988
$\Delta_d=0$, $tr\{P\}=0.01$, RLS=ON
$N_1=1$, $N_2=10$, $N_u=1$, $\lambda=10000$, $R_w/R_v=0.05$
(a) Total Outlet Poisons
(b) Hydogen Flow
(c) Total Inlet Poisons
(d) Fresh Feed Flow
(e) a Parameter Trajectory
(f) b Parameter Trajectory
(g) Model Prediction Error

4.3.8 MAP Control of Hydrofiner 210
7 December 1988
$N_1=4$, $N_2=10$, $N_u=1$, $\lambda=1200$, $R_w/R_v=0.05$, $tr\{P\}=0.01$
(a) Total Outlet Poisons
(b) Hydogen Flow
(c) Total Inlet Poisons
(d) Fresh Feed Flow
(e) a Parameter Trajectory
(f) b Parameter Trajectory
(g) Model Prediction Error
(h) Residual Estimated Auto-Correlation Sequence

4.3.9 MAP Control of Hydrofiner 212
10 December 1988
$N_1=4$, $N_2=10$, $N_u=2$, $\lambda=400$, $R_w/R_v=0.001$
(a) Total Outlet Poisons
(b) Hydogen Flow
(c) Total Inlet Poisons
(d) Fresh Feed Flow
(e) a Parameter Trajectory
(f) b Parameter Trajectory
(g) Model Prediction Error
(h) Residual Estimated Auto-Correlation Sequence

4.3.10 MAP Control of Hydrofiner 214
11 December 1988
$N_1=4$, $N_2=10$, $N_u=2$, $\lambda=400$, $R_w/R_v=0.05$, RLS=OFF
(a) Total Outlet Poisons
(b) Hydogen Flow
(c) Total Inlet Poisons
(d) Fresh Feed Flow
(e) a Parameter Trajectory
(f) b Parameter Trajectory
(g) Model Prediction Error
(h) Residual Estimated Auto-Correlation Sequence

LIST OF FIGURES (...cont)

Figure Page

4.3.11 MAP Control of Hydrofiner 216
12 December 1988
$N_1=4$, $N_2=10$, $N_u=2$, $\lambda=400$, $R_w/R_v=0.005$, RLS=ON
(a) Total Outlet Poisons
(b) Hydogen Flow
(c) Total Inlet Poisons
(d) Fresh Feed Flow
(e) a Parameter Trajectory
(f) b Parameter Trajectory
(g) Model Prediction Error
(h) Residual Estimated Auto-Correlation Sequence

4.3.12 MAP Control of Hydrofiner 218
17 December 1988
$N_1=4$, $N_2=10$, $N_u=2$, $\lambda=400$, $R_w/R_v=0.005$
(a) Total Outlet Poisons
(b) Hydogen Flow
(c) Total Inlet Poisons
(d) Fresh Feed Flow
(e) a Parameter Trajectory
(f) b Parameter Trajectory
(g) Model Prediction Error
(h) Residual Estimated Auto-Correlation Sequence

4.3.13 MAP Control of Hydrofiner 220
19 December 1988
$N_1=4$, $N_2=10$, $N_u=2$, $\lambda=400$, $R_w/R_v=0.005$
(a) Total Outlet Poisons
(b) Hydogen Flow
(c) Total Inlet Poisons
(d) Fresh Feed Flow
(e) a Parameter Trajectory
(f) b Parameter Trajectory
(g) Model Prediction Error
(h) Residual Estimated Auto-Correlation Sequence

4.3.14 PID Control of Hydrofiner 222
10-13 March 1989
$K_o=30$, $K_1=0.0016$, $K_2=0$
(a) Total Outlet Poisons
(b) Hydogen Flow
(c) Total Inlet Poisons
(d) Fresh Feed Flow

NOMENCLATURE

Technical Abbreviations

AR	Auto-Regressive
ARIMA	Auto-Regressive Integrated Moving Average
BPH	Barrels per Hour
CARIMA	Controlled Auto-Regressive Integrated Moving Average
CSTH	Continuous Stirred Tank Heater
DMC	Dynamic Matrix Control
DMI	Dynamic Matrix Identification
ELS	Extended Least Squares
GPC	Generalized Predictive Control
HOIS	Higher Olefins Imperial Sarnia
IDSA	Identification, Design, Simulation and Analysis
ILS	Improved Least Squares
IMC	Internal Model Control
KFP	Kalman Filter Predictor
KSCF/HR	Thousands of Standard Cubic Feet per Hour
LPDMC	Linear Programmed Dynamic Matrix Control
MA	Moving Average
MAPC/MAP	Multi-Step Adaptive Predictive Control
MISO	Multiple Input, Single Output
MKFP	Modified Kalman Filter Predictor
MPE	Model Prediction Error
MPM	Model-Plant-Mismatch
PID	Proportional-Integral-Derivative

PRBS	Pseudo Random Binary Sequence
QDMC	Quadratic Dynamic Matrix Control
RLS	Recursive Least Squares
S/N	Signal to Noise ratio
SISO	Single Input, Single Output

Alphabetic

$A(z^{-1})$	Polynomial corresponding to the process output
$a_1, \ldots, a_n$	Coefficients of $A(z^{-1})$
$B(z^{-1})$	Polynomial corresponding to the process input
$b_1, \ldots, b_n$	Coefficients of $B(z^{-1})$
$C(z^{-1})$	Polynomial corresponding to stochastic disturbance
$c_1, \ldots, c_n$	Coefficients of $C(z^{-1})$
c	Floating point characterstic
d	Integer discrete time delay of process
J	Cost function for control
k	Discrete time interval
L	Kalman gain vector
$L_\rho, \ldots, L_{n+d}$	Elements of Kalman gain vector
M	Mantissa
m_x	Mean of sequence x_i
N_1	Minimum prediction horizon
N_2	Maximum prediction horizon
N_u	Control horizon
$P(k)$	Estimation covariance matrix
R_v	Measurement noise covariance

R_w	Process noise covariance
tr	Trace of a matrix
T_s	Sample time
T_{sw}	PRBS generator switching time
$u(k)$	Process input
$v(k)$	Measurement noise
$w(k)$	Process noise
$\mathbf{x}(k)$	State vector
x_i	Discrete time sequence
$X(\omega)$	Power spectrum of sequence x_i
$y(k)$	Process output
z^{-1}	Backward shift operator

Greek

Δ	Differencing operator
δ	Order of a polynomial
$\boldsymbol{\Phi}$	State transition matrix
$\boldsymbol{\phi}$	Regressor vector
Γ	Process noise transition vector
$\gamma_1, \ldots, \gamma_n$	First n elements of Γ
Λ	Input transition vector
λ	Used as forgetting factor, or control weighting
Θ	Output transition vector
$\boldsymbol{\theta}$	Model parameter vector
σ_x	Standard deviation of x_i
σ_x^2	Variance of x_i
$\xi(k)$	White noise sequence

Superscripts

^	Estimated value

1.0 INTRODUCTION

Long range adaptive predictive control strategies have recently been demonstrated to be very robust in the presence of changing process and disturbance dynamics (Clarke, Mohtadi and Tuffs, 1987), (McIntosh, 1988), (Foley, 1988). Industrial chemical processes are known to exhibit such time-varying dynamics and thus provide a rich environment for the implementation and evaluation of such control strategies.

This thesis focused on implemention and evaluation of Multi-Step Adaptive Predictive Control (Sripada, 1988) in an industrial environment. The environment was provided by Esso Chemical Canada in Sarnia at their higher olefins plant. The thesis has been written in a manner which provides an individual with a complete picture of both the relevant MAPC theory and the experiments that were performed to understand the behaviour of the controller in both academic and industrial settings.

Chapter 2 provides a brief summary of the theory and development of the RLS estimator and MAPC controller. Detailed derivations and discussions may be found in Sripada, (1988) and Foley, (1988).

Chapter 3 describes some of the practical considerations and analysis techniques that may be used to better understand the dynamic data associated with a chemical process. It also presents the general framework of the Honeywell distributed control network, which is in place at the higher olefins unit, and the MAPC software development.

Chapter 4 presents and discusses the results obtained from the university and industrial experiments. The experiment on the continuous stirred tank heater provided initial training and guidance on the use of the MAPC. This knowledge was then used as a starting point for the industrial experiments. The polychamber reactor temperature control and hydrofiner total outlet poisons control were selected for the industrial experiments.

Finally, Chapter 5 discusses the conclusions, contributions and recommended future work to improve the MAPC controller.

2.0 THEORETICAL DEVELOPMENT OF THE MULTI-STEP ADAPTIVE PREDICTIVE CONTROLLER

2.1 THE PLANT MODEL

The dynamics of a chemical process may be described by either a transfer function or state-space model. The following section presents both representations for a plant that may be characterized as having linear, stochastic, non-stationary behavior about some operating point.

2.1.1 Transfer Function Models

The dynamics of a stochastic, non-stationary continuous time plant may, in the most general case, be described by the following discrete time model, provided that the plant input and output have been sampled at a rate that includes all desired frequency components. This is normally done by sampling at a rate of $\frac{1}{5}$ to $\frac{1}{10}$ the dominant time constant of the continuous time plant. The dominant time constant of the plant may be defined at the frequency which the plant's magnitude repsonse demonstrates a -3 decibel roll-off. This is also called the crossover frequency. The discrete plant transfer function describes a plant which is non-stationary. A stationary random process may be defined as a process whose statistical properties are invariant to a shift in the time origin. Namely, the mean and the variance are independent of time and the autocorrelation function is only a function of the time difference (Oppenheim and Shaefer,1975), (Bendat and Piersol, 1971). A non-stationary process would thus violate this invariance to time. Equation 2.1.1 describes the input to the disturbance transfer function, $G_d(z^{-1})$, as a discrete white noise process. Passing $\xi(k)$, a white noise process through a filter $1/\Delta$ effectively produces a non-stationary random output.

$$y(k) \quad = \quad z^{-d}\, G_p(z^{-1})\, u(k-1) \quad + \quad \frac{G_d(z^{-1})\, \xi(k)}{\Delta} \qquad (2.1.1)$$

where

$G_p(z^{-1})$ =	Process Transfer Function
$G_d(z^{-1})$ =	Disturbance Transfer Function
z^{-1}	Backward Shift Operator
Δ	Integrating Operator $1-z^{-1}$
d	Process Time Delay (Integer)
$y(k)$	Process Output
$u(k)$	Process Input
$\xi(k)$	Zero-mean Gaussian Noise

Any plant may be described by a transfer function which represents the dynamics between its input and output and a complimentary transfer function which describes the measurement and process noise. The general model may be presented in the following form, which has been referred to in the literature as the Box and Jenkins [illegible]:

$$\Delta y(k) = z^{-d} \cdot \frac{G_p^N(z^{-1})}{G_p^D(z^{-1})} \cdot \Delta u(k-1) + \frac{G_d^N(z^{-1})}{G_d^D(z^{-1})} \cdot \xi(k) \tag{2.1.2}$$

where

$$G_p^N(z^{-1}) = g_{p_1}^N \cdot z^{-1} + g_{p_2}^N \cdot z^{-2} + \cdots + g_{p_n}^N \cdot z^{-n} \tag{2.1.3}$$

$$G_p^D(z^{-1}) = 1 + g_{p_1}^D \cdot z^{-1} + \cdots + g_{p_n}^D \cdot z^{-n} \tag{2.1.4}$$

$$G_d^N(z^{-1}) = 1 + g_{d_1}^N \cdot z^{-1} + \cdots + g_{d_n}^N \cdot z^{-n} \tag{2.1.5}$$

$$G_d^D(z^{-1}) = 1 + g_{d_1}^D \cdot z^{-1} + \cdots + g_{d_n}^D \cdot z^{-n} \tag{2.1.6}$$

where $G_p^D(z^{-1})$, $G_d^D(z^{-1})$ and $G_d^N(z^{-1})$ are monic polynomials in the backward shift operator. It should be understood that the Box and Jenkins model completely separates the plant and disturbance dynamics, unlike the models which are normally referred to in the literature as the CARIMA (Controlled Auto-Regressive Integrated Moving Average) or ARIMA (Auto-Regressive Integrated Moving Average w/ Auxiliary Noise Input) models.

For purposes of on-line recursive estimation and adaptive control, the structure of the ARIMA model is as follows :

$$A(z^{-1})\cdot y(k) \quad = \quad z^{-d}B(z^{-1})\cdot u(k-1) \quad + \quad \frac{C(z^{-1})\cdot \xi(k)}{\Delta} \qquad (2.1.7)$$

where

$$A(z^{-1}) \quad = \quad 1 + a_1 z^{-1} + a_2 z^{-2} + \cdots + a_n z^{-n} \qquad (2.1.8)$$

$$B(z^{-1}) \quad = \quad b_1 + b_2 z^{-1} + b_3 z^{-2} + \cdots + b_n z^{-n} \qquad (2.1.9)$$

$$C(z^{-1}) \quad = \quad 1 + c_1 z^{-1} + c_2 z^{-2} + \cdots + c_n z^{-n} \qquad (2.1.10)$$

This ARIMA model incorporates both the plant and disturbance dynamics into the AR (Auto-Regressive) and MA (Moving-Average) components of the plant model. If the Box and Jenkins model is re-written as in equation (2.1.11) then it is apparent that the $A(z^{-1})$, $B(z^{-1})$ and $C(z^{-1})$ polynomials are a function of both the plant and disturbance dynamics.

$$\begin{aligned} G_p^D(z^{-1})\cdot G_d^D(z^{-1})\cdot \Delta y(k) \quad = \quad & z^{-d}\cdot G_p^D(z^{-1})\cdot G_d^N(z^{-1})\cdot \Delta u(k-1) \\ & + \; G_p^D(z^{-1})\cdot G_d^N(z^{-1})\xi(k) \qquad (2.1.11) \end{aligned}$$

If Equation (2.1.11) is compared with the ARIMA model, it can be seen that the $A(z^{-1})$ polynomial is a function of both the AR components of the plant and the disturbance dynamics. Similarly, the $B(z^{-1})$ polynomial is affected by the AR component of the disturbance dynamics. This correlation of plant with disturbance dynamics will become much more important later on, when a good model of the plant dynamics must be estimated. It will be essential that during estimation periods that the AR component of the disturbance dynamics is significantly less in magnitude than the AR component of the plant dynamics.

2.1.2 State-Space Models

An equivalent discrete time representation of a linear time-invariant plant is the state-space representation. A plant may be described in many different canonical forms (Kailath, 1980) and thus there exists no single unique representation. The canonical form chosen is an observable form as used by Walgama, 1986 and may be written for SISO systems as :

$$\mathbf{x}(k+1) = \Phi\cdot\mathbf{x}(k) + \Lambda\cdot u(k) + \Gamma\cdot w(k) \tag{2.1.12}$$

$$y(k) = \Theta\cdot\mathbf{x}(k) + v(k) \tag{2.1.13}$$

where

$$\Phi = \begin{bmatrix} 1 & 0 & 0 & \cdots & & 0 & 0 & \cdots & 0 \\ \gamma_1 & 1 & 0 & \cdots & & -a_n & 0 & \cdots & 0 \\ \vdots & & \ddots & & & \vdots & \vdots & & \vdots \\ \gamma_n & 0 & 0 & \cdots & 1 & -a_1 & 0 & \cdots & 0 \\ 0 & & & \cdots & & 1 & 0 & & 0 \\ & & & & & 0 & 1 & & \\ \vdots & & & & & \vdots & & \ddots & \vdots \\ 0 & & & \cdots & & 0 & \cdots & 1 & 0 \end{bmatrix} \quad \Lambda = \begin{bmatrix} 0 \\ b_n \\ \vdots \\ b_1 \\ 0 \\ 0 \\ \vdots \\ 0 \end{bmatrix} \quad \Gamma = \begin{bmatrix} 1 \\ 0 \\ \vdots \\ 0 \\ 0 \\ 0 \\ \vdots \\ 0 \end{bmatrix} \tag{2.1.14}$$

$$\Theta = \begin{bmatrix} 0 & \cdots & 0 & 1 \end{bmatrix} \tag{2.1.15}$$

$$\mathbf{x}(k) = \begin{bmatrix} x_\rho(k) & x_1(k) & \cdots & x_n(k) & x_{n+1}(k) & \cdots & x_{n+d}(k) \end{bmatrix}^T \tag{2.1.16}$$

Φ ≡ state transition matrix

Λ ≡ input transition vector

Θ ≡ output transition vector

Here w(k) and v(k) represent uncorrelated, Gaussian distributed noise sequences with a mean of zero, and covariances $R_w=E[w^T(k)\cdot w(k)]$ and $R_v=E[v^T(k)\cdot v(k)]$. This model is basically a direct realization of the ARIMA transfer function model with the exception that the noise dynamics have been separated into two uncorrelated components of a given standard deviation. The non-stationary component of the noise is represented in the state space model by the augmentation of the state transition matrix with a pure integrator as in equation (2.1.14).

Comparing the state-space and ARIMA models further, it is easily noticed that the state transition matrix contains the AR component of the process. Similarly, the input transition vector describes the MA component. Since the state transition matrix contains no additional noise parameters, the state space model lumps the AR process and disturbance dynamics together as does the ARIMA model. This fact will have a significant impact on the model parameters during on-line estimation when a disturbance with AR dynamics is present.

2.2 PLANT IDENTIFICATION

The dynamics of most chemical processes that have been sampled at a rate which allows identification of the desired process bandwidth may be characterized by the following n^{th} order discrete time ARIMA model :

$$A(z^{-1})\cdot y(k) = z^{-d}\cdot B(z^{-1})\cdot u(k-1) + \frac{C(z^{-1})\cdot \xi(k)}{\Delta} \qquad (2.2.1)$$

where

$$A(z^{-1}) = 1 + a_1 z^{-1} + a_2 z^{-2} + \cdots + a_n z^{-n} \qquad (2.2.2)$$

$$B(z^{-1}) = b_1 + b_2 z^{-1} + b_3 z^{-2} + \cdots + b_n z^{-n} \qquad (2.2.3)$$

$$C(z^{-1}) = 1 + c_1 z^{-1} + c_2 z^{-2} + \cdots + c_n z^{-n} \qquad (2.2.4)$$

$$\Delta = 1 - z^{-1}$$

$$d = \text{true process time delay} \in \mathit{Integer}$$

Here d is the true process time delay and an integral multiple of the sampling time T_s. Similarly, the Δ operator is used to define the non-stationary behavior of the process, as a random walk.

With time invariant processes, the parameters of the ARIMA model may be estimated off-line by a batch least squares or maximum likelihood technique. However, plants which exhibit time varying dynamics and/or non-linearities which are non-repeatable will require the model parameters to be estimated by some on-line technique. This will have to be done either in the open or closed loop depending on the safe operating limits of the process. From the literature it is obvious that there are a large number of techniques to perform this on-line estimation, but the most commonly used technique is recursive least squares estimation. The following sections describe the basic RLS algorithm and the modifications that are required in order for it to provide stable and accurate estimates of the plant parameters in an industrial environment, i.e. an environment which is continuously being corrupted by both MA and AR type disturbances.

2.2.1 Basic Least Squares Algorithm

If, for the moment, the structured MA dynamics of the noise are neglected, the ARIMA plant model of Equation (2.2.1) may be re-written in the following convenient vector form :

$$\Delta y(k) = \frac{B(z^{-1})}{A(z^{-1})} \cdot \Delta u(k-d-1) + \xi(k) \qquad (2.2.5)$$

$$\Delta y(k) = \phi(k)^T \cdot \hat{\theta}(k-1) + \xi(k) \qquad (2.2.6)$$

where

$$\phi(k) = \left[\Delta y(k-1) \cdots \Delta y(k-n) \;\; \Delta u(k-d-1) \cdots \Delta u(k-d-n) \right] \qquad (2.2.7)$$

$$\hat{\theta}(k-1) = \left[\hat{a}_1 \cdots \hat{a}_n , \hat{b}_1 \cdots \hat{b}_n \right]^T \qquad (2.2.8)$$

Since the ultimate interest here is in adaptive control, the plant parameters must be estimated by some on-line technique. In the literature, the most common technique is one which minimizes a quadratic cost function. The elements of the algorithm which must be updated at each sample interval may be summarized as :

A) gain calculation :

$$L(k-1) = \frac{P(k-1)\cdot\phi(k)}{1 + \phi^T(k)\cdot P(k-1)\cdot\phi(k)} \tag{2.2.9}$$

B) parameter update :

$$\hat{\theta}(k) = \hat{\theta}(k-1) + L(k-1)\cdot[\,\Delta y(k) - \phi^T(k)\cdot\theta(k-1)\,] \tag{2.2.10}$$

C) covariance update :

$$P(k) = P(k-1) - \frac{P(k-1)\cdot\phi(k)\cdot\phi^T(k)\cdot P(k-1)}{1 + \phi^T(k)\cdot P(k-1)\cdot\phi(k)}$$

$$\text{where} \quad P(0) = \alpha\cdot I \quad \alpha > 0 \tag{2.2.11}$$

Although this algorithm will work for a certain class of systems, it has many shortcomings and must be modified in order for it to function in an environment where the excitation may be small for extended periods of time.

A common first problem of the basic least squares algorithm is that after the initial process excitation and identification, the covariance matrix, P(k) will decay to zero in an exponential fashion. This decaying of the auto and cross correlation terms in the matrix to zero, causes the corresponding Kalman estimator gain vector to become increasingly small, and thus the estimator will not be able to track changing plant dynamics. At this point the estimator is said to have gone to "sleep" and no level of regressor excitation will cure the problem. In process control computers, this covariance decay may also lead to numerical problems and may cause the P(k) matrix to loose its positive definite nature.

A common solution to the covariance decay is to introduce a forgetting factor into the quadratic cost function :

$$J = \sum_{k=1}^{N} \lambda^{N-k} \cdot \left(\Delta y(k) - \phi^{T}(k)\cdot\hat{\theta}(k-1) \right) \qquad (2.2.12)$$

For this cost function the updates now become,

gain calculation

$$L(k-1) = \frac{P(k-1)\ \phi(k)}{\lambda + \phi^{T}(k)\cdot P(k-1)\cdot\phi(k)} \qquad (2.2.13)$$

covariance update

$$P(k) = \frac{P(k-1)}{\lambda} - \frac{P(k-1)\cdot\phi(k)\cdot\phi^{T}(k)\cdot P(k-1)}{\lambda + \phi^{T}(k)\cdot P(k-1)\cdot\phi(k)}$$

where $\lambda = (\ 0,\ 1\ ]$

(2.2.14)

A forgetting factor of $\lambda \le 1$ is typically chosen such that the estimator can track the changing dynamics of the plant at an appropriate speed. Selecting $\lambda \cong 1$ causes slow parameter tracking, and would thus be used when the plant dynamics change gradually over an extended period of time. Equivalently, selecting $\lambda \ll 1$ causes fast parameter tracking. λ may also be thought of as the estimator filter constant. It must be noted that if the signal/noise is small, selecting a λ that is relatively small will cause radical fluctuations in the estimated parameters, as the estimator attempts to fit the resulting fluctuations caused by the noise. Although the forgetting factor solves the problem of covariance decay, it presents another problem when the regressor excitation is low, $\phi(k)\cong 0$. The covariance update with $\phi(k)\cong 0$ becomes $P(k)=P(k-1)/\lambda$. With $\lambda<1$, the covariance matrix, $P(k)$ will grow exponentially large. This is typically known as covariance "windup" or "blow up". This "windup" condition must be controlled because once the regressor is excited, the parameters will also burst as now the estimator gain vector has also grown exponentially large. Naturally, there are numerical constraints on the size of the values that a digital computer may handle, and thus it is important to prevent this phenomena from occurring.

There have been several solutions proposed to improving the robustness of the Basic Recursive Least Squares algorithm . A number of these solutions have been summarized and discussed (Ljung and Soderstrom, 1983). Many of these ideas (Shah, 1986), (Sripada, 1988) have been incorporated in their version of Improved Least Squares (ILS) which addresses many of the robustness problems of the basic algorithm. The following section summarizes the improvements that were made to the RLS algorithm and used in this work.

2.2.2 Recursive Least Squares Estimation For An Industrial Enviroment

There are three main concerns in developing a recursive estimator for an industrial environment. First, the estimator must be numerically stable in order for it to operate over extended periods of time without having to be restarted or re-initialized. Second, it must provide the "tuning knobs" which are both reasonable and easily comprehensible such that the estimator can be easily maintained with a minimal amount of engineering effort. Thirdly, the estimator must provide monitoring information which allows the user to evaluate the performance of the algorithm. The following sections describe the items which are required to implement such an estimator.

Data Scaling

In general, the regressor vector, $\phi(k)$ contains both input and output terms when estimating an ARIMA type model. With the ARIMA structure the regressor vector is written as :

$$\phi(k) = \left[\, \Delta y(k-1) \cdots \Delta y(k-n) \;\; \Delta u(k-d-1) \cdots \Delta u(k-d-n) \,\right]$$

Sripada,(1988) has suggested that this regressor should be normalized in the following manner :

$$\Delta y_n(k) = \Delta y(k) \, / \, \eta \qquad (2.2.15)$$

$$\phi_n(k) = \phi(k) \, / \, \eta \qquad (2.2.16)$$

where $\eta = \max(\, 1, \, \|\, \phi(k) \,\| \,)$

Although it may seem logical to scale the regressor to a value less than or equal to one, numerical problems may result if the dynamic ranges of the input and output are not identical. For example, if typically $\Delta y(k) \cong 10^{2}$ and $\Delta u(k) \cong 10^{-1}$ then normalizing the regressor using equation (2.2.16) will yield $0.1 \le \Delta y \le 1$ and $10^{-4} \le \Delta u \le 10^{-3}$. Possible overflow problems have been eliminated by scaling the data to less than one, however, the truncation/round-off problems may cause difficulties due to the lack of significant digit representation in the input.

Most arithmetic computations are performed in computers which either have floating point hardware or software emulation of floating point operations coded in firmware. A floating point number may be represented in binary as $2^{c} \cdot M$, where c is the characteristic and M is the mantissa. During an addition/subtraction the floating point hardware must equalize the characteristic of the two numbers. It does this by increasing the characteristic of the smaller number by shifting the binary point to the left and padding with zeros. Depending on the size of the mantissa, M, this may create some real numerical problems during the addition of two numbers if one of the numbers is relatively small.

Thus a solution to this problem is to scale the regressor components separately based on whether they are inputs or outputs.

The regressor elements may be scaled as follows :

$$\eta_y = \max(\ 1,\ \|\ \phi_y(k)\ \|\ ) \tag{2.2.17}$$

$$\eta_u = \max(\ 1,\ \|\ \phi_u(k)\ \|\ ) \tag{2.2.18}$$

$$\Delta y_n(k) = \Delta y(k)\ /\ \eta_y$$

$$\Delta u_n(k) = \Delta u(k)\ /\ \eta_u$$

$$\text{where} \quad \phi(k) = \left[\ \phi_y(k) \quad \phi_u(k)\ \right]$$

$$\phi_y(k) = \left[\ \Delta y(k-1)\ \Delta y(k-2) \cdots \Delta y(k-n)\ \right]$$

$$\phi_u(k) = \left[\ \Delta u(k-d-1)\ \Delta u(k-d-2) \cdots \Delta u(k-d-n)\ \right]$$

This normalization scheme will ensure that both the $\phi_y(k)$ and $\phi_u(k)$ values are contained in the same order of magnitude which will prevent the floating point hardware from having to equalize the characteristics, thus possibly removing valuable dynamic information by shifting it out of the mantissa. It should also be noted that utilizing values less than one also prevents the occurrence of overflow/underflow.

Data Filtering

The complete ARIMA model from Section 2.1 was written as :

$$A(z^{-1})\cdot y(k) = z^{-d}\cdot B(z^{-1})\cdot u(k-1) + \frac{C(z^{-1})\cdot \xi(k)}{\Delta} \tag{2.2.19}$$

This ARIMA model describes a linear, non-stationary process where the noise dynamics are parameterized by the $C(z^{-1})$ polynomial. If the noise, $\xi(k)$, were measurable, then the $C(z^{-1})$ polynomial could be estimated by appending the $\xi(k)$, $\xi(k-1)$ ... terms to the regressor vector as follows :

$$\phi(k) = \left[\, \Delta y(k-1) \cdots \Delta y(k-n) \;\; \Delta u(k-d-1) \cdots \Delta u(k-d-n) \;\; \xi(k-1) \cdots \xi(k-n) \,\right] \tag{2.2.20}$$

However, since $\xi(k)$ is not measurable, a pseudo, linear regression (Goodwin and Sin, 1984) algorithm may be used where the $\xi(k)$ terms are replaced by an approximation to these noise components. The approximations are found by using the old parameter vector and the newly updated regressor vector :

$$\hat{\xi}(k) = \Delta y(k) - \Delta\hat{y}(k) = \Delta y(k) - \phi^T(k-1)\cdot\hat{\theta}(k-1) \tag{2.2.21}$$

This form of parameter estimation is commonly referred to as Extended Least Squares (ELS), and in practice is very difficult to perform due to the slow convergence of the $C(z^{-1})$ polynomial parameters. In order to improve the estimation Tuffs and Clarke, (1985) have proposed the $T(z^{-1})$ filter in order to reduce or eliminate the effects of the structured noise component.

With the $T(z^{-1})$ filter the ARIMA model may be re-written as :

$$\frac{A(z^{-1})\cdot\Delta y(k)}{T(z^{-1})} = z^{-d}\cdot\frac{B(z^{-1})\cdot\Delta u(k-1)}{T(z^{-1})} + \frac{C(z^{-1})\cdot\xi(k)}{T(z^{-1})} \tag{2.2.22}$$

where

$$\frac{1}{T(z^{-1})} = \frac{1 + t_1 + \cdots + t_n}{1 + t_1\cdot z^{-1} + \cdots + t_n\cdot z^{-n}}$$

$1/T(z^{-1})$ is essentially a low pass or MA filter, responsible for removing the structured high frequency noise components in the plant input/output. When implemented as in equation (2.2.23), it adds no bias or DC gain to the I/O components, but rather shapes their frequency/phase characteristics. It should be noted that the use of a $1/T(z^{-1})$ filter does not remove the low frequency noise that may be present. This low frequency noise typically takes a form of slow moving AR type disturbances due to the addition or removal of loads to the system. If the disturbances are steps in the output, the Δ operator will account for their effects. The Δ operator differences the input and output data and is one way of providing stationary data for the estimator. Stationary process data is required if a stable process model is to be estimated.

Typically, for a first order system, the $1/T(z^{-1})$ filter is chosen as $0.2/(1-0.8\cdot z^{-1})$. Looking at the denominator, the filter pole location suggests that a good choice for the bandwidth of the filter is the bandwidth of the plant itself, where the bandwidth is defined as the -3dB roll-off frequency. If a first order system is sampled at a rate of $\frac{1}{5}\tau_p$ the discrete time pole location will be approximately 0.8.

Bierman's UD-Factorization

The gain and covariance update for weighted least squares was given as :

gain calculation

$$L(k) = \frac{P(k-1)\cdot\phi(k)}{\lambda + \phi^T(k)\cdot P(k-1)\cdot\phi(k)}$$

covariance update

$$P(k) = \frac{P(k-1)}{\lambda} - \frac{P(k-1)\cdot\phi(k)\cdot\phi^T(k)\cdot P(k-1)}{\lambda + \phi^T(k)\cdot P(k-1)\cdot\phi(k)}$$

In modern computers where register lengths may be 256 bits, the above computations may be implemented directly without much concern for numerical problems and instabilities. However, the majority of existing chemical process control computers are limited to 24-32 bit word lengths, and thus it is quite conceivable that numerical problems may occur with the covariance update when more than 2 or 3 parameters are being estimated. Since it is critical to maintain the positive definite property of the covariance matrix, several factorization algorithms (i.e. Cholesky, Bierman's UD-factorization) are available which will ensure that this property is maintained.

In Bierman's UD-factorization algorithm(Bierman,1977) the covariance matrix P(k) is replaced by $U(k)\cdot D(k)\cdot U^T(k)$

where,

$$U(k) = \begin{bmatrix} 1 & u_{1,2} & \cdots & u_{1,m} \\ & 1 & & \vdots \\ & & \ddots & \\ & 0 & & u_{m-1,m} \\ & & & 1 \end{bmatrix} \qquad (2.2.24)$$

$$D(k) = \begin{bmatrix} d_1 & & & \\ & d_2 & & 0 \\ & & \ddots & \\ & 0 & & \\ & & & d_m \end{bmatrix} \qquad (2.2.25)$$

U(k) is an upper triangular matrix with 1's along the diagonal and D(k) is a diagonal matrix of dimension $m=n_a + n_b$ (n_a = number of $A(z^{-1})$ parameters, n_b = number of $B(z^{-1})$ parameters). The complete computation algorithm may be found in Ljung and Söderström, (1984).

Although the UD-factorization adds an additional burden on the computer, the fact that it contributes significantly to the robustness of the parameter estimator far outweighs the burden.

Constant Trace, Variable Forgetting Factor

As was mentioned earlier, the covariance matrix can either decay to zero ($\lambda=1$), or "wind-up" during periods of low regressor excitation ($\lambda<1$). To eliminate these phenomena from occurring (Sripada and Fisher, 1987) have proposed a variable forgetting factor which maintains the *tr*{ P(·) } constant at a user-specified value. The variable forgetting factor may be written as :

$$\lambda(k) = 1 - \frac{1}{2}\left(g(k) - \left[g^2(k) - \frac{4 \, || \, P(k-1)\,\phi(k) \, ||^2}{tr\{ \, P(k-1) \, \}} \right]^{1/2} \right)$$

$$\text{where} \quad g(k) = 1 + \phi^T(k)\cdot P(k-1)\cdot\phi(k) \qquad (2.2.26)$$

The *tr*{ P(·) } is chosen by the user such that the model parameters will adequately track the changing plant parameters. The higher the *tr*{ P(·) }, the larger will be the resultant Kalman gain vector elements. In fact, since the parameter update equation is written as,

$$\hat{\theta}(k) = \hat{\theta}(k-1) + L(k)\cdot[\ \Delta y_f(k) - \phi^T(k)\cdot\hat{\theta}(k-1)\ ] \qquad (2.2.27)$$

$$\Delta\hat{\theta}(k) = L(k-1)\cdot\hat{\xi}(k) \qquad (2.2.28)$$

the Kalman gains directly determine the incremental adjustment that is made to the individual parameters. It can be seen that if the model error $\hat{\xi}(k)$ has a large variance, then the parameters may fluctuate excessively and thus model based control may not be practical. Also, this is where data filtering becomes extremely important, since high frequency noise in the plant output may cause the model parameters to fluctuate wildly. To eliminate the effects of high frequency noise, digital data filtering may be used in the form of the $\Delta/T(z^{-1})$ filter, as was already discussed.

Thus the choice of the $tr\{\ P(\cdot)\ \}$ is important to achieving and maintaining a good set of model parameters. In order to do this, the variance of the plant dynamics and noise must be understood.

ON/OFF Criterion

During periods of low excitation, or periods where the plant dynamics are not changing, it is desirable to turn the estimator off. This is done to prevent low frequency or auto-regressive type disturbances from corrupting the model parameters, which under these conditions will tend to drift. This drifting may cause the plant model to become unstable, and thus adequate, stable prediction is not possible when the model is to be used for control purposes. In order to prevent this from occurring the estimator is turned off when $||\ \Delta y_f(k) - \phi^T(k)\cdot\theta(k)\ || \le \Delta_d$, the absolute value of the model prediction error, is less than some user specified deadzone. The literature provides alternatives to the use of the deadzone. Sripada, (1988) has used $||P(k-1)\cdot\phi(k)||$ and Cond{P(k)} as indicators of persistent excitation. As with the deadzone on the prediction error, user-specified limits can be set around the indicators of persistent excitation. The RLS estimator would then be turned off during periods of low excitation.

2.3 MODIFIED KALMAN FILTER PREDICTOR

Since the introduction of the Kalman Filter (Kalman and Bucy, 1961), the filter has found many applications in a wide spectrum of industries ranging from aerospace to the biochemical industry. In this section the Kalman filter is presented as an optimal, single-step predictor.

Consider a linear state space model of a plant,

$$\mathbf{x}(k+1) = \Phi\cdot\mathbf{x}(k) + \Lambda\cdot u(k) + \Gamma\cdot w(k) \qquad (2.3.1)$$

$$y(k) = \Theta\cdot\mathbf{x}(k) + v(k) \qquad (2.3.2)$$

$$\Phi = \begin{bmatrix} 1 & 0 & \cdots & 0 & 0 & 0 & \cdots & 0 & 0 \\ \gamma_1 & 1 & \cdots & 0 & -a_n & 0 & \cdots & 0 & 0 \\ \gamma_2 & & \ddots & & -a_{n-1} & \vdots & & & \vdots \\ \vdots & & & & \vdots & & & & \\ \gamma_n & 0 & \cdots & 1 & -a_1 & 0 & \cdots & 0 & 0 \\ 0 & & \cdots & & 1 & 0 & \cdots & 0 & 0 \\ \vdots & & & & \vdots & 1 & \ddots & & \vdots \\ 0 & & \cdots & & 0 & 0 & \cdots & 1 & 0 \end{bmatrix}_{(n+d+1)\times(n+d+1)}$$

$$\Lambda = \begin{bmatrix} 0 \\ b_n \\ b_{n-1} \\ \vdots \\ b_1 \\ 0 \\ \vdots \\ 0 \end{bmatrix}_{(n+d+1)\times 1} \qquad \Gamma = \begin{bmatrix} 1 \\ 0 \\ 0 \\ \vdots \\ 0 \\ 0 \\ \vdots \\ 0 \end{bmatrix}_{(n+d+1)\times 1}$$

$$\Theta = \begin{bmatrix} 0 & 0 & \cdots & 0 & 1 \end{bmatrix}_{1\times(n+d+1)}$$

where w(k) is the process noise with covariance R_w and v(k) is the measurement or output noise with covariance R_v. If the dynamics of the process are non-stationary then it is desirable to augment the state transition matrix with an additional noise or integrating state. The use of this augmented state space model in the Kalman Filter update equations is referred to by Walgama, (1986) as the modified Kalman filter predictor.

The on-line computation and updating of the Kalman filter may be performed by the two-step method as proposed by (Aström, 1970),

A) gain calculation

$$L(k) = \frac{M(k)\cdot\Theta^T(k)}{\Theta(k)\cdot M(k)\cdot\Theta^T(k) + R_v} \qquad (2.3.3)$$

B) measurement update

i) posteriori state update

$$\hat{\mathbf{x}}(k) = \bar{\mathbf{x}}(k) + L(k)\cdot[\, y(k) - \Theta\cdot\bar{\mathbf{x}}(k) \,] \qquad (2.3.4)$$

ii) posteriori covariance update

$$P(k) = M(k) - L(k)\cdot\Theta(k)\cdot M(k) \qquad (2.3.5)$$

C) time update

i) priori state update

$$\bar{\mathbf{x}}(k+1) = \Phi\cdot\hat{\mathbf{x}}(k) + \Lambda\cdot u(k) \qquad (2.3.6)$$

ii) priori covariance update

$$M(k+1) = \Phi\cdot P(k)\cdot\Phi^T + \Gamma\cdot R_w\cdot\Gamma^T \qquad (2.3.7)$$

Although these equations may be implemented directly on a digital computer, it is usually much more beneficial to use a factorization (Cholesky, Bierman's UD) on the covariance matrix. By using a factorization, the matrix elements being updated are standard deviations rather that auto/cross covariances. This normally implies that the relative value of the covariance elements will be closer to 1 and thus less prone to numerical round-off or truncation errors. The algorithm also ensures that the covariance matrix maintains its positive, definite property which is essential to having stable control action.

A very powerful technique for analyzing and obtaining an equivalent transfer function form of the Modified Kalman Filter Predictor (MKFP) is the innovations analysis. Both Walgama,(1986) and Foley,(1988) used it extensively to illustrate the equivalence of the Smith predictor (Smith, 1959) and the MKFP. Foley,(1988) also went further and illustrated the steady state equivalence of the diophantine identity to the MKFP using this same technique. The diophantine identity has been used extensively in both generalized minimum variance (Clarke and Gawthrop, 1979) and generalized predictive control (Clarke, Mohtadi and Tuffs, 1987).

If the innovations analysis is performed as by Foley,(1988) the modified Kalman filter predictor may be summarized by the following equations and block diagram given in Figure 2.3.1 :

$$\hat{y}(k+d|k) \;=\; y_p(k) \;+\; G_F(k,z^{-1})\cdot[\; y(k) - y_m(k)\;] \qquad (2.3.8)$$

where

$$y_m(k) \;=\; z^{-d}\cdot \frac{B(z^{-1})}{A(z^{-1})}\cdot u(k-1) \qquad (2.3.9)$$

$$y_p(k) \;=\; \frac{B(z^{-1})}{A(z^{-1})}\cdot u(k-1) \qquad (2.3.10)$$

$$G_F(z^{-1}) \;=\; \frac{K_5(z^{-1})}{C(z^{-1})} \qquad (2.3.11)$$

$$K_5(z^{-1}) \;=\; z^{+1}\cdot[\; K_1(z^{-1})\cdot\Delta - L_n\cdot A(z^{-1})\cdot\Delta \;+\; D(z^{-1})\;] \qquad (2.3.12)$$

$$C(z^{-1}) \;=\; [\; A(z^{-1})\cdot(\; 1 + K_2(z^{-1})\;) + z^{-d}\cdot K_1(z^{-1})\;]\cdot\Delta \;+\; z^{-d}\cdot D(z^{-1}) \qquad (2.3.13)$$

$$K_1(z^{-1}) \;=\; L_n + L_{n-1}\cdot z^{-1} + \cdots + L_1\cdot z^{-n+1} \qquad (2.3.14)$$

$$K_2(z^{-1}) \;=\; L_{n+d-1} + L_{n+d-2}\cdot z^{-1} + \cdots + L_{n+1}\cdot z^{-(d+2)} \qquad (2.3.15)$$

$$D(z^{-1}) \;=\; L_\rho\cdot[\; \gamma_n\cdot z^{-1} + \cdots + \gamma_1\cdot z^{-n}\;] \qquad (2.3.16)$$

From equation (2.3.8) and the block diagram realization, it can be seen that the Smith predictor and the modified Kalman filter predictor are equivalent, with the one exception being that the MKFP uses a non-linear, time-varying, optimal disturbance filter, $G_F(z^{-1})$, in order to shape the residuals formed between the model and the current output measurement. $G_F(z^{-1})$ consists of both a

Figure 2.3.1 Block Diagram of Kalman Filter Predictor

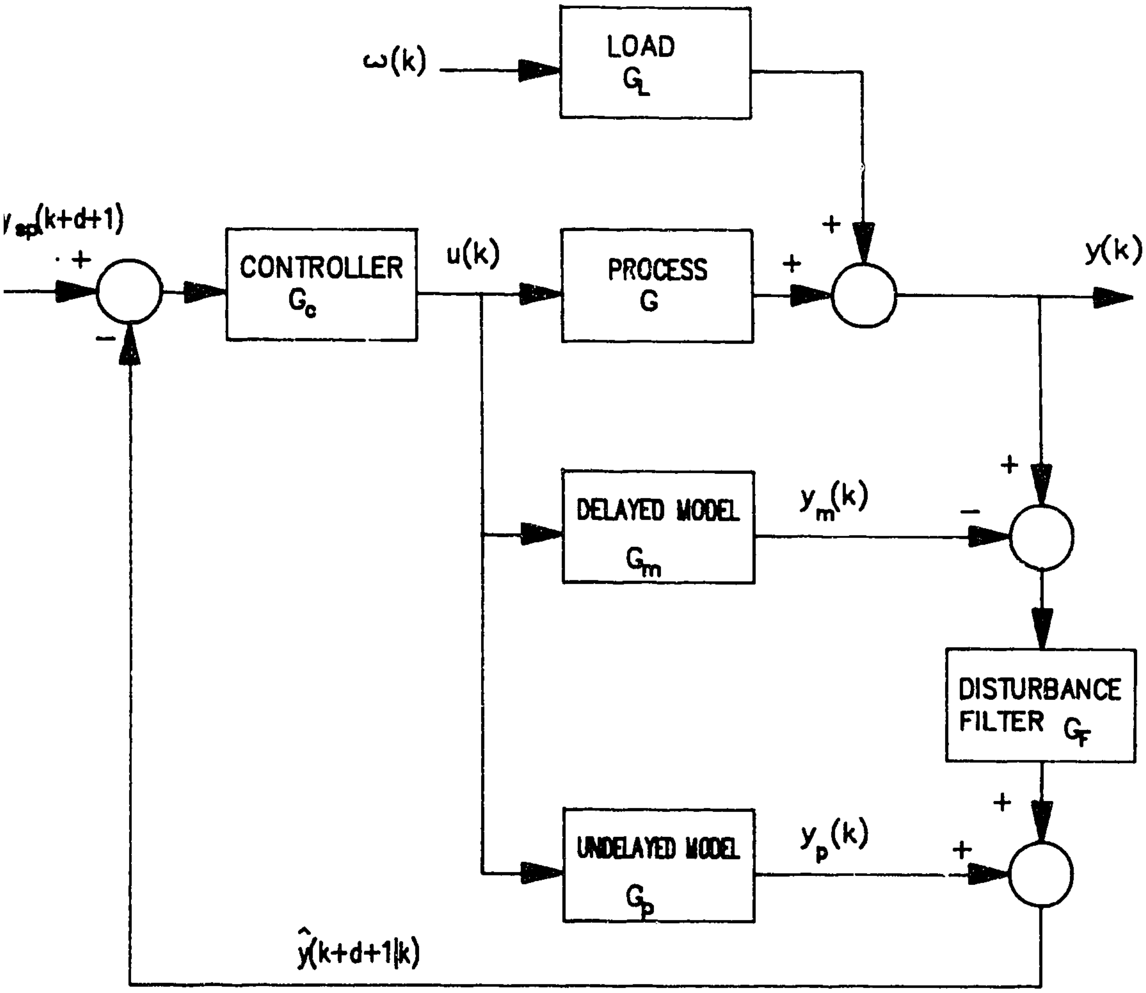
ω(k)
LOAD
G_L
$y_{sp}(k+d+1)$
+
−
CONTROLLER
G_c
u(k)
PROCESS
G
+
+
y(k)
+
−
DELAYED MODEL
G_m
$y_m(k)$
DISTURBANCE
FILTER G_F
+
+
UNDELAYED MODEL
G_p
$y_p(k)$
$\hat{y}(k+d+1|k)$

numerator and denominator polynomial. The denominator, $C(z^{-1})$ is an optimal low pass filter whose bandwidth may be manipulated by altering the ratio of the process and measurement noise covariances, R_w/R_v. This low-pass filter is analogous to the $T_c(z^{-1})$ filter which has been used to improve the overall robustness of GPC. Mohtadi,(1987) and McIntosh,(1988) both discuss the implementation and selection of such a filter. Similarly, the numerator of the disturbance filter may be thought of as a single series forecast of the residual. Man,(1984) discussed the use of such a forecaster to improve the overall robustness of IMC.

2.4 THE MULTI-STEP PREDICTIVE ALGORITHM

In Section 2.3 the single step modified Kalman filter predictor was developed. It was shown to provide a single step prediction of the output, which when modified with the integrating state, guarantees asymptotically zero prediction offset in the presence of non-stationary disturbances.

In 1986, Clarke and Mohtadi developed the Generalized Predictive Control algorithm (GPC) which was shown to provide very good, robust control in presence of model plant mismatch (McIntosh, 1988). The GPC algorithm makes use of the CARIMA model and uses the diophantine identity to provide the series or horizon of future output predictions which are later used in a complimentary control law.

In 1987, Sripada, Foley and Fisher have similarly developed the Multi-Step Adaptive Predictive Controller (MAPC). This controller relies on a state space model augmented with an additional noise state as in Walgama's, (1986) MKFP, and the future state and output predictions are provided by using the two-step Kalman filter equations given in Section 2.3.

2.4.1 The Basic Algorithm

The multi-step predictive algorithm may be developed by extending the results of Section 2.3 in the following manner. First, the two-step Kalman filter state update equations may be summarized as

$$\hat{x}(k+1) \;=\; \Phi\cdot\hat{x}(k) + \Lambda\cdot u(k) + L(k+1)\cdot\xi(k) \qquad (2.4.1)$$

$$\text{where} \quad \xi(k) = y(k+1) - \Theta\cdot\Phi\cdot\hat{x}(k) - \Theta\cdot\Phi\cdot u(k) \qquad (2.4.2)$$

By recursive substitution of equation (2.4.1) the following expression may be written for the future state vector predictions,

$$\hat{x}(k+j|k) \;=\; \Phi^{j}\cdot\hat{x}(k|k-1) + \sum_{l=k}^{k+j} \Phi^{k+j-l-1}\cdot\Lambda\cdot u(l-1) + \sum_{l=k+1}^{k+j} \Phi^{k+j-l}\cdot L(k+1)\cdot\xi(l) \qquad (2.4.3)$$

The future state predictions require knowledge of the current and future plant inputs u(k-1), u(k) ... u(k+j-1), as well as the future noise terms $\xi(k+1)$, $\xi(k+2)$ ... $\xi(k+j)$. Once the Kalman gains L_{ρ}, L_1, ... L_{n+d} have converged to their steady state values, the noise term $\xi(k)$ will be a white noise sequence with a mean of zero. Since the noise sequence has a mean of zero, the future noise terms are assumed to be zero and the future state predictions may now be written as in equation (2.4.4) :

$$\hat{\mathbf{x}}(k+j|k) = \Phi^{j}\cdot\hat{\mathbf{x}}(k|k-1) + \sum_{l=k}^{k+j} \Phi^{k+j-l-1}\cdot\Lambda\cdot u(l-1) \tag{2.4.4}$$

Similarly, the future output predictions may be written as :

$$\hat{y}(k+j|k) = \Theta\cdot\Phi^{j}\cdot\hat{\mathbf{x}}(k|k-1) + \sum_{l=k}^{k+j} \Theta\cdot\Phi^{k+j-l-1}\cdot\Lambda\cdot u(l-1) \tag{2.4.5}$$

At this time it is appropriate to introduce the minimum and maximum prediction horizons, N_1 and N_2. With these two horizons defined, equation (2.4.5) may be rewritten in the following vector-matrix form:

$$\{\, \hat{y}(k+j|k),\ j\in[N_1,N_2]\,\} = \{\, \Theta\cdot\Phi^{j}\cdot\hat{\mathbf{x}}(k|k-1),\ j\in[N_1,N_2]\,\} + \mathbf{A'}\cdot\{\, u(k+j-1),\ j\in[N_1,N_2]\,\} \tag{2.4.6}$$

where

$$\mathbf{A'} = \begin{bmatrix} \Theta\Phi^{N_1-1}\Lambda & \Theta\Phi^{N_1-2}\Lambda & \cdots & \Theta\Lambda & 0 & 0 & \cdots & 0 \\ \Theta\Phi^{N_1-2}\Lambda & \Theta\Phi^{N_1-3}\Lambda & \cdots & & \Theta\Lambda & 0 & \cdots & 0 \\ \vdots & \vdots & & & & & \ddots & \vdots \\ & & & & & & & 0 \\ \Theta\Phi^{N_2-1}\Lambda & \Theta\Phi^{N_2-2}\Lambda & \cdots & & \Theta\Phi^{N_2-N_1-1}\Lambda & & \cdots & \Theta\Lambda \end{bmatrix}_{(N_y \times N_2)} \tag{2.4.7}$$

The $\mathbf{A'}$ matrix consists of the plant impulse co-efficients and is of dimension $N_y \times N$ $N_y = N_2 - N_1 + 1$. Typically, N_1 is chosen to be d+1 where d is the integral plant time delay not including the zero-order hold. Choosing $N_1 \leq d$ causes the first d rows of the **A'** matrix to be zero since the corresponding impulse co-efficients will also be zero.

Although this form of the future predictions may be implemented in an appropriate control law, it becomes more convenient to rewrite the future output predictions in terms of incremental control actions or inputs so that knowledge of the absolute steady state future plant input is not required. Thus, the vector-matrix equation may be written such that incremental control actions are used in the prediction equation, and the only absolute plant input required is the current input sample u(k-1). This may be done by recursively substituting u(k-1) = u(k) - Δu(k) into equation (2.4.6). When this is done the new vector-matrix form will assume the following form:

$$\{\ \hat{y}(k+j|k),\ j \in [N_1, N_2]\ \} = \{\ \Theta \cdot \Phi^j \cdot \hat{\mathbf{x}}(k|k-1),\ j \in [N_1, N_2]\ \} +$$

$$\left\{ \left(\sum_{j=1}^{i} a'_{i-N_1+1,\,j} \right) u(k-1),\ i \in [N_1, N_2] \right\} +$$

$$\mathbf{A}\{\ \Delta u(k+i-1),\ i \in [1, N_u]\ \} \tag{2.4.8}$$

with $\mathbf{A} = \mathbf{A}'\mathrm{S}$, $\mathrm{S} = \begin{bmatrix} 1 & 0 & & \cdots & 0 \\ 1 & 1 & 0 & \cdots & 0 \\ \vdots & \vdots & & \ddots & \vdots \\ & & & & 0 \\ 1 & 1 & & \cdots & 1 \\ 1 & 1 & & \cdots & 1 \\ \vdots & \vdots & & & \vdots \\ 1 & 1 & & \cdots & 1 \end{bmatrix}_{(N_2 x N_u)}$ (2.4.9)

Looking at equation (2.4.8), a new horizon was introduced, namely N_u which is defined as the control horizon. Beyond this control horizon, all incremental control actions are assumed to be zero, and thus, it is only necessary to compute the current control increment $\Delta u(k)$ and the future increments $\Delta u(k+1)$, ... $\Delta u(k+N_u-1)$ where $N_u \geq 1$, $\in I$. Also, it should be noticed that the **A** matrix is a matrix which contains the step response co-efficients, as opposed to the **A'** matrix which contained the impulse response co-efficients.

The multi-step predictive algorithm will now be rewritten in a more simplified form which will be useful in the next section when the control law is defined.

Defining, $\hat{Y}(k)$, $Y^{*}(k)$, and $\Delta u(k)$ as,

$$\hat{Y}(k) = \{ \hat{y}(k+j|k),\ j\in[N_1,N_2] \} \tag{2.4.10}$$

$$Y^{*}(k) = \{ \Theta\cdot\Phi^{j}\cdot\hat{\mathbf{x}}(k|k-1),\ j\in[N_1,N_2] \} + \left\{ \left(\sum_{j=1}^{i} a'_{i-N_1+1,j} \right) u(k-1),\ i\in[N_1,N_2] \right\} \tag{2.4.11}$$

$$\Delta u(k) = \{ \Delta u(k+i-1),\ i\in[1,N_u] \} \tag{2.4.12}$$

equation (2.4.8) may be written as,

$$\hat{Y}(k) = Y^{*}(k) + \mathbf{A}\cdot\Delta u(k). \tag{2.4.13}$$

Equation (2.4.13) can be described as being the addition of two components. The first component, $Y^{*}(k)$, contains information regarding the effects of past plant inputs. The second component, $\mathbf{A}\cdot\Delta u(k)$, summarizes the effects of future incremental input values.

This section has described the manner in which the state updates may be used in order to provide a horizon or trajectory of future predicted outputs. The parameters of the model may be fixed or adapted. The important tuning parameters of the predictor are N_1, N_2 and N_u. The minimum costing horizon, N_1 is typically chosen to be $d+1\le N_1\le N_2$ so that the step/impulse co-efficient matrix is non-singular. The maximum costing horizon, N_2 is typically chosen to encompass the dynamic response of the plant up to some steady state value.

2.4.2 Feedforward Variables

When a plant has measurable inputs that affect the output, but are not being used to manipulate the output, it is still possible to use them in order to improve the overall prediction. The state space model with a measurable disturbance variable may be written as :

$$\mathbf{x}(k+1) = \Phi\cdot\mathbf{x}(k) + \Lambda\cdot u(k) + w(k) \qquad (2.4.14)$$

$$y(k) = \Theta\cdot\mathbf{x}(k) + v(k) \qquad (2.4.15)$$

where

$$\Phi = \begin{bmatrix} 1 & 0 & & 0 & 0 & 0 \\ \gamma_1 & 1 & & -a_n & & \\ \gamma_2 & & \ddots & -a_{n-1} & & \\ \gamma_n & 0 & 1 & -a_1 & 0 & 0 \\ 0 & & & 1 & 0 & 0 \\ & & & & \ddots & \\ 0 & & & 0 & 0 \; 1 & 0 \end{bmatrix} \quad \Lambda = \begin{bmatrix} 0 & 0 \\ b_{n,1} & b_{n,2} \\ b_{n-1,1} & b_{n-1,2} \\ \vdots & \vdots \\ b_{1,1} & b_{1,2} \\ 0 & 0 \\ \vdots & \vdots \\ 0 & 0 \end{bmatrix}$$

$$\Theta = \begin{bmatrix} 0 & \cdots & 0 & 1 \end{bmatrix}$$

$$\mathbf{x}(k) = \begin{bmatrix} x_p(k) & x_1(k) & \cdots & x_n(k) & x_{n+1}(k) & \cdots & x_{n+d}(k) \end{bmatrix}^T$$

$$u(k) = \begin{bmatrix} u_1(k) & u_2(k-q-d) \end{bmatrix}^T \qquad q\geq d,\ q,d\in I$$

Here $u_1(k)$ is the manipulated variable normally used to control the output, and $u_2(k)$ is a measurable disturbance or feedforward input which may have either a MA or ARIMA structure. As was discussed in Section 2.1, if the disturbance is of a MA structure then the parameters associated with the input transition matrix/vector are sufficient to describe its dynamics. However, if the disturbance has an AR, or ARMA structure, then the order of the state transition matrix will have to be increased in order to accommodate the additional $A(z^{-1})$ parameters. The $A(z^{-1})$ parameters will now be a convolution of the AR dynamics of all plant inputs that have been modelled. For example, if the plant dynamics are first order, and similarly, the measurable disturbance dynamics are first order, then the number of parameters required for the state transition matrix is 2, and they involve the convolution of both plant dynamics.

Another important factor is that the time delay associated with the measurable disturbance must be equal to, or larger than the time delay involved with the manipulated input. This is necessary for causality to apply.

An additional system input may be easily incorporated into the overall prediction by modifying equation (2.4.5) :

$$\begin{aligned}\hat{y}(k+j|k) \;=\; & \Theta\cdot\Phi^{j}\cdot\hat{x}(k|k-1) + \sum_{l=k}^{k+j} \Theta\cdot\Phi^{k+j-l-1}\cdot\Lambda_1\cdot u_1(l-1) \\ & + \sum_{l=k}^{k+j} \Theta\cdot\Phi^{k+j-l-1}\cdot\Lambda_2\cdot u_2(l-q-d-1)\end{aligned} \qquad (2.4.16)$$

where q = integral time delay of $u_2(k)$

From this equation the final multi-step prediction algorithm is derived in a similar fashion as before with the exception that all future increments of the measurable disturbance input are assumed to be zero, that is $\Delta u_2(k)$ $\Delta u_2(k+1)$ ... $\Delta u_2(k+N_u-1)= 0$. Therefore the final prediction equation may be summarized as follows :

$$
\begin{aligned}
\{\, \hat{y}(k+j|k),\ j\in[N_1,N_2] \,\} &= \{\, \Theta\cdot\Phi^{j}\cdot\hat{\mathbf{x}}(k|k-1),\ j\in[N_1,N_2] \,\} \\
&+ \left\{ \left(\sum_{j=1}^{i} {}^{1}a'_{i-N_1+1,\,j} \right) u_1(k-1),\ i\in[N_1,N_2] \right\} \\
&+ \left\{ \left(\sum_{j=1}^{i} {}^{2}a'_{i-N_1+1,\,j} \right) u_2(k-1),\ i\in[N_1,N_2] \right\} \\
&+ \mathbf{A}\cdot\{\, \Delta u(k+i-1),\ i\in[1,N_u] \,\} \qquad (2.4.17)
\end{aligned}
$$

where

$$
{}^{1}A' = \begin{bmatrix}
\Theta\Phi^{N_1-1}\Lambda_1 & \Theta\Phi^{N_1-2}\Lambda_1 & \cdots & \Theta\Lambda_1 & 0 & 0 & \cdots & 0 \\
\Theta\Phi^{N_1-2}\Lambda_1 & \Theta\Phi^{N_1-3}\Lambda_1 & \cdots & & \Theta\Lambda_1 & 0 & \cdots & 0 \\
\vdots & \vdots & & & & \ddots & & \vdots \\
 & & & & & & & 0 \\
\Theta\Phi^{N_2-1}\Lambda_1 & \Theta\Phi^{N_2-2}\Lambda_1 & \cdots & & \Theta\Phi^{N_2-N_1-1}\Lambda_1 & & \cdots & \Theta\Lambda_1
\end{bmatrix}_{(N_y \times N_2)}
$$

$$
{}^{2}A' = \begin{bmatrix}
\Theta\Phi^{N_1-1}\Lambda_2 & \Theta\Phi^{N_1-2}\Lambda_2 & \cdots & \Theta\Lambda_2 & 0 & 0 & \cdots & 0 \\
\Theta\Phi^{N_1-2}\Lambda_2 & \Theta\Phi^{N_1-3}\Lambda_2 & \cdots & & \Theta\Lambda_2 & 0 & \cdots & 0 \\
\vdots & \vdots & & & & \ddots & & \vdots \\
 & & & & & & & 0 \\
\Theta\Phi^{N_2-1}\Lambda_2 & \Theta\Phi^{N_2-2}\Lambda_2 & \cdots & & \Theta\Phi^{N_2-N_1-1}\Lambda_2 & & \cdots & \Theta\Lambda_2
\end{bmatrix}_{(N_y \times N_2)}
$$

2.4.3 Innovations Analysis of MAPC

As was done with the MKFP, an innovations analysis may also be performed on the multi-step prediction algorithm to yield an equivalent transfer function form. This analysis was performed by Foley,(1988) in order to show the equivalence of GPC (Clarke, Mohtadi and Tuffs,1987) and MAPC (Sripada,1988). The basic results of the analysis are summarized in the equations below.

$$\hat{y}(k+j|k) = \frac{B(z^{-1})}{A(z^{-1})} u(k+j-1) + \frac{K_{4,j}(z^{-1})}{C(z^{-1})} \left\{ y(k) - z^{-d} \frac{B(z^{-1})}{A(z^{-1})} u(k-1) \right\} \tag{2.4.18}$$

where

$$K_{4,j}(z^{-1}) = z^{j-d} \left[(K_1(z^{-1}) - K'_{3,j}(z^{-1}) \cdot A(z^{-1}))\Delta + D(z^{-1}) \right] \tag{2.4.19}$$

$$C(z^{-1}) = A(z^{-1})(1 + K\ (z^{-1}))\Delta + z^{-d} \cdot [K\ (z^{-1})\Delta + D(z^{-1})] \tag{2.4.20}$$

$$K'_{3,j}(z^{-1}) = k_{d+1} + k_{d+2} z^{-1} + \ldots + k_j z^{-j+d+1} \tag{2.4.21}$$

$$k_i = \Theta\Phi^{i-1}L$$

The block diagram representation of the above equations in Figure 2.4.1, illustrates clearly that the multi-step predictor structure is essentially a bank of parallel Smith predictors, with a time-varying, optimal disturbance filter. It is this disturbance filter, $K_{4,j}$, that provides offset free future output

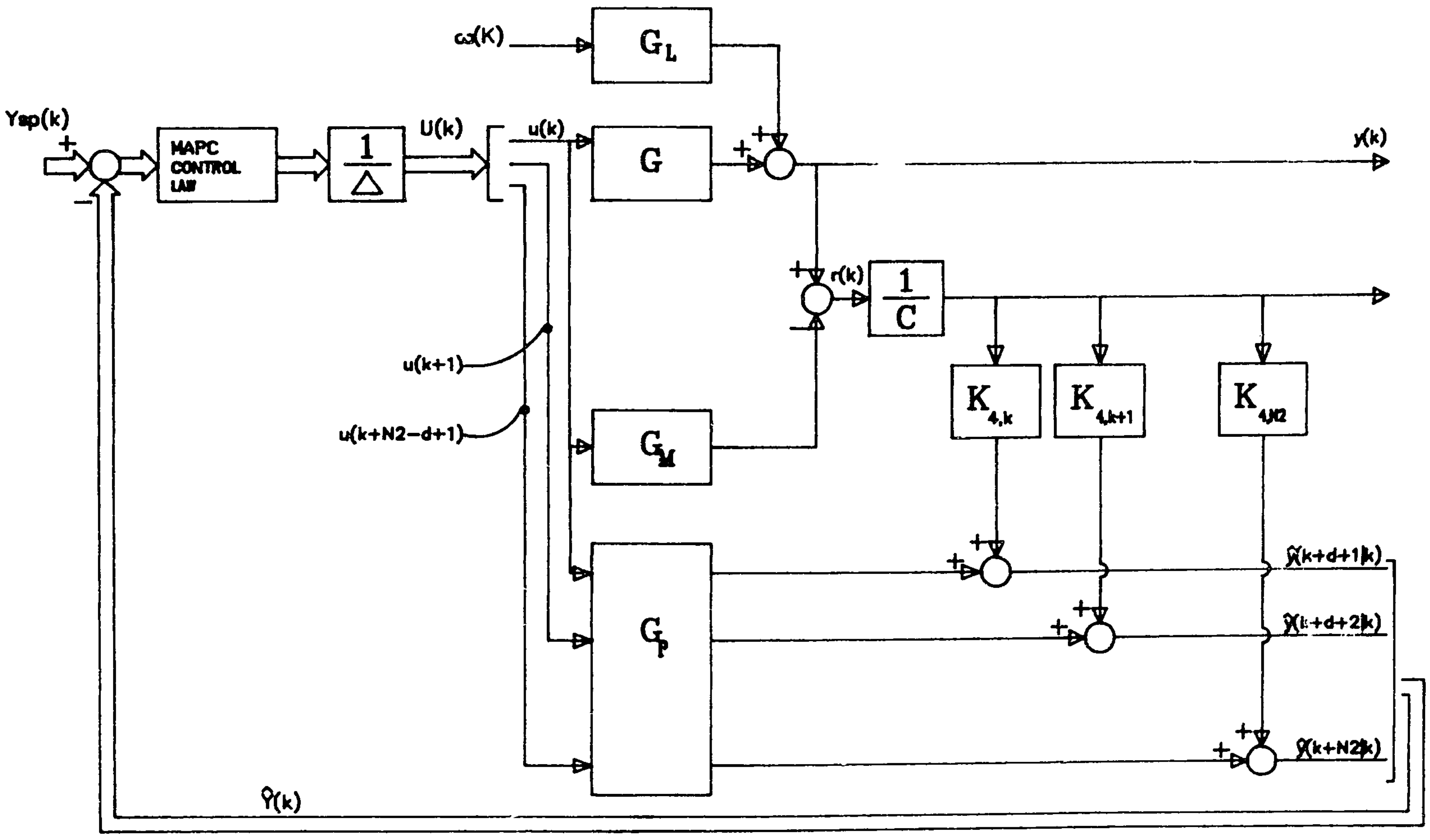
ω(K)
G_L
Ysp(k)
+
−
MAPC CONTROL LAW
1/△
U(k)
u(k)
G
+
+
y(k)
+
r(k)
1/C
−
u(k+1)
u(k+N2−d+1)
G_M
K_4,k
K_4,k+1
K_4,N2
G_p
+
+
ŷ(k+d+1|k)
ŷ(k+d+2|k)
ŷ(k+N2|k)
Ŷ(k)

Figure 2.4.1 Block Diagram of Multi-Step Adaptive Predictive Controller

prediction in the presence of load disturbances and model-plant mismatch (MPM). The minimum requirement is that this filter is $G_F(z^{-1})=1$, which is what the Smith predictor uses. In the case of MAPC, $G_F(z^{-1})$ is a combination of both a low-pass filter, $1/C(z^{-1})$, and a single series forecaster $K_{4,j}(z^{-1})$. The low-pass filter is responsible for removing high frequency measurement and MPM noise, and can be tuned by manipulating the ratio of the covariance noises, R_w/R_v, as was done with the MKFP. Decreasing the ratio, decreases the bandwidth of the filter and thus provides heavy low-pass filtering. Similarly, the single series forecaster provides future estimates of the filtered residual. It should be noted that when no MPM exists, the servo and regulatory responses may be tuned independent of each other. However, when MPM does exist, R_w/R_v must be carefully selected such that the effects of MPM are minimized.

2.5 THE MULTI-STEP CONTROL LAW

In Section 2.4, the multi-step prediction equation was developed so that for a horizon or trajectory of future outputs could be generated. With such an optimal prediction of the future outputs available, it is now possible to develop a complimentary optimal control law. In the literature, this has been done by several authors (Cutler and Ramaker, 1980), (Clarke, Mohtadi and Tuffs, 1986), (Sripada, 1988). Although in each case, the prediction of the future outputs is obtained differently, the same control law may be used. The control law as implemented in the multi-step adaptive predictive controller minimizes the following quadratic cost function :

$$J = \sum_{j=N_1}^{N_2} \{ y_{sp}(k+j) - \hat{y}(k+j|k) \}^2 + \sum_{j=1}^{N_u} \lambda \cdot \Delta u^2(k+j-1) \tag{2.5.1}$$

The quadratic cost function, equation (2.5.1) may also be rewritten in the following convenient vector form as was the prediction equation in Section 2.4 :

$$J = [\mathbf{Y}_{SP}(k) - \hat{\mathbf{Y}}(k)]^T [\mathbf{Y}_{SP}(k) - \hat{\mathbf{Y}}(k)] + \lambda \Delta u^T(k) \Delta u(k) \tag{2.5.2}$$

where

$$\mathbf{Y}_{SP}(k) = \left[y_{sp}(k+N_1) \quad y_{sp}(k+N_1+1) \quad \ldots \quad y_{sp}(k+N_2) \right]^T$$

$$\hat{\mathbf{Y}}(k) = \left[\hat{y}(k+N_1|k) \quad \hat{y}(k+N_1+1|k) \quad \ldots \quad \hat{y}(k+N_2|k) \right]^T$$

$$\Delta u(k) = \left[\Delta u(k) \quad \Delta u(k+1) \quad \ldots \quad \Delta u(k+N_u-1) \right]^T$$

Also from Section 2.4, $\hat{\mathbf{Y}}(k) = \mathbf{Y}^*(k) + \mathbf{A}\cdot\Delta u(k)$. Substituting this expression into equation (2.5.2) leads to :

$$J = [\ \mathbf{Y}_{SP}(k) - \mathbf{Y}^*(k) - \mathbf{A}\Delta U(k)\ ]^T [\ \mathbf{Y}_{SP}(k) - \mathbf{Y}^*(k) - \mathbf{A}\Delta U(k)\ ] + \lambda \Delta u^T(k)\Delta u(k) \tag{2.5.3}$$

Expanding equation (2.5.3) and taking $\frac{\partial J}{\partial \Delta u(k)} = 0$, we obtain the expression for the incremental control vector :

$$\Delta u(k) = (\ \mathbf{A}^T\mathbf{A} + \lambda I\ )^{-1}\cdot\mathbf{A}^T\cdot\{\ \mathbf{Y}_{SP}(k) - \mathbf{Y}^*(k)\ \} \tag{2.5.4}$$

When the incremental control vector is obtained, the control action is applied in a receding horizon fashion, and thus only the first element, Δu(k), in the control vector is implemented at time k.

In order to solve for the control vector, the $\mathbf{A}^T\mathbf{A}+\lambda I$ matrix must be inverted. This matrix is a positive definite, symmetric matrix of dimension $N_u \times N_u$. Clearly, when $N_u = 1$, the matrix inversion is trivial. Also, when the multi-step predictive control is non-adaptive, the inversion can be performed off-line as is done with Dynamic Matrix Control (DMC). When $N_u > 1$, the inversion must be performed on-line using some robust numerical tool. For an excellent summary of these techniques refer to Mohtadi, (1986).

2.5.1 LU Decomposition

In this implementation of MAPC, the technique used to solve for the incremental control vector was LU decomposition (Burden et al, 1981) together with forward and backward substitution. The $\mathbf{A}^T\mathbf{A}+\lambda\mathbf{I}$ matrix is decomposed into the following upper and lower triangular matrices :

$$(\mathbf{A}^T\mathbf{A} + \lambda\mathbf{I})\Delta\mathbf{u} = \mathbf{A}^T\mathbf{e} \qquad \text{where } \mathbf{e} = Y_{SP}(k) - Y^*(k)$$

$$\mathbf{LU}\cdot\Delta\mathbf{u} = \mathbf{A}^T\mathbf{e} \qquad (2.5.5)$$

$$\mathbf{L} = \begin{bmatrix} l_{1,1} & 0 & \cdots & 0 \\ l_{2,1} & l_{2,2} & & \vdots \\ \vdots & & \ddots & 0 \\ l_{N_u,1} & & \cdots & l_{N_u,N_u} \end{bmatrix} \qquad \mathbf{U} = \begin{bmatrix} 1 & u_{1,2} & \cdots & u_{1,N_u} \\ 0 & 1 & & \vdots \\ \vdots & & \ddots & u_{N_u-1,N_u} \\ 0 & \cdots & & 1 \end{bmatrix}$$

In the actual computer implementation the LU matrices may occupy the same $N_u \times N_u$ storage matrix, since the 0's are irrelevant and the 1's along the main **U** diagonal may be implied in the algorithm. This allows memory storage savings of N_u^2. The basic algorithm then solves for the $\Delta\mathbf{u}$ vector by successive backward and forward substitution.

2.5.2 Selection of Tuning Values for MAPC

From the development of MAPC, it is obvious that there are several parameters which may be specified by the user. The proper selection of these parameters will determine the closed loop servo and regulatory responses. The following section provides some insight into the use of these tuning parameters.

Minimum and Maximum Prediction Horizons

The minimum and maximum prediction horizons, N_1 and N_2, may be chosen in a variety of ways. N_1 is typically chosen to be one unit greater than the integral discrete time delay of the plant. Remembering that the **A** matrix consists of elements which are step response coefficients of the plant, if N_1 is chosen to be 1, then the matrix will contain 0's in the first d rows. Choosing $N_1 \geq d+1$ eliminates these redundant zeros in the **A** matrix, thus reducing the number of matrix computations.

The maximum prediction horizon, N_2 may also be chosen in several ways. The selection of N_2 has been shown to reduce the GPC algorithm to a number of known controller types. With GPC, the selection of $N_2=10$ is a default mode, and has been shown to be a good choice leading to an adaptive controller which is fairly robust in light of changing plant dynamics and dead time (Clarke, Mohtadi and Tuffs,1986), (McIntosh,1988). To provide some further insight into its selection, N_2 is typically chosen as $\tau_d+\tau_r/T_s$ or $\tau_d+\tau_s/T_s$ where τ_d, τ_r, τ_s are continuous time parameters which characterize the plant dead time, rise-time and settling time. Rise-time is used when the open loop plant response is damped, and similarly the settling time is used for under-damped plants. For plants which have non-minimum phase dynamics, N_2 should be chosen large enough to provide the controller with the correct information with respect to the correct sign of the steady state gain.

The Control Horizon

In developing the multi-step prediction algorithm, N_u was introduced to specify the number of finite future control increments. Beyond this horizon, the control increments were assumed to be zero, or equivalently the control weighting on the input was infinite. N_u is typically chosen to be 1, but may be chosen > 1 if it is desired to have stronger control action. N_u may be thought of as the number of control increments desired to achieve the final target or setpoint. Increasing N_u allows the controller to take larger initial actions, because the later control moves made possible by the increased N_u value can correct for over reactions. With $N_u=1$ and $N_2\cong10$ the controller has only 1 degree of freedom to achieve the desired steady state, and thus, this control increment will be small leading to a fairly slow and sluggish control.

Control Weighting

Once the prediction and control horizons are selected, further tuning may be accomplished by adjusting λ, the control weighting. McIntosh, (1988) showed that as $\lambda\to\infty$, the closed loop poles approach the open loop poles and an additional pole at z=1. Since $0 \le \lambda \le \infty$, it is not immediately apparent how λ can be chosen. However, it may be observed that ($\mathbf{A}^T\mathbf{A} + \lambda I$) constitutes the matrix which must be inverted to solve for the incremental control vector. Choosing $\lambda I \cong \lambda_{rel}[B(1)]^2$ has been shown by McIntosh,(1988) to maintain a constant output performance, in the presence of changing plant dynamics. B(1) is the steady state gain of the $B(z^{-1})$ polynomial and λ_{rel} is a constant which is chosen by the user. A good initial choice for λ_{rel} was shown by McIntosh,(1988) to be :

$$\lambda_{rel} = \frac{m \mid Tr(\mathbf{A}^T\mathbf{A}) \mid}{N_u} \tag{2.5.6}$$

If m=0 there would be no control weighting and so a deadbeat control response would result. Increasing the value of "m" progressively decreases, or dampens the size of the incremental control actions.

Ratio of Process/Measurement Covariances

The final "tuning knob" for MAPC is the ratio of the process and measurement noise covariances, R_w/R_v. This tuning knob naturally arises from the use of the Kalman filter, and was shown to affect the bandwidth of the disturbance filter in the MKFP. Increasing this ratio, increases the bandwidth of the filter, thus allowing higher frequency components to be compensated for by the controller. Walgama,(1986) also showed that the MKFP can be interpreted as a series of proportional-derivative controllers, and hence R_w/R_v may be thought of as a tuning knob which adjusts the amount of predictive action taken on the residual.

MAPC falls into the same category as GPC in terms of being a controller with "two degrees of freedom". That is, for the limiting case when no model-plant mismatch is present, the servo and regulatory responses may be tuned separately. R_w/R_v allows the regulatory response to be tuned independently from the servo response. When MPM is present, the ratio R_w/R_v is tuned to provide the best compromise between noise filtering and disturbance dynamics. When measurement noise is high it is desirable to select a conservative or low value for R_w/R_v. Not doing so may cause oscillatory, unstable control. When low frequency disturbance dynamics dominate the process output, it is then desirable to select a higher value for R_w/R_v. The predictive nature of the MKFP will enable strong compensation of unmeasurable disturbance dynamics.

3.0 ADAPTIVE CONTROLLER IMPLEMENTATION

Since the introduction of the self tuning regulator (Astrom, 1970) people have been attempting to "black box" adaptive or self-tuning control so that it would be available to the average technician for day to day use. Current examples of such products with this objective are the Turnbull Control System TCS-6355 and the Foxboro EXACT, both of which have been received extensive use in industry. However, in recent years it has become increasingly apparent that adaptive control is not something that should be "black boxed", but rather understood. It is only through better comprehension of its capabilities and limitations that a successful application can be implemented in an industrial environment. Goodwin and Salgada, (1988) speak of intelligent control, where the concepts and methods of adaptation and robustness are fused to form a controller which is capable of performing in a non-ideal environment.

The following sections describe some of the key elements in implementing and maintaining an adaptive controller. The first section deals with the open and/or closed loop testing of the plant and provides information regarding the approach and execution of these tests. Section 3.2 discusses the valuable information that can be gained from off-line analysis and model identification using the plant test data. Initial parameter selection, model order, parameter bounds, and residual dynamics all play an important role in providing the control engineer with the information necessary to design and maintain the on-line recursive estimator. Section 3.3 summarizes the need for both analog and digital data filtering, and provides some rules of thumb to select filter constants. Finally, Section 3.4 reviews the manner in which the adaptive control software for this industrial application was written. It also discusses the common items found in most advanced process control machines, such as anti-windup status, manual, automatic and computer modes, output and setpoint clamping, etc.

3.1 CONSIDERATIONS IN PARAMETER ESTIMATION

There is little doubt that the single most critical component of adaptive control is the parameter estimator. Incorrect or poor model parameters will lead to a controller which is extremely sluggish, oscillatory, or simply unstable. This will, in turn, lead operating staff to turn the controller off and run the process manually, or worse yet, place the previous, ill-tuned PID controller on.

To prevent such embarrassment, there are certain steps that can be taken to ensure that the parameter estimation is both valid and a good reflection of the current plant dynamics. Naturally, the first step is to conceptually understand the process by observing the day to day operation. Once a working knowledge of the process is obtained, some additional a priori information must be gathered to aid the control engineer in making suitable choices for items such as the magnitude of test signals, model order, etc. The second step is to then apply the test signal to the process and perturb it sufficiently to obtain the necessary dynamic information about the process. The following sections elaborate on the above.

3.1.1 A priori Information

The first step in any parameter estimation procedure is to gain as much a priori information as possible about the physical processes that comprise the complete plant. Once a good understanding is established, the process loop which is being considered for adaptive control should be analyzed both at the input and the output for the statistical mean and variance. The sample mean and variance can be easily computed as follows:

Sample Mean

$$\hat{m}_x = \frac{1}{N} \sum_{i=0}^{N-1} x_i \qquad (3.1.1)$$

Sample Variance

$$\hat{\sigma}^2_x = \frac{1}{N-1} \sum_{i=0}^{N-1} (x_i - \hat{m}_x)^2 \qquad (3.1.2)$$

where $x_i = u_i$ or y_i and N = sample length

For most typical chemical processes, the sample length N may be chosen from 1-5 days. With today's process control computers, this data is readily accessible through the historical data base. If the process is currently operated without automatic feedback control , good information regarding the output mean and variance can be obtained. If the input is not manipulated, then knowledge may only be gained about the noise dynamics that influence the output. Thus collecting data during this period would allow an estimate of the process noise variance, $\hat{\sigma}_y^2$, to be determined. On the other hand, if the input is manipulated then some information regarding the overall process dynamics may be determined.

For closed loop systems, the mean and variance will provide information with respect to the operating point, as well as the relative magnitudes of the input and output during this period. The variance of the input σ_u^2 and the output σ_y^2 will eventually determine the magnitude of the test signal that will be applied to the setpoint or input of the process to perform the recursive estimation.

If the input/output data is now segmented into several windows of equal length and the sample mean and variance are computed for these individual windows, information regarding the stationarity of the process can be determined. If the sample mean and variance are not the same among the individual windows of data then the process is non-stationary and the data will have to be differenced during the parameter estimation. It should be noted that the ARIMA model which is the basis of the recursive least squares algorithm, assumes that the noise dynamics are step type random walk disturbances, and thus uses the Δ operator to difference the regressor vector. The use of the Δ operator on the regressor vector induces stationarity into the process model, and thus removes the mean or bias from the regressor vector (Box and Jenkins, 1976).

The next step is to perform an open loop step in order to obtain an initial estimate of the following continuous time parameters :

τ_d = process dead-time
τ_p = process time constant
K_p = process gain

It is important to perform the step test above and below the desired operating point to determine whether the system is asymmetric. For example, exothermic chemical processes may require only a small adjustment in the input to initiate the reaction, implying τ_p may be small and K_p large. However to reduce the reaction rate, a very large adjustment in the input may be required leading to a large τ_p and small K_p.

The magnitude of the step input must also be selected with caution. A value too small may be masked by the noise dynamics of the process. Similarly, a value too large may lead to identification of process dynamics which are governed by the effect of plant recycles, or up-stream processes. Typically, plant recycles or interacting processes are responsible for under-damped dynamics in processes where the input has been moved quickly over a large magnitude.

In any event the size of the input should be perturbed by an amount $p\cdot\pm\sqrt{\sigma^2_{u,y}}$ (i.e. $p>1$) where "p" is a user chosen factor based on the considerations discussed above.

3.1.2 PRBS Generation and Plant Testing

The application of pseudo random binary sequences (PRBS) to open and closed loop plants has become a popular technique for providing the process excitation required for good parameter identification (Bendat and Piersol,1971), (Davies,1970), (Nikiforuk and Gupta,1969). This section outlines two basic considerations :

1. The manner in which to generate these PRBS signals.
2. The different ways to apply these sequences for good plant identification.

Generation of PRBS Signals

An ideal PRBS signal would be a random noise sequence with a Gaussian distribution and a mean of zero. Such a white noise sequence is capable of exciting all frequency components of a plant, which is necessary if the identified parameters are to be a good, stable representation of the plant parameters.

PRBS signals are not totally random, but have some repeatability to them, and so the term "pseudo random" is used to describe them. They also tend to excite only over a finite frequency bandwidth. A technique which is used to generate them involves the use of a binary linear-shift feedback register as shown in Figure 3.1.1. By taking the contents of the last two registers, performing an exclusive-or operation and feeding the result back to the first

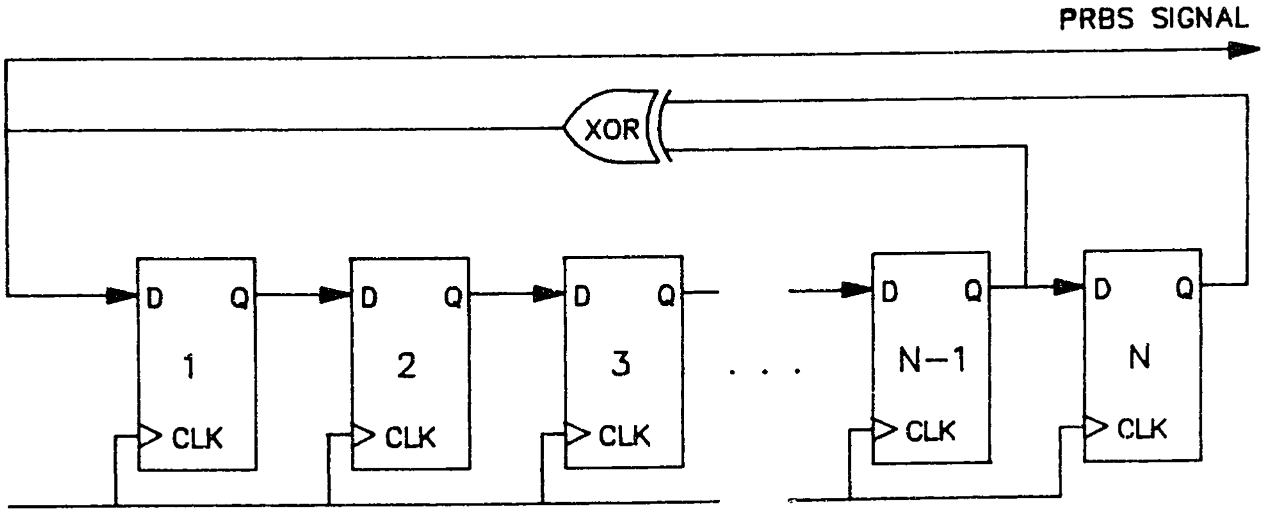
PRBS SIGNAL
XOR
D
Q
1
CLK
D
Q
2
CLK
D
Q
3
CLK
. . .
D
Q
N−1
CLK
D
Q
N
CLK

Figure 3.1.1 Binary Linear-Shift Feedback Register

element, a pseudo random binary sequence may be generated. This sequence is repeated every $2^{\eta}-1$ times, where η is the number of binary memory elements comprising the shift-register (Nikiforuk and Gupta, 1969), (Davies, 1970), (Brown, 1983). For example, if a register size of 9 elements is selected, then a sequence which is repeatable every 511 times is generated.

Another distinguishing feature of the PRBS signals is the switching interval, T_{sw}, which defines the period of time between each decision to change the PRBS signal level and is typically chosen to be $\frac{1}{2}\tau_p \leq T_{sw} \leq \tau_p$, where τ_p is the dominant time constant of the process. The decision is made by the pseudo random binary number generator. If the number is a 1, then the signal level is switched, and if the number is 0, then the current level is maintained until a period of T_{sw} has elapsed. Selecting a large switching interval, T_{sw}, will produce a PRBS sequence which provides good low frequency excitation. A switching interval, T_{sw}, which is small relative to the process time constant will provide good high frequency excitation. It is very important that the finite bandwidth of the PRBS signal be matched to the important dynamics of the process.

The final feature of PRBS signals is the selection of a mean level and magnitude of the signal. The mean level is the difference between the maximum and minimum values between which the PRBS is switched. The magnitude is often selected as a multiplicative factor of the standard deviation of the input or output noise dynamics. This was shown to be $m\cdot\pm\sqrt{\sigma_u^2}$ or $m\cdot\pm\sqrt{\sigma_y^2}$ where m is chosen as a compromise between the allowable process upset and high signal to noise (*S/N*) ratio. For purposes of definition, *S/N* ratio may be defined as follows :

$$y(k) = G_o(z^{-1})\cdot u(k-1) + H_o(z^{-1})\cdot\xi(k) \qquad (3.1.3)$$

$$S/N = \frac{E\{\ [\ G_o(z^{-1})\cdot u(k)\ ]^2\ \}}{E\{\ [\ H_o(z^{-1})\cdot\xi(k)\ ]^2\ \}} = \frac{\sigma_y^2}{\sigma_e^2} \qquad (3.1.4)$$

The true process is defined in equation (3.1.3) as a superposition of the plant and the noise dynamics. It has been assumed that $G_o(z^{-1})$ and $H_o(z^{-1})$ are linear transfer functions in the backward difference operator z^{-1}. Thus the signal-to-noise ratio is obviously governed by the size of the input. Increasing the magnitude of the PRBS input leads to a higher *S/N* ratio.

Figures 3.1.2 to 3.1.5 show the time and spectral density plots of two PRBS sequences which were generated by using a linear-shift feedback register of length $\eta=9$. The sequence will naturally repeat itself every $2^9-1 = 511$ iterations. PRBS signal 1 was generated with a $T_{sw}=1$ minute and represents one complete cycle of random steps as governed by the size of the linear-shift feedback register. On the other hand, PRBS signal 2 was generated with a $T_{sw}=5$ minutes and thus does not represent a complete cycle of the PRBS generator.

Figure 3.1.2 Time Plot of PRBS Sequence with Tsw=1 min.

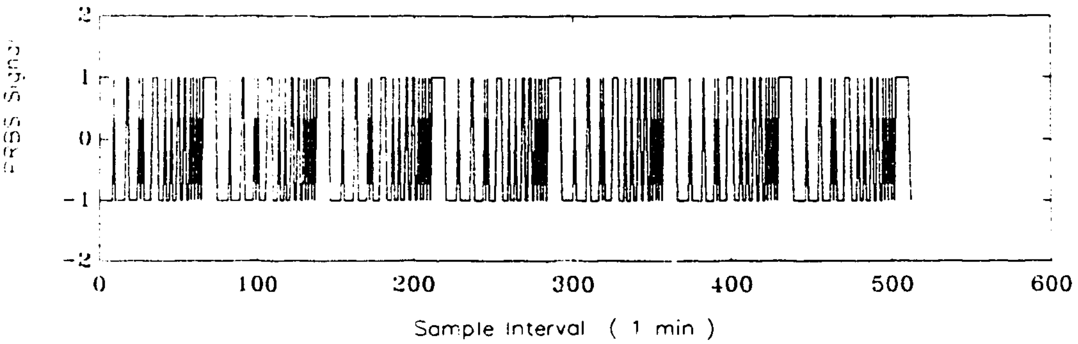

Figure 3.1.3 Time Plot of PRBS Sequence with Tsw=5 min.

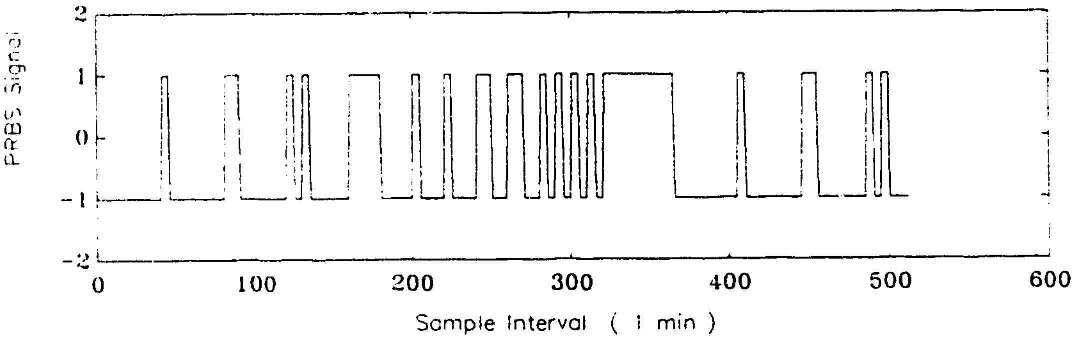

Figure 3.1.4 Spectral Density Plot of PRBS Sequence with Tsw=1 min.

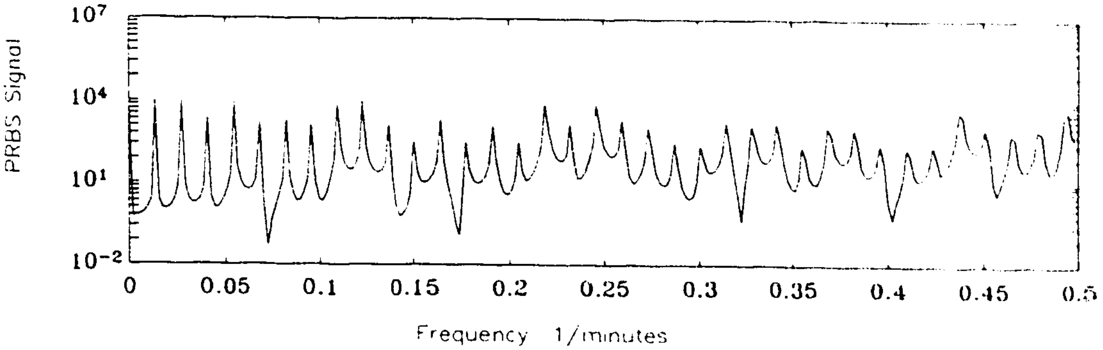

Figure 3.1.5 Spectral Density Plot of PRBS Sequence with Tsw=5 min.

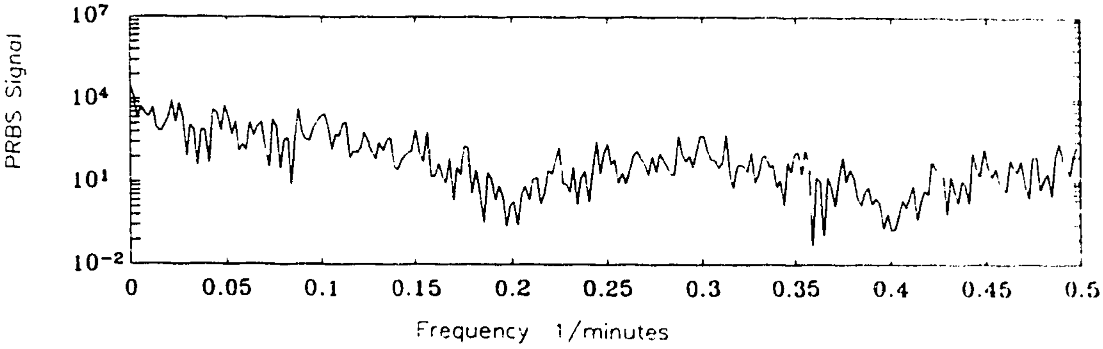

The accompanying plots show the power spectral density characteristics of the two signals. The estimate of the power spectral density was accomplished by computing the periodogram as described in Oppenheim and Schaefer, (1975). This includes taking the discrete Fourier transform of the time signal and then multiplying the resulting Fourier transform by its complex conjugate. Figure 3.1.4 illustrates the spectral density plot of PRBS signal 1. The spectral density is evenly distributed across the entire discrete frequency spectrum from 0 to 0.5 min^{-1}. The peaks in the spectrum represent the dominant harmonics of the PRBS and are evenly spaced due to the exact completion of 1 cycle of the PRBS generator.

In contrast to this, PRBS signal 2 where the T_{sw} was 5 minutes, concentrates the signal power in the lower frequencies for a sequence of the same length (note the logarithmic magnitude scale in Figure 3.1.4 and 3.1.5). This second sequence has not exactly repeated itself yet due to the switching time of 5 minutes. From the spectral density plots it can be seen that varying the switching interval will shape the frequency content of the PRBS signal. Prior to plant testing it is essential to understand the desired PRBS frequency content so as to excite the desired bandwidth of the system (Bendat and Piersol, 1971).

3.1.3 Plant Identification

Process excitation and identification may be performed in either the open or closed loop. Although open loop identification is preferred, closed loop identification has become quite popular in the petrochemical industry. Closed loop tests allow the process to remain within reasonable limits in the presence of non-stationary noise dynamics which, in the open loop would cause a process upset or incident.

Figure 3.1.6 illustrates the manner in which open and closed loop identification may be performed. In an industrial environment this will normally involve injecting a PRBS signal directly to a valve, or to a setpoint of a controller which will be the secondary controller of a cascaded adaptive control strategy. A typical example of the latter may be drawn from distillation control, where an overhead composition controller is cascaded to reset the setpoint of a secondary controller such as a reflux flow controller. In this case, the reflux flow controller setpoint would have a PRBS signal applied to provide a composition/reflux model.

Some guidelines for open/closed loop identification center around the stability and frequency bandwidth of the process. The guidelines are summarized below :

1. Ensure that the process in the open loop is stationary.

Figure 3.1.6 Open and Closed Loop Identification Configurations

Open Loop Test

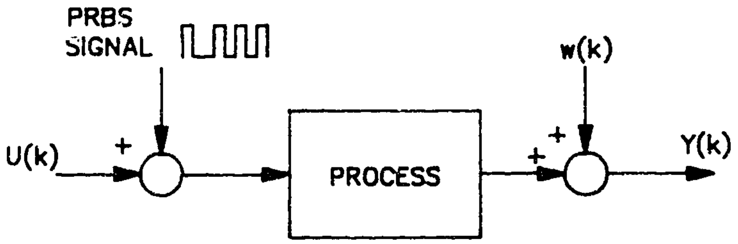
PRBS
SIGNAL
w(k)
U(k)
+
+
+
PROCESS
Y(k)

Closed Loop Test

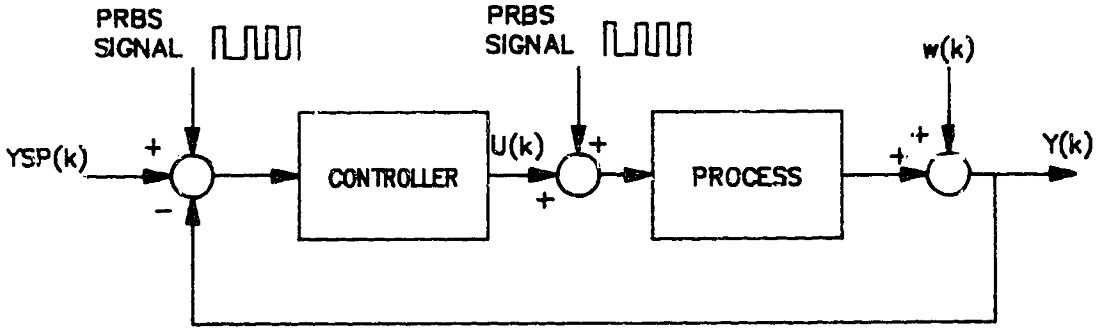
PRBS
SIGNAL
PRBS
SIGNAL
w(k)
YSP(k)
+
−
CONTROLLER
U(k)
+
+
PROCESS
+
+
Y(k)

This involves maintaining a steady and consistent plant upstream of the process. Downstream processes may have to be considered if the plant contains any recycles. Also, the process should be at the desired operating point, so that an accurate model is identified for the region of interest.

2. Next, the PRBS signal may be applied either directly to the valve, or to the setpoint of a secondary controller. In this case the secondary controller must be tuned tightly, so that the dynamics of this loop do not influence the identification of the model of interest. This is generally not a problem in the chemical industry, since the dynamics of the primary loop are generally longer than those of the secondary.

   In the closed loop, the PRBS signal may be applied to the setpoint of the primary controller. Since the dynamics of the controller affect the correlation of the input with the output noise, it is necessary that the primary controller is tuned fairly tight. A sluggish controller will not introduce the needed "kicks" to the process that are necessary for good high frequency excitation.

   The recommended procedure is to estimate in the open loop. This means opening the primary loop and exciting the setpoint of the secondary loop or the control valve directly. This prevents the plant input from being correlated with the plant output noise which is necessary for good, unbiased parameter estimation.

3. Choose the magnitude of the PRBS signal to be consistent with the computations of input/output variance that were obtained as part of the a priori knowledge and the plant operating limits. For open loop identification, it may

not be obvious from the a priori knowledge what a good magnitude for the PRBS signal should be. This is not a concern, since the PRBS signal magnitude may be adjusted on-line to yield the desired excitation. For closed loop estimation, the choice of PRBS magnitude is simple since the engineer may choose a magnitude which is directly related to the variance of the process output, and thus no knowledge regarding the input is necessary.

The switching time, T_{sw}, must be selected to best reflect the bandwidth of interest. Selecting a T_{sw} of 1/2 the dominant time constant has been suggested by (MacGregor, 1987). Other references for the use of PRBS tests may be f[illegible] Bendat and Piersol, (1971) and Jenkins and Wa[illegible] This allows the PRBS signal to focus the excitation in the lower frequencies, where process movement will occur. It has been suggested by several authors (Sripada, 1988), (McIntosh, 1988) that in the petrochemical industry, good low frequency models are necessary for long range predictions. An alternative to the selection of switching time is to filter the PRBS sequence or the input/output data as suggested by (Mohtadi, 1988). The use of $T(z^{-1})$ filters is discussed in Section 3.3.

4. The final guideline is on selecting the amount of time that is required to perform the identification. This again is very much dependent on the process time constant and time delay, τ_p and τ_d. In the petrochemical industry these parameters may range from a couple of minutes to several hours. A good identification period will collect enough data to adequately characterize the plant in the desired bandwidth.

3.2 OFF-LINE ANALYSIS AND MODEL IDENTIFICATION

Although adaptive control is concerned with the simultaneous identification of plant parameters and the use of these estimated parameters in a complimentary control cost function, there is still considerable knowledge to be gained from off-line analysis. This off-line analysis has become increasingly easier to do with the introduction of the personal computer as well as some excellent scientific software packages such as MATLAB-386 (Mathworks Inc.,1984) , IDSA (MacGregor and Taylor,1987). Additionally, the use of a Fast Fourier Transform (FFT) algorithm permits the engineer to gain valuable information about the process. Performing off-line analysis and simulation will allow the control engineer to gain an intimate understanding of the following items, which are needed for robust, adaptive control :

1) Model structure selection,
2) Estimator tuning, and
3) Model residual analysis.

3.2.1 Model structure selection

Processes may have an infinite number of frequency modes, however, most successful applications of model based control have involved model orders of 1 or 2. In selecting the model structure, the following parameters are determined by non-parametric or parametric techniques :

1. Process Gain, K_p
2. Process time constant, τ_p
3. Process time delay, τ_d
4. Order of $A(z^{-1})$ polynomial, δA
5. Order of $B(z^{-1})$ polynomial, δB

In the past, non-parametric techniques have provided a relatively good estimate of the above parameters. A simple step test may be used to identify the first 3 parameters as shown in [illegible] 3.2.1. The order of the A and B polynomials may be then selected based on the following criteria :

Process Characteristic	Polynomial Order
Overdamped Response (Minimum Phase)	$\delta A = 1$ $\delta B = 1$
Overdamped Response (Non-Minimum Phase)	$\delta A = 1$ $\delta B = 2$
Underdamped Response	$\delta A = 2$ $\delta B = 1$ or 2

The step test normally yields enough information about the process such that a good on-line recursive parameter estimation may be performed when the PRBS signal is used. However, once the PRBS test is completed and the model identified on-line, the u-y data may be collected and further analyzed to better understand the process order and dynamics. The following two tools allow for a

Figure 3.2.1 Identification of Continuous Time Parameters From Open Loop Step Test

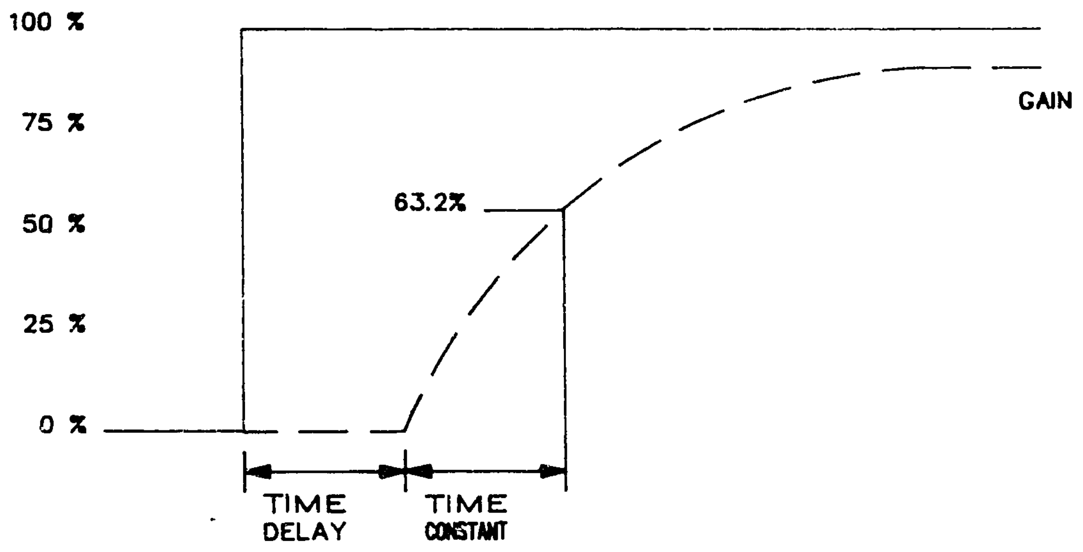
100 %
75 %
50 %
25 %
0 %
63.2%
GAIN
TIME DELAY
TIME CONSTANT

more accurate estimate of the process parameters mentioned above:

1. Cross-correlation analysis of u-y data.
2. Smoothed spectral estimates of u-y data.

The first analysis that may be performed on the input/output data collected from the PRBS test is a cross-correlation analysis, which will yield a more exact estimate of the discrete process time delay, $d=\tau_p/T_s$, (MacGregor, 1987). Naturally the resolution of the discrete process time delay will be dependent on the sampling period with which the u-y data was collected. The smaller the sampling period the better the resolution. An estimate of the cross-correlation sequence may be obtained by the following computation :

$$c_{uy}(m) = \frac{1}{N} \sum_{i=0}^{N-m-1} [u(i)-\hat{m}_u]\cdot[y(i+m)-\hat{m}_y] \qquad (3.2.1)$$

where

$$\hat{m}_u = \frac{1}{N} \sum_{i=0}^{N-1} u(i) \qquad \hat{m}_y = \frac{1}{N} \sum_{i=0}^{N-1} y(i)$$

The means, $\hat{m}_u$ and $\hat{m}_y$ are subtracted from the u-y data over the data set of N, in order to induce stationarity to the data. This is a requirement if the estimate of the cross-correlation is to be unbiased. Foley (1988) has shown that the alternative to subtracting the mean is to simply difference the data using the Δ operator. The discrete time delay may be obtained by plotting the $c_{uy}(m)$ sequence, and identifying the location of the largest single peak. This peak may be referenced to the discrete time scale to identify the discrete process time delay + 1 lag for the discretization delay.

Figure 3.2.2 illustrates an open loop PRBS test which was simulated using the following first order + time delay model :

$$Y(s) = \frac{10 \cdot e^{-25s}}{30s + 1} U(s) \tag{3.2.2}$$

The sample time used to collect the data was 5 minutes, which leads to a discrete time delay of d=5. Adding the delay associated with discretization of 1 unit, the peak may be found at the sixth lag in the plot of the cross-correlation sequence.

This analysis works best for data which has been collected from an open loop PRBS test. However, if a closed loop PRBS test is performed and the signal is injected at the setpoint, the dynamics of the controller influence the analysis, and thus the discrete delays associated with the controller must be known so that they may be subtracted to yield the estimate of the discrete process delay.

The second tool or analysis that may be used to identify the process order and characteristics is the use of smoothed power spectral estimates (Blackman and Tukey,1958), (Jenkins and Watts,1968), (Bendat and Piersol,1971), (Oppenheim and Schafer,1975), (Bendat,1980).

Figure 3.2.2 Time Delay Analysis Using Cross-Correlations

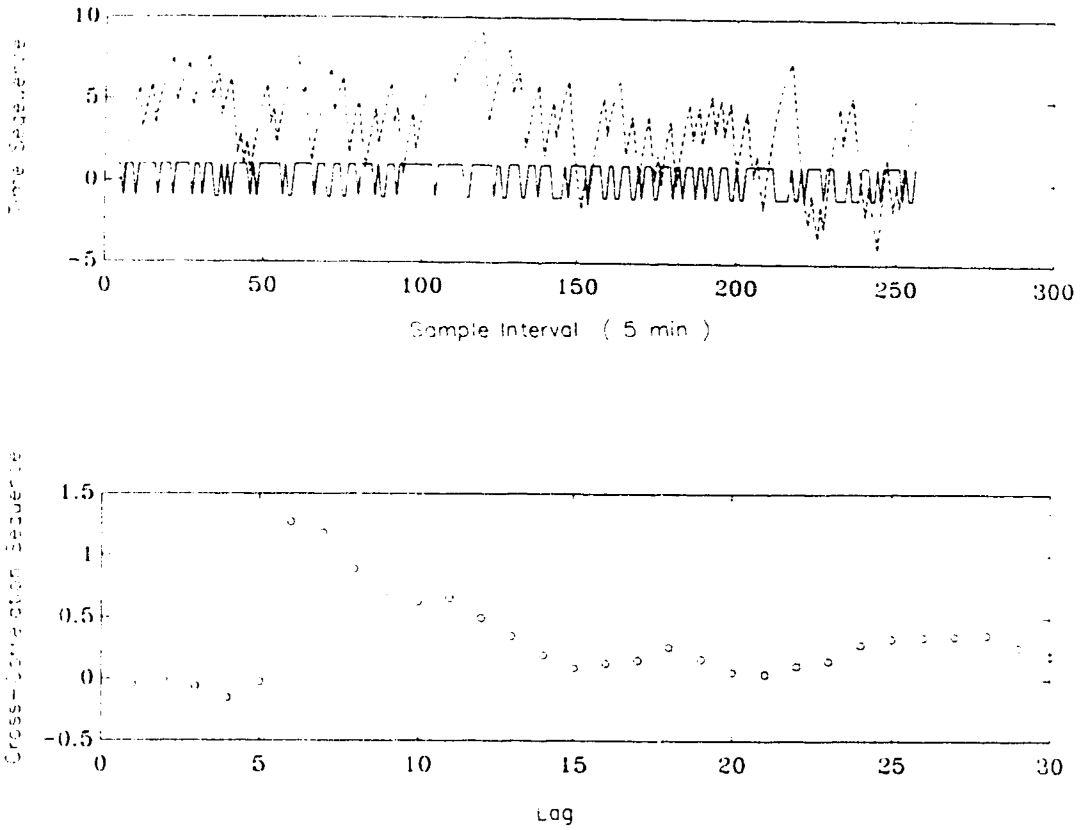

Although spectral analysis has been used extensively in the communications industry, the petrochemical industry has yet to explore its benefits. The last section used the periodogram as an estimate of the spectral density (Oppenheim and Schafer, 1975) to analyze the frequency components of the two PRBS signals. Using the periodogram to analyze a time series may yield a spectral estimate that has a high variance irrespective of the number of discrete data points that are used (Jenkins and Watts, 1968). A common technique to reduce the variance of the spectal estimate is to smooth the discrete data by windowing it. Oppenheim and Schafer, (1975) describe the use of the Welch or Bartlett method for obtaining a smoothed spectral estimate. The discrete estimate of the spectral density is given by,

$$B_{xx}^{\omega}\left(\frac{2\pi}{M}k\right) = \frac{1}{K}\sum_{i=1}^{K} J_M^{(i)}\left(\frac{2\pi}{M}k\right) \qquad k = 0,\ 1,\ \ldots,\ M-1 \tag{3.2.3}$$

where

$$J_M^{(i)}\left(\frac{2\pi}{M}k\right) = \frac{1}{MU}\left|\sum_{n=0}^{M-1} x^{(i)}(n)\cdot w(n)\cdot e^{-j2\pi kn/M}\right|^2$$

for $i = 1,\ 2,\ \ldots,\ K$

and $$U = \frac{1}{M}\sum_{n=0}^{M-1} w^2(n)$$

To obtain the smoothed spectral estimate, the data set of length N is divided into K segments of length M. Each segment is then windowed by using any of the several data windowing techniques such as the Bartlett, Hanning, Hamming techniques (Oppenheim and

Schafer, 1975), (Jenkins and Watts, 1968), (Blackman and Tukey, 1958). Windowing of the data is necessary in order to reduce the variance of the power spectral estimate. Reducing the variance of the spectral estimate will allow better analysis of the plant's frequency repsonse. An unfortunate result of smoothing is that the bias between the estimate and the true spectral density increases. Depending on the window used (i.e. Bartlett, Hanning, Hamming, Blackman, etc) the variance and bias of the spectral estimate will vary.

The variance and bias of the spectral estimate for a specific window will also vary as K, the number of segments is varied for a fixed data size, N. As the segments are increased, the bias decreases, and there is an increase in the variance of the spectral estimate. This may also be regarded as a loss of resolution of the spectral estimate when the variance increases. Naturally, the opposite is true as the number of segments are decreased. Ultimately a decision must be made about how much smoothing is desired to obtain a spectral estimate that achieves a compromise between the variance and bias.

Once the K segments have been windowed the Fourier transform of each segment may be taken to form the corresponding periodogram. Then the K periodograms may be summed up and divided by KMU to form the smoothed spectral estimate of the individual signal.

To obtain the cross-spectral estimate, $B^{\omega}_{uy}(\frac{2\pi}{M}k)$, the Fourier transforms of each individual windowed signal segment are multiplied and accumulated as shown below :

$$B^{\omega}_{uy}(\frac{2\pi}{M}k) = \frac{1}{KMU}\sum_{i=1}^{K} X^{(i)}_{y}(\frac{2\pi}{M}k)\cdot X^{*(i)}_{u}(\frac{2\pi}{M}k) \qquad (3.2.4)$$

$$k = 0,\ 1,\ \ldots\ ,\ M-1$$

where $X_y(\omega)$ = Fourier Transform of y(n)w(n)

and $X^{*}_{u}(\omega)$ = Complex Conjugate Fourier Transform of u(n)w(n)

In process control, transfer functions may be represented in the frequency domain by the use of Bode diagrams. With the power spectral estimates, it is now possible to obtain an estimate of the magnitude and phase diagrams for the system being tested. The Bode magnitude plot may be formed by normalizing the cross-spectral density with the spectral estimate of the input, and the phase estimate may be obtained from the angle formed between the real and imaginary components of the cross-spectral estimate.

This may be performed as shown below :

Estimate of Process Magnitude Repsonse :

$$\hat{T}_{xy}(\frac{2\pi}{M}k) = B^{\omega}_{xy}(\frac{2\pi}{M}k)\ /\ B^{\omega}_{xx}(\frac{2\pi}{M}k) \qquad k = 0,\ 1,\ \ldots\ ,\ M-1 \qquad (3.2.5)$$

Estimate of Process Phase Response :

$$\hat{\theta}_{xy}(\frac{2\pi}{M}k) = \tan^{-1}\left(\frac{\mathrm{Im}\left[B^{\omega}_{xy}(\frac{2\pi}{M}k)\right]}{\mathrm{Re}\left[B^{\omega}_{xy}(\frac{2\pi}{M}k)\right]}\right) \qquad (3.2.6)$$

It becomes quite evident by examining the power spectrum of the process signals, the importance of exciting the proper frequency modes, so that a good estimate is obtained. Once the estimates of the magnitude and phase response are obtained, certain important features about the process can be determined, that otherwise could not be obtained if the signals were examined in the time domain.

First of all, the magnitude response will reveal the steady state gain of the process, K_p and the dominant time constant, τ_p. K_p may be found by looking at the magnitude response of the lowest frequency mode that was excited. Similarly, τ_p is found by locating the corner frequency. The corner frequency is defined as the point where the steady state gain decreases by 3dB. This represents the half power point of the process. Also the order of the process dynamics may be obtained by examining the rate at which the slope of the magnitude response decreases after the corner frequency. Typically, processes with n^{th} order dynamics will decrease at a rate of $-n \cdot 20$dB/decade. The decrease is due to the number of poles in the left half plane. Similarly, a zero in the left half plane will cause an increase in slope by an amount of 20dB/decade. If the poles and zeros are located in the right half, or unstable plane, then they have the opposite affect on the magnitude response plot.

To confirm the order of the numerator and denominator of a continuous time process, the phase response plot is used. As was true of the magnitude response, stable poles and zeros cause the slope of the phase response to decrease and increase by an amount of 90°/decade. Unstable poles and zeros cause the opposite effect. For further details see Dorf,(1980).

3.2.2 Estimator Tuning

One of the prime advantages of off-line estimation is that the plant u-y data which is obtained from a PRBS test may be used repeatedly with different estimator simulations. By performing off-line simulations with plant test data the control engineer can experiment with the estimator "tuning knobs" to achieve a desired response in the model parameters.

Section 2.2 describes the recursive least squares estimation algorithm as was used in the industrial implementation of MAPC. The main "tuning knobs" of the estimator are the tr{ P(·) } and the deadzone Δ_d on the model prediction error. An additional tuning knob for the industrial implementation of the estimator was the $\Delta \cdot T^{-1}(z^{-1})$ filtering of the regressor vector. The choice of filtering co-efficients will be further discussed in Section 3.3.

The tr{ P(·) } directly affects the magnitude of the estimator gain vector L(k). Increasing the tr{ P(·) } causes the gain vector to increase and thus stronger and faster action is taken to decrease the size of the model residuals. Similarly, the opposite is true when the tr{ P(·) } is decreased. Although the tr{ P(·) } may be adjusted by viewing the trajectories of the parameters, a better indicator of the tuning is the response of the variable forgetting factor, $\lambda(k)$. Since $\lambda(k)$ is a function of both the covariance matrix P(·) and the regressor vector $\phi(k)$, its trajectory may be examined during off-line simulations to determine a good value for tr{ P(·) } that will not exceed a lower limit on the forgetting factor λ(k). For instance, if plant parameter variations are slow, then λ should be near unity for information to be discounted slowly. This is typically the case with most chemical processes. If plant parameter variations are fast then λ must be smaller so that information is discounted much faster. Clarke and Gawthrop, (1975) speak about the "asymptotic sample length" α of the estimator which is given by

$$\alpha = \sum_{i=0}^{\infty} \lambda^{i} = \frac{1}{1 - \lambda} \qquad (3.2.8)$$

To understand what α represents, the cost function for the least squares estimator may be examined

$$J_{est} = \sum_{i=0}^{\infty} \lambda^{i} \cdot e^{2}(k-i) = \sum_{i=0}^{\infty} \beta^{2 \cdot i} \cdot e^{2}(k-i) \qquad (3.2.9)$$

where $\beta^2 = \lambda$

Now using Parseval's theorem to describe the estimator cost function as a representation of the power spectral density, (Mohtadi, 1988)

$$J_{est} = \frac{1}{2\pi} \int_{0}^{2\pi} X_{w}(\omega) \circledast X_{e}(\omega) \cdot d\omega \qquad (3.2.10)$$

where $X_w(\omega)$ is the power spectrum of the exponential window and similarly, $X_e(\omega)$ is the power spectrum of the model prediction error, and $\otimes$ is the convolution operator. The window size is then determined by α, the asymptotic sample length. If the results of finite sample lengths are extended to infinite sample lengths, then as the window size decreases, $\lambda \to 0$ and similarly as $\lambda \to 1$ the window size increases to encompass all the data. In both cases, the shape of the exponential window also changes, since a variable forgetting factor factor is used. This window shape and size is governed by the amount of excitation that is present in the system. Sripada,(1988) showed that a measure of excitation may be computed as

$$\nu = \| P(k-1)\cdot\phi(k) \|_{\infty} \qquad (3.2.11)$$

The second tuning knob that is required in an industrial environment is the specification of an estimator on-off criterion such as a deadzone, Δ_d, on the prediction error. If the prediction error is given by,

$$\hat{\xi}(k) = \Delta y_f(k) - \phi^T(k)\cdot\hat{\theta}(k-1) \qquad (3.2.12)$$

where $|\hat{\xi}(k)|<\Delta_d$, then the estimator is turned off. This is done so that during steady state operation of the process, any natural or common variation does not cause parameter bias. Since the estimated process is forced to be stationary by band-pass filtering of the regressor vector, the model prediction error will also be void of any random step type disturbances in the process output. Thus, the expected mean and variation of the model prediction error should be a white noise process with a mean of zero, and a variance of σ_{ξ}^{2} once the parameters have converged. This variance can be easily computed and thus allows an initial estimate of the deadzone to be

$$\Delta_{d} = 3\cdot\pm\sqrt{\sigma_{\xi}^{2}} \tag{3.2.13}$$

The deadzone has been chosen to be three standard deviations of the model prediction error. If the model prediction error increases beyond the deadzone, then the estimated model is no longer valid and the estimator will be turned on to estimate an improved model. This very much depends on the current plant conditions. If the estimator has turned itself on during a process upset or large disturbance, then the previously estimated model may be corrupted and the resultant control may be either extremely sluggish or unstable.

3.2.3 Analysis of Model Prediction Error

Once the parameters have converged, the model prediction errors or residuals should ideally be a noise sequence with a Gaussian distribution and a mean of zero. This implies that there exists no correlation among the sequence and the noise spectrum is flat over the entire discrete frequency range. Although this is desirable, in practice it is rarely attained and thus analysis of the model prediction errors will further reveal any unmodelled dynamics that are present. Box and Jenkins, (1976) as well as MacGregor, (1987) give a detailed method for analyzing the residuals using auto-correlation and partial-correlation analysis.

Using both these analysis techniques allows the structure of the residuals to be identified. More specifically, the residuals may be characterized as having Auto-Regressive (AR), Moving-Average (MA) or ARMA dynamics. Once the residuals are characterized, a suitable discrete transfer function model of the residuals may be estimated by some off-line batch least squares or maximum likelihood technique. Provided that the residual dynamics do not change, it is then possible to use this residual transfer function model to filter the regressor vector.

If the correlation analysis is extended to the frequency domain, an estimate of the power spectrum may be obtained to reveal dominant frequency components in the model residual sequence.

3.3 ANALOG AND DIGITAL DATA FILTERING

The need for analog and digital pre-filtering of the u-y data prior to estimation has become increasingly more important for robust implementations of adaptive control. Tuffs and Clarke,(1985), Mohtadi,(1988), McIntosh,(1988) all speak about using a band pass pre-filter prior to estimation to remove any high and low frequency disturbance components in the u-y data. The following sections describe the use of analog and digital filters for estimation and control. Analog filters are typically used prior to signal sampling to remove frequency components which are higher than the sample frequency. Digital filters are later used to condition the data for the recursive least squares estimation algorithm.

3.3.1 Analog Anti-Aliasing Filters

In chemical process control, most signals that are monitored are continuous in nature. Temperatures, pressures, levels are typically monitored by measuring devices which provide a continuous signal. This continuous signal will have dynamics that are associated with the process itself as well as the measuring instrument. The measuring instrument dynamics are normally fast relative to the process dynamics. These signals are transmitted to the digital control system, where they are sampled at a fixed frequency f_s.

A continuous time signal of finite energy and infinite duration may be represented as x(t). If x(t) is now sampled with a period of T_s, then the corresponding discrete time signal may be represented as $x(nT_s)$ or simply x(n). To determine the effect of over-sampling or under-sampling x(t), the continuous and discrete time Fourier and inverse Fourier transforms may be examined. This type of analysis is described in almost every book on the topic of signal processing and may be found in Haykin,(1978) and Oppenheim and Schafer,(1975).

If $X(e^{j\omega})$ is the discrete Fourier transform of x(n), and $X_c(e^{j\Omega})$ is the continuous Fourier transform of x(t), where $\Omega=\omega/T_s$, then the two Fourier transforms are related as follows

$$X(e^{j\omega}) = \frac{1}{T_s}\sum_{r=-\infty}^{\infty} X_c\left(\frac{j\omega}{T_s} + j\frac{2\pi r}{T_s}\right) \qquad (3.3.1)$$

or

$$X(e^{j\Omega T_s}) = \frac{1}{T_s}\sum_{r=-\infty}^{\infty} X_c\left(j\Omega + j\frac{2\pi r}{T_s}\right) \qquad (3.3.2)$$

If the signal x(t) is band-limited, and has a corner frequency of $\Omega_o/2$, then for purposes of demonstration let the Fourier transform of the continuous time signal look as shown below :

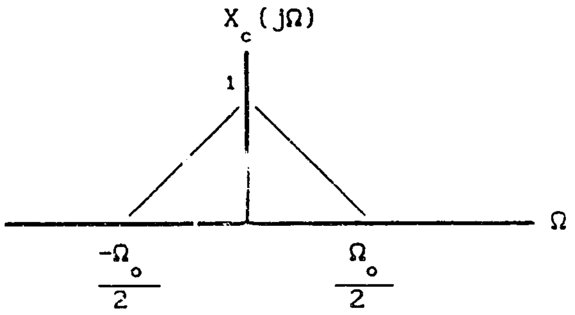
$X_c(j\Omega)$
1
Ω
$\frac{-\Omega_o}{2}$
$\frac{\Omega_o}{2}$

If the signal x(t) is sampled at a rate faster than the Nyquist rate, that is

$$\frac{\pi}{T_s} \geq \frac{\Omega_o}{2} \tag{3.3.3}$$

then the corresponding discrete Fourier transform of x(t) will look as follows ;

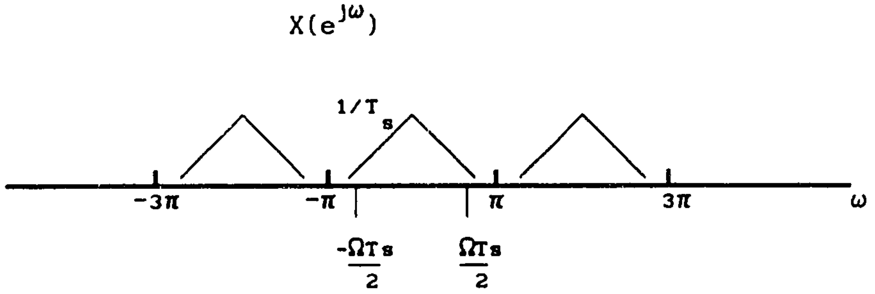
$X(e^{j\omega})$
$1/T_s$
-3π
$-\pi$
π
3π
ω
$\frac{-\Omega T_s}{2}$
$\frac{\Omega T_s}{2}$

As can be seen from the diagram, when the sampling frequency is greater than the corner frequency, the periodic repetitions of the continuous time transform do not overlap. In fact they are separated by $2\cdot(\pi-\Omega T_s/2)$.

When

$$\frac{\pi}{T_s} \le \frac{\Omega_o}{2} \tag{3.3.4}$$

the repetitions of the continuous time transform do overlap as shown below.

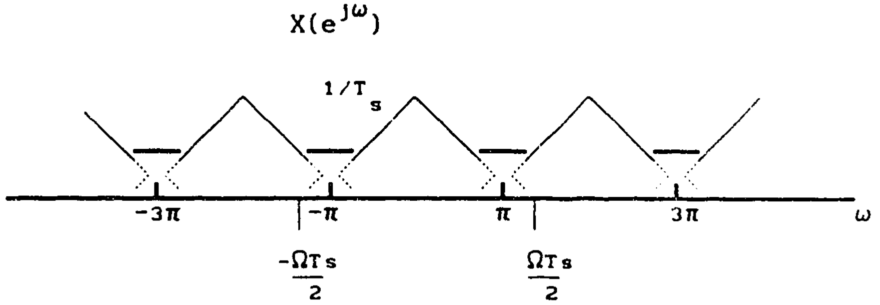

In the above diagram the high frequencies are being over-lapped into the lower frequencies. This is commonly referred to as "aliasing", and will cause the signal to be distorted both in magnitude and in phase. In fact, the original signal cannot be restored.

A simple and common solution to this problem is to use an "anti-aliasing" filter prior to sampling the continuous time signal. The filter is a low pass type, with the corner frequency being the highest desirable frequency in the discrete time signal. Similarly, the sample frequency will be chosen to be twice the corner frequency of the "anti-aliasing" filter. This will prevent frequencies which are higher than the sample frequency from over-lapping into the lower frequencies and causing the undesirable distortion in frequency magnitude and phase.

An analog "anti-aliasing" low pass filter may be easily constructed with a simple RC network and an amplifier as shown in Figure 3.3.1. The resultant transfer function for a ρ-order cascade arrangement of individual filters is

$$\frac{V_o(s)}{V_i(s)} = \left(\frac{-R_1}{R_2}\right)^{\rho}\left(\frac{1}{sCR_1 + 1}\right)^{\rho} \tag{3.3.5}$$

For control purposes a first or second order filter is sufficient. A second order, low pass filter with the RC network demonstrated will provide a final output signal which is similar in phase to the input signal. If a first order filter is used, then the signal will be -180° out of phase due to the sign change.

Wittenmark,(1988) discusses the possible interaction of the "anti-aliasing" filter with the estimation and control algorithms. If the sampling frequency is not 20-100 times larger than the desired closed loop system bandwidth, then interactions between the anti-aliasing filter and the process must be considered and accounted for when the order of the model polynomials is chosen. For instance, if the physical process is first order, and the anti-aliasing filter is second order, the order of the overall dynamics is third order.

In modern day distributed control systems, this problem has been

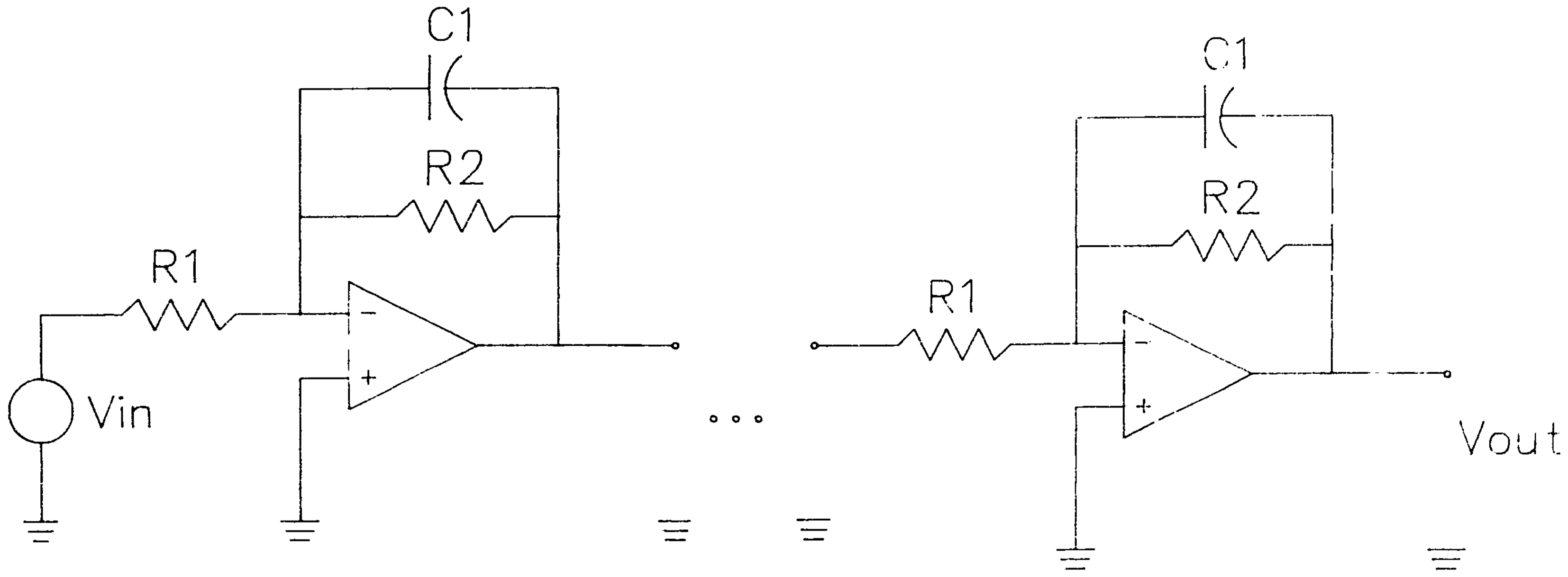
C1
R2
R1
Vin
−
+
C1
R2
R1
−
+
Vout

Figure 3.3.1 Simple Electronic Realization of Analog Anti-Aliasing Filter

solved by over-sampling the continuous time signal. For example, in the Honeywell distributed control system, the process variable is pre-filtered by a 1^{st} order filter with a -3dB corner frequency of 1Hz. It is then sampled at a frequency of 3Hz. Supervisory control is then performed by the PMX-45000 mini-computer once every 1-6 minutes depending on the process time constant. This suggests that if the process time constant is 60 minutes and the desired closed loop time constant is to be 12 minutes, then sampling the process variable at 1/3 seconds, suggests that the sampling frequency is 360 times the bandwidth of the closed loop. Thus the anti-aliasing filter will have little influence on the overall closed loop system response under these circumstances.

3.3.2 Digital Data Filtering

With the plant u-y data discretized, there exists the potential for pre-conditioning the data prior to estimation and control. It has been suggested by many authors that filtering the data is necessary in order to achieve robust adaptive control. Tuffs,(1984), Clarke and Mohtadi,(1986) and McIntosh,(1988) have shown that the use of the $\Delta/T(z^{-1})$ filter effectively reduces the effect of low frequency process load disturbances and high frequency measurement and unmodeled dynamics noise on the u-y data. From Section 2.2 the $\Delta/T(z^{-1})$ filter was integrated with the ARIMA model as follows,

$$A(z^{-1})\cdot\frac{\Delta y(k)}{T(z^{-1})} = B(z^{-1})\cdot\frac{\Delta u(k-d-1)}{T(z^{-1})} + \frac{C(z^{-1})}{T(z^{-1})}\,\xi(k) \qquad (3.3.6)$$

Thus if $T(z^{-1}) \cong C(z^{-1})$ then the process output and input were effectively free of any high and low frequency disturbances. It must be noted that the removal of low frequency disturbances is performed by the Δ operator. The assumption that has been made about the auto-regressive portion of the noise dynamics is that the noise occurs as random step type disturbances in the output. Similarly the $1/T(z^{-1})$ polynomial filters the moving-average or high frequency noise dynamics. Mohtadi,(1988) has shown that the proper, theoretical choice for the order of the $T(z^{-1})$ filter is $\delta A+1$. McIntosh,(1988) suggests that this order need not be larger than 2 in most applications.

Although the filter order may be selected quite easily, the roots of the $1/T(z^{-1})$ are somewhat more complicated to select. It has been shown by Mohtadi,(1988) and McIntosh,(1988) that good estimation occurs when the filter has the following coefficients,

$$\frac{1}{T(z^{-1})} = \frac{0.2}{1 - 0.8z^{-1}} \qquad (3.3.7)$$

For most chemical processes which demonstrate overdamped 1st or 2nd order dynamics, this filter selection is adequate. It must be noted that if an overdamped process is sampled at $\frac{1}{5}\tau_p$, then the corresponding discrete time pole location will be approximately equal to 0.8. This suggests that if u-y filtering is performed to accentuate the frequency content around the dominant time constant of the process that a good model may be estimated in that region.

However, the use of filtering without some knowledge of the process dynamics may lead to the estimation of a model which does not accurately describe the dynamics of the actual process. If an $1/T(z^{-1})$ filter designed for overdamped systems is used for systems with underdamped behavior, then the filter will mask the true dynamics of the process. Thus if a second order process with underdamped behavior is to be filtered, the filter will have to have complex poles in order for the process dynamics to be estimated with a minimal amount of model-plant mismatch. Alternatively, the $1/T(z^{-1})$ filter will have to be designed with a discrete pole location which is approximately 1 decade greater than the corner frequency of the 2nd order process. It becomes evident that the selection of this filter may not be as straight forward as many authors have suggested. This reinforces the need for off-line analysis of any PRBS data that is available. Section 3.2 described the use of smoothed power spectral estimates which allow the control engineer to determine the order and physical characteristics of the process.

So far, much has been said about filtering the high frequency components contained in the u-y data, and it has been assumed that the low frequency disturbances can be filtered by using the Δ operator, which effectively results in differencing the u-y data. This data differencing induces stationarity to the regressor vector which is needed if the process mean and variance change with time. Once the data is differenced, it still may contain some low frequency disturbance components and, if possible, it would be advantageous to the estimation algorithm if these components could be removed without influencing the low frequency process components.

If the process is represented in the following form :

$$y(k) \;=\; G_o(z^{-1})\cdot u(k-d-1) \;+\; \frac{H_o(z^{-1})\cdot\xi(k)}{\Delta} \qquad (3.3.8)$$

where

$$G_o(z^{-1}) \;=\; \frac{G_o^N(z^{-1})}{G_o^D(z^{-1})} \quad \text{and} \quad H_o(z^{-1}) \;=\; \frac{H_o^N(z^{-1})}{H_o^D(z^{-1})}$$

then a filter would have to be designed to eliminate the effect of the noise transfer function, $H_o(z^{-1})$. This could be done if the $\Delta/T(z^{-1})$ was modified to include a numerator component $F(z^{-1})$. The resulting filter would be

$$\frac{\Delta\cdot F(z^{-1})}{T(z^{-1})} = \frac{\Delta(\ 1+t_1+\ \ldots\ +t_{n_t}\ )\ (\ 1+f\ z^{-1}+\ldots+f_{n_f} z^{-n_f})}{(\ 1+f_1+\ \ldots\ +f_{n_f}\ )\ (\ 1+t\ z^{-1}+\ldots+t_{n_t} z^{-n_t})} \tag{3.3.9}$$

It should be noted that when

$$\frac{\Delta\cdot F(z^{-1})}{T(z^{-1})} \cong \frac{H_o^N(z^{-1})}{\Delta\cdot H_o^D(z^{-1})} \tag{3.3.10}$$

then all disturbances will be removed from the process, and the model parameters will be a good representation of the true process dynamics. Sripada, (1988) has proposed an elaborate scheme for estimating the $F(z^{-1})$ and $T(z^{-1})$ polynomials using a recursive least squares technique. These polynomials would be estimated during periods of low excitation or active low frequency disturbances by holding the process model parameters constant. Foley, (1988) discussed the difficulty with this technique being two-fold. First, the variation in the model prediction error, $\hat{\xi}(k)$, cannot always be attributable to high and/or low frequency disturbances. In fact, the variation may actually be due to changing plant parameters, which would show up in the filter dynamics rather than the process model parameters, defeating the purpose of adaptive control. The second difficulty is with trying to estimate a stable, parametric noise model. In most instances, parameters associated with estimating the noise converge very slowly and there is no guarantee that the noise model will be stable. Some form of spectral factorization must be done in order to maintain the noise model poles within the unit circle. This leads to an ever increasing magnitude of complexity which is difficult to perform in real-time, not to mention maintain in the long term.

An alternative to on-line estimation of the u-y data filters is by using time series analysis (Box and Jenkins,1976). By using the data acquired during the PRBS test, a process and noise model may be obtained using an analysis program such as the IDSA package (MacGregor and Taylor,1987). By estimating a suitable process model and then examining the auto-correlation sequence of the model prediction errors, a suitable structure for the noise model may be selected. Once this is done, the process and noise models are simultaneously identified to yield the final overall model. This time series analysis produces two results. First, it provides an excellent initial and default process model parameter set, and second, it provides a stable noise model which when inverted can be used as the $\Delta \cdot F(z^{-1})/T(z^{-1})$ u-y data filter for further on-line recursive estimates of the process model parameters.

3.4 COMPUTER SYSTEM AND ADAPTIVE CONTROL SOFTWARE

With the implementation of any control algorithm in an industrial environment, it is generally good engineering practice to be familiar with the overall control system. Modern day, digital control systems in even the smallest plants may at first appear overwhelmingly complex and sophisticated. It is only through a good understanding of both the control system hardware and software that a successful control application can be commissioned and maintained for an indefinite period.

This section deals with the description of the control system hardware and software that was specific to the application of the multi-step adaptive predictive controller at the Esso Chemical Higher Olefins plant in Sarnia, Ontario. It briefly outlines the hardware associated with the Honeywell TDC-2000/PMX-45000 distributed control system and describes the manner in which the MAPC software was written and implemented. The final section deals with some of the practical issues surrounding the implementation of the software in order to maintain a consistent "look, touch and feel" for the console operators.

3.4.1 Control System Architecture

The complete control system architecture may be described as in Figure 3.4.1. The lowest layer of the system encompasses all the field instrumentation and final control elements. Instrumentation is responsible for measuring temperatures, pressures, differential pressures, levels, etc. Similarly, analyzers are used to measure boiling points and carbon number distributions. All these instruments are terminated in the TDC-2000 hardware which consists of Honeywell Basic Controller Files (CB-Files), Low Energy Process Interface Units (LEPIU), High Level Process Interface Units (HLPIU), and Data Hiway Ports (DHP-II).

The CB-Files provide two way communication to the process and provide the first layer of SISO automatic plant control. The CB-files provide for 8 process variables and 8 remote variables to be measured and digitized. In conjunction with the measurements, 8 analog outputs are provided so that the process variables may be maintained at a specific target. The remote variables allow for additional plant measurements to be made or for cascading of individual controllers.

The LEPIU's allow for low-energy signals, specifically the millivolt analog signals associated with temperature measurements to be conditioned, linearized according to thermocouple type, and then digitized. This device provides an inexpensive alternative for the acquisition and monitoring of temperature measurements.

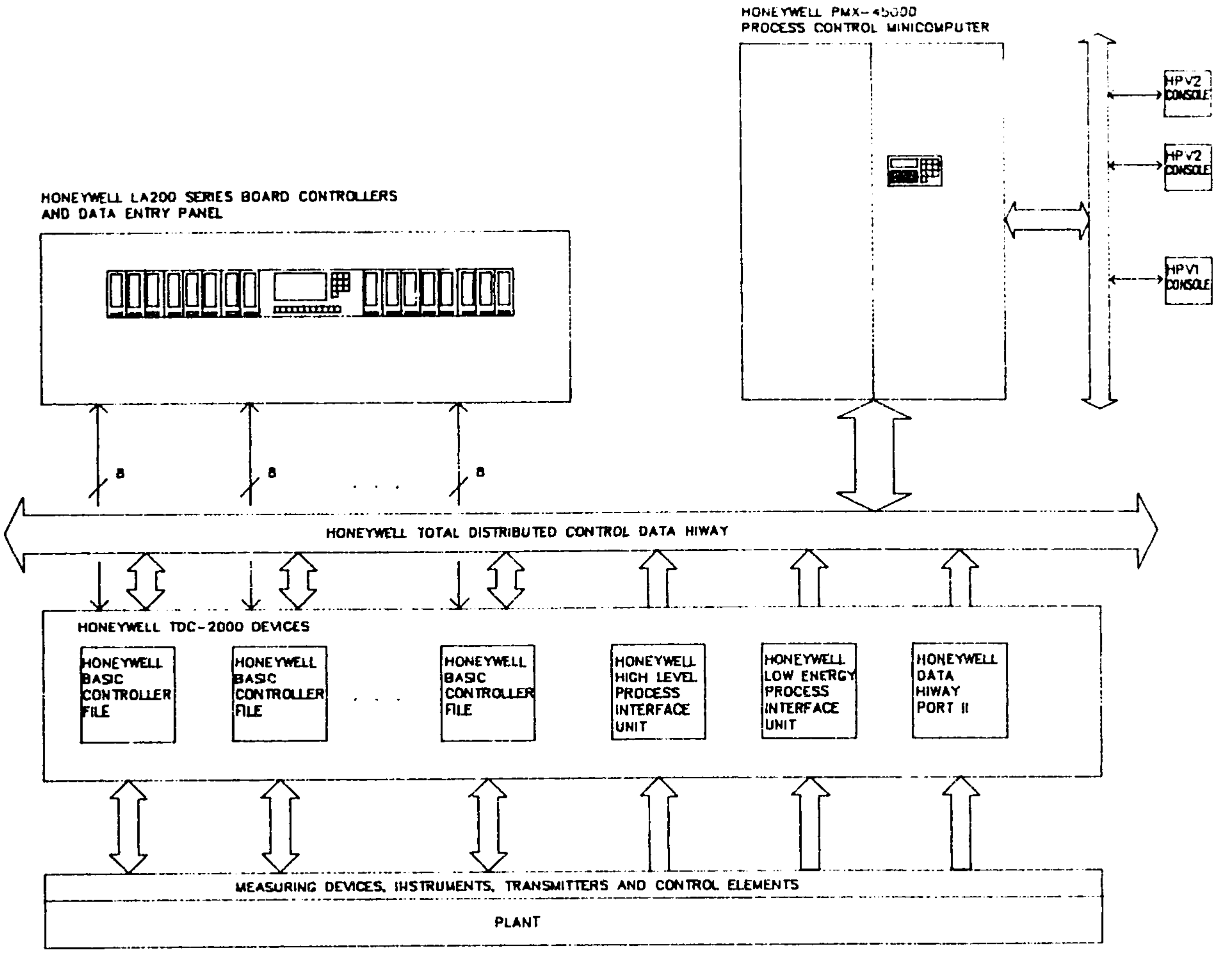
HONEYWELL PMX-45000
PROCESS CONTROL MINICOMPUTER
HPV2 CONSOLE
HPV2 CONSOLE
HPV1 CONSOLE
HONEYWELL LA200 SERIES BOARD CONTROLLERS
AND DATA ENTRY PANEL
8
8
8
HONEYWELL TOTAL DISTRIBUTED CONTROL DATA HIWAY
HONEYWELL TDC-2000 DEVICES
HONEYWELL BASIC CONTROLLER FILE
HONEYWELL BASIC CONTROLLER FILE
HONEYWELL BASIC CONTROLLER FILE
HONEYWELL HIGH LEVEL PROCESS INTERFACE UNIT
HONEYWELL LOW ENERGY PROCESS INTERFACE UNIT
HONEYWELL DATA HIWAY PORT II
MEASURING DEVICES, INSTRUMENTS, TRANSMITTERS AND CONTROL ELEMENTS
PLANT

Figure 3.4.1 Process Control System Architecture at the Higher Olefins Plant

The HLPIU provides the same service as the LEPIU, with the exception that it is used for high level current or voltage signals in the range of 4-20mA or 1-5Volts. It is a device which only allows process variables to be monitored, and thus sends no control signals to the field.

The final common TDC-2000 device is a DHP. The DHP allows for other non Honeywell computing devices to reside on the TDC-2000 Hiway. Examples are intelligent measuring devices such as component analyzers, which have RS-232, IEEE-488 bus protocol communication capabilities.

All these devices described above are linked together via a high speed dual coaxial link, which in practice allows the TDC-2000 devices to be distributed plant wide. The individual controllers within the CB-Files may be manipulated in two fashions. Either board mounted LA201 devices which are hard wired into the CB-Files are used, or TDC-2000 operator consoles are used which reside on the Hiway. Figure 3.4.1 does not show the operator consoles, since they are currently not used at the higher olefins plant.

The final and most desirable item from the point of high level control and unit optimization is the PMX-45000 (Process Management Exxon - 45000) process control minicomputer. This computer allows for all resident Hiway devices to be scanned on a user specified frequency for purposes of supervisory or advanced control and improved process monitoring. By using the HPV2 (high performance video 2) consoles, the plant schematics may be made available to the console operator. Naturally these schematics allow the console operators to monitor all process variables which have been incorporated into the distributed control system. The HPV2 console may be thought of as a window into the process which allows the console operator to monitor and control the overall health and operation of the plant. The HPV1 console allows the control engineer to develop and implement advanced control strategies to improve unit quality, production and energy utilization.

The PMX-45000 computer is a single processor, multi-user, multi-tasking, interrupt-based system which uses RTMOS (real time management operating system) to coordinate user and device activities with the appropriate priority and schedule. The concepts of "realtime" and "freetime" are used to distinguish between activities that must run on a fixed schedule and priority, and activities which may run in the background only after all realtime tasks have been completed for the defined period.

The PMX-45000 system has extended memory capability which its predecessor the PMX-4500 system does not have. This allows for additional information to reside in main or "core" memory, and reduces the amount of page swapping that was necessary with the older system. However, page swapping is still performed with realtime and freetime FORTRAN programs. The page swapping scheme used is one with a fixed page size of 8 kilowords, with a word size of 24 bits. The page allocation is static, and thus the program is always swapped into the same "core" memory location provided that it is not occupied by a program of higher priority. If a program of higher priority is occupying the memory location, it must finish executing, and be placed back on "bulk" or secondary memory if a program of lower priority is to be executed in the same "core" location. Understanding the manner in which page swapping is done is necessary if a program is larger than 8 words, thus occupying several pages or segments in main memory. If the system loading is high and the program is poorly segmented, "thrashing" may occur by which the computer spends all of its time communicating with the "bulk" controller. The term "thrashing" is used when the program segments spend their time moving from "core" to "bulk" memory and back.

The PMX-45000 system supports 3 computer languages for software development. The first is simply called PAL (Programming Assembler Language) and is used primarily for additions and modifications to the existing RTMOS and PMX operating systems. The second language is BPL (Basic Programming Language). It is used to enhance and provide special computations for the standard control and calculation algorithms that are an integral part of the PMX software. The final and third language is ANSI X3.9-1966 FORTRAN IV. The FORTRAN language is specifically used for application software that requires special features such as mathematical functions, matrix manipulations, and file handling.

FORTRAN programs may be written either as real-time or free-time programs. Once written, they are compiled and loaded onto the "bulk" or secondary memory system. If written for free-time, they are typically invoked manually. If written for real-time, they will be automatically invoked by a BPL program which has been appropriately scheduled. PMX-45000 also allows FORTRAN users to have access to the complete "point record" historical and on-line data base through the use of "multi-point" lists. Each multi-point list allows for 64 points or process parameters to be accessed by any FORTRAN program which has requested the list. A further programming requirement that the PMX system provides is "working" or "scratch pad" memory for FORTRAN programs which is needed to save intermediate results or variables between executions. This memory is easily defined and is referred to as a real-time or a free-time data table.

3.4.2 Structure of Adaptive Control Software

In implementing MAPC much consideration was given to the future use, readability and maintainability of the software. In order to accomplish these objectives the software was written in FORTRAN with modularity stemming from the generic operations that were required. Figure 3.4.2 illustrates the manner in which the MAPC software was segmented and the logic that links each segment based on the digital switches that were defined to allow the user to turn specific segments on and off.

Figure 3.4.2 Task Structure of the MAP Controller Software

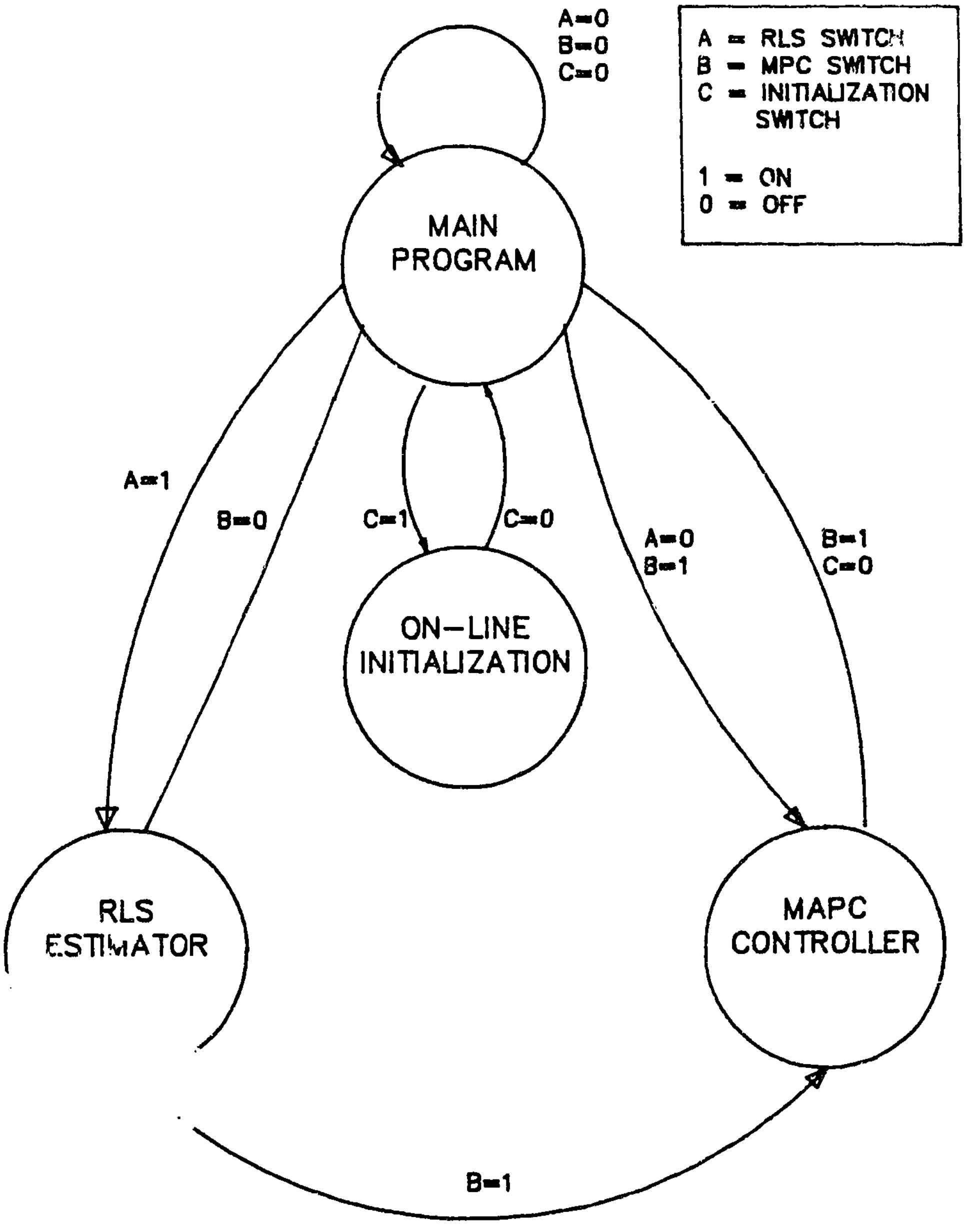
A=0
B=0
C=0
A = RLS SWITCH
B = MPC SWITCH
C = INITIALIZATION SWITCH
1 = ON
0 = OFF
MAIN PROGRAM
A=1
B=0
C=1
C=0
A=0
B=1
B=1
C=0
ON-LINE INITIALIZATION
RLS ESTIMATOR
MAPC CONTROLLER
B=1

The MAPC software was written in 4 distinct segments. The "main" segment is run on a scheduled frequency and is responsible for data scaling, data filtering and the maintenance of all data vectors required for the recursive estimator and the multi-step controller segments. An "on-line initialization" segment allows the user to re-initialize all vectors and matrices to user-specified initial values. This may be invoked by placing the "initialization" switch to the on position. The initialization segment will then toggle all switches to the off position, and thus, allow only the main program to run. The user then has the flexibility to select a complete adaptive multi-step controller or can separately enter the model parameters and have a fixed parameter multi-step controller. This flexibility was built to facilitate evaluation of the adaptive controller, and for future non-adaptive applications.

The RLS estimation segment will run when the RLS switch is in the "on" position. The segment is responsible for scaling the covariance matrix based on the current $tr\{P(\cdot)\}$ specification, the use of Bierman's UD-factorization for covariance updating and estimation gain vector computation, and model parameter updating. It should be noted that this segment need not exist if a non-adaptive controller is desired. The removal of the segment will in no way affect the remaining software.

The MPC segment performs all the computations required to compute the control vector Δu of dimension $N_u x1$ and implement the first element in that vector. It is responsible for the covariance and Kalman gain updates of the two-step Kalman Filter, the formation of the impulse and step response co-efficient matrices, the computation of the future output vector, and the solution of the $\Delta u = (A^TA + \lambda I) \cdot A^T\{ Y_{sp}(k) - Y^{\bullet}(k) \}$ equation. It should be noted that the two-step Kalman filter was implemented such that the incremental control value is implemented prior to performing the time update to the Kalman filter. This allows the processor to perform the computation intensive time update during the intermediate period between control intervals.

3.4.3 Practical Considerations

When implementing any controller in an industrial environment there exist certain items which must be considered if the application is to be successful. This is no different with adaptive control, and the importance of providing a consistent, standard system cannot be over-emphasized. Typically, the console operators are not technically versed with the technology that has been implemented and thus it is important to educate them on the limitations of the technology. With the implementation of MAPC at Esso Chemical's higher olefins plant, the application was made completely transparent to the console operator. The MAP controller was made to resemble a standard PID controller for the console operator, so that any changes that had to be made on-line to the setpoint, output clamps, or controller status could be performed as before. This was an attempt to maintain a consistent "look, touch and feel" for the console operator as well as for future application engineers.

Control applications at the PMX level may be implemented as setpoint or direct digital controllers. With setpoint control, the PMX control application manipulates the setpoint of a secondary controller which is typically a TDC-2000 PID controller. Console operators will limit movement in the secondary loop by setting setpoint high and low clamps. Similarly, with direct digital controllers, the control value computed by the PMX application is sent directly to the final control element. In this case console operators will limit movement by setting clamps to the output of the valve. It should be noted that these clamps are soft in that they reside in the Honeywell process control system rather than in the field. Naturally hard limits also exist in the field due to the limited capacity or movement of final control elements. Typically, the soft limits have smaller ranges to prevent and warn console operators of potential process or control application problems.

With setpoint or output clamps being violated, the anti-windup status (AWS) word or field associated with the point record is set to true. This allows suitable software to be written to prevent the MAP controller from running. In any event, when the AWS is set to true, estimation is disabled to prevent saturation non-linearities or process drift to corrupt the model parameters.

At the same time, the incremental control action is taken is set to $\Delta u=0$. Once the process output or secondary setpoint are no longer limited, the estimation and multi-step control will resume as before.

In adaptive control there always exists the possibility of having the model parameters unexpectedly drift into unstable regions. Although this should be prevented by having a deadzone on the model prediction errors, experience has shown that during plant upsets the deadzone is violated and the estimation algorithm attempts to produce a new set of parameters which may or may not be a good reflection of the true process dynamics. To prevent such an occurrence, the parameters may have upper and lower limits. These limits may be selected based on the natural variation of the parameters during a PRBS test, and are best computed by off-line simulation and analysis. MacGregor, (1987) computes the upper and lower bounds on each individual parameter by measuring the individual model parameter variation over the fixed data set. The upper and lower bounds are computed as the $\pm 2\sqrt{\hat{\sigma}^2_{a,b}}$ standard deviations. These bounds are then used during on-line parameter estimation to guard against a poor parameter set from being identified. Once confidence is gained in the parameter estimation these parameter limits may be widened. These upper and lower bounds must be implemented in a manner which does not interfere with the estimation algorithm. Techniques such as parameter projection (Shah, 1986) illustrate how to handle parameter limits in an elegant manner, without upsetting the estimation algorithm.

4.0 EXPERIMENTAL APPLICATION OF MULTI-STEP ADAPTIVE PREDICTIVE CONTROL IN THE ACADEMIC AND INDUSTRIAL ENVIRONMENT

The multi-step adaptive predictive controller (MAPC) discussed in the previous chapters was applied to 3 processes. The first process was a continuous stirred tank heater and constituted the university application of MAPC. The purpose of this application was to examine and analyze the capabilities and limitations of the MAP controller in a stable and controlled atmosphere. The following two applications were performed at the higher olefins plant at Esso Chemical Canada in Sarnia, Ontario. The first of the industrial applications was implemented on a polychamber reactor, to adaptively control the outlet temperature on the 5th catalyst bed. The second application was later performed on the unit hydrofiner which is responsible for the removal of poisons from the propylene feed.

The following sections describe the operation of these processes and present the experiments that were performed to test the capabilities and limitations of the MAP controller. The industrial applications provided a true testing ground for the controller. It had to deal with a variety of conditions that are typically not found in the laboratory. Finally, the results are summarized to show both the advantages and disadvantages of the MAP controller.

4.1 CONTINUOUS STIRRED TANK HEATER

4.1.1 Process Description

The continuous stirred tank heater (CSTH) consists of a an open vessel approximately 12.5 cm in diameter and 130 cm in height. Cold water enters the tank at the top and is heated by a steam coil. The steam is supplied from the university heating utility. The level in the tank is controlled via a local pneumatic proportional controller which regulates the valve at the tank outlet. Prior to the outlet valve are four thermocouples which are situated at different positions from the tank outlet along a long copper tube. For the experimental configuration refer to Figure 4.1.1.

The control objective in this configuration is to maintain one of the four thermocouples at a user-specified temperature by manipulating the steam valve position. Servo response is possible by varying the temperature setpoint. Similarly, regulatory response is witnessed when the cold water rate is adjusted. The cold water produces a disturbance which alters the process steady state and also the transportation time delay. By reducing the cold water flow rate, the time delay associated with temperature is lengthened. Thus, there exists an inverse relationship between the cold water flow rate and the process time delay.

Uncontrollable disturbances may also arise with the experimental

Figure 4.1.1 Process Diagram of Continuous Stirred Tank Heater

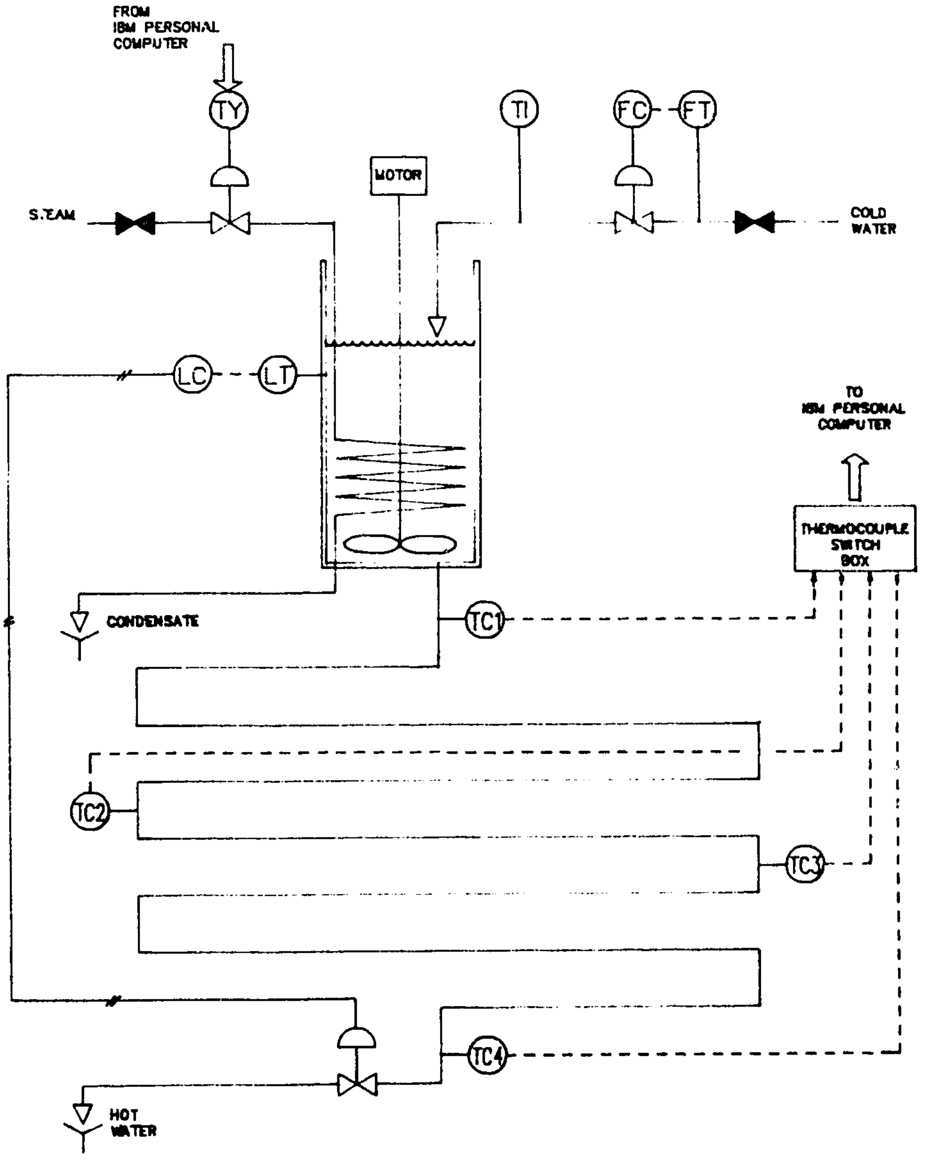
FROM
IBM PERSONAL
COMPUTER
TY
TI
FC
FT
MOTOR
STEAM
COLD
WATER
LC
LT
TO
IBM PERSONAL
COMPUTER
THERMOCOUPLE
SWITCH
BOX
CONDENSATE
TC1
TC2
TC3
TC4
HOT
WATER

equipment. A common uncontrollable disturbance was associated with the oversized steam trap. Condensate build-up in the steam lines resulted in poor heat transfer. With a sudden release of the condensate from the steam trap, the heat transfer increased and resulted in a sudden temperature increase. To circumvent this problem, the process was brought to a steady state operation where the steam flow rate was quite high. This managed to clear the condensate from the steam lines and steam trap much more readily.

For all the experiments that were performed, the steady state operating conditions were on average as shown in Table 4.1.1.

Table No. 4.1.1 CSTH Steady State Operation Conditions

Inlet Cold Water Temperature	19°C
Inlet Cold Water Rate	80 cm^3/s
Water Level in Tank	100 cm
Steam Valve Position	50 %
Outlet Water Temperature	38°C

Based on the above steady state operating conditions, the process reaction curves were obtained on a strip chart recorder so that knowledge could be gathered pertaining to the continuous time plant parameters. Knowing the continuous time plant parameters would allow a correct discrete process ARIMA model to be selected for the recursive identification as well as selecting the appropriate order and time constant of the $\Delta/T(z^{-1})$ filter.

The results of the open loop step tests that were performed on the on the CSTH for the three thermocouples is as shown in Table 4.1.2. In each case, the responses were plotted on a strip chart recording, which revealed a first order + time delay continuous time model was more than adequate to describe the open loop dynamics. Table 4.1.2 represents the average response obtained throughout the various experiments that were performed. The continuous time parameters which were obtained are defined by the first order transfer function model in the s-domain as shown below,

$$Y(s) = \frac{K_p \cdot e^{-\tau_d \cdot s}}{\tau_p \cdot s + 1} \cdot U(s)$$

Table No. 4.1.2 Continuous Time Process Parameters

Thermocouple Number	Time Constant τ_p (s)	Deadtime τ_d (s)	Gain K_p (%/%)
1	35	4	-1.80
2	40	25	-1.625
3	40	35	-1.50

4.1.2 CSTH Experimental Results

This section describes the experimental tests that were performed on the CSTH to evaluate the performance of the MAP controller. It must be stated that the CSTH is not an ideal candidate for adaptive control since it does not demonstrate time-varying behavior or highly non-linear dynamics. Due to this fact emphasis was then placed on quick identification of an ARIMA model, and then the immediate use of this model in the MAP controller. The results obtained from the various tests with the MAP controller were then compared with the results obtained by using a standard PID (proportional-integral-derivative) controller which was tuned to give a quick, over-damped servo response for thermocouple No. 1.

The items which were investigated using the CSTH as the process may be summarized as follows:

I RLS Open Loop Identification in a Noisy Environment
II Interaction Between the Kalman Filter and RLS
III Servo Response of MAP Controller
IV Regulatory Response of MAP Controller
V MAP Controller Behavior in presence of Changing Deadtime Dynamics

4.1.3 RLS Open Loop Identification in a Noisy Environment

The behavior of the RLS algorithm and identification was investigated by choosing the CSTH thermocouple which exhibited the highest amount of measurement variation. This, without doubt, was thermocouple No. 1. The variation in the measurement was approximately 4% of the temperature range. The variation was mainly caused by the poor location of the thermocouple which was situated at the immediate outlet of the CSTH tank. The cold water would channel through the tank leading to a poor mixing with the warmer water which resulted in a noisy temperature measurement.

Based on an open loop step test which was performed, the continuous time transfer function model which describes the dynamics of the CSTH for TC#1 is,

$$y_1(t) = \frac{-1.506}{35s + 1} \cdot u(t)$$

$y_1(t)$ = Temperature Measurement (0-100%)
$u(t)$ = Steam Valve Position (0-100%)

Similarly, a discrete time transfer function may be obtained by selecting a suitable sample time and then mapping the continuous time model into the discrete domain. The sample time selected was about 1/6 of the τ_p or 6 seconds. Based on this T_s and selecting the n_a and n_b as 1, the discrete time transfer function may be written as,

$$\Delta y(k) = \frac{-0.23735}{1 - 0.8425 \cdot z^{-1}} \cdot \Delta u(k-1)$$

The negative sign in the gain is due to the fact that the steam valve is "air to close", so that increasing the signal from 4-20mA closes the valve and causes a subsequent drop in water temperature.

Figures 4.1.2, 4.1.3 and 4.1.4 show the behavior of the parameters under open loop identification when three different orders of the $1/T(z^{-1})$ filter are used on the regressor vector. Table 4.1.3 summarizes the discrete time model parameters for the three tests as well as the filter order and pole location.

Table 4.1.3 Summary of Estimated Discrete Time Models For TC 1

Test No.	Estimated Plant Model	$\frac{\Delta}{T(z^{-1})}$ Filter	σ_e^2
1	$\frac{-0.0912 \cdot z^{-1}}{1 + 0.4239 \cdot z^{-1}}$	$\frac{\Delta}{1}$	4.654
2	$\frac{-0.7514 \cdot z^{-1}}{1 - 0.3527 \cdot z^{-1}}$	$\frac{\Delta \cdot 0.200 \cdot z^{-1}}{1 - 0.800 \cdot z^{-1}}$	0.351
3	$\frac{-0.3751 \cdot z^{-1}}{1 - 0.8375 \cdot z^{-1}}$	$\frac{\Delta \cdot 0.04 \cdot z^{-1}}{1 - 1.6 \cdot z^{-1} + 0.64 \cdot z^{-2}}$	0.006

In all three cases the *tr(P)* was held at a constant value of 1 during steady state operation and at a value of 10 during the pulses in the steam valve. The *tr(P)* was increased during the pulses to facilitate a quick identification of the plant model. Based on the tests performed there is no doubt that the third test provided the best discrete time model. The third test used a 2nd order residual filter with a discrete pole location of 0.8. This filter pole location was chosen to be somewhat smaller than the actual plant pole location of 0.8425.

The first test used only the Δ operator on the regressor vector, which would effectively eliminate any low frequency disturbances in the temperature output, but would not filter the high frequency components that were present with this particular temperature measurement. As a result, a high frequency model was estimated that had a pole location in the left half plane of the unit circle suggesting that the plant dynamics were oscillatory.

The second test used a first order residual filter. This test again revealed a high frequency model, however its dynamics are not oscillatory as in the first case. The residual filter in this case has a finite high frequency gain and thus influences the estimation to identify a model with much more significant high frequency components.

Looking at the variance of the residual sequences, it is evident that the third test minimized this variance best. Its value was 0.0056, compared with 4.6541 and 0.3505 for the first and second tests. This emphasizes the fact that using the correct order of $\Delta/T(z^{-1})$, the parameter identification may be both fast and stable. In the third test the parameters converged in about 40 sample intervals, or 240 seconds, to values which were approximately equal to the discrete time model determined from a continuous, process reaction curve.

4.1.4 Interaction Between The Kalman Filter & RLS Algorithm

Chapter 2.0 described the manner in which the MAP controller was implemented. The ARIMA model parameters are estimated on-line and then used in an observable state-space model to provide the basis for the modified Kalman filter predictor. During the time that the parameters are adapting, fluctuations in the ARIMA parameters will cause similar fluctuations in the Kalman gain vector elements. This variation in the Kalman gain vector elements will also cause variations in the residual filter bandwidth. Variations in this bandwidth must be maintained to a safe minimum, otherwise, in a noisy environment, the expansion of the bandwidth may cause instability in the controller. The manner in which the bandwidth may be kept artificially small is by selecting an appropriate value for the ratio of the process to measurement noise covariances, R_w/R_v.

The experimental results from the CSTH revealed, that in the closed loop, severe changes in the bandwidth of the residual or Kalman filter during parameter estimation caused highly non-linear temperature behavior during servo changes. The intensity of this non-linear response could be regulated by 2 "tuning knobs". First, the gain of the RLS algorithm may be reduced by adjusting the *tr{P}*. Lowering the *tr{P}* causes slower parameter changes resulting in slower and smoother bandwidth transitions in the residual Kalman filter.

The second tuning "tuning knob", R_w/R_v, allows the user to artificially adjust the bandwidth of the Kalman filter. Decreasing R_w/R_v causes the bandwidth to decrease allowing high frequency disturbances to be masked. As a result, the controller will take little or no action on these disturbances. Naturally, increasing this ratio has the opposite effect on the bandwidth and so the controller will see these disturbances and attempt to compensate for them.

Theoretically, if the model prediction errors were zero, R_w/R_v, would have no effect on servo response. In practice, this is seldom the case, and so the selection of R_w/R_v is also important when considering the servo response. Figures 4.1.5 to 4.1.7 illustrate the experiments which revealed the non-linear behavior of the MAP controller in the closed loop when the Kalman filter and the RLS algorithm interacted. In all three cases the temperature measurement used was T/C #2. Figure 4.1.5 shows the effect of a quick $\hat{a}$ parameter change that was caused by increasing the gain of the estimator during the setpoint change. As $\hat{a}$ increased from -0.92 to -0.904 the *tr{M}* experienced a similar transient causing the temperature to overshoot and settle out.

Figure 4.1.6 shows the result of slow $\hat{a}$ transitions. If $\hat{a}$ has a slow transient during identification the *tr{M}* will also experience a slow transient. This resulted in a servo response which was damped illustrating that it was not significantly affected by the RLS and Kalman filter transients.

Figure 4.1.7 shows an extreme example of what happens with the MAP controller when both the *tr{P}* and R_w/R_v are chosen high. The result is an $\hat{a}$ parameter which responds quickly causing the *tr{M}* to have a fast transient. This leads to the extreme non-linear temperature response which was only stabilized once both the $\hat{a}$ parameter and *tr{M}* reached their steady-state values.

4.1.5 Servo Response of the MAP Controller

This section investigates the behavior of the MAP controller during servo changes with the RLS algorithm turned off. The previous section showed the possible non-linear response which results if the RLS algorithm is on. The tuning parameter which was manipulated was the control weighting, λ. All other parameters were maintained constant. McIntosh,(1988) showed that a good selection of λ can be made by scaling it according to the magnitude of the $tr(\mathbf{A}^T\mathbf{A})$ matrix. Selecting

$$\lambda I = m \cdot \frac{tr(\mathbf{A}^T\mathbf{A})}{N_u}$$

where m is some arbitrary factor used to determine the amount of energy to be expended in controlling the output. Choosing λ to be large relative to the $tr(\mathbf{A}^T\mathbf{A})$ will reduce the incremental control actions. Choosing λ to be small or zero as is the default case with the GPC controller (Clarke, Mohtadi and Tuffs,1987) will cause the control action to be fast and very responsive to deviations from the setpoint.

Two experiments were performed with the CSTH to demonstrate the servo behavior of the MAP controller. The first order model was identified prior to the servo tests and then held constant throughout the test to prevent any non-linear responses in the Kalman filter.

The model identified for TC#2 was :

$$\Delta y(k) = \frac{-0.45\cdot z^{-1}}{1 - 0.8\cdot z^{-1}} \Delta u(k-3)$$

The remaining controller parameters were selected to be :

$$N_1 = 1 \quad N_2 = 10 \quad N_u = 1 \quad R_w/R_v = 2.0$$

The values selected for the three horizons were fairly standard, however, the selection of the ratio of process/measurement noise covariance was chosen to be abnormally high. This was done because of a high confidence in the model parameters. With a good model any noise contained in the model residuals can typically be characterized to be auto-regressive or of a low frequency. Low frequency noise occurs when unexpected loads are imposed on the system. With the CSTH, such a load could be generated by suddenly varying the cold water flow rate into the tank.

Figure 4.1.8 shows the response of the CSTH to a 10% setpoint increase in temperature with $\lambda = 10$. This is similar to choosing the value of $m \cong 1$. The output and input responses are smooth. They show no signs of high frequency fluctuations. The response time in this case is 114 seconds. It should be remembered that this includes the deadtime of approximately 30 seconds. The deadtime is included as part of the overall response time due to the fact that setpoint changes at time k are actually implemented by the MAP controller at time k+d+1.

Figure 4.1.9 illustrates a similar servo response except $\lambda=0$. In this case the output response remains fairly smooth as in Figure 4.1.8. However, the input response which is the manipulation of the steam valve is rapid and jittery. This is what was expected when λ is selected to be small or zero. The response time was a fast 60 seconds. Subtracting the dead-time of 30 seconds leads to a process response time, τ_r, of 30 seconds which is faster than the open loop τ_p.

This demonstration of λ-weighting is important because it shows that it has two qualities which become important in an industrial environment. First, λ-weighting allows the user to tune the output response for servo type changes. With some off-line simulation, a desired response can be achieved. Second, the appropriate choice of λ also permits the user to have smooth control action. This prevents unnecessary manipulations of control elements which may, in a large plant, effect other upstream/downstream processes.

4.1.6 Regulatory Response of MAP Controller

It has been stated in previous sections that the MAP controller has 2 degrees of freedom. Holding the horizons constant, the servo and regulatory behaviors can be tuned individually provided the model prediction errors are white noise. Naturally, this will not always be the case, however a good selection of the R_w/R_v parameter will ensure that unmodelled disturbances will be compensated adequately by the controller. Walgama, (1986) showed that this ratio is similar to derivative action. The larger the value, the stronger the predictive action taken on unmodelled disturbances that fall within the bandwidth of the plant.

The regulatory ability of the MAP controller was tested on the CSTH by providing an unmodelled disturbance. This was performed by varying the flow rate of the cold water injection into the tank. The flow rate was changed by ±10%. This experiment used the model which was identified for the servo response tests. The controller horizons were maintained as before, and the control weighting was set to $\lambda=10$.

Figures 4.1.10 and 4.1.11 show the regulatory response of the controller to a 10% decrease and then a similar increase in cold water flow rate. During this time, the cold water temperature was constant. In Figure 4.1.10, the temperature deviated by 8% and it took the controller 400 seconds to settle the temperature to its intial setpoint. Figure 4.1.11 refers to a 10% increase in cold water flow. Unfortunately during this time another disturbance occurred which was associated with the steam trap. This disturbance which occurred several times without warning throughout all the experiments typically caused a rise in the temperature. This is evident from Figure 4.1.11.

Figure 4.1.12 illustrates a 10% decrease in cold water flow with a noise covariance ratio set to R_w/R_v=2.0. In this case the temperature deviated only 6%, however it still took approximately 400 seconds for the TC#2 temperature to settle within ±5% of the temperature setpoint.

These two experiments suggest that increasing the R_w/R_v tuning knob allows the MAP controller to compensate for unmodelled disturbances in a manner which reduces the overall impact of the disturbance on the controlled variable.

4.1.7 MAP Controller Behavior in Presence of Changing Deadtime Dynamics

Varying time delay dynamics can seriously degrade the performance of any controller. This section describes the experimental tests that were performed to test the MAP controller under extreme variations in time delay dynamics. Results are then compared with a well tuned PID controller.

In all three experiments that were performed, a first order model was used. The prediction and control horizons, as well as the control weighting and ratio of process/measurement noise covariance, were maintained constant. Adjustments to these parameters were only made when controller behavior became oscillatory or unstable in order to stabilize the CSTH temperature.

Results from the first experiment are shown in Figure 4.1.13. The process model estimated for TC#1 was first order with no time delay. From the actual process reaction curves, TC#1 has approximately 3 seconds of time delay. This was considered to be insignificant when using a sample time, T_s=10 seconds. Figure 4.1.13 shows the trajectories of the model parameters. The parameters converge during an open loop identification to their steady state values by 40T_s after which the MAP controller is turned on. After a short transient in the *tr*(**M**) which determines the bandwidth of the Kalman filter, the controller begins to regulate the CSTH temperature by manipulating the steam valve. To introduce the change in time delay the thermocouple switch is changed to TC#2 at 110T_s. TC#2 has approximately three sample intervals of time delay which is significant relative to the process model which has been estimated for TC#1. With the RLS identification still active, the model parameters begin to drift and diverge from their originally estimated values. The discrete pole location exits the unit circle leading to an unstable process model. The resultant closed loop control of the CSTH temperature becomes unstable and the controller must be placed into manual mode to prevent the underdamped oscillations.

The second experiment involved the identification of the same model as used in the first experiment. This open loop identification occurs from 160-220T_s. The results are summarized in Figure 4.1.14. After the parameters have reached their steady state values and the controller has gone through an initial transient with the Kalman filter, the switch is used to select TC#2. During this entire experiment the RLS estimator was left active. The gain of the estimator is summarized in the diagram of the $tr\{\mathbf{P}\}$. The controller in this instance does not become unstable immediately. However, after a servo change of +10% is implemented, the parameters begin to drift. Once the discrete pole moves outside the unit circle, the control action immediately becomes unstable and oscillatory. During the initial stages of the parameter drift, the control weighting was increased to $\lambda=25$ in an attempt to limit rapid control actions from occurring. This seemed to have little effect on stabilizing the CSTH temperature.

The last experiment was less severe in that the increase in time delay was restricted to a single unit of discrete time delay. A first order plus time delay model was open loop identified for TC#2 this time as shown in Figure 4.1.15. After identification of the model parameters the RLS algorithm was shut off at $T_s \cong 210$. Once the Kalman filters reached their steady state, the time delay was increased by about one sample interval (10 seconds) by selecting TC#3. Figure 4.2.15 demonstrates the controller performance to a +10% increase in temperature setpoint. The resulting temperature response exhibits a small overshoot with rapid recovery to the desired setpoint. The regulatory behavior is then tested by decreasing the cold water flow by 10% at $T_s \cong 375$. A corresponding deviation of 10% occurs in the CSTH temperature. The temperature then oscillates in a damped manner towards its original setpoint. To aid the controller in recovering from the oscillatory behavior the maximum prediction horizon, N_2, is increased from 10 to 14.

The experiments performed were both adaptive and non-adaptive. The adaptive experiments clearly illustrate that incorrect time delay specification in the model, or simply having a process whose time delay varies significantly, will cause the MAP controller to become unstable. In this case, the time delay variation was in the neighborhood of the process time constant.

The non-adaptive experiment illustrated that the MAP controller continues to be quite robust. Its servo response becomes faster with the increase in time delay, but most important it continues to maintain a stable temperature for the CSTH. Similarly, it provides fairly good regulation of the CSTH temperature in the presence of cold water disturbances. In this experiment it required some adjustment of the prediction horizon N_2 to more quickly dampen the resulting oscillations.

It is convenient to compare these results with those obtained with an ordinary PID controller. Figure 4.1.16 illustrates these results. The discrete PID controller was initially tuned to have good servo and regulatory response for TC#1. TC#1 demonstrated no no time delay when using a sample period of T_s=10 seconds. "Good tuning" was considered to be a damped servo response and non-oscillatory regulation. Figure 4.1.16(a) shows that the PID controller drives the temperature to a new setpoint value in 44 seconds. Similarly, the regulation of temperature to a 10% change in cold water flow is fast and non-oscillatory.

To understand the behavior of the PID controller to successive increases in time delay the thermocouple switch was used to select TC#2 and TC#3 which have 25 and 35 second time delays. Figure 4.1.16(b) illustrates that with the increase in time delay the servo response is no longer damped. However the temperature does settle out quickly with no oscillation. When the regulatory behavior is examined, the results demonstrate that the PID controller has degraded and a continuous oscillation results with a period and magnitude of 200 seconds and ±5% of the temperature range for TC#2. Similar results were obtained when TC#3 was used. Here the temperature overshoot is in excess of 5% for the 10% servo change. The temperature response also demonstrates a 4% undershoot before it finally settles to the desired setpoint. The regulatory response to an increase in cold water flow rate produces a similar cycle as with TC#2. In this case the oscillation magnitude is similar to that of TC#2.

The behavior of the PID controller is predictable with subsequent increases in time delay. As the time delay increases for a given set of tuning constants the degree of oscillatory behavior also increases. To circumvent this problem the PID controller would have to be de-tuned and thus could not respond as quickly to process disturbances as would the MAP controller.

Figure 4.1.2 Open Loop RLS Identification

TC#1 tr(P)=1 No Regressor Filter

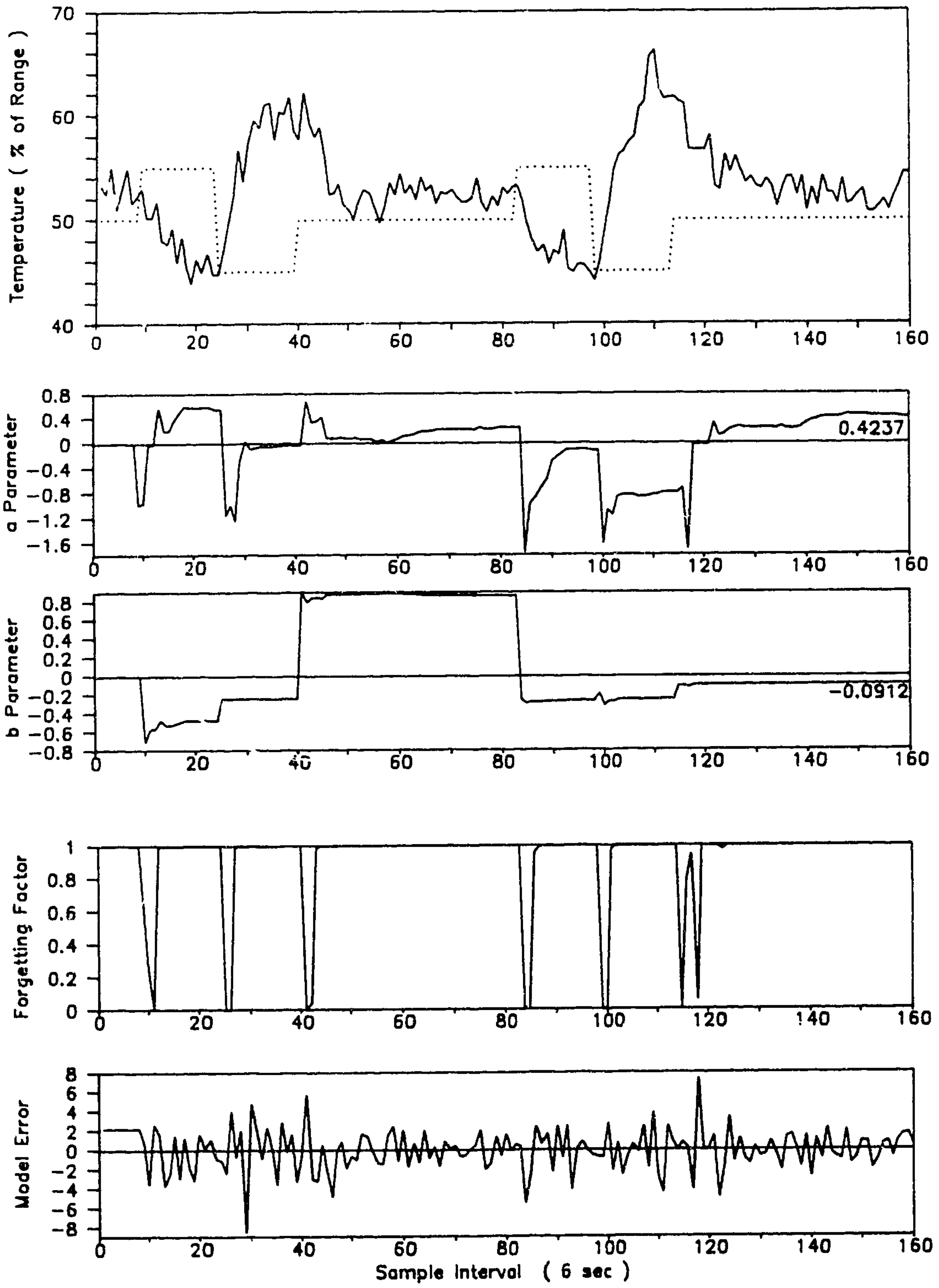

Figure 4.1.3 Open Loop RLS Identification

TC#1 tr(P)=1 1st Order T Filter (Tp=0.8)

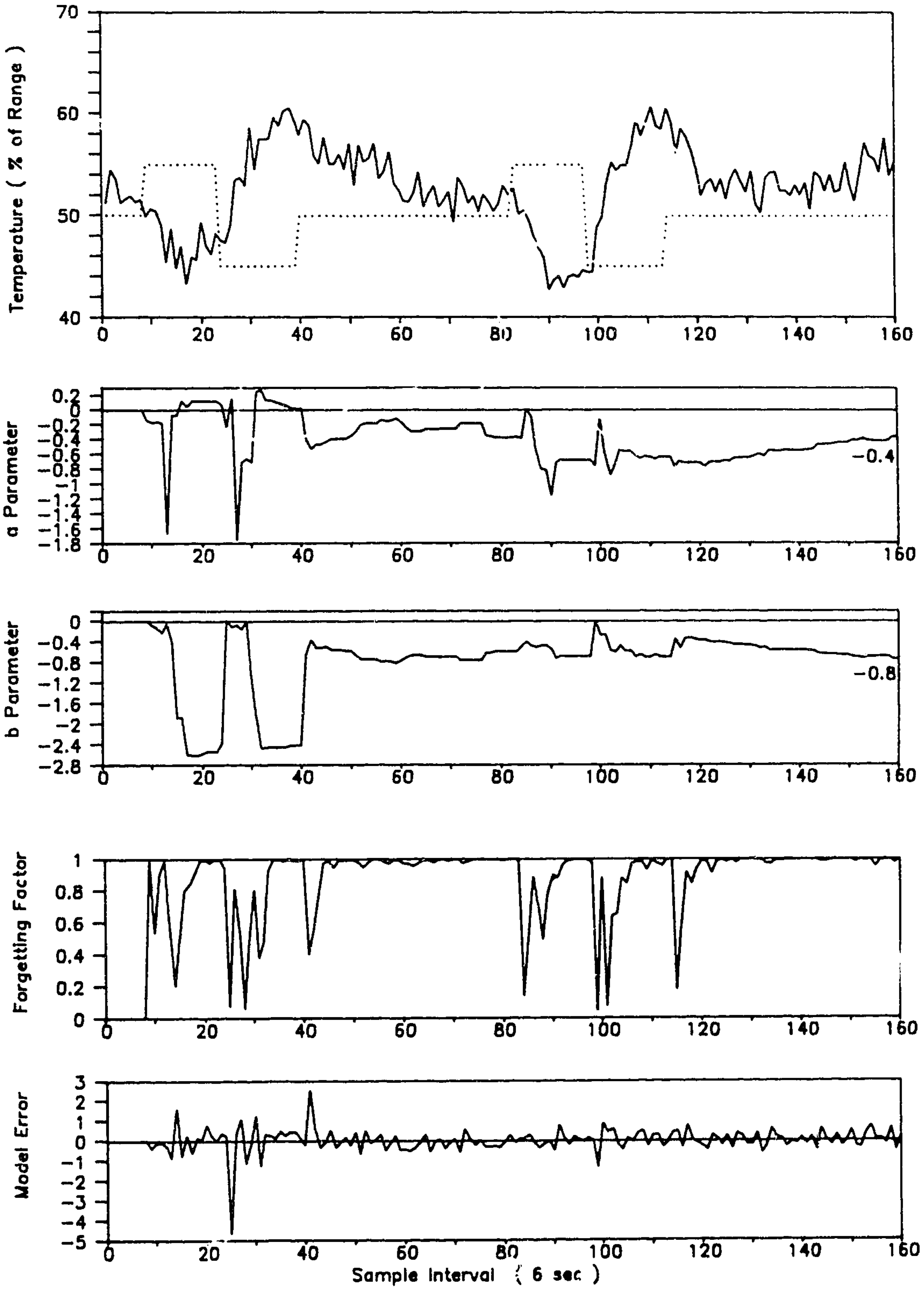

Figure 4.1.4 Open Loop RLS Identification
TC#1 tr(P)=1 2nd Order T Filter (Tp=0.8)

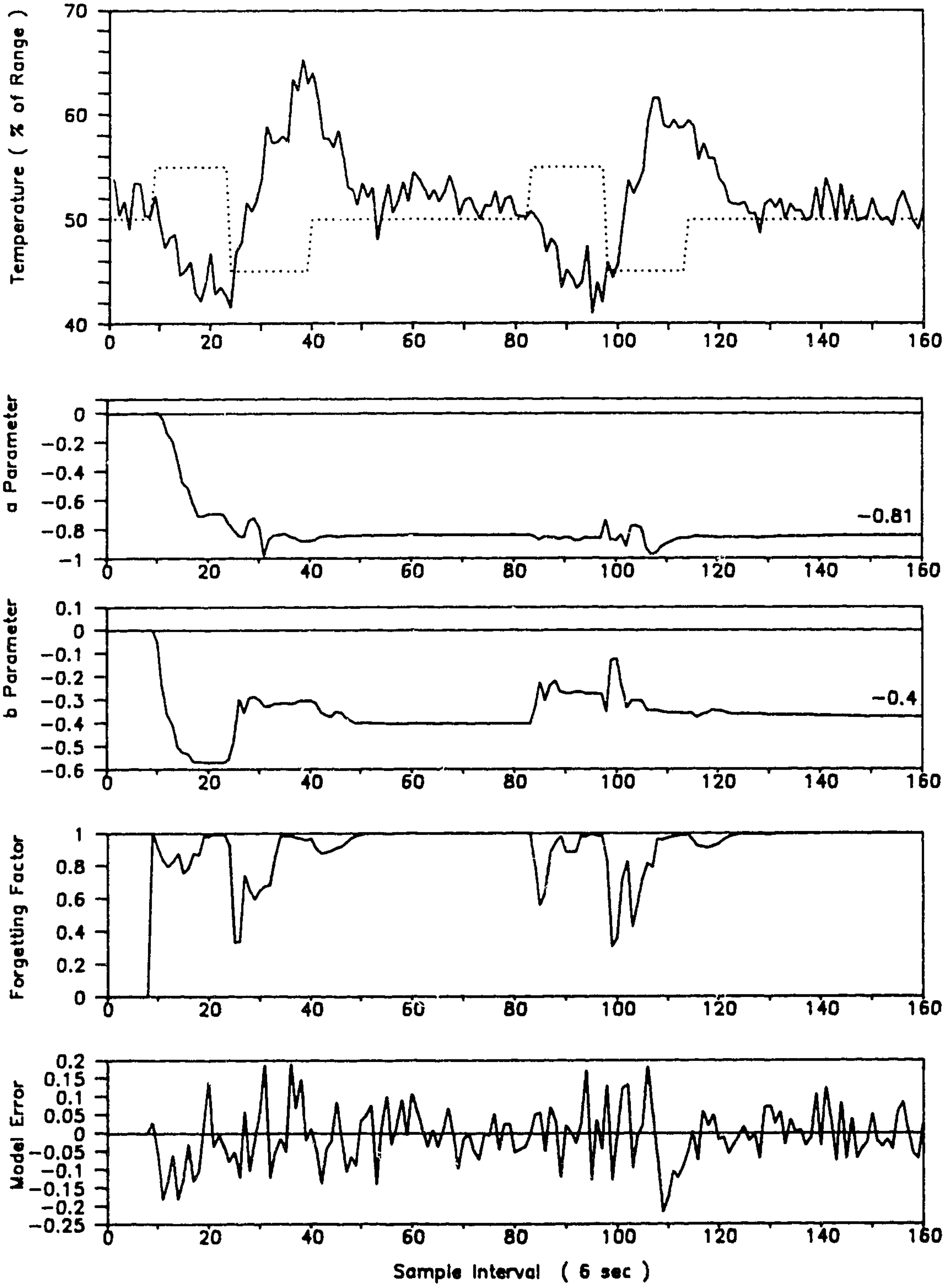

Figure 4.1.5 Multi-Step Adaptive Predictive Control of CSTH

N1=1, N2=10, Nu=1, Lambda=10, Rw/Rv=0.01, RLS=ON, tr(P)=1

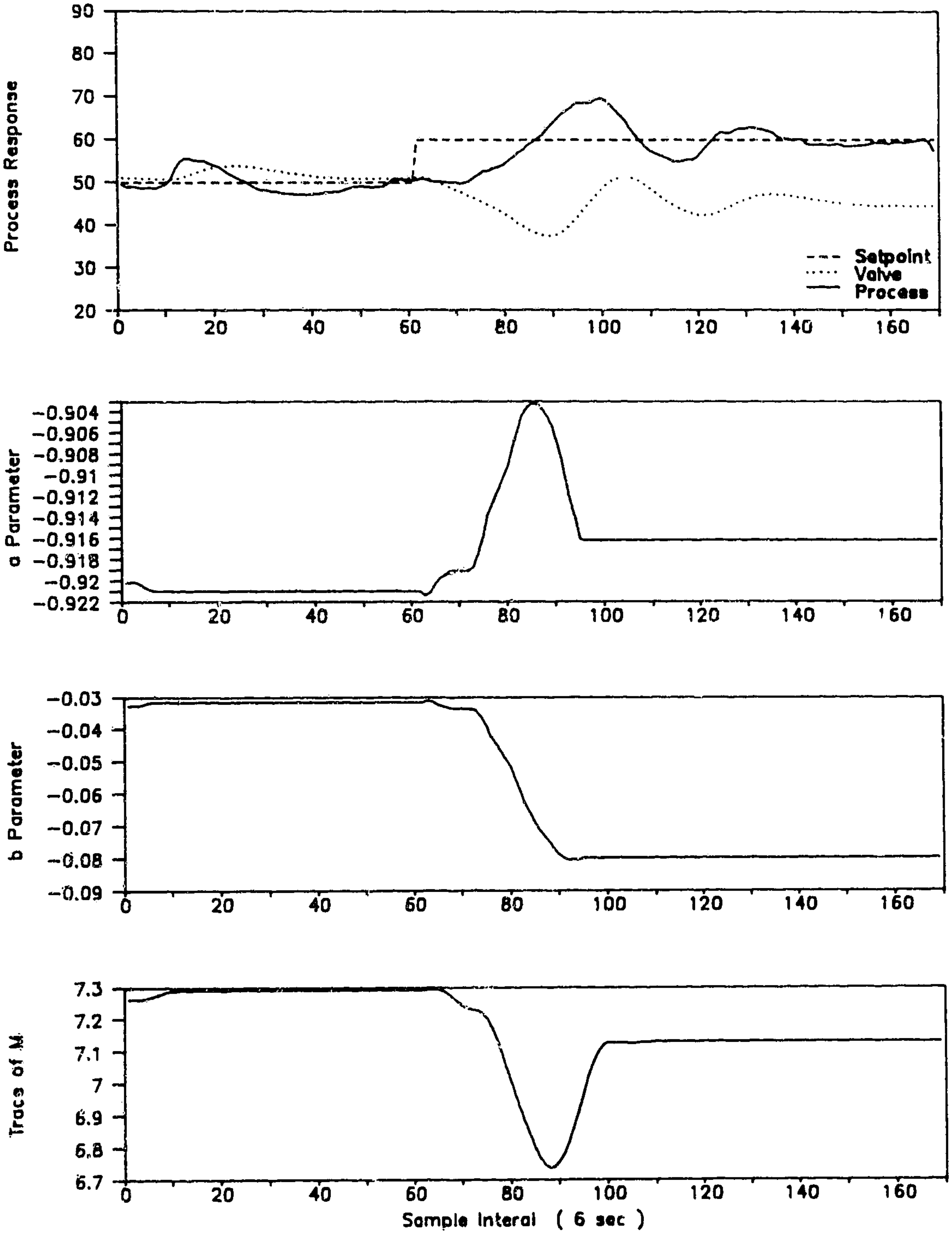

Figure 4.1.6 Multi-Step Adaptive Predictive Control of CSTH

N1=1, N2=10, Nu=1, Lambda=10, Rw/Rv=0.9, RLS=ON, tr(P)=1

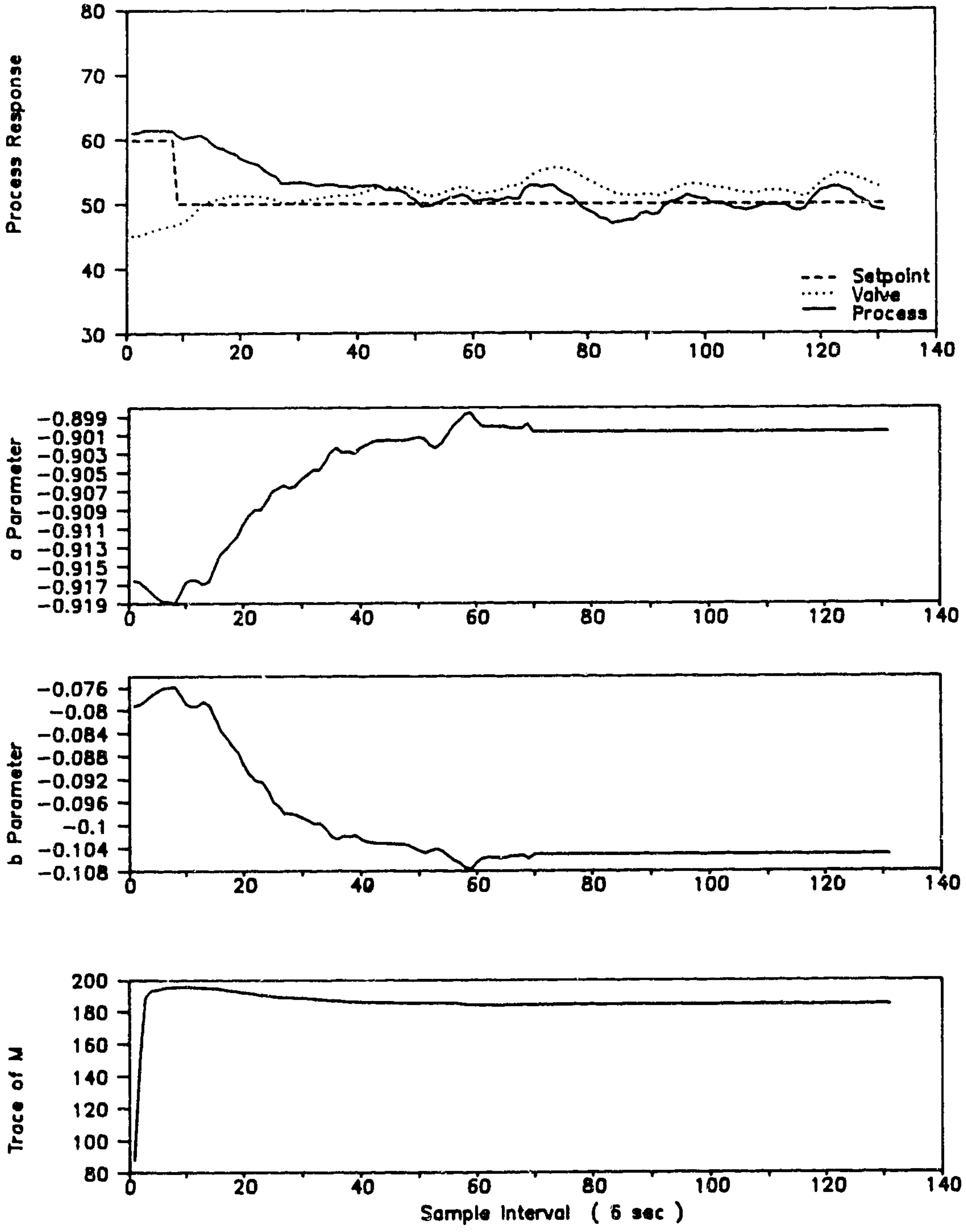

Figure 4.1.7 Mulit-Step Adaptive Predictive Control of CSTH

N1=1, N2=10, Nu=1, Lambda=10, Rw/Rv=2.0, RLS=ON

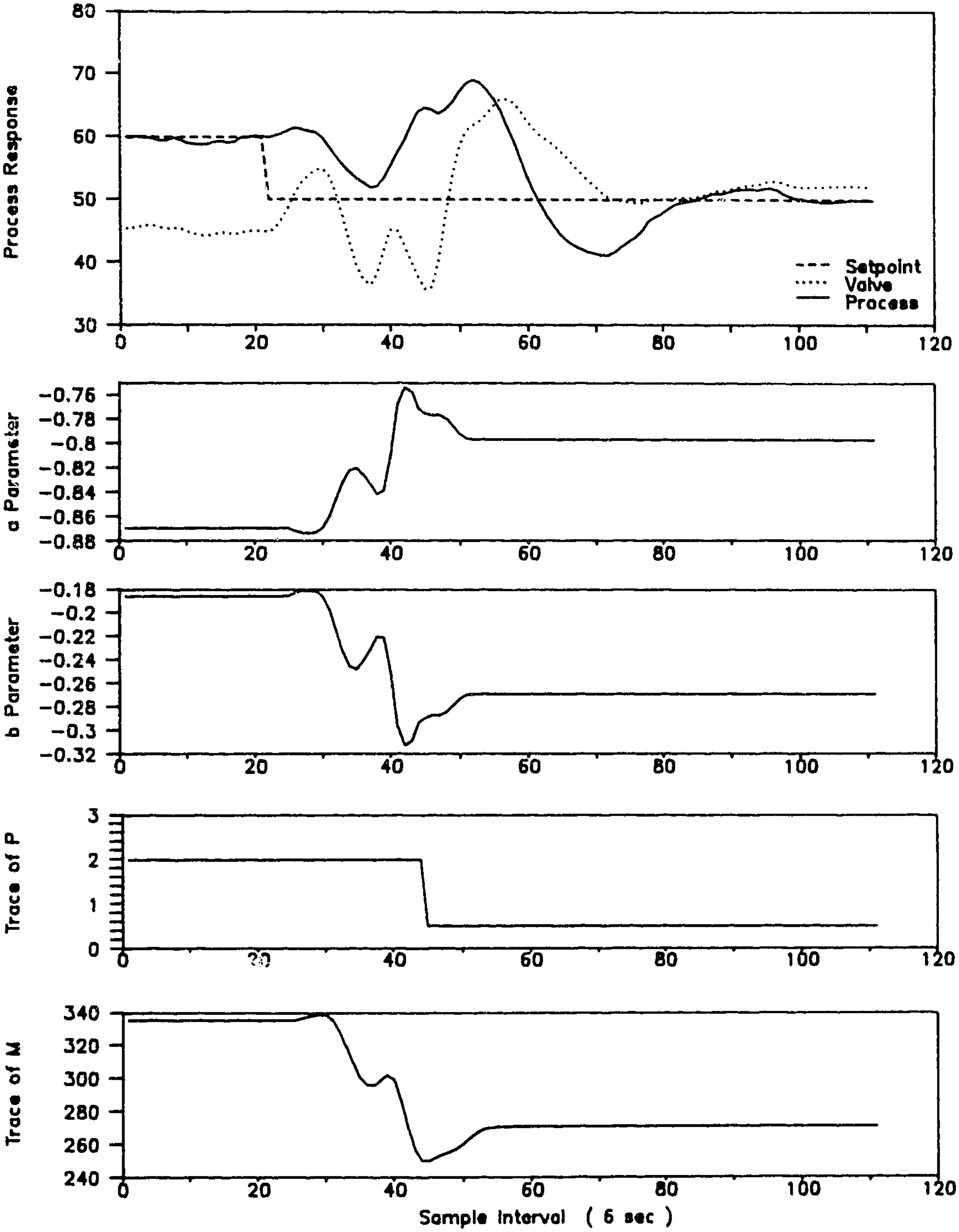

Figure 4.1.8 Multi-Step Adaptive Predictive Control of CSTH Servo Response

N1=1, N2=10, NU=1, Lambda=10, Rw/Rv=2.0, RLS=OFF, TC#2

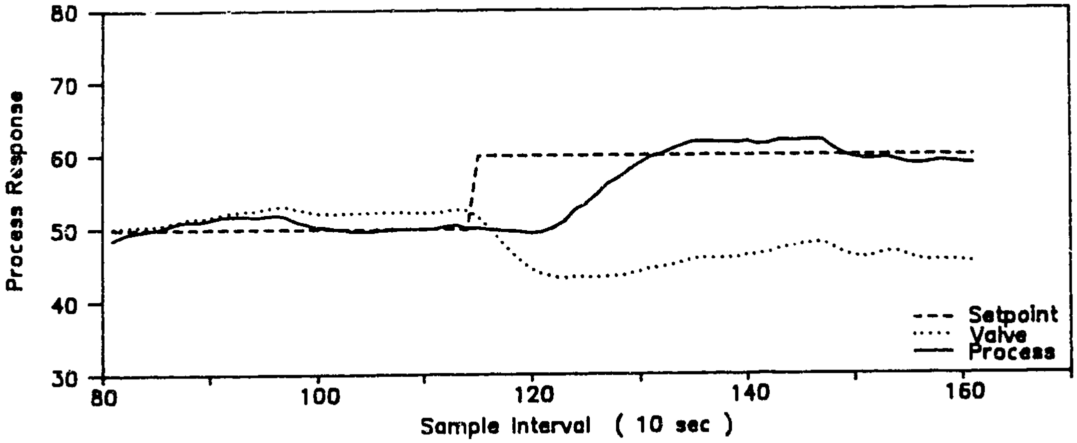

Figure 4.1.9 Multi-Step Adaptive Predictive Control of CSTH Servo Response

N1=1, N2=10, Nu=1, Lambda=0, Rw/Rv=2.0, RLS=OFF, TC#2

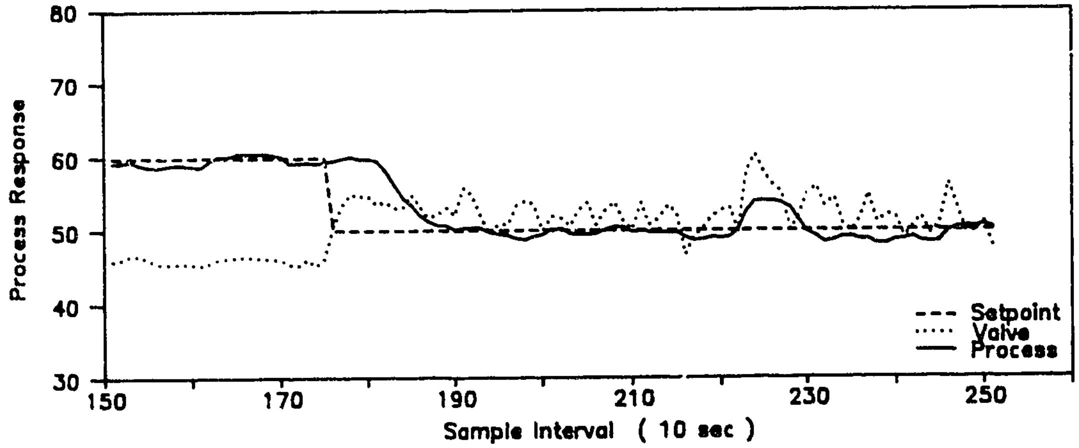

Figure 4.1.10 Multi-Step Adaptive Predictive Control of CSTH TC#2 Regulatory Response

N1=1, N2=10, Nu=1, Lambda=10, Rw/Rv=0.9, tr(M)=184, RLS=OFF

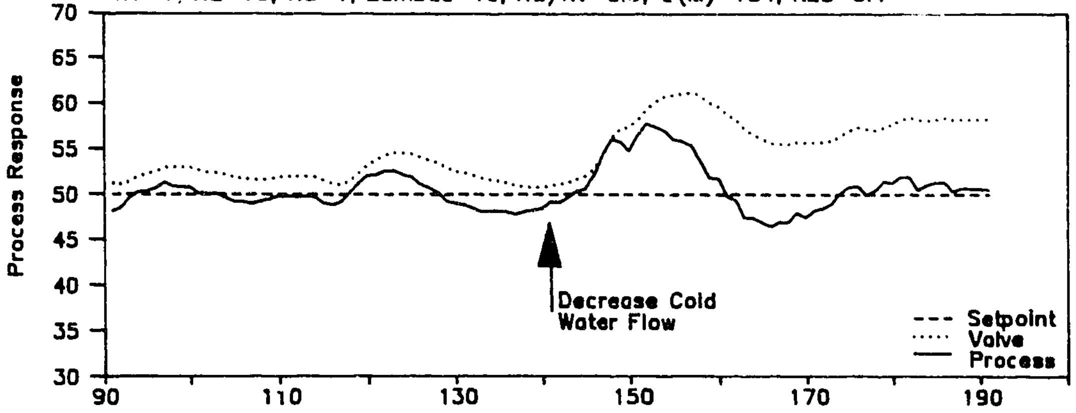

Figure 4.1.11 Multi-Step Adaptive Predictive Control of CSTH TC#2 Regulatory Response

N1=1, N2=10, Nu=1, Lambda=10, Rw/Rv=0.9, tr(M)=184, RLS=OFF

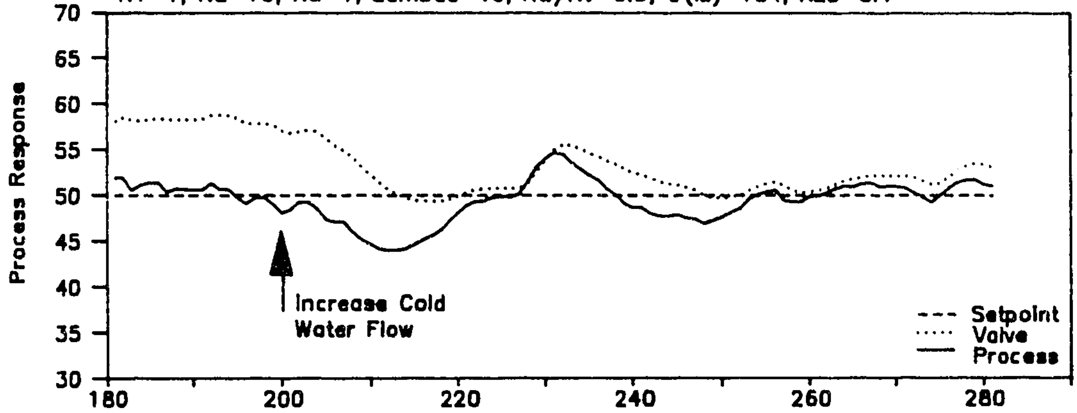

Figure 4.1.12 Multi-Step Adpative Predictive Control of CSTH TC#2 Regulatory Response

N1=1, N2=10, Nu=1, Lambda=10, Rw/Rv=2.0, tr(M)=369, RLS=OFF

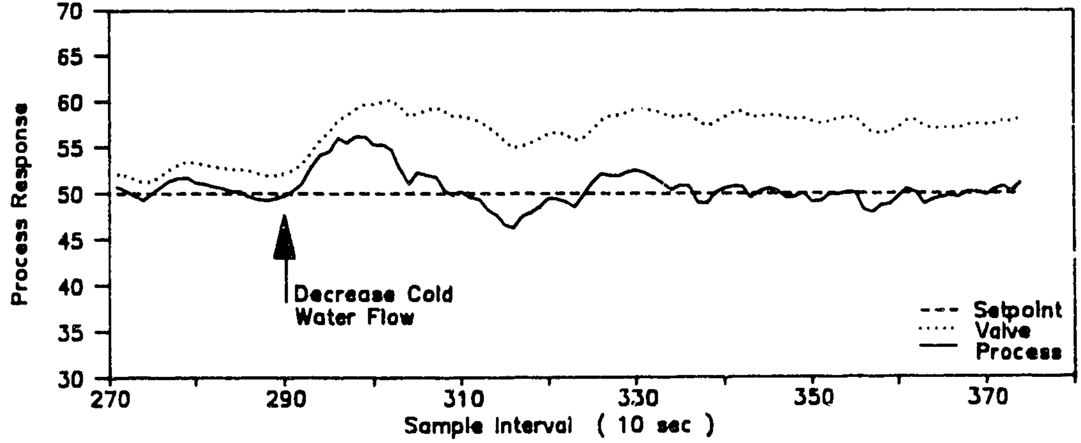

Figure 4.1.13 Multi-Step Adaptive Predictive Control of CSTH
Changing Deadtime Performance

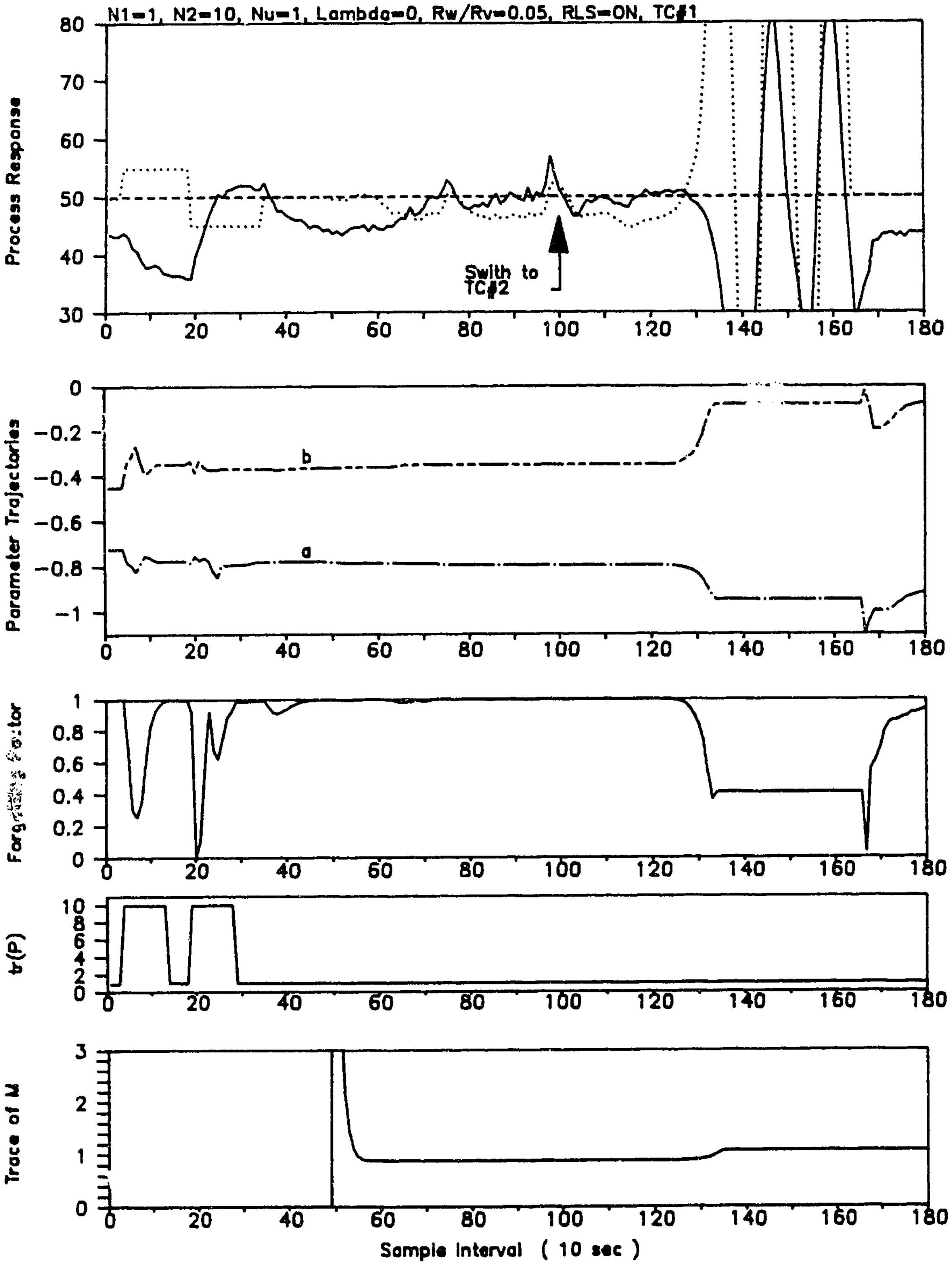

Figure 4.1.14 Multi-Step Adaptive Predictive Control of CSTR
Varying Deadtime Dynamics

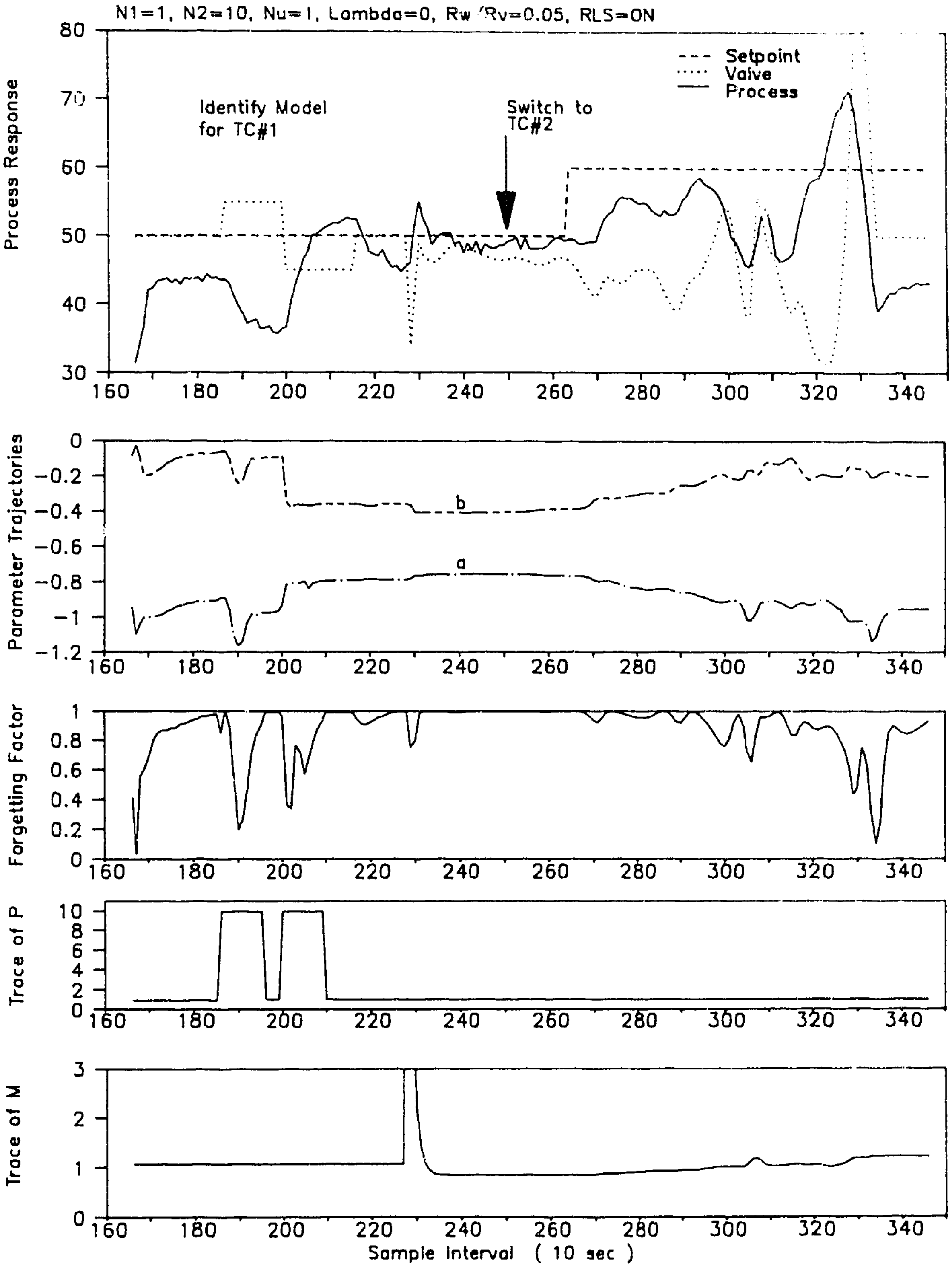

Figure 4.1.15 Multi-Step Adaptive Predictive Contro of CSTH
Varying Deadtime Dynamics

N1=1, N2=10, Nu=1, Lambda=1, Rw/Rv=0.05, RLS=OFF after ID

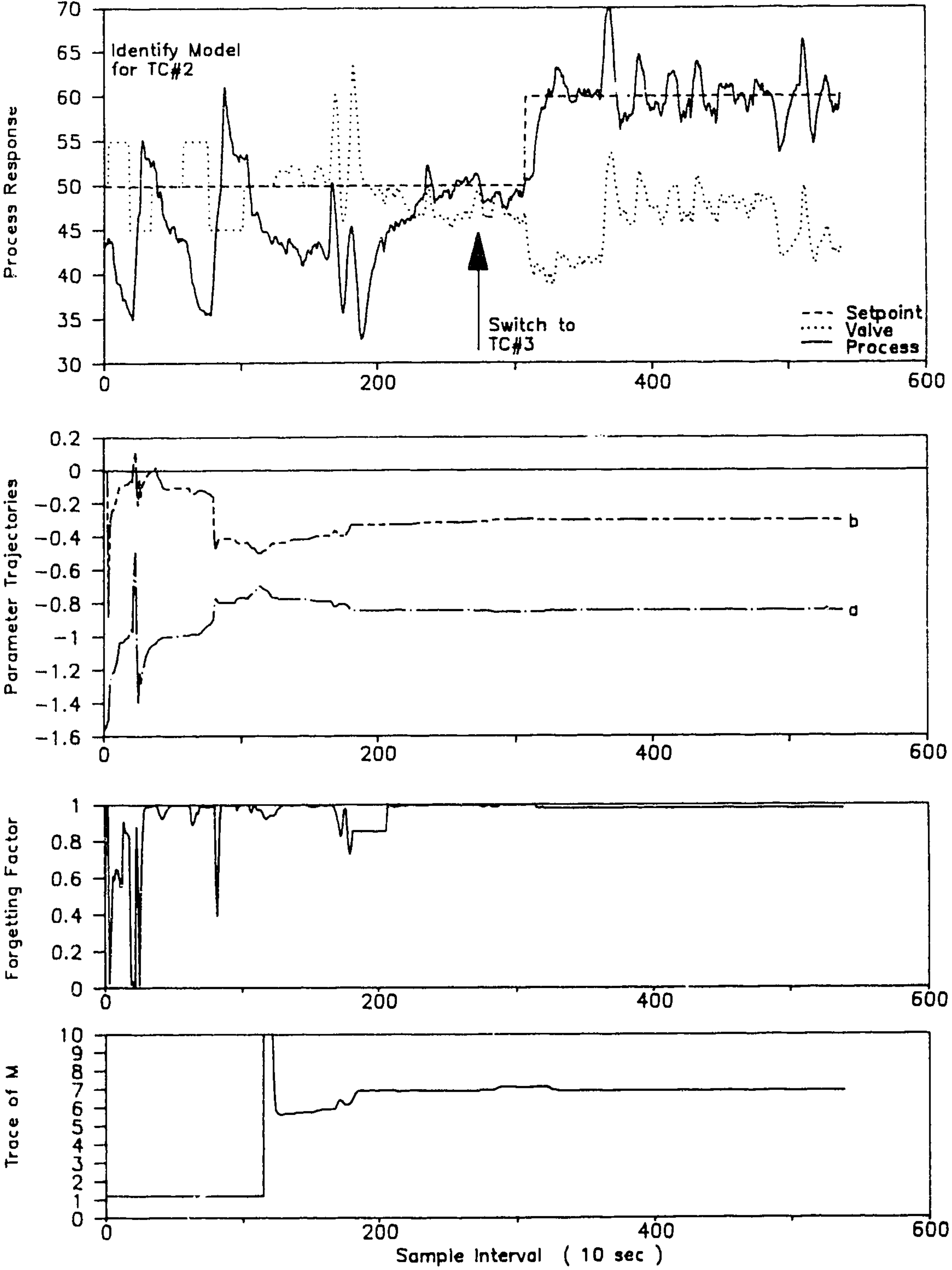

Figure 4.1.16 PID Control of CSTH
Servo And Regulatory Behaviour With Varying Deadtime Dynamics

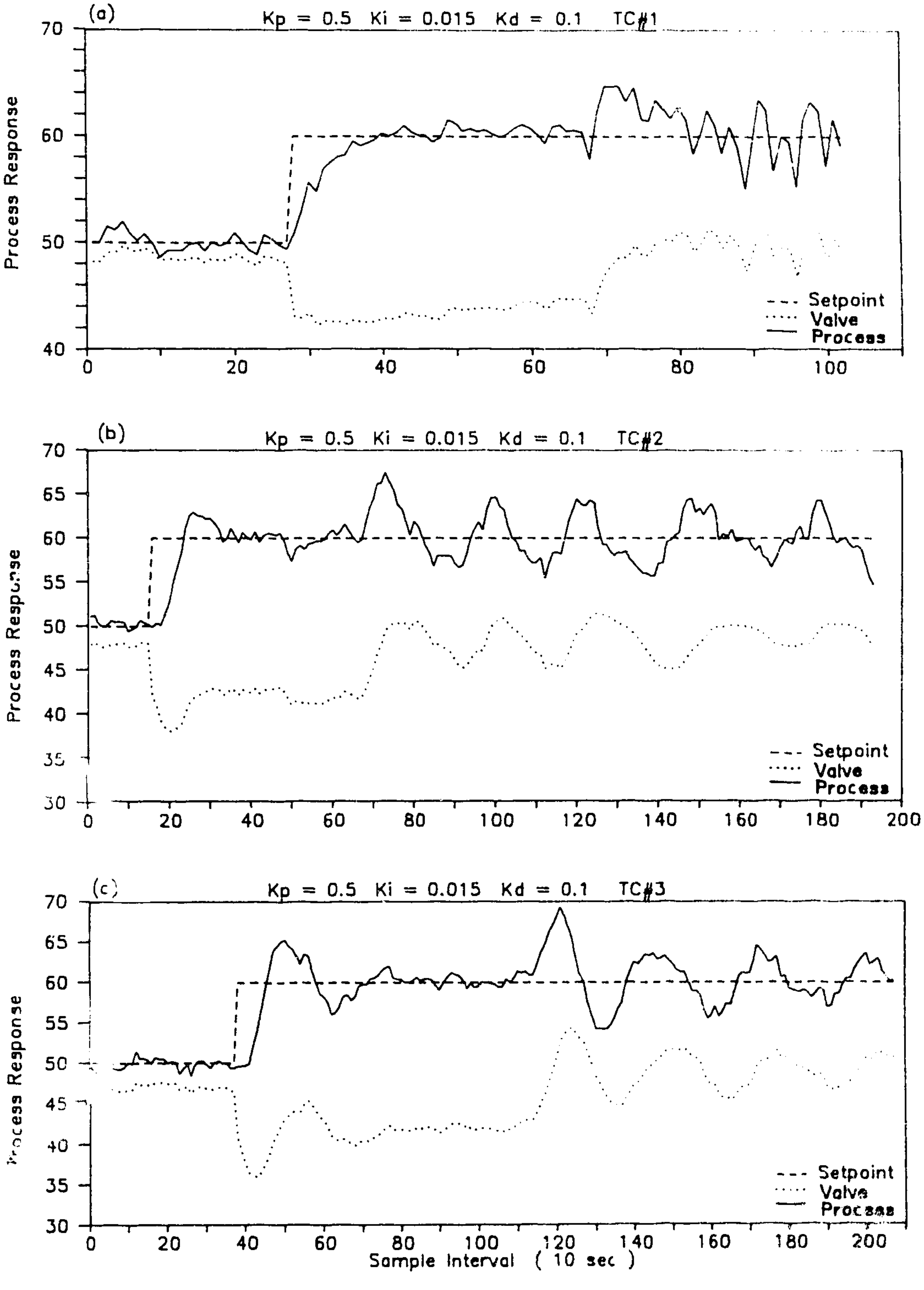

4.2 REACTOR BED TEMPERATURE CONTROL

4.2.1 Process Description

[illegible] first industrial application was performed on a relatively simple process control problem. The higher olefins unit in Sarnia uses 2 polychamber reactors to oglimerize dilute propylene to higher chain olefins, namely nonene and tetramer. Figure 4.2.1 shows the simple process flow diagram for a single reactor. The dilute propylene enters the top of the reactor and then passes over five beds of catalyst. These beds of catalyst provide the medium in which the propylene is gradually converted through a highly exothermic reaction to a higher chain olefin. To provide additional cooling and maintain a stable polymerization, the individual beds are quenched using a liquid which is relatively unreactive. The liquid is predominantly propane and represents a recycle stream from the first level of separation downstream.

The bed outlet temperature control on the individual reactors is maintained by four PID controllers. The target or outlet temperature setpoint is maintained by manipulating "air to close" quench valves. There are two peculiarities of the quench system which can cause temperature control problems and also represent unmodelled system disturbances. The first one deals with the fact that all the bed quench lines are connected to a single header and fed from a single pump. Pressure fluctuations on the header caused by an ill-tuned controller moving a valve too fast causes

Figure 4.2.1 Process Diagram of Reactor Bed Temperature Control

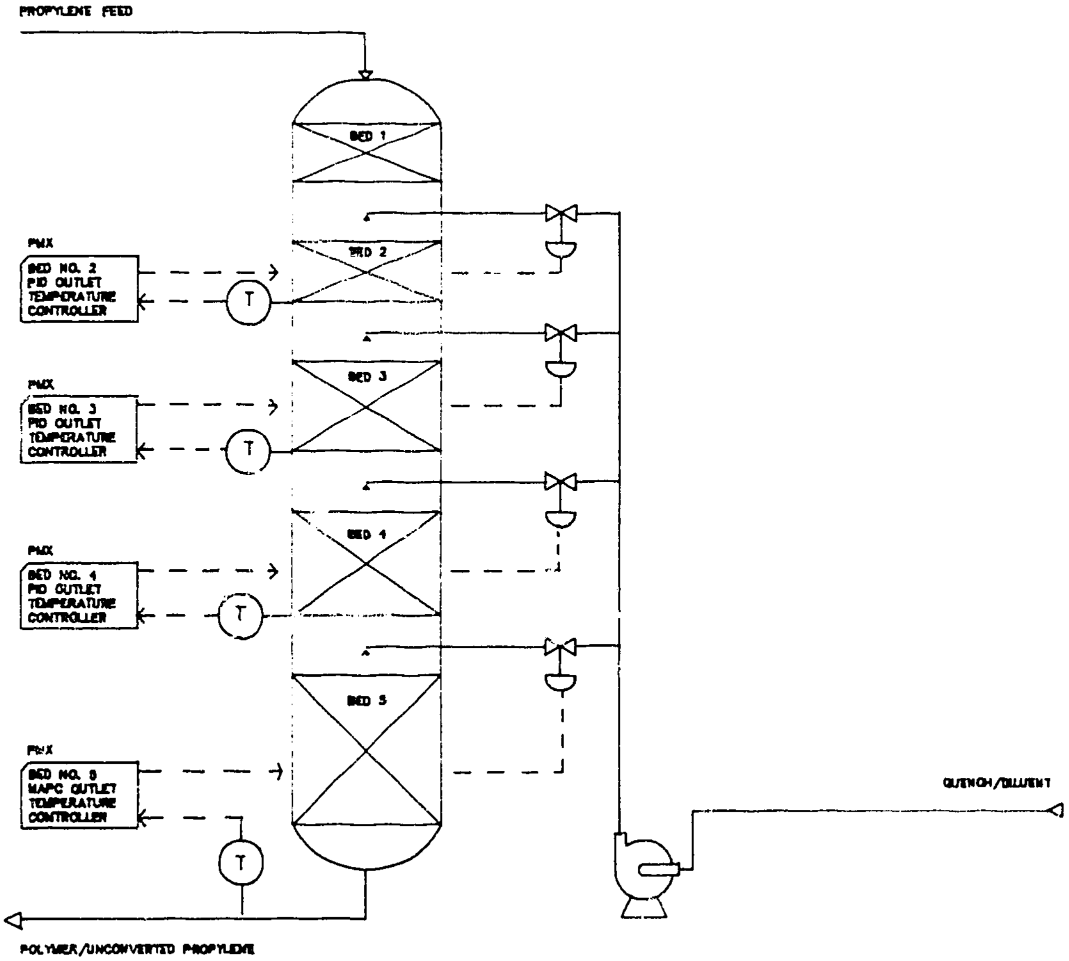
PROPYLENE FEED
BED 1
BED 2
BED 3
BED 4
BED 5
PMX
BED NO. 2 PID OUTLET TEMPERATURE CONTROLLER
PMX
BED NO. 3 PID OUTLET TEMPERATURE CONTROLLER
PMX
BED NO. 4 PID OUTLET TEMPERATURE CONTROLLER
PMX
BED NO. 5 MAPC OUTLET TEMPERATURE CONTROLLER
T
T
T
T
QUENCH/DILUENT
POLYMER/UNCONVERTED PROPYLENE

subsequent bed outlet temperature fluctuations. The second peculiarity is with the temperature of the quench. Quench temperature is controlled by a series of fin-fan coolers which are either off or on. Sudden cooling or heating will cause bed outlet temperature fluctuations.

Finally, the exothermic process may be considered "ill-conditioned". During open loop experiments it was found that the process gain and time constant can vary depending on whether quench is increased or decreased. Increasing the quench causes a small temperature decrease suggesting the process has a small steady state gain. On the other hand, decreasing the quench will cause a rapid and large temperature increase indicating that the gain is large and time constant small.

For the industrial experiment the fifth bed was selected for the primary reason that it offered the largest relative time delay as compared to the other beds. The fifth bed is the deepest bed and therefore provides the longest liquid transport delay. It was initially felt that this would be a good application for adaptive control due to the decay of catalyst activity over the reactor life.

The sections which follow describe the steps that were taken to understand the process dynamics in order to identify a process model. With the experimental data, it was then also possible to tune the RLS estimator off-line. Finally, some results are presented that show the performance of the complete MAP controller as applied to the fifth bed outlet temperature control.

4.2.2 Process Model Selection and Identification

The first implementation of the MAP controller to an industrial process proceeded with several on-line tests and then some intense off-line analysis of the data. This was done to establish the confidence necessary to run the MAP controller continuously and without an incident.

Chapter 3 described some of the practical considerations involved in implementing a more sophisticated adaptive model based controller. Prior to placing the MAP controller on-line the following steps were performed :

1. Open loop test.
2. PRBS test.
3. Off-line analysis to determine model order and time delay.
4. Simulation study to tune RLS estimator.

Figure 4.2.2 illustrates the open loop step test that was performed on the fifth bed characteristic outlet temperature. The PID controller was placed into manual mode, and the output was manually operated to provide the open loop step test. The series of steps reveal that the process is predominantly first order, however the potential for second order dynamics does exist with large movements in the quench valve. A large decrease in the fifth bed quench valve will cause a rapid increase in quench header pressure. This increase in quench header pressure causes more quench to flow to the fourth bed for a given valve position and thus causes the fourth bed outlet temperature to drop. The drop in fourth bed outlet temperature will cause a subsequent drop in the fifth bed outlet temperature. The reverse is true when the fifth bed quench valve is opened quickly. Table 4.2.1 summarizes the continuous time parameters from the successively performed step tests :

Table 4.2.1 Summary of Reactor Step Tests

Step Test Number	τ_p (min)	τ_d (min)	K_p (^{o}F/%)
1	6	0	-0.48
2	5	5	-0.60
3	3	9	-0.30
4	13	6	-0.40

Looking at Table 4.2.1 the average values of the parameters are τ_p=7min , τ_d=5min and K_p=-0.445^{o}F/%. The negative gain is caused by the fact that as the valve is opened, the quench flow increases causing a drop in the bed outlet temperature. The step tests also suggest that there is significant variation in the continuous time parameters and that a longer test may be required in order to provide good process data for model identification.

The step tests provided an initial guess for the model structure. The structure may be defined as :

T_s = 2 minutes
n_a = 1
n_b = 1
d = 3

In order to achieve a better understanding of the process dynamics a closed loop PRBS test was performed. The closed loop test was selected for 2 reasons. First, it is important to prevent a temperature runaway in the reactors and so any extended testing must be performed with caution. Second, it presented a good opportunity to determine how good a process model a closed loop test could yield.

The existing PID controller was altered to provide proportional action on the error ($y_{sp}(k) - y(k)$) rather than on the process variable ($y(k) - y(k-1)$). This was done to ensure that the manipulated variable, in this case the valve, provided the necessary "proportional kick" to the process in the closed loop. This is required in order to minimize the correlation between the manipulated variable and the process output noise.

Prior to performing the test, some steady state operating data was analyzed to determine the natural variation of the bed outlet temperature in the closed loop. The standard deviation of the output was $\sigma_y = \pm 1^{\circ}F$. Based on this output variation, the magnitude of the PRBS signal was selected to be ±3°F. The sample time was chosen as $T_s = 2$ min. and the PRBS switching interval as $T_{sw} = 4$ min. The PRBS test was then performed over a 6 hour period as shown in Figures 4.2.3 (a)-(d).

From these 4 figures, it can be seen that the selection of the PRBS magnitude of ±3°F was a good one, as it did not influence the fourth bed temperature as drastically as the open loop step tests did. Also, the downward drifting valve position over the 6 hour period demonstrates the non-stationary characteristic of the process. As the daily temperature began to rise, it caused a similar rise in the quench temperature. If the test were performed in the open loop, this drifting would have caused an unacceptable rise in the bed outlet temperature. However, since the test was performed under closed loop conditions, the rise in quench temperature was automatically compensated for by the PID controller which increased the amount of quench flow to the reactor catalyst bed. With this test, the outlet temperature was maintained within a comfortable ±10°F range which was deemed acceptable by the higher olefin operators.

With this PRBS data, a more sophisticated analysis of the process dynamics could be made using some of the techniques discussed in Chapter 3.0. A cross-correlation analysis identified the process time delay to be 3 sample periods or 6 minutes. Figure 4.2.4(c) illustrates the step response formed from the estimate of the cross-correlation sequence. From the estimate of the step response, the time delay of 3 sample intervals corresponded well with the reactor step test data.

Figure 4.2.4 (b) and (c) illustrate the impulse and step response coefficients obtained from using the IDSA Software Package (McGregor, 1988). The step response shows that a first order process + time delay model is satisfactory. Thus n_a and n_b were chosen as 1.

The next step after identifying the process model order and time delay, was to perform several simulations using the PRBS data to tune the RLS estimator. To do this, an off-line version of the RLS estimator was used. This off-line simulation allowed for the following estimator "tuning knobs" to be selected :

$tr\{\mathbf{P}\}$ = trace of the covariance matrix

$T(z^{-1})_p$ = regressor filter discrete pole location

Δ_d = prediction error deadzone

Figure 4.2.4 (d) shows the most successful simulation where the RLS tuning parameters were selected as :

$$tr\{\mathbf{P}\} = 8, \quad T(z^{-1})_p = -0.8, \quad \Delta_d = 0.0$$

The $T(z^{-1})$ order was selected appropriately as second order. The parameter trajectories show how quickly the model can adapt when a good PRBS test is performed. In this case, the test was performed under closed loop conditions with the setpoint of the fifth bed

PID temperature controller being manipulated. The identified model may be summarized in the following discrete form :

$$\Delta y(k) = \frac{0.17092 \cdot z^{-1}}{1 - 0.8885 \cdot z^{-1}} \cdot \Delta u(k-3)$$

To verify the goodness of model fit to the data, the model prediction error may be examined by looking at the residual auto-correlation sequence. Figure 4.2.4 (g) illustrates the residual auto-correlation sequence with the standard error limits. Notice that the first 3 lags exceed the positive standard error limit. This states that the model residuals still contain some structure to them. In this case the structure may be identified as first order AR in nature based on the rules found in Box and Jenkins, (1984). To remove this structure a residual filter similar to the $1/T(z^{-1})$ filter would have to be designed. This has been explained in Section 3.3.2 as the $F(z^{-1})$ filter. The $F(z^{-1})$ filter is much harder to design in the adaptive case since it requires a priori knowledge of the residual dynamics. Sripada, (1988) describe a technique for estimating such a filter on-line and then conditioning the regressor vector. This was not performed in these experiments as it was felt that the complexity was unjustified.

4.2.3 Multi-Step Adaptive Predictive Control Of Reactor Bed Outlet Temperature

With the off-line analysis complete, it was now possible to go to the higher olefins unit and attempt to control the bed outlet temperature with the MAP controller. This section briefly describes some of the features that the Honeywell PMX III computer interface provided for the engineer/operator. It also reviews the experimental results which best demonstrated the operation of the MAP controller.

4.2.3.1 Operator/Engineer Interface

The interface for both the operator and the engineer was through the use of the Honeywell PMX-III color console, which is capable of allowing descriptive schematics to be built to display information more readily. Figure 4.2.5 illustrates the interface to the MAP controller. The operators were educated on how to turn the controller ON and OFF. This can be done by simply placing the secondary TDC-2000 controller into automatic mode from computer mode. Additionally, the PID controller could be placed back on by changing the primary MAP controller into manual, and switching the PID temperature controller into automatic mode. All other information found on this display was strictly for monitoring and tuning the MAP controller, which would be performed by the engineer.

The monitoring and tuning information for the controller and estimator were displayed independently of each other on the same schematic. The table below summarizes the parameters that could be changed on-line and the parameters that were displayed for monitoring the MAP controller.

	Controller	Estimator
Tuning Parameter	N_1, N_2, N_u λ_u, R_w/R_v	$tr\{P\}$, Δ_d, θ^T
Monitor Parameter	Δu, $\|\|K\|\|$, $tr\{M\}$	$\hat{e}(k)$, $\lambda(k)$

Similarly, the same schematic provided the digital switches that allowed the engineer to select on-line controller initialization, RLS estimator on/off and MAP controller on/off. This logic has already been described in Chapter 3.0.

4.2.3.2 Experimental Results

The experimental results that are presented in this section span a period of testing from November 1988 to January 1989. During this time the MAP controller was run continuously on the HOIS reactors. The predominant use of the MAP controller in this setting was for regulation of the fifth bed outlet temperature. There was little attention given to the servo response. The controller had to perform well given the unmodelled disturbances which could arise, with the constraint that fast movement of the quench valve was undesirable because it would cause the entire temperature profile in the reactor to cycle. Based on this criteria the controller parameters were selected to be as follows:

$$N_1 = 4, \quad N_2 = 10, \quad N_u = 1, \quad \lambda_u = 100, \quad R_w/R_v = 0.05$$

The selection of the prediction and control horizons was fairly standard given that this is a long range predictive controller. The control weighting and ratio of covariance noises were selected based on an off-line simulation of the MAP controller. This tuning gave the control valve a smooth response without excessively sacrificing the output or temperature response to step type disturbances. The results that follow demonstrate the performance of the MAP controller in the presence of disturbances. The data that is shown was collected on a daily basis using the historical data base that is available on the Honeywell PMX computer. Although the controller sample interval was 2 minutes, the data collected represents 6 minute averages which are readily available from the computer database for a period of 4 days. Each plot represents a single day of 6 minute averages or 240 samples.

Figure 4.2.6 represents the controller behavior with the RLS estimator turned off. It should be noted that the values of the model parameters at this point were identified by the off-line simulation. The parameters were identified as $\theta^T=[-0.854\ -0.142]$.

The RLS estimator was turned off after the initial estimation so that during periods of regulation the parameters would not drift and cause instability in the controller. From the experiments performed on the CSTH, this was the correct decision since the CSTH results demonstrated that during regulation the controller could easily become unstable if the RLS estimator remained on. Figure 4.2.6 illustrates the effect of suddenly cooling the quench flow to the reactors. Prior to turning on the fin-fan coolers at T_s=140 the quench temperature was slowly rising. This quench temperature rise manifested itself in a subsequent rise in the bed outlet temperatures. This caused the fifth bed quench valve to open 100%. After the quench was cooled, the valve came back to a range where the bed outlet temperature could be controlled. Although it seems that the controller took a significant amount of time to recover, this is desired because of the fact that rapid valve movement may cause further oscillations in the reactor temperature profile.

Looking at Figure 4.2.7 the fifth bed temperature came to setpoint by T_s=15 the following day. This represents a period of 11 hours on November 14 to recover from a -15°F deviation from a 405°F setpoint. Figure 4.2.7 also illustrates the MAP controller response to a disturbance caused by an increase in the fourth bed outlet temperature at T_s=120. The MAP controller was able to regulate the fifth bed outlet temperature to ±15°F given that the temperature disturbance on the fourth bed was ±20°F. The controller is again relatively slow in bringing the bed temperature to setpoint.

Figures 4.2.8 to 4.2.10 represent three days of testing during which the model parameters were re-estimated using the natural excitation of the process. In Figure 4.2.8 the model parameter vector elements were $\theta^T=[\ -0.854\ \ -0.148\ ]^T$. The corresponding controller parameters which were monitored to give an indication Kalman filter bandwidth were $||K(k)||=1.18$ and $tr(\mathbf{M})=7.139$. K(k) is the current computed Kalman gain vector and **M** is the error covariance matrix used in the computation of the Kalman gains. A rise in these two monitoring parameters indicated an increase in the Kalman filter bandwidth. During this day, the controller adequately compensated for a quench temperature disturbance. This is shown by the movement of the quench valve from 70% to 60% starting at $T_s=40$. This corresponds well with the gradual decrease in quench temperature. The model prediction error is shown in Figure 4.2.8(e). The estimated standard deviation and mean of this randomly fluctuating signal are $\hat{\sigma}_e=0.0111$ and $\hat{m}_e=-0.0028$. The prediction error indicates how well the model represents the movement of the process. Figure 4.2.8 (f) illustrates the auto-correlation sequence of the residuals. It provides information regarding the "whiteness" of the residual sequence. In this case the sequence decays below the standard error limits within 5 lags. This suggests that the MPE is not as "white" as would be desired. This may be due to several reasons the main one being that the current model does not account for all the process dynamics. Residual dynamics will be influenced by unmodelled disturbance dynamics. Low frequency disturbances such as quench temperature fluctuations will "colour" the MPE. In most cases, the MPE will have AR(1) dynamics as was true in this case. The rules for identifying residual dynamics are summarized in Box and Jenkins, (1976).

Figure 4.2.9 shows 24 hours of data that caused much excitation in the process. During this period the estimator had been left on with its tuning parameters set to the following values,

$$\Delta_d = 0.1 \quad \text{and} \quad tr\{\mathbf{P}\} = 0.1$$

From the diagrams it may be observed that the model parameters reach a new steady state of $\theta^T = [\ -0.918 \quad -0.091\ ]$. These new parameters caused a similar shift in the bandwidth of the Kalman filter. The steady state values of the Kalman filter parameters were $||\mathbf{K}(k)||=1.312$ and $tr\{\mathbf{M}\}=8.596$. In both cases, the ratio of the noise covariances was, $R_w/R_v=0.05$. Figure 4.2.9 (g) and (h) demonstrate the behaviour of the MPE. The residual time plot shows significant peaks occurring that correspond with the unmodelled disturbances. Naturally, this leads to an MPE with a high variance since the estimated model cannot account for the disturbance dynamics. The residual auto-correlation sequence can now be used to identify the structure of the unmodelled dynamics. This sequence is slowly oscillating suggesting that the disturbance dynamics are AR(2) with the discrete pole locations being complex.

Figure 4.2.10 represents the following day after the re-estimation. The controller response may be observed for two transitions in the fourth bed outlet temperature. In this case the MAP controller responds relatively quickly. It must be noted that during these three days the control weighting had been adjusted from a previous value of λ_u=100 to λ_u=50. Figure 4.2.10(e) illustrates the model prediction error. The model prediction error now has an estimated standard deviation and mean of $\hat{\sigma}_e$=0.0102 and $\hat{m}_e$= -0.00023. The reduction in residual variance suggests that the model is providing a better prediction than it had with the previous parameter set. Additionally, controller response to the fourth bed outlet temperature disturbance was excellent. The objective of quick disturbance rejection with smooth manipulation of the fifth bed quench valve was well executed.

Figure 4.2.11 and 4.2.12 illustrate the MAP controller's response to servo changes. In Figure 4.2.11 the RLS estimator was turned off and thus the model parameters were not permitted to adapt. The setpoint change from 416°F to 411°F was implemented at T_s=80. By T_s=100 or 2 hours later the fifth bed outlet temperature had reached its new setpoint.

Figure 4.2.12 illustrates the same MAP controller with the exception that the control horizon has been changed to a value of N_u=2. All other controller tuning parameters had remained the same. The data which is displayed was collected based on a sample period of 2 minutes. This was equivalent to the controller sample period. Additionally, this on-line experiment was performed with the RLS estimator on. The gain of the estimator was set by holding the *tr(P)*=0.1. The low gain trace specification was chosen such that large swings in the Kalman filter bandwidth would not occur rendering the controller unstable as was shown to be the case with the CSTH experimental results.

Figure 4.2.12 (e) and (f) show the resulting parameter trajectories during the servo changes. It can be seen that the model parameters do not change significantly. This may be explained by looking at the model prediction error in Figure 4.2.12 (g). The variance of the model prediction error appears to be small, however as was true in Figure 4.2.8, the residual auto-correlation sequence can reveal details of the unmodelled dynamics that simply analyzing the time residual sequence cannot. The auto-correlation sequence decays exponentially below the standard error limits within 4 lags. It again breaks these limits on the negative side from the 9 to 13 lags. This suggests that the unmodelled disturbance dynamics may be AR(2) with imaginary roots. It is the imaginary roots that will cause the oscillations in the auto-correlation sequence. These oscillations that were detected in the residuals may be explained by looking at Figure 4.2.12 (c) and (d). Both Figures show low frequency oscillations to be present in the quench and fourth bed outlet temperatures which would directly influence the estimation and control of the fifth bed reactor outlet temperature.

In summary, this first application of the MAP controller demonstrated that the technology could be easily applied to an industrial process without a major upset in operations.

Both the open loop step tests and closed loop PRBS tests provided sufficiently rich data in order to estimate a good process model. Off-line data analysis of the PRBS data and subsequently controller simulation provided the needed confidence with which to run the on-line controller application.

The MAP controller was tuned to provide good regulatory response which was similar to the existing PID controller. The use of natural process excitation proved to be successful in establishing a new model parameter set which minimized the residual variation.

The application of the MAP controller operated side by side with the existing controller technology at the HOIS. Acceptance by the operators was good, once they were trained and convinced by operating data that the MAP controller satisfied the necessary control objectives.

4.2.4 PID Control Of Reactor Bed Outlet Temperature

Figure 4.2.13 illustrate the behavior of the existing PID-DDC controller for the fifth bed outlet temperature control. The Honeywell PMX-III PID control equation is incremental and non-interacting in the time domain and may be written in the following form :

$$\Delta u(k) = K_1 \left(\Delta y(k) + \frac{K_2}{T_s} \Delta y(k) + \frac{T_s}{K_o} (y_{sp}(k) - y(k)) \right)$$

where,

K_o = reset constant (minutes)

K_1 = linear gain constant

K_2 = derivative constant (minutes)

T_s = sample time (minutes)

The PID controller provides proportional action on the process variable rather than on the error. This prevents the controller from "kicking" the process in response to step type servo changes. It was previously mentioned that slow response is desired in order to prevent large temperature oscillations from occurring within the reactor. There exists a greater interest in the input or manipulated variable response rather than on the output response, because fast input responses cause other bed temperatures to cycle.

The PID controller tuning constants during this period of of experimentation were :

K_o = reset constant = 15 minutes
K_1 = linear gain constant = 2.2
K_2 = derivative constant = 0.05 minutes
T_s = sample time = 2 minutes

Comparing the MAP to the PID controller for this experiment there were no real gains in performance with the MAP controller. It could be stated that the MAP controller performed equivalent to the PID controller. This experiment provided a good first application of the MAP controller in an environment which provided good step and ramp type disturbances. Figure 4.2.13 (b) shows the valve response of the PID controller. This response is similar to that of the MAP controller. Both controllers were able to achieve the desired smooth control valve movement to unmodelled disturbances.

In this case, the step quench temperature disturbance at T_s=20 did not have much affect on the fifth bed outlet temperature control. However, the fourth bed outlet temperature had a significant affect on the fifth bed outlet temperature. The PID controller was able to more than adequately control the temperature to a target of 416°F.

Although there were no significant improvements in performance with the MAP controller, it may be concluded that the RLS estimation was very successful when used in the closed loop with the existing PID controller. A good model could be estimated very quickly and resulted in a successful application of the MAP controller. The ability to rapidly estimate a process model without upsetting the process is significant, because it allows a controller to be commissioned faster in an industrial environment. Once the MAP controller was placed on, very little additional tuning needed to be done. In contrast, the existing PID controller on the reactor outlet temperature may need periodic changes made to the tuning constants to meet the desired control objective.

Figure 5.12 Reactor 5th Bed Temperature STEP Test

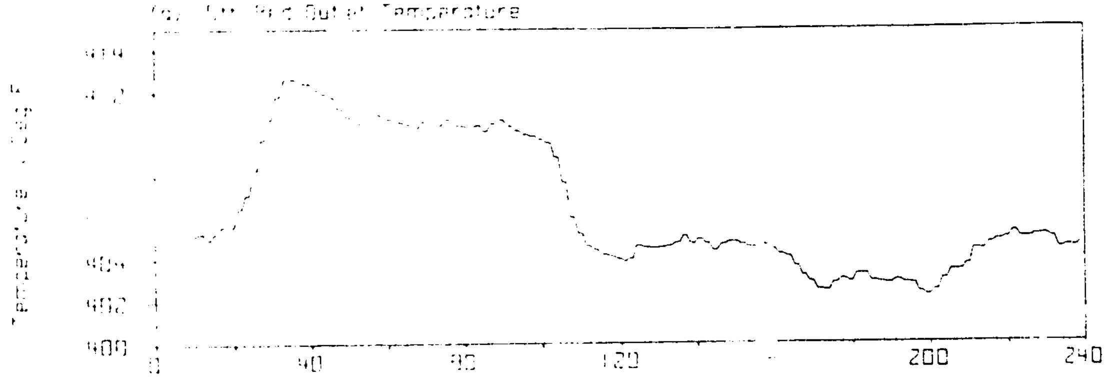
(a) 5th Bed Outlet Temperature

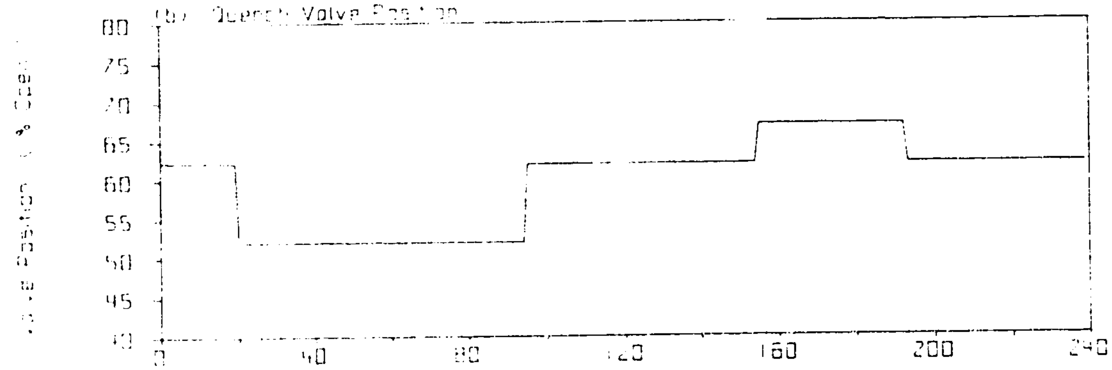
(b) Quench Valve Position

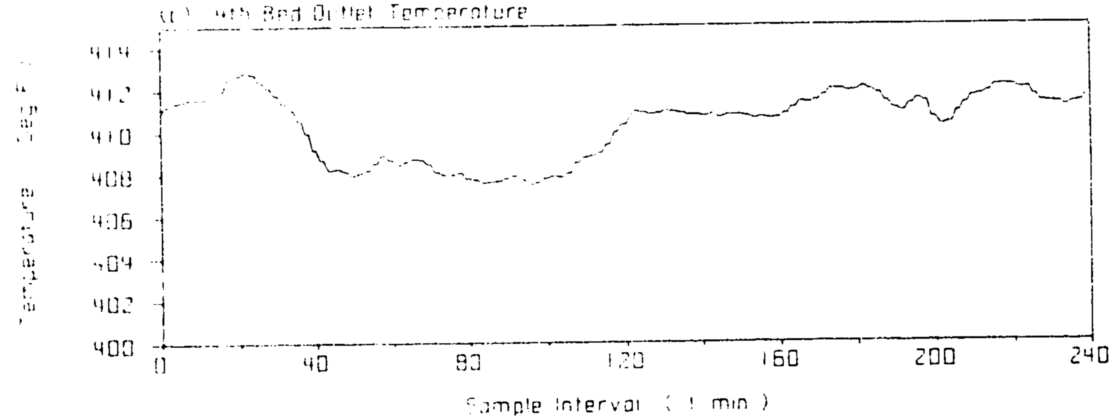
(c) 4th Bed Outlet Temperature

Figure 4.2.3 Reactor Closed Loop PRBS Test

(a) 5th Bed Outlet Temperature

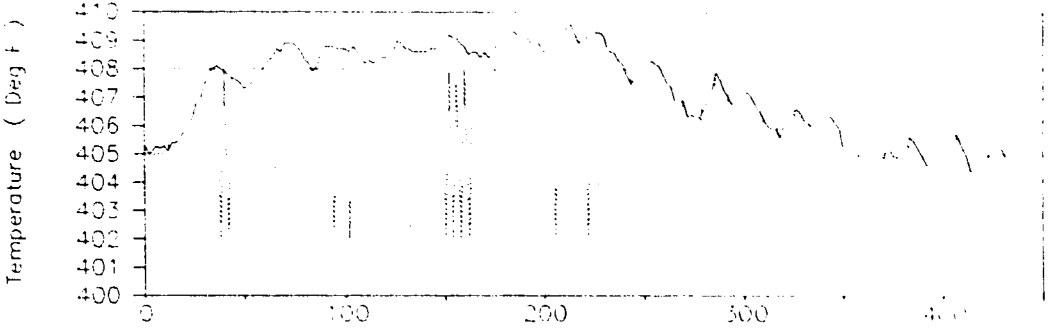

(b) Quench Valve Position

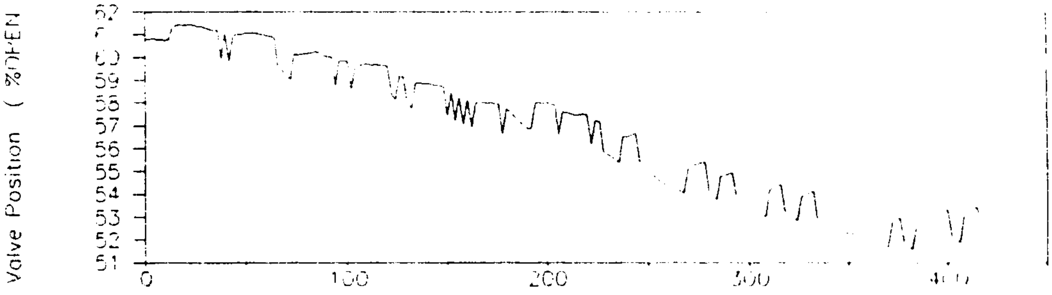

(c) Quench Temperature

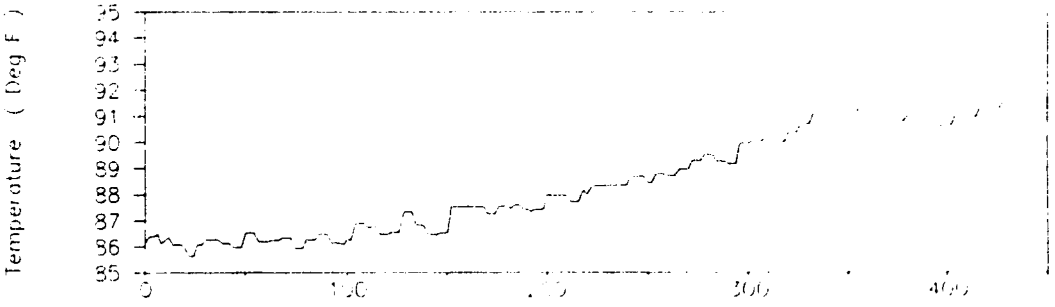

(d) 4th Bed Outlet Temperature

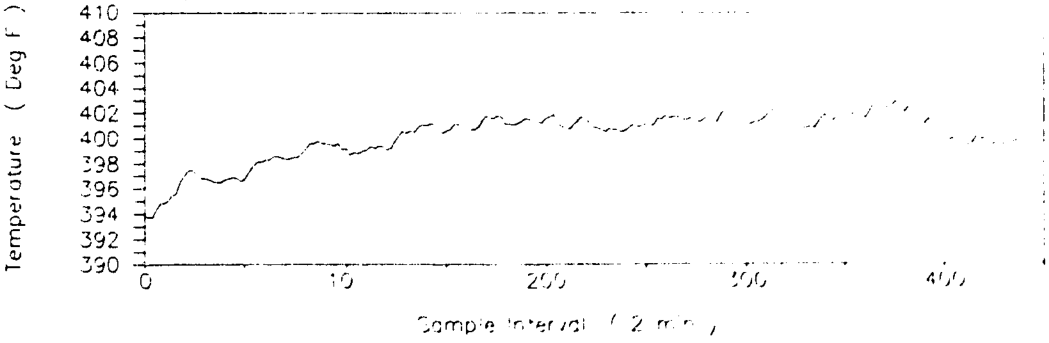

Figure 4.2.4 Off-line Analysis of Reactor PRBS Data

(a) X Correlation of Valve vS 5 Bed Outlet Temp

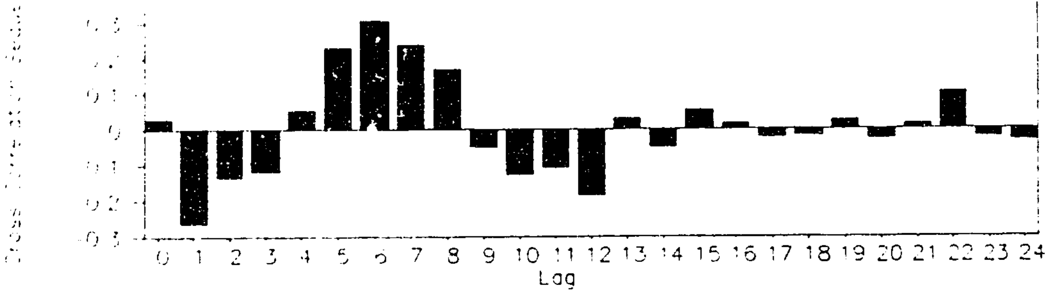

(b) Impulse Response

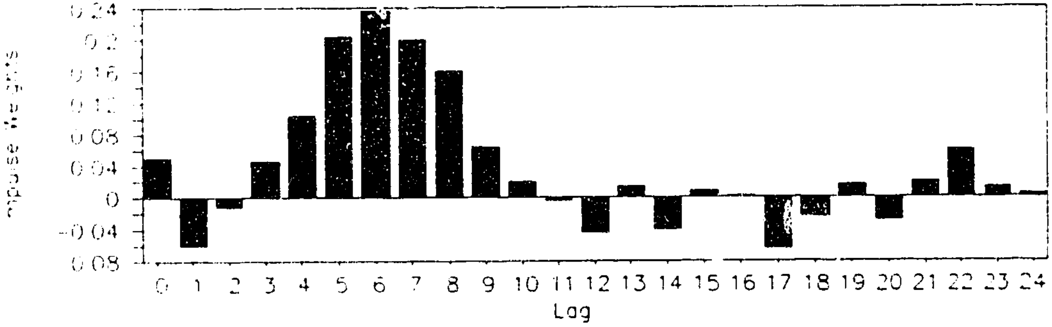

(c) Step Response

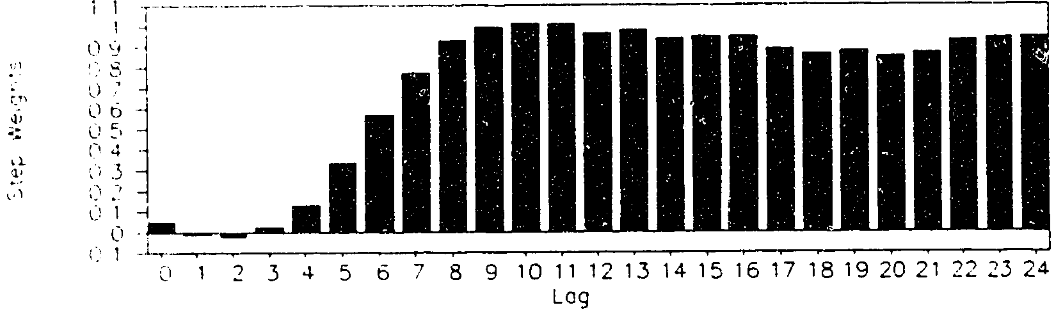

(d)

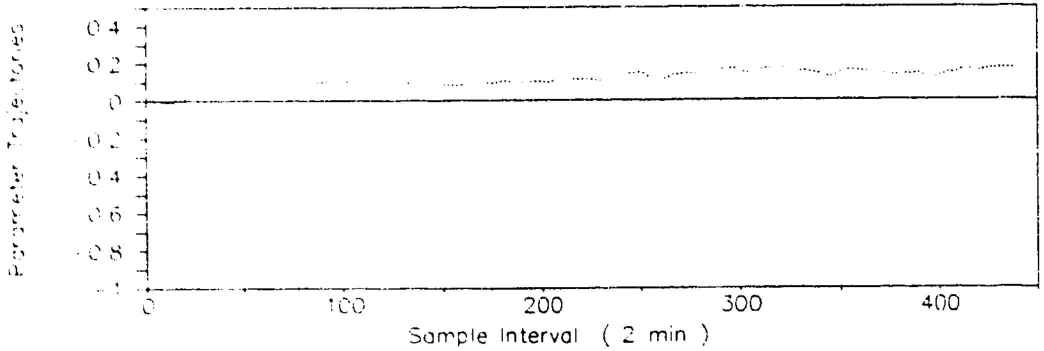

Figure 4.2.4 Off-line Statistical Analysis of PRBS Data

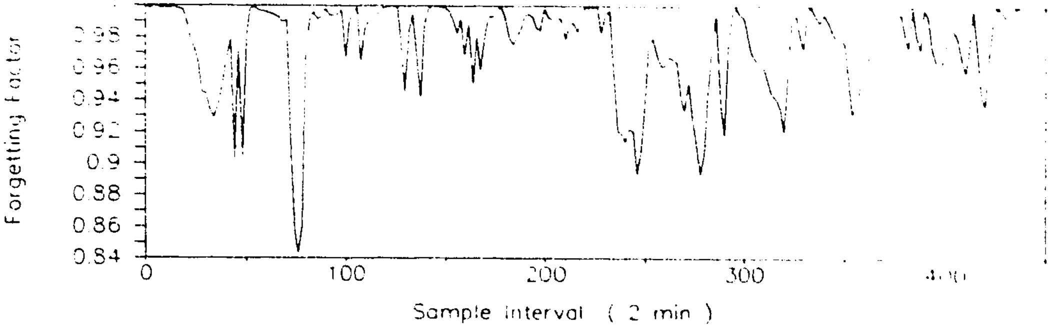

(e) Constant Trace Variable Forgetting Factor

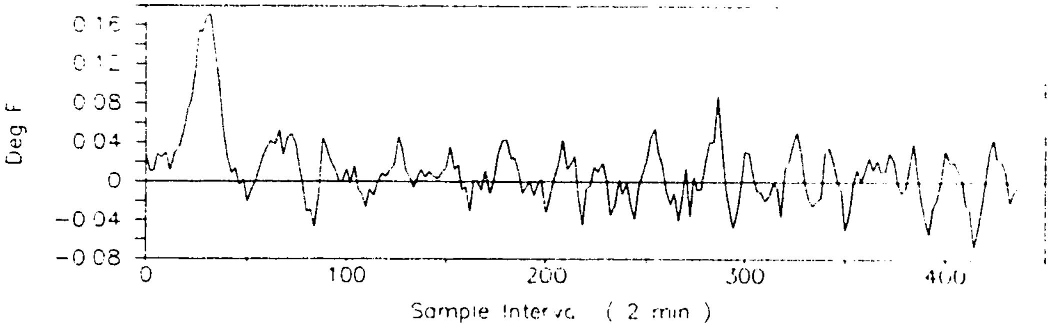

(f) Model Prediction Error

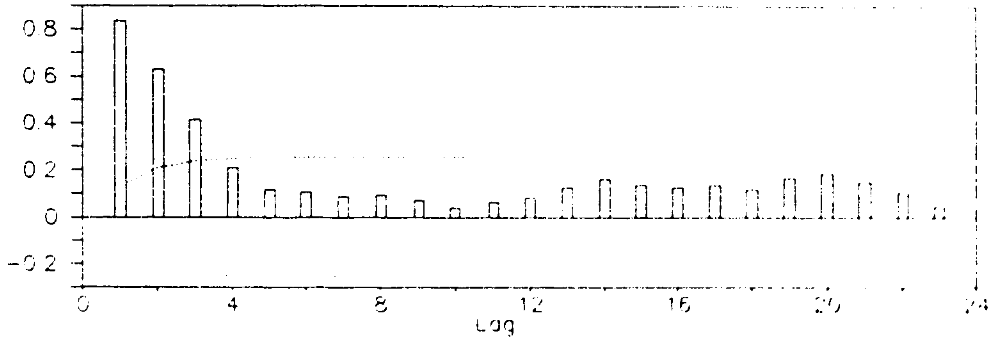

(g) Residual Auto-Correlation Sequence

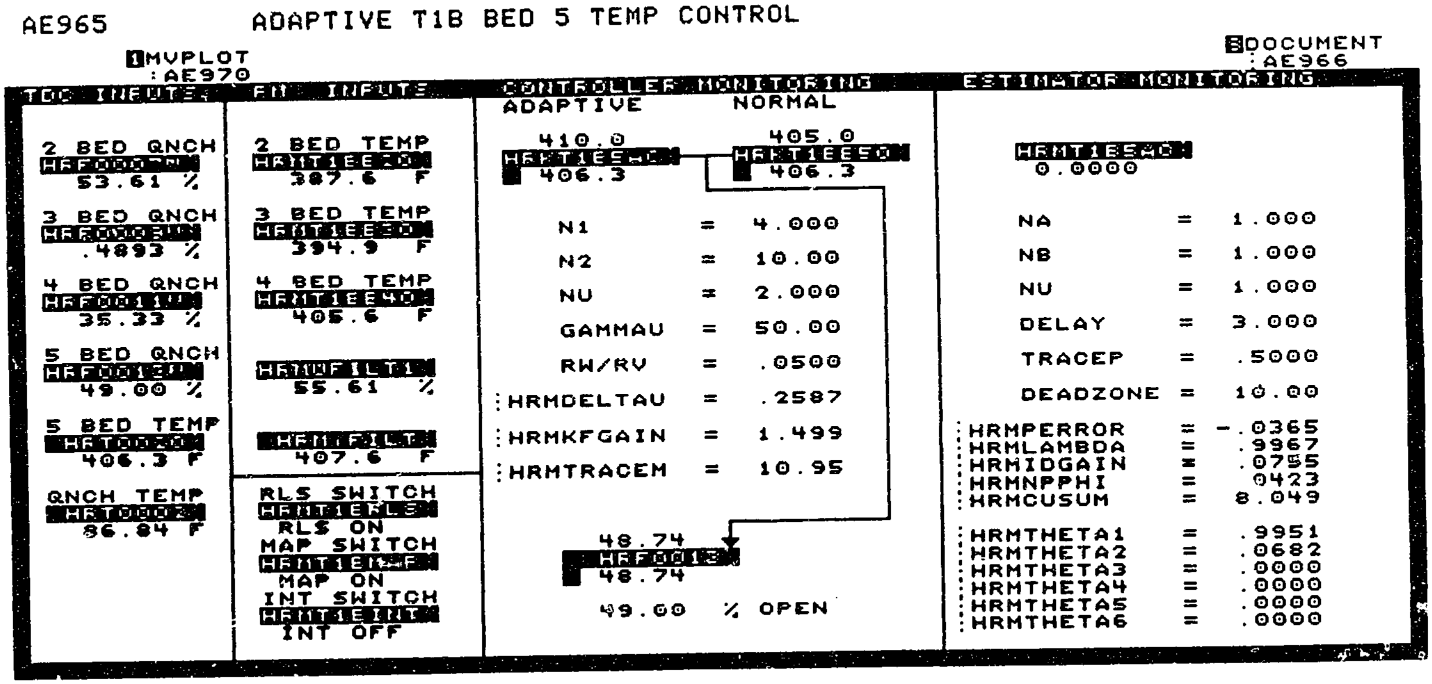

```
AE965          ADAPTIVE T1B BED 5 TEMP CONTROL
          1MVPLOT                                                              8DOCUMENT
           :AE970                                                               :AE966
TDC INPUTS     FN INPUTS       CONTROLLER MONITORING           ESTIMATOR MONITORING
                               ADAPTIVE        NORMAL
2 BED QNCH     2 BED TEMP        410.0          405.0
HRF000[illegible]      HRMT1EE20      HRKT1E5[illegible]   HRKT1EE50          HRMT1E5A[illegible]
  53.61 %        387.6  F          406.3          406.3             0.0000

3 BED QNCH     3 BED TEMP        N1         =   4.000              NA          =   1.000
HRF000[illegible]      HRMT1EE30        N2         =   10.00              NB          =   1.000
  .4893 %        394.9  F        NU         =   2.000              NU          =   1.000
                                 GAMMAU     =   50.00              DELAY       =   3.000
4 BED QNCH     4 BED TEMP        RW/RV      =   .0500              TRACEP      =   .5000
HRF0011[illegible]     HRMT1EE40                                          DEADZONE    =   10.00
  35.33 %        405.6  F       :HRMDELTAU  =   .2587
                                :HRMKFGAIN  =   1.499             :HRMPERROR   =  -.0365
5 BED QNCH     HRMWFILT1        :HRMTRACEM  =   10.95             :HRMLAMBDA   =   .9967
HRF0012[illegible]       55.61  %                                         :HRMIDGAIN   =   .0755
  49.00 %                                                         :HRMNPPHI    =   0423
               HRMMFILT            48.74                          :HRMCUSUM    =   8.049
5 BED TEMP       407.6  F         HRF00013
HRT00020                           48.74                          :HRMTHETA1   =   .9951
  406.3 F      RLS SWITCH                                         :HRMTHETA2   =   .0682
               HRMT1ERLS           49.00   % OPEN                 :HRMTHETA3   =   .0000
QNCH TEMP        RLS ON                                           :HRMTHETA4   =   .0000
HRT00002       MAP SWITCH                                         :HRMTHETA5   =   .0000
  86.84 F      HRMT1E[illegible]                                             :HRMTHETA6   =   .0000
                 MAP ON
               INT SWITCH
               HRMT1EINT
                 INT OFF
```

Figure 4.2.5 Honeywell PMXIII Multi-Step Adaptive Predictive Controller Operator/Engineer Interface

Figure 4.2.6 Reactor MAP Controller 24 Hour Test
14 November 1988

(a) 5th Bed Outlet Temperature

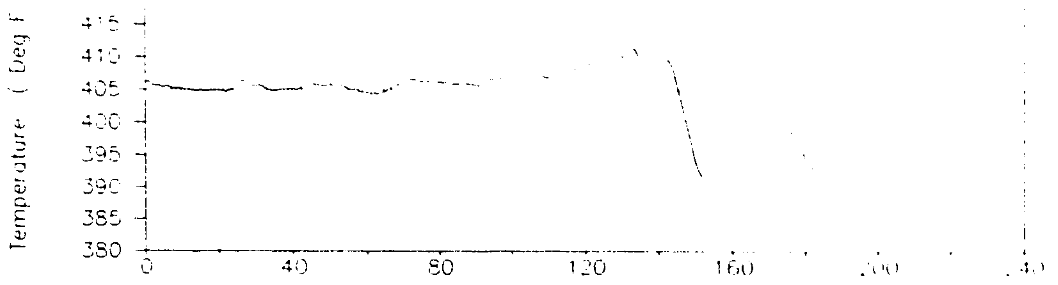

(b) 5th Bed Quench Valve Position

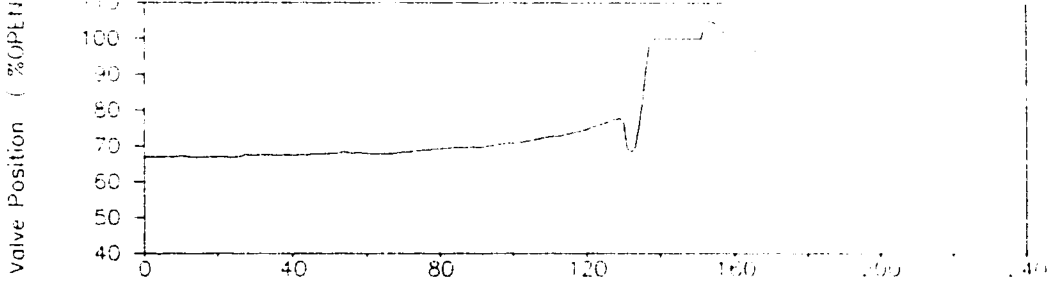

(c) Quench Temperature

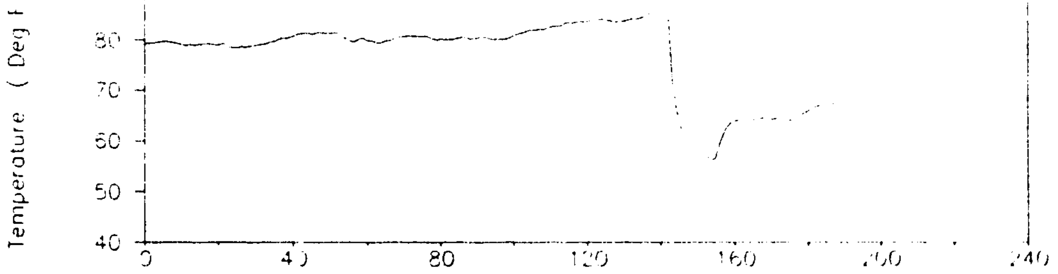

(d) 4th Bed Outlet Temperature

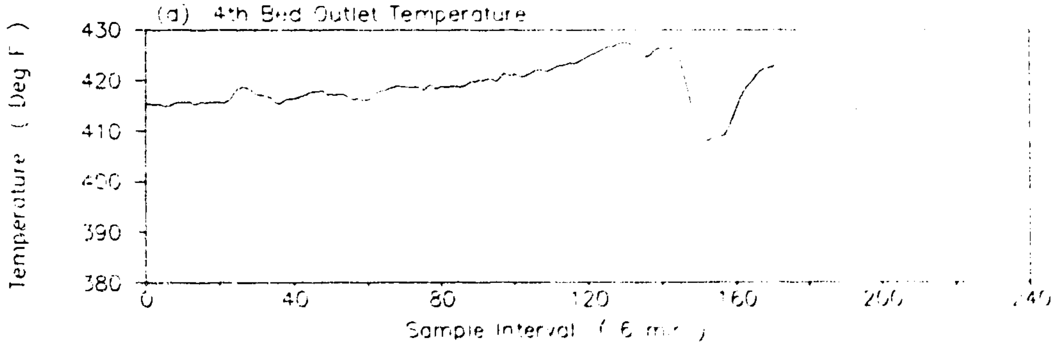

Figure 4.2.7 Reactor MAP Controller 24 Hour Test on 15 November 1988

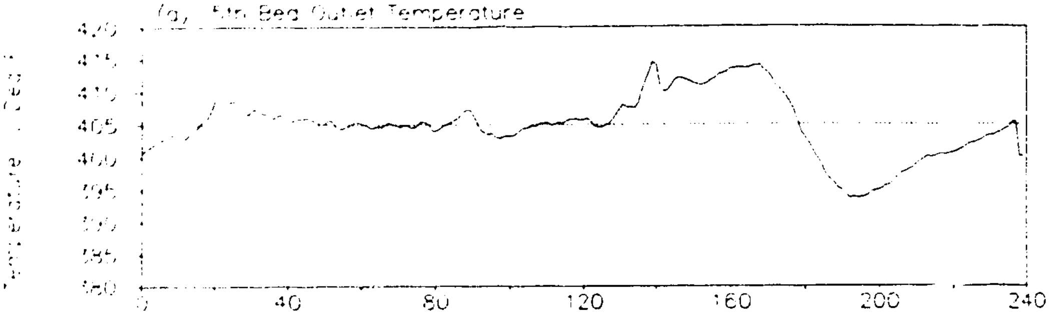
(a) 5th Bed Outlet Temperature

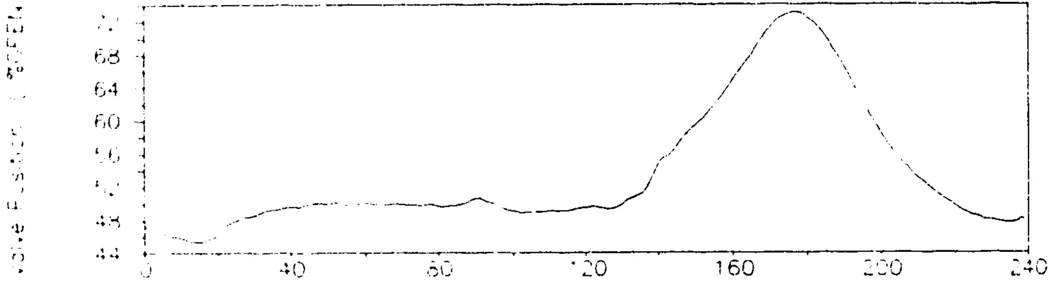
(b) 5th Bed Quench Valve Position

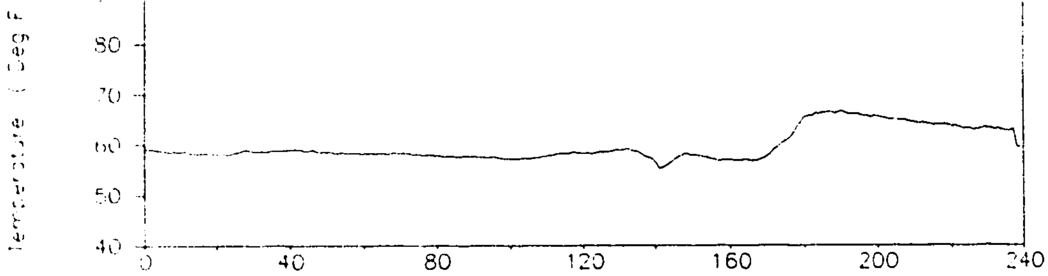
(c) Quench Temperature

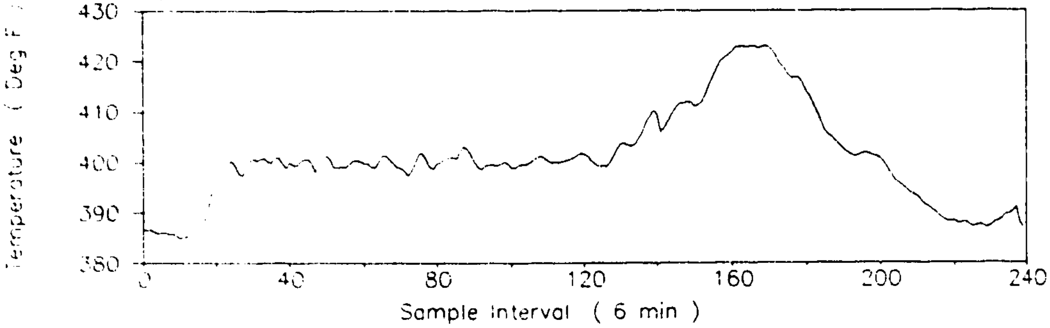
(d) 4th Bed Outlet Temperature

Figure 4.2.8 Reactor MAP Controller 24 Hour Test on 8 December 1988

(a) 5th Bed Outlet Temperature

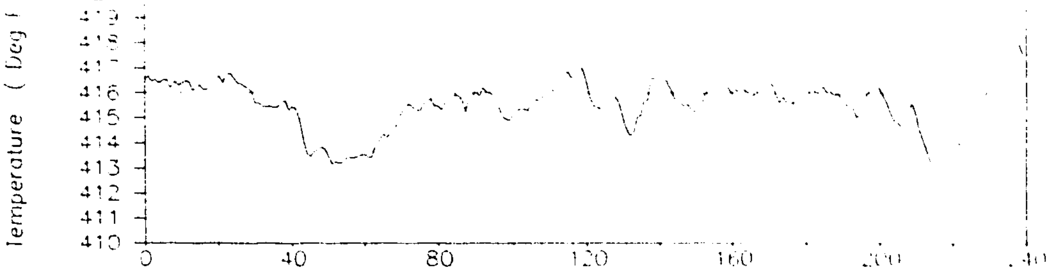

(b) 5th Bed Quench Valve Position

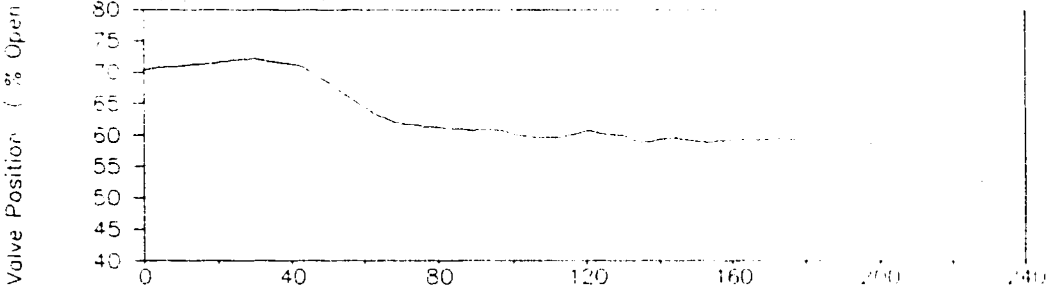

(c) Quench Temperature

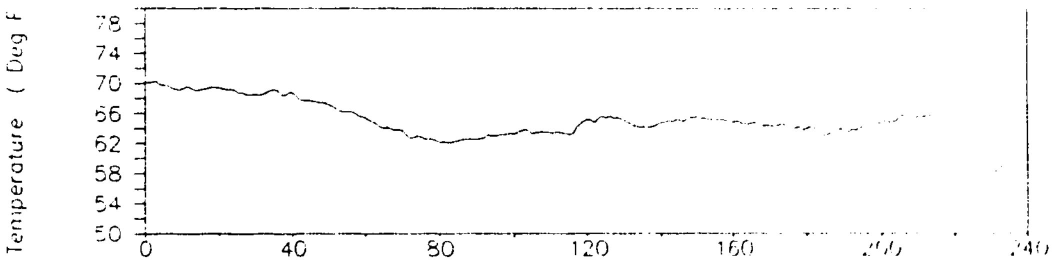

(d) 4th Bed Outlet Temperature

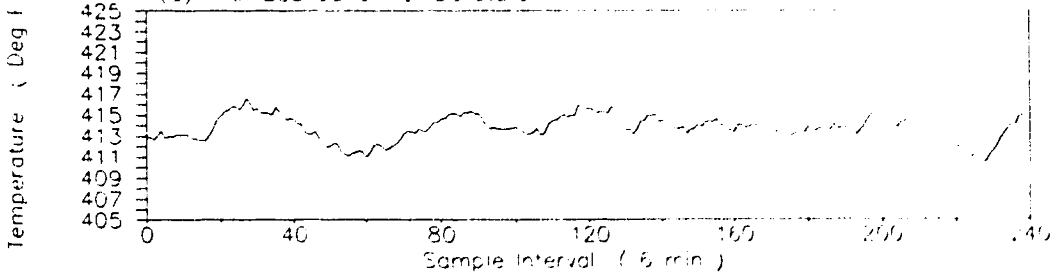

Figure 4.2.8 Reactor MAP Controller 24 Hour Test on 8 December 1988 (...cont)

(e) Model Prediction Error

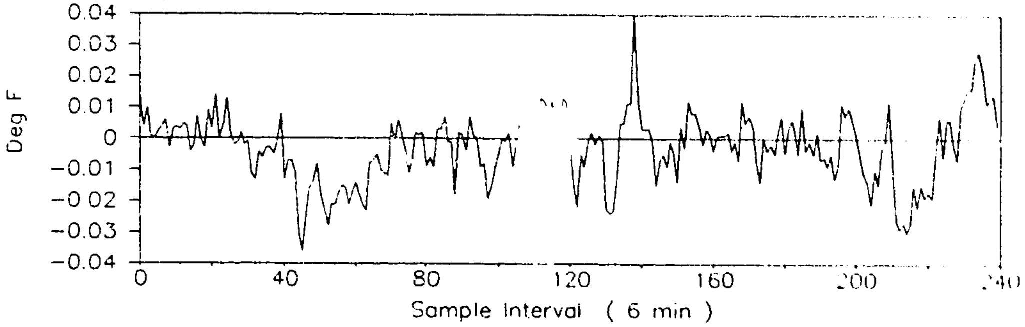

(f) Auto Correlation Sequence

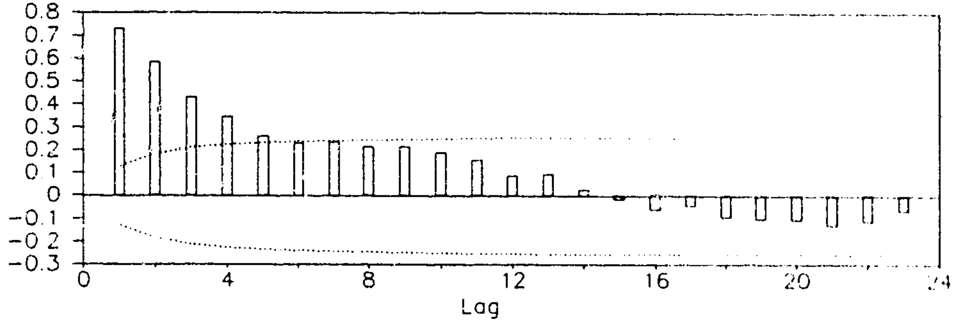

Figure 4.2.9 Reactor MAP Controller 24 Hour Test
9 December 1988

(a) 5th Bed Outlet Temperature

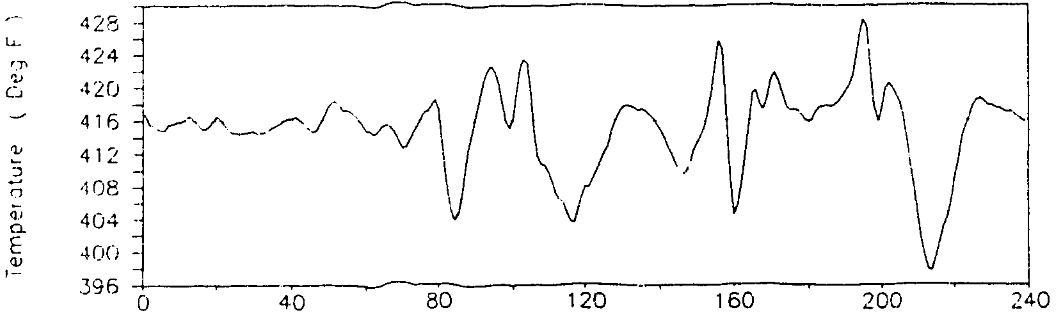

(b) Quench Valve Position

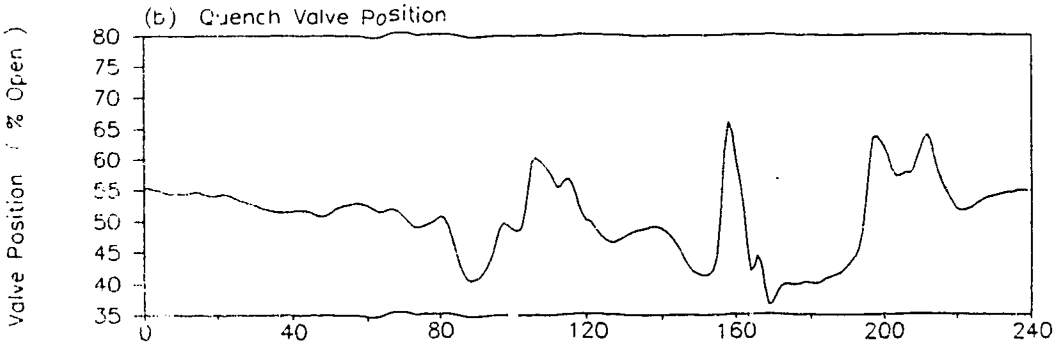

(c) Quench Temperature

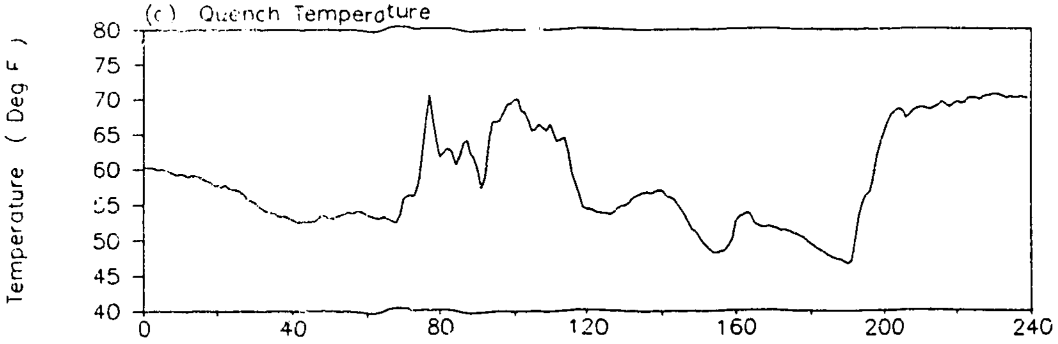

(d) 4th Bed Outlet Temperature

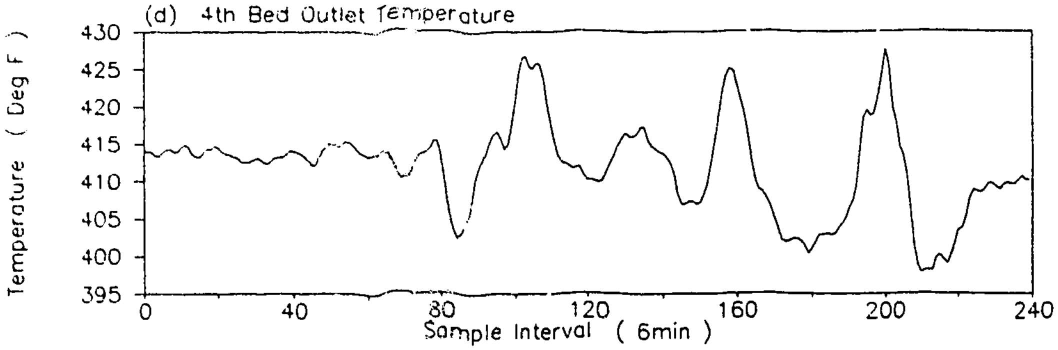

Figure 4.2.9 Reactor MAP Controller 24 Hour Test
9 December 1988

(e) Model Parameter Trajectories

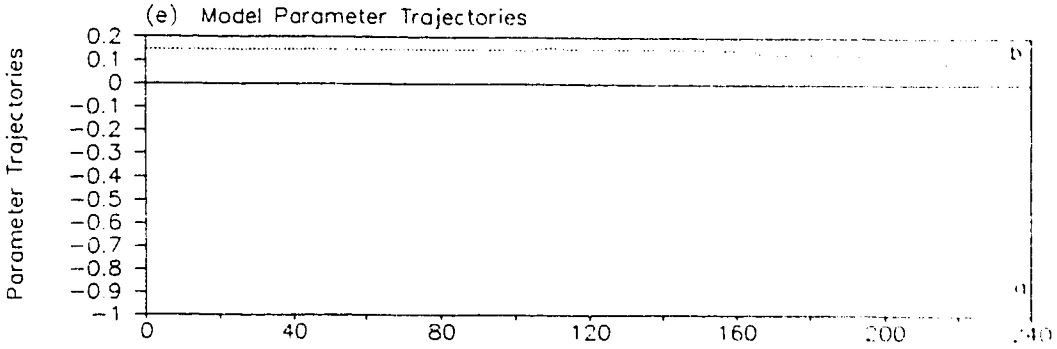

(f) Trace of M

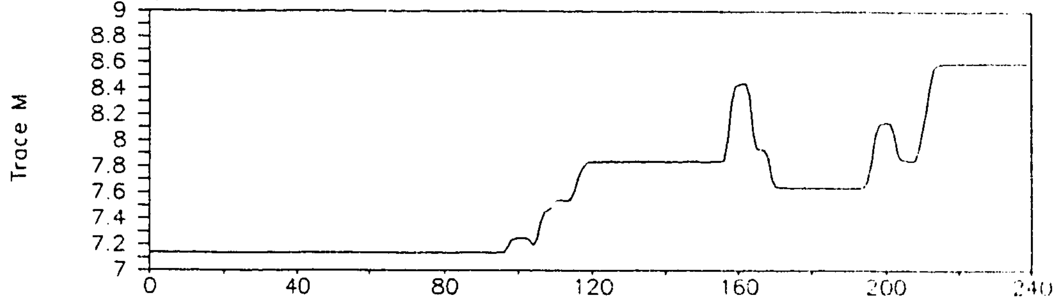

(g) Model Prediction Error

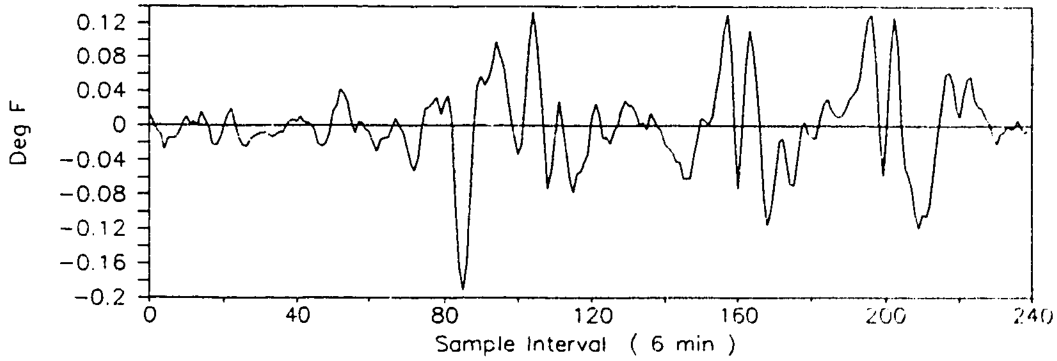

(h) Residual Auto-Correlation Sequence

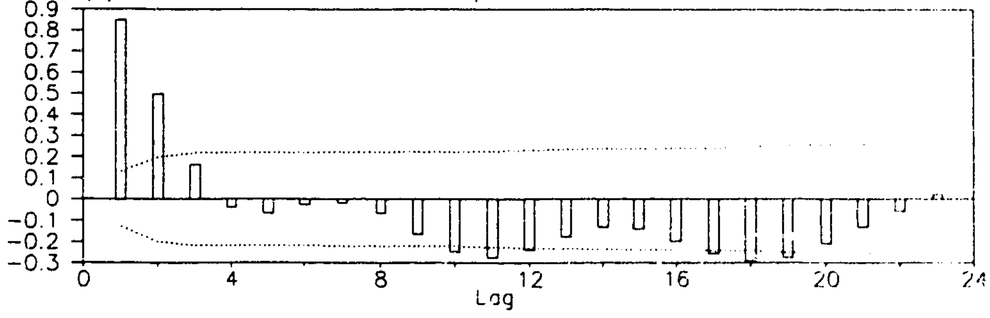

Figure 4.2.10 Reactor MAP Controller 24 Hour Test
10 December 1988

(a) 5th Bed Outlet Temperature

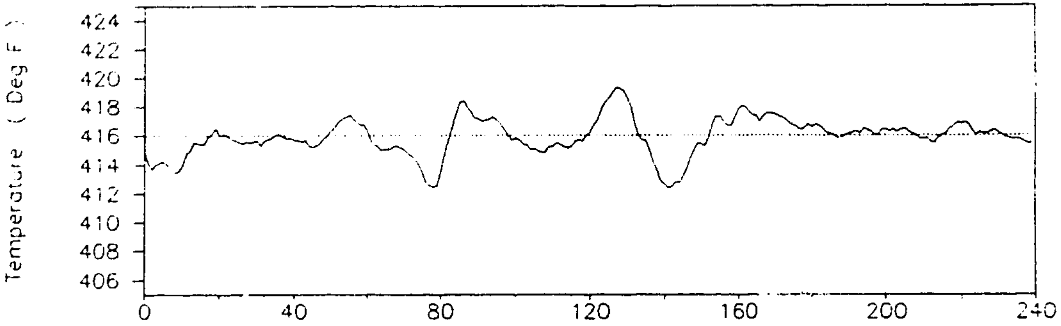

(b) 5th Bed Quench Valve Position

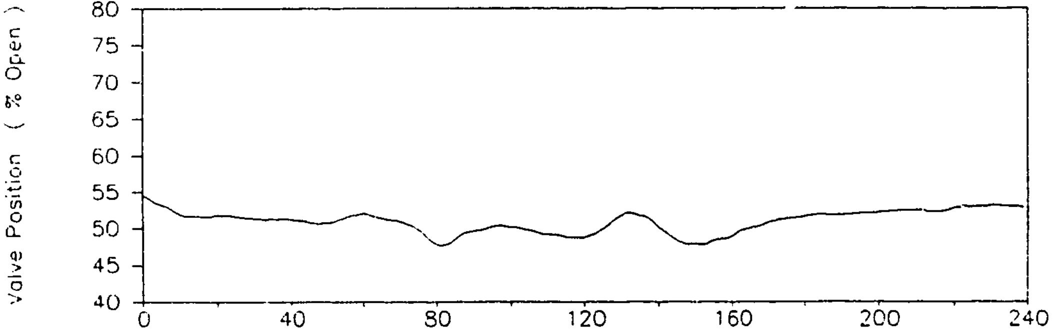

(c) Quench Temperature

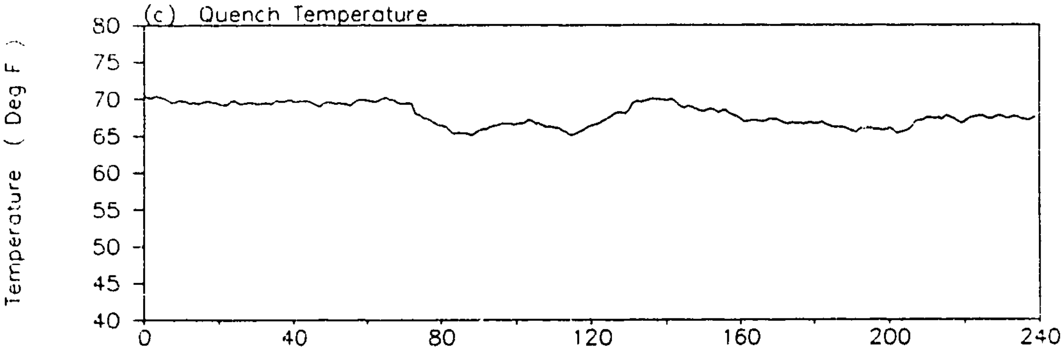

(d) 4th Bed Outlet Temperature

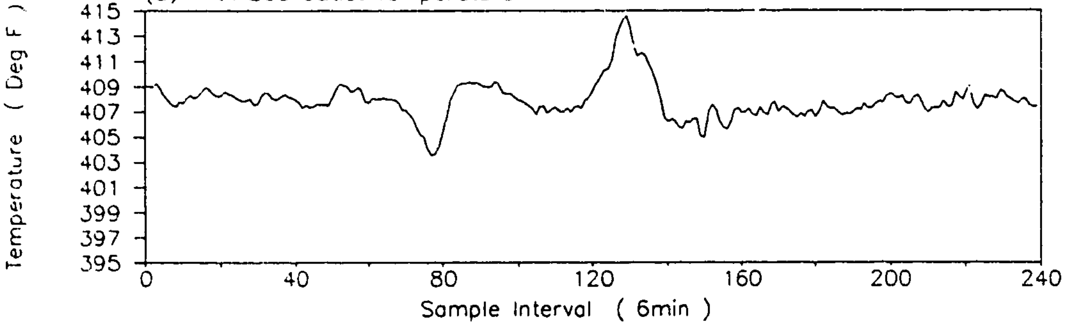

Figure 4.2.10 Reactor MAP Controller 24 Hour Test
10 December 1988 (... cont)

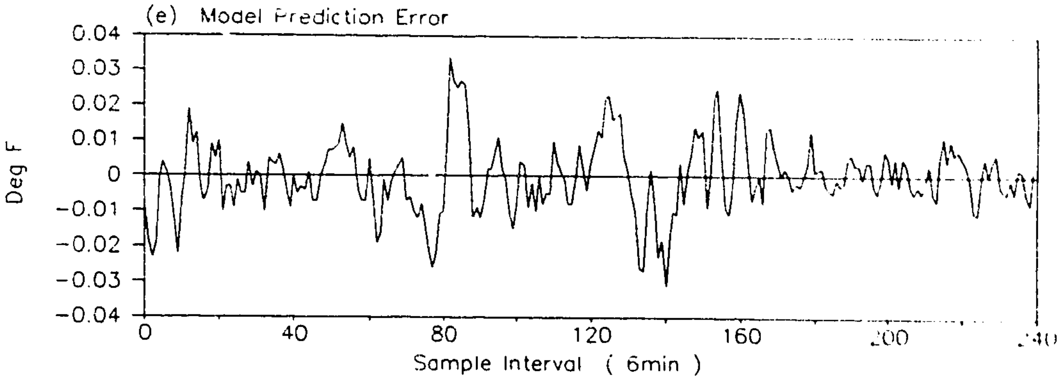

Figure 4.2.11 Reactor MAP Controller 24 Hour Test
12 December 1988

(a) 5th Bed Outlet Temperature

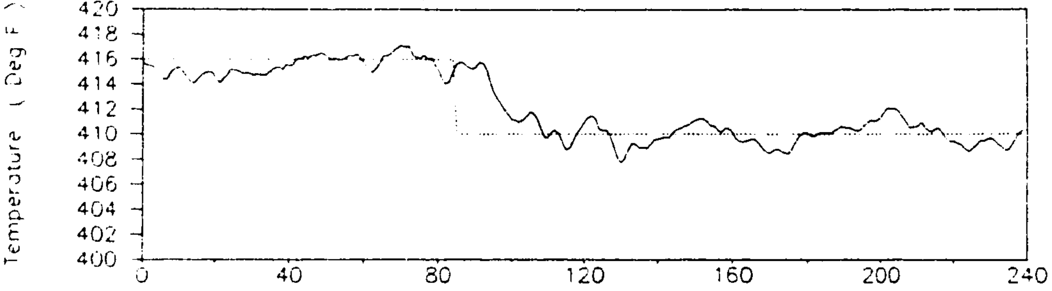

(b) Quench Valve Position

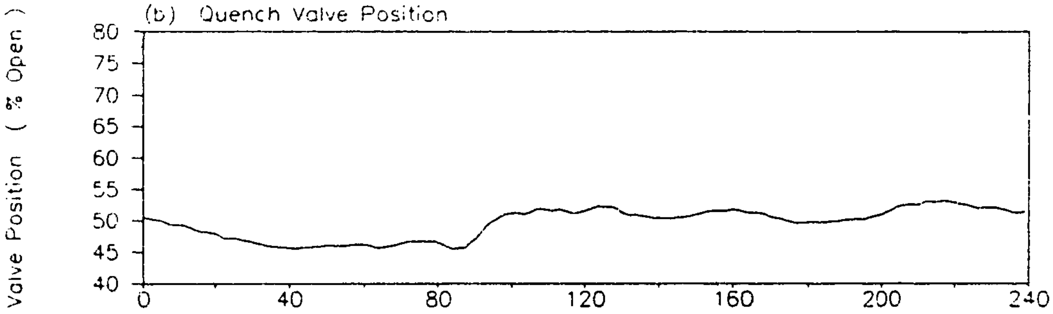

(c) Quench Temperature

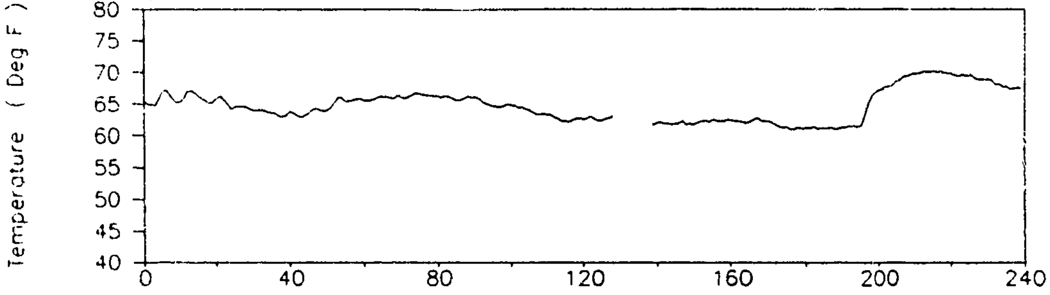

(d) 4th Bed Outlet Temperature

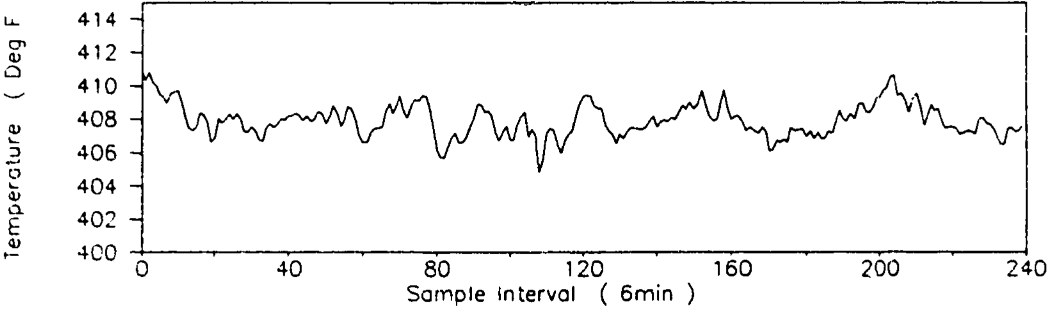

Figure 4.2.12 Reactor MAP Controller Servo Response Test
5 January 1989
N1=4 N2=10 Nu=2 Lambda=50 Rw/Rv=0.05

(a) 5th Bed Outlet Temperature

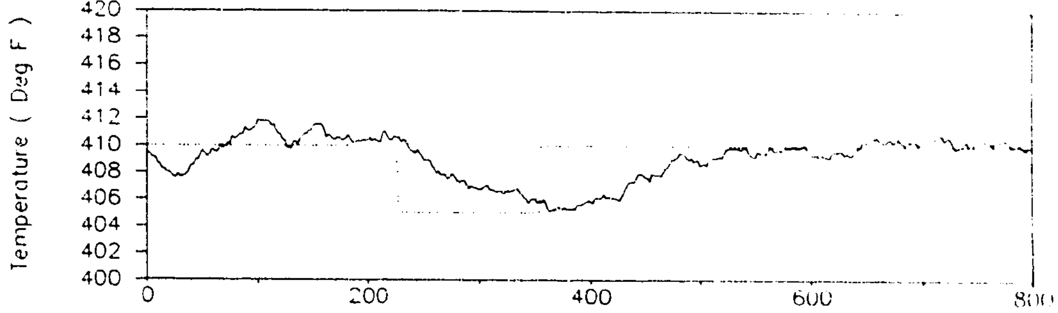

(b) Quench Valve Position

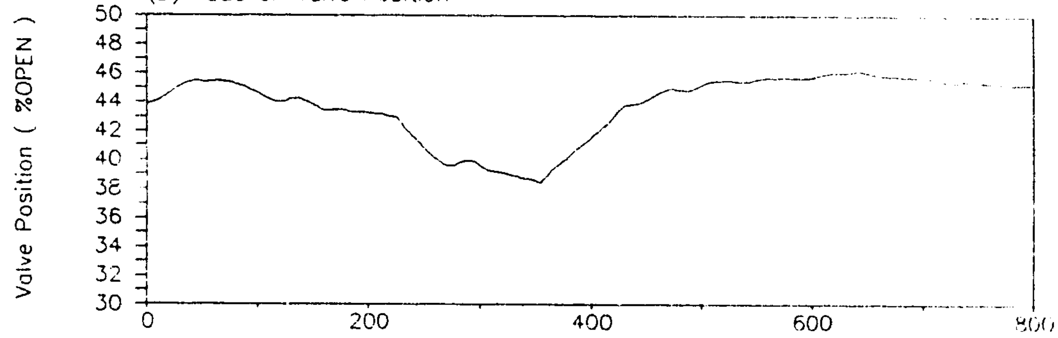

(c) Quench Temperature

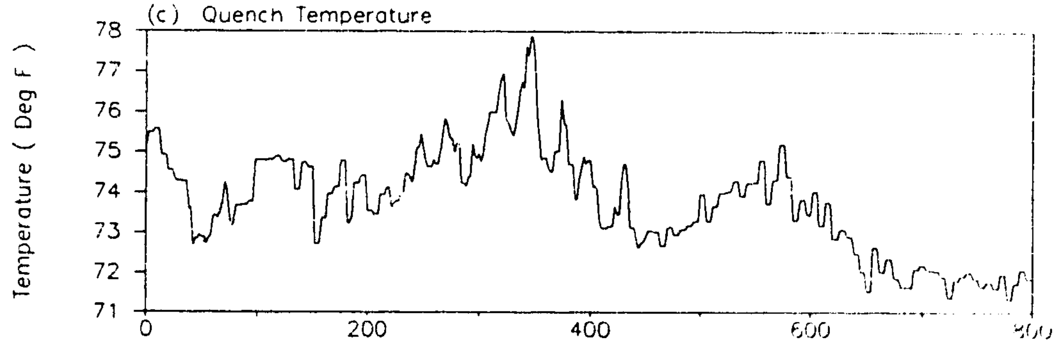

(d) 4th Bed Outlet Temperature

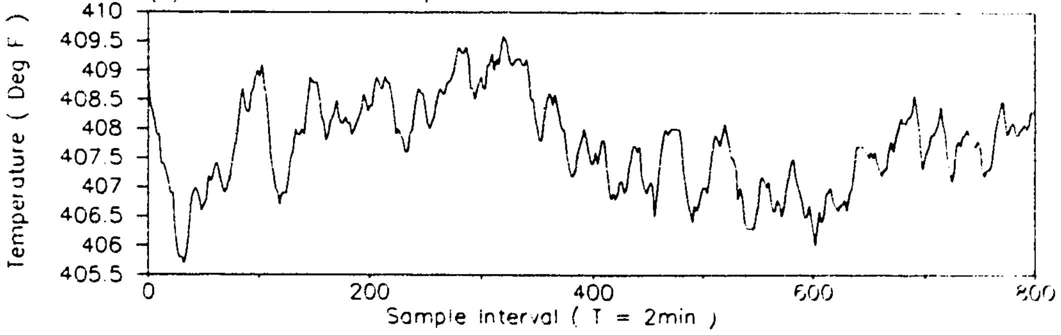

Figure 4.2.12 Reactor MAP Controller Servo Response Test
5 January 1989 (...cont)
N1=4 N2=10 Nu=2 Lambda=50 Rw/Rv=0.05

(e) a Parameter Trajectory

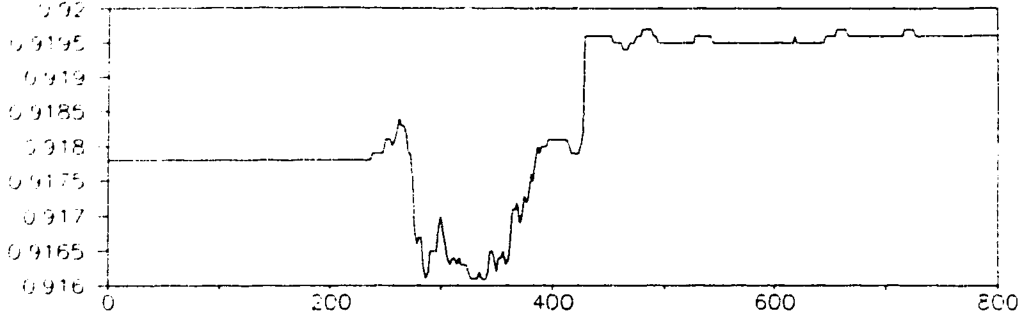

(f) b Parameter Trajectory

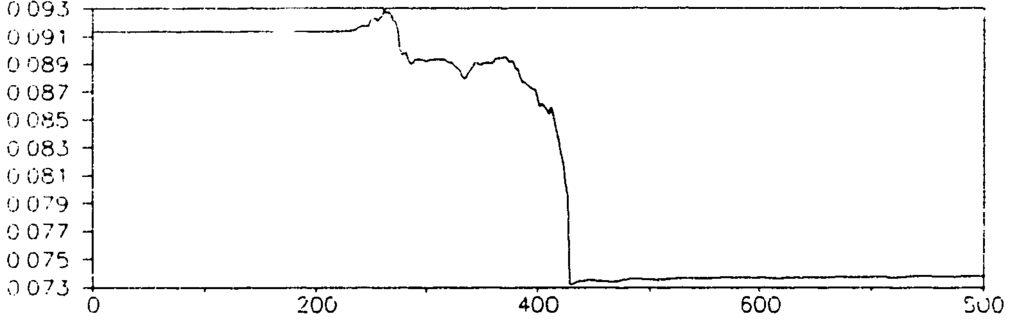

(g) Model Prediction Error

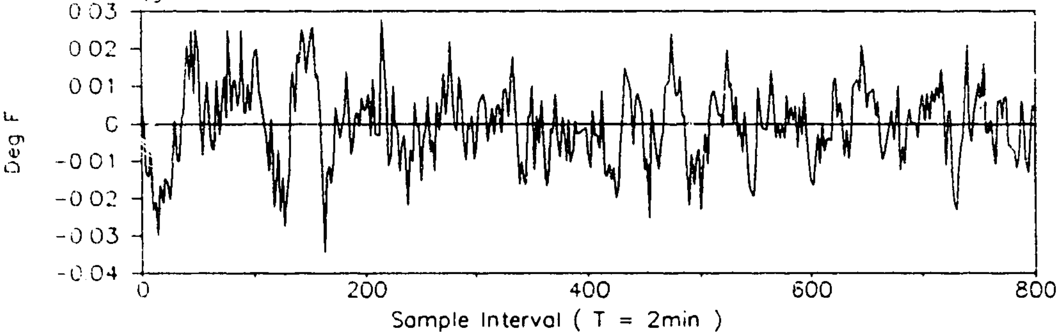

(h) Residual Auto-Correlation Sequence

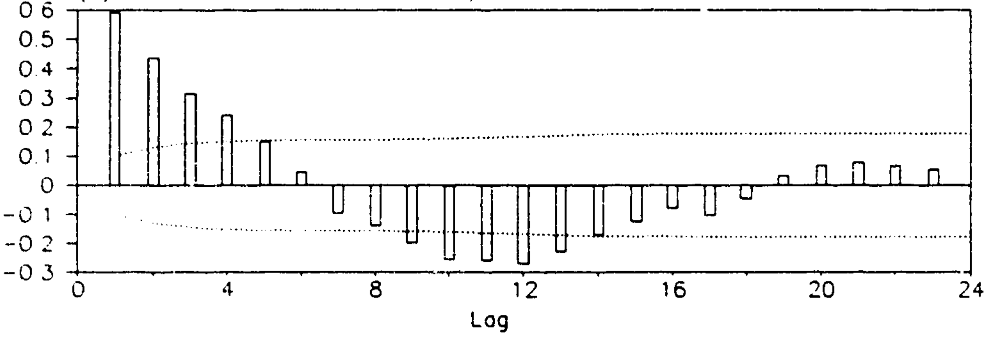

Figure 4.2.13 24 Hour PID Controller Test
30 November 1988
Ko=15, K1=2.2, K2=0.05

(a) 5th Bed Outlet Temperature

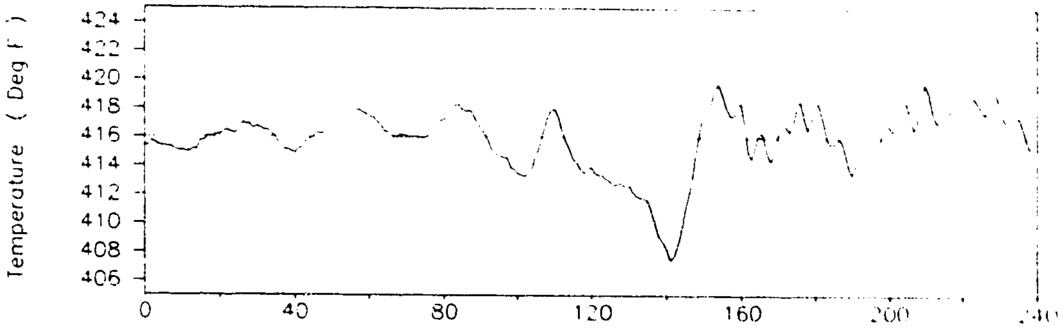

(b) Quench Valve Position

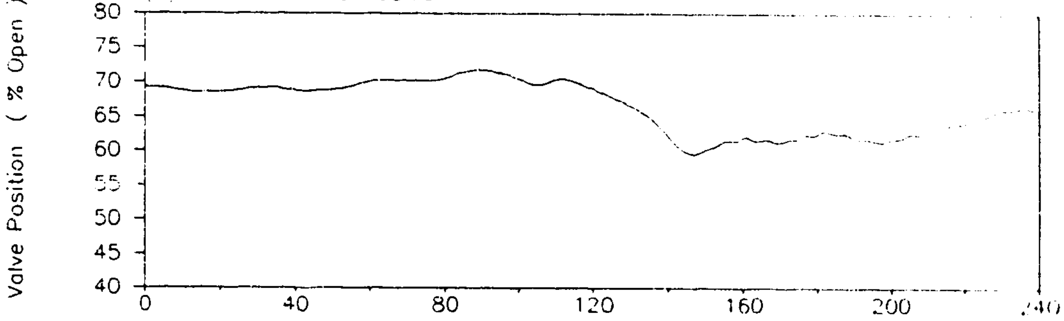

(c) Quench Temperature

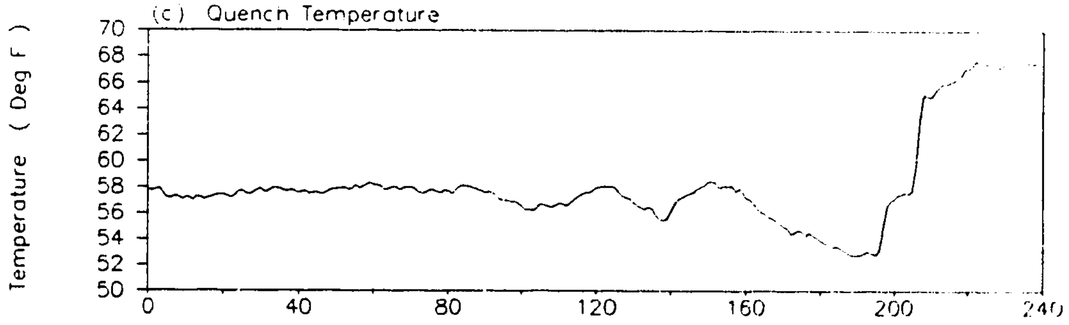

(d) 4th Bed Outlet Temperature

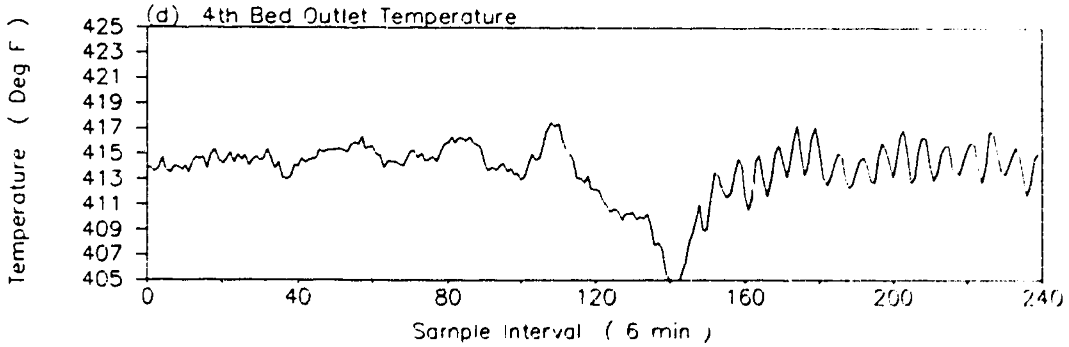

4.3 HYDROFINER TOTAL OUTLET POISONS CONTROL

4.3.1 Process Description

The second industrial application was performed on a somewhat more difficult process than the first. This second process involves the conversion of butadienes, propadienes and methyl acetylenes to butylene and propylene. The main feed to the HOIS unit is propylene which comes directly from the bottom stream of the de-ethanizer at the light ends recovery section of the gas cracking plant. This stream contains alkenes which may cause premature deactivation of the polymer reactor catalyst. In order to prevent this deactivation the propylene stream must be hydrofined.

Figure 4.3.1 illustrates the basic hydrofining operation. Hydrogen gas and propylene flow into a reactor vessel containing a catalyst which selectively converts the methyl acetylene and propadiene to propylene. In controlling the hydrofiner operation, the effluent recycle is maintained constant. The hydrofiner outlet is analyzed on-line for specific poisons using a gas chromatograph. The cycle time of the gas chromatograph is 18 minutes. The poisons are controlled by adjusting the pure hydrogen stream which is injected together with the propylene at the inlet of the hydrofiner.

There are two major disturbances which affect the performance of

Figure 4.3.1(a) Process Diagram of Hydrofiner Control

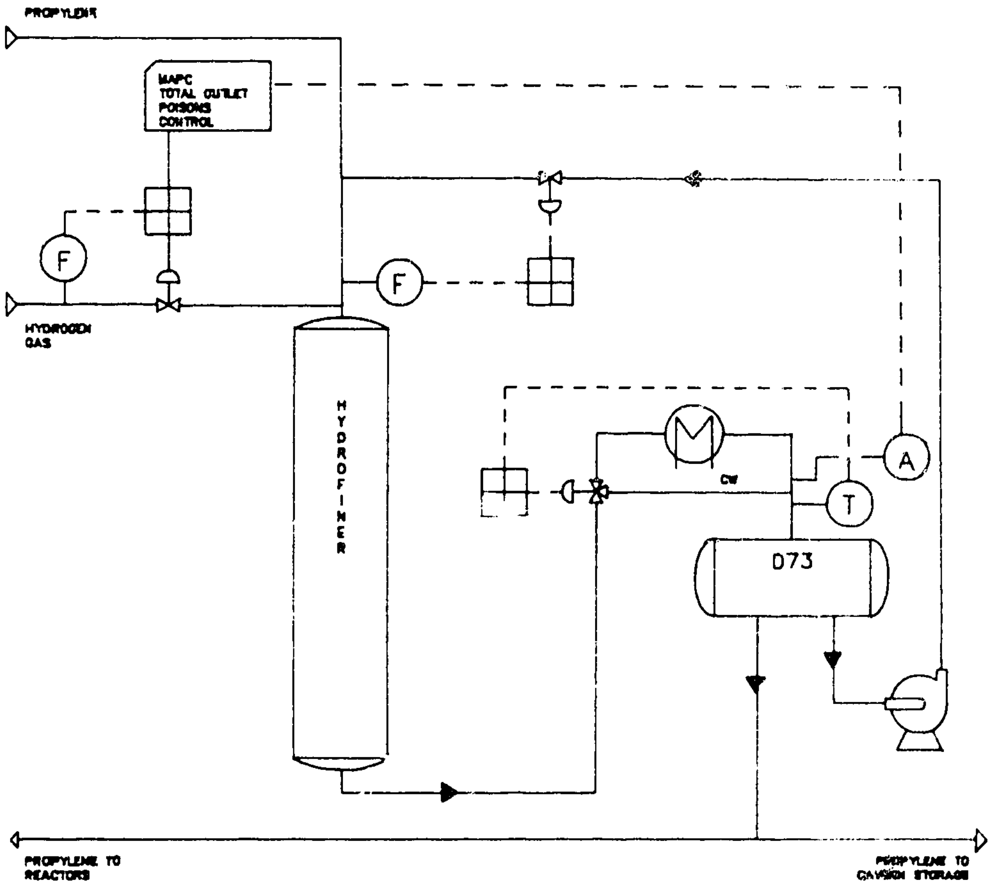
PROPYLENE
MAPC
TOTAL OUTLET
POISONS
CONTROL
F
HYDROGEN
GAS
F
HYDROFINER
CW
A
T
D73
PROPYLENE TO
REACTORS
PROPYLENE TO
CAVERN STORAGE

the hydrofining operation. First the propylene flow varies continuously depending on the inventory in the unit feed surge drum. An increase in propylene flow leads to additional hydrogen being required in order to maintain the total outlet poisons at setpoint. Second, the amount of total poisons contained in the propylene will vary based on the upstream operation. Again, additional hydrogen will be required when an increase in the total inlet poisons is detected.

To control the total outlet poisons, any feedback control strategy will cascade to the Honeywell TDC-2000 hydrogen flow controller. The hydrogen flow may be manipulated by incrementally varying the setpoint of the hydrogen PID flow controller. This strategy differed from the first implementation of the MAP controller in that the first one directly manipulated the valve.

The following section describes the implementation of the MAP controller to the hydrofining process. It summarizes several days of consecutive on-line estimation and control. This application of the MAP controller was significantly more challenging, although not as much caution was exercised as with the first application. This was mainly due to the fact that the hydrogen flow was a "free" manipulated variable, and thus quick, exaggerated fluctuations would not upset any upstream or recycle processes.

4.3.2 Process Model Selection and Identification

The second implementation of the MAP controller followed the same basic steps as the first implementation. Several open loop step tests were done to determine the basic hydrofiner dynamics. Secondly, an open loop PRBS test was performed to more rigorously define the dynamics and include them in a discrete time model which could then be used by the MAP controller. These parameters would form the basis for the on-line model.

This second implementation of the MAP controller did not utilize much off-line simulation or modelling. Confidence gained in the first implementation allowed for a quicker and smoother commissioning. The following section describes the details of establishing the initial model. The remaining sections focus on the experiments performed with the MAP controller.

Open Loop Step Tests

The HOIS operators often run the hydrofiner in open loop due to problems with the existing PID control strategy. Because of this, it was very simple to perform and obtain data for the open loop step tests. Figure 4.3.2 and 4.3.4 clearly show two individual step tests that were performed on different days in an attempt to keep the total outlet poisons to a target value of 350 ppm. The total inlet poisons on both days ranged from 5300 to 7200 ppm.

The fresh feed to the hydrofiner in the Figure 4.3.2 is approximately 20-30 BPH higher than in Figure 4.3.3. These two parameters, mainly the total inlet poisons and fresh feed, significantly influence the performance of the hydrofiner. Specifically, these two parameters will cause the process gain K_p to fluctuate as they represent loads and different operating points to the overall system.

Figure 4.3.2 shows the first step test occurs at T_s= 148, when the hydrogen flow was increased from 2.9 to 3.5 KSCF/HR. This resulted in a reduction of the total outlet poisons from 1981.7 to 190.3 PPM, and a continuous time gain of K_p= -29.85. The corresponding time constant τ_p=48 minutes and the time delay τ_d=18 minutes. As was discussed in Chapter 3, it is advantageous to have both the input and output units in the same dynamic range for numerical purposes. In this case the input, or the hydrogen flow was multiplied by 100. This factor would aid in reducing numerical round-off problems.

Similar continuous time parameters may be established when Figure 4.3.3 is examined. In this Figure the gain is K_p= -12.4. The time constant and time delay are τ_p= 42 min. and τ_d= 18 min. The resulting discrete time process models from the step tests may be summarized as follows when the sample time is $T_s = 6$ min.

$$\Delta y(k) = \frac{-3.50 \cdot z^{-1}}{1 - 0.8824 \cdot z^{-1}} \cdot \Delta u(k-3)$$

and

$$\Delta y(k) = \frac{-1.657 \cdot z^{-1}}{1 - 0.8668 \cdot z^{-1}} \cdot \Delta u(k-3)$$

The sample time was chosen to be approximately $\frac{1}{7}\tau_p \cong 6$ minutes. This sample time was a good selection as it corresponds well with the manner in which the Honeywell PMX computer schedules the processing of real-time programs.

Open Loop PRBS Test

Figure 4.3.3 illustrates the open loop PRBS test that was performed. At $T_s \cong 70$ the total outlet poisons were brought to 600 ppm by stepping the hydrogen flow from 3.1 to 3.3 KSCF/HR. After this the PRBS test began with a hydrogen mean level of 3.3 KSCF/HR. The PRBS signal magnitude was chosen to be ±200 SCF/HR and the switching interval was $T_{sw} = 12$ minutes. The PRBS controller was scheduled to run every 6 minutes, and incrementally adjusted the hydrogen flow controller. Both the mean level and signal magnitude could be adjusted on-line so that the total outlet poisons target could be maintained by the operators. This on-line mean level adjustment occurred soon after the PRBS test began. The mean level was changed from 3.3 to 3.1 KSCF/HR. At the conclusion of the test the hydrogen was adjusted to 3.4 KSCF/HR which allowed the total outlet poisons to be maintained at a target of 350 ppm.

This PRBS data was then used to identify an off-line discrete time model using the IDSA software package (McGregor and Taylor, 1986). The results of the off-line identification produced the following model :

$$\Delta y(k) = \frac{-4.0383 \cdot z^{-1}}{1 - 0.7060 \cdot z^{-1}} \cdot \Delta u(k-3)$$

Again the sample time was T_s=6 minutes. When the step test and PRBS test models are compared they seem to agree very well. The PRBS model has a somewhat higher gain and faster time constant. This was shown in the last experiment not to be a serious concern once the on-line estimator is functioning.

Figure 4.3.5 illustrates the parameter trajectories that correspond to the on-line step test that was performed on 3 December 1988. The $tr\{P\}$=0.005 and Δ_d=0.0 for the identification period. The initial parameter estimates were taken from the model parameters identified using the PRBS data. By the end of the identification period, the parameter vector has settled to $\theta^T=[-0.836, -1.92\ ]^T$. These parameters correspond well with the discrete models identified by non-parametric techniques. During this identification period a second order $\Delta/T(z^{-1})$ regressor filter was used with a discrete time pole location of 0.7.

By performing the on and off-line identification, confidence was obtained in the use of the on-line RLS estimator for the hydrofining control problem. Both the step and PRBS test showed good agreement among the various model parameter sets that were identified. Also, the off-line identification allowed for the tuning and initial parameter sets to be determined.

4.3.3 Multi-Step Adaptive Predictive Control of Hydrofiner Total Outlet Poisons Control

The testing of the MAP controller on the hydrofiner took place during the month of December, 1988. The results that are presented correspond to several days of testing where the controller was shown to operate both successfully and poorly over a variety of process conditions.

As was done with the reactor MAP control application, a separate operator/engineer window was built for operating and monitoring the performance of the hydrofiner MAP controller. Figure 4.3.6 illustrates the operator/engineer interface. This interface is identical to the one used for the reactor experiments and thus no further explanation will be made. To turn the MAP controller on the hydrogen flow controller would simply be changed from AUTOmatic mode to COMputer mode.

Figure 4.3.7(a)-(h) illustrates the first attempt to place the MAP controller on-line. Prior to placing the controller on, the RLS estimator was allowed to run for several days with the following tuning parameters:

$$tr\{P\} = 0.005, \quad \Delta_d = 0, \quad \text{and} \quad \frac{\Delta}{T(z^{-1})} = \frac{0.09\cdot(1-z^{-1})}{1-1.4\cdot z^{-1}+0.49\cdot z^{-2}}$$

At $T_s=80$, an open loop PRBS test was attempted by manipulating the hydrogen flow controller setpoint. Unfortunately, soon after the test was started, the gas chromatograph analyzer failed, and was brought back on-line at about T_s=110. During the analyzer outage the RLS estimator was turned off as is indicated by the constant model prediction error in Figure 4.3.7(g). At T_s=110, the MAP controller was turned on with its tuning parameters set as follows:

$$N_1 = 1, \quad N_2 = 10, \quad N_u = 1, \quad \lambda = 10\,000, \quad R_w/R_v = 0.05$$

As the controller was turned on, the RLS estimator trace specification was set to *tr(P)*=0.1 during the period from $130<T_s<160$. After this period, the *tr(P)* was set back to a value of 0.005. Figures 4.3.7(e)-(f) illustrate the parameter trajectories during this period. The final steady state model parameter values are $\theta^T = [\ -0.82 \quad -3.5\ ]^T$. With the parameters identified, the gain of the estimator was reduced to *tr(P)*=0.005. This value was chosen as it would allow the estimator to respond slowly to any parameter changes. Also, it would prevent any significant interactions with the controllers Kalman Filter. Looking at the MPE plot, Figure 4.3.7(g) shows a reduction in the residual variance after the identification period. This would indicate the the newly identified model will perform better than the old, as it will be able to provide a better prediction of the future process output.

Figures 4.3.8(a)-(g) illustrate the results of the previous days estimation and controller tuning. During the sample interval $0\le T_s \le 80$, the total outlet poisons began to drift from 350ppm towards an asymptotic value of 2000ppm. This was caused by the slow increase in the total inlet poisons, which caused a similar drift in the $\hat{b}$ or discrete gain parameter. In fact, Figure 4.3.8(f) shows a sign reversal in the $\hat{b}$ trajectory. Because the controller was extremely detuned with a control weighting of λ=10,000, it did not respond to the $\hat{b}$ parameter shift.

At $T_s \cong 100$ the controller tuning was changed to,

$$N_1 = 4, \quad N_2 = 10, \quad N_u = 2 , \quad \text{and} \quad \lambda = 1200$$

These new tuning parameters would permit the controller to respond much faster to disturbances which affect the total outlet poisons. With the tuning changes and the slow decrease in inlet poisons, the parameters again drifted and were re-identified by T_s=210 as θ^T=[-0.875 -4.00]^T. At this point, the estimator was turned off to allow viewing of the MAP controller in a non-adaptive role. With the new model parameter set identified, it was also noticed that the standard deviation in the model prediction error had decreased from $\hat{\sigma}_e$=7.44ppm to a $\hat{\sigma}_e$=1.73ppm. This represents a significant reduction in MPE variation with the newly identified parameters.

Figure 4.3.8(h) represents the auto-correlation sequence for the MPE of Figure 4.3.8(g). The auto-correlation sequence identifies the degree of whiteness in the MPE. Ideally all values corresponding to lags>0 should be below the $2\hat{\sigma}$ limits. However, since a low order model is being fitted to a process which may possess several higher frequency pole locations there exist structured model errors. The auto-correlation sequence in this diagram reveals that some correlation does exist as is evident from the first 3 lags being above the $2\hat{\sigma}$ limits. Once inside the $2\hat{\sigma}$ limits, any trends in the data are investigated to reveal the structure of the noise. In this case, it is apparent that after the 16th lag, the MPE is positively biased. This would suggest that the prediction of the total outlet poisons is typically lower than the actual value. This could be corrected by some additional noise filtering of the regressor vector if an AR model was fitted to the MPE and then used as the regressor filter. This typically is extremely difficult to do in the adaptive case. Several authors have demonstrated that estimating a $C(z^{-1})$ or noise polynomial can be extremely difficult because it takes the parameters of the polynomial so long to converge.

Figures 4.3.9(a)-(g) illustrate the performance of the MAP controller with the RLS estimator turned off. Figures 4.3.9(e) and (*f*) show that throughout the entire 24 hour test period no identification was performed with the parameter vector being $\theta^T=[\ -0.877\ \ -3.98\ ]^T$. The controller tuning parameters were set as follows,

$$N_1 = 4,\quad N_2 = 10,\quad N_u = 2,\quad \lambda = 400 \quad \text{and} \quad R_w/R_v = 0.001$$

These controller tuning parameters would allow the controller to manipulate the hydrogen flow setpoint quite strongly as compared to the previous tests. In this instance, $\lambda=400$ corresponded to an *m*-factor of 0.6149.

Figures 4.3.9(a) and (b) illustrate the controllers response to step type disturbances in the inlet poisons and fresh feed flows. The first disturbance was noted in Figure 4.3.9(d) at $T_s \cong 70$ where the fresh feed to the hydrofiner has increased from 125 to 180 barrels per hour (BPH). During this time the inlet poisons had remained fairly steady. The fresh feed disturbance caused a subsequent increase in the total outlet poisons from 350 to 950ppm. The controller responded quickly as is shown by the rapid increase in hydrogen flow which caused the outlet poisons to return to its initial target of 350ppm in 25 sample intervals or 150 minutes.

At $T_s = 145$ the HOIS operators had noticed a dramatic step increase in inlet poisons of 700ppm and proceeded to turn the MAP controller off. At this time, they manually increased the hydrogen flow to 3.05 KSCF/HR and then turned the MAP controller back on. It should be noted that in a similar instance with the PID controller, that the operators would have performed the same function, and assisted the process to return to steady state in a manual fashion. With the controller back on-line, it continued to provide excellent regulation of total outlet poisons. This regulation is again illustrated at $T_s \cong 145$ where another step increase of 50 BPH of fresh feed occurred. Again, the total outlet poisons were reduced from a level of 1000ppm to their desired target of 350ppm in a matter of 20 sample intervals or 120 minutes.

Soon after recovering from this 50 BPH increase the fresh feed to the hydrofiner was cut by 90 to 100 BPH. This represents a dramatic decrease in fresh feed and the result to the total outlet poisons was a reading of 0ppm. The MAP controller was unable to manipulate the hydrogen flow quick enough to bring the outlet poisons to the 350ppm target by the end of the 24 hour test period.

Looking at Figure 4.3.9(g) the MPE fluctuated in conjunction with the disturbances that occurred during this period. As the fresh feed increased rapidly, the total outlet poisons also increased. Since the model did not account for the disturbances, the prediction was lower than the actual output. This resulted in an increased MPE magnitude during periods where the outlet poisons were above the 350ppm target due to the fresh feed and inlet poisons disturbances. From the time plot of the MPE, it is also apparent that the noise is structured rather than white. This structuring is again due to the disturbances that were occurring during this period.

The next test period is illustrated by Figures 4.3.10(a)-(g). The model parameter set and controller tuning constants were maintained similar to those in the last test described by Figures 4.3.9(a)-(g). During this period, the RLS estimator also remained off as is indicated by the constant parameter trajectories shown in Figures 4.3.10(e) and (f).

This 24 hour test period provided a good example of how well the MAP controller can perform when the disturbances are restricted to slow, ramp type functions. Both the total inlet poisons and fresh feed had demonstrated fluctuations similar in magnitude as in Figure 4.3.9, however they were restricted to ramps rather than step type disturbances. The regulation of the total outlet poisons was excellent compared to previous results.

Looking at the MPE, it is apparent that it is more white than the MPE in Figure 4.3.9(g). This of course is due to the lack of marked step type disturbances which heavily influence the MPE. Comparing the mean and standard deviations of the MPE during the two periods,

Figure 4.3.9(g)	Figure 4.3.10(g)
$\hat{m}_e = -0.62$	$\hat{m}_e = -0.02$
$\hat{\sigma}_e = 3.86$	$\hat{\sigma}_e = 1.66$

it is evident that the ramp type disturbances influence the MPE to a lesser degree than step type disturbances, even though the magnitudes of the disturbances are relatively equal.

Figures 4.3.11(a)-(g) illustrate a 24 hour test period where the MAP controller failed. During this period the controller tuning constants were as follows,

$$N_1 = 4, \quad N_2 = 10, \quad N_u = 2, \quad \lambda = 400 \quad \text{and} \quad R_w/R_v = 0.005$$

At the beginning of the test, the model parameters were similar to the parameters in the last test, with $\theta^T=[\ -0.877\ \ -3.98\ ]^T$. For the beginning of the test the estimator remained off. During this initial period the total outlet poisons control was poor and so it was decided to re-estimate the model parameters to improve the control. It must be noted that the estimator had been turned off for about 4 days and was now turned on at $T_s \cong 90$. The estimator tuning parameters were set to Δd=0 and *tr(P)*=0.001.

Figure 4.3.11(e)-(f) show the rapid fluctuation in the model parameters. In fact, the $\hat{b}$ parameter changes signs for a short period and causes the MAP controller to drive the hydrogen flow to zero. The parameters are permitted to identify for approximately 2 hours and then the estimator is turned off. The new parameter set is $\theta^T=[\ -0.767\ \ -1.75\ ]^T$. It is evident from the remaining test period, that this parameter set is poor since the control has become oscillatory during a period where the fresh feed and total inlet poisons disturbances were minimal. The MPE shown in Figure 4.3.11(g) also illustrates the poor ability of the model to predict the total outlet poisons. From $T_s \geq 140$ the MPE is completely structured indicated by the periodic low frequency sine wave. Here the estimator did not remain on long enough for the model parameters to properly converge and so the residual auto-correlation sequence demonstrates an oscillatory MPE behavior.

Figures 4.3.12(a)-(g) illustrate a test period where the deadzone on the prediction error was used and was the cause of oscillatory controller response. The *tr(P)* and Δ_d specification for the 24 hour period were 0.05 and 3ppm. From $0 \le T_s \le 50$, the model parameters exhibited no movement due to the fact that the $e(k) \le \Delta_d$. As a result the controller response was very good in holding the outlet poisons to a target of 350ppm. The controller tuning parameters for this period were,

$$N_1 = 4, \quad N_2 = 10, \quad N_u = 2, \quad \lambda = 400 \quad \text{and} \quad R_w/R_v = 0.005$$

At $T_s \ge 50$, a step increase of 400ppm inlet poisons occurred. This resulted in a sudden increase in the MPE beyond the Δ_d of 3ppm. With the MPE beyond the deadzone limits, the model parameters began to move because the estimator was now functioning outside the deadzone. Once the MPE was reduced to within the Δ_d, then the estimator stopped adapting the parameters. Although it seems to be a good idea to have some criteria to prevent adaptation during periods of low excitation, it appears that in this case the choice of Δ_d was poor as it initiated a cycle in the outlet poisons control. This could be directly attributed to the fact that the parameters were not allowed to adapt continuously as they would be able to do if the $\Delta_d=0$.

Figure 4.3.13 shows the same controller as was used in Figure 4.3.12, however $\Delta_d=0$ and thus the RLS estimator was on during the entire test period. The *tr(P)* was set to 0.05 as in the previous case with the exception of the time period extending from $140 \le T_s \le 155$ where the *tr(P)*=0.1. The *tr(P)* was increased in order to accelerate the identification of the parameters and thus improve the control of the total outlet poisons. This increase coincided with the fresh feed and total inlet poisons disturbances which occurred at T_s=155. The disturbances which occurred caused sufficient excitation for the RLS estimator to identify a new set of model parameters. The resulting parameter trajectories are shown in Figures 4.3.13 (e) and (f). Notice that the discrete gain parameter $\hat{b}$ increased as the fresh feed decreased. This trajectory intuitively makes sense since the hydrofiner requires less hydrogen with less fresh feed. Also, with less fresh feed, more poisons can be converted with the same quantity of hydrogen. With the increase in fresh feed after $T_s \geq 200$ from 140 to 200 BPH, the $\hat{b}$ parameter returned to its original value of -2.4.

Several conclusions may be made from the hydrofiner experiments. First, off-line analysis of the step and PRBS test data is important in deciding the plant model order and approximating an initial discrete time parameter set. Simulations using the RLS algorithm allowed for proper selection of the *tr(P)* parameter, which controls the estimator gain and subsequent model parameter trajectories. In this application, a low *tr(P)* specification had to be used in order to prevent large model parameter fluctuations. This was due to the fact that the plant gain was very high. Very small changes in hydrogen flow would significantly influence the hydrofiner total outlet poisons.

In all the experiments, the MAP controller prediction and control horizons remained constant. It was the control weighting, λ, and the ratio of process and measurement noise covariances, R_w/R_v, that were used to tune the controller. This tuning was consistent with the guidelines that were established by McIntosh,(1988). Initially, λ was chosen to be very high leading to slow and small control hydrogen movement. This caused the process to drift unacceptably from the target of 350 PPM. After some re-tuning, the best choice of λ was found to be 400. The noise covariance term was difficult to select. The experimental results demonstrate a high amount of process noise. Typically, measurement noise associated with a GC is small and thus the logical selection of the ratio would be to select it high. However, the experiments showed that the best choice was in the range of 0.001 to 0.005.

The use of the deadzone on the MPE proved to be unsuccessful as it lead to an oscillatory process response. A poor choice of a non-linear technique to turn the estimator on/off can prove to be disastrous as in this case. Best on-line estimation results were obtained with an engineer present to monitor the performance and behavior of the model parameter trajectories. Good estimation results were also obtained when the deadzone, Δ_d=0 and the RLS estimator trace specification was low allowing for a slow parameter identification. With the hydrofiner experiments on-line estimation proved to be valuable when control performance deteriorated. Since the hydrofiner is subjected to large variations in fresh feed and total inlet poisons, its ability to convert the poisons fluctuates. This directly manifests itself in large process gain changes. In addition, process gain is affected by the steady state level of total outlet poisons. On-line estimation permitted the estimation of an improved model, which subsequently improved the MAP controller performance. Figure 4.3.8 and 4.3.9 provide data that demonstrate improved controller performance after re-identification.

An obvious difficulty with adaptive control is selecting the appropriate time to activate the estimator. In most cases the estimator activated when the model prediction error became large and subsequently controller performance became oscillatory. The estimator was then detuned or turned off, when the model parameter trajectories seemed to reach some stable steady state.

Finally, operator acceptance was enthusiastic. Again, once the operators were educated and trained, they used the technology in harmony with the existing PID controllers. Operators would turn the strategy off to make needed corrections to the hydrogen flow when the MAP controller could not handle an excessive load of fresh feed or total inlet poisons. Also, step and PRBS testing posed no significant unit problems.

4.3.4 PID Feedback-Feedforward Control of Hydrofiner Total Outlet Poisons

The existing PID control strategy was compared versus the performance of the MAP controller. This strategy has two components to it. A feedforward component looks at the total lb-moles of poisons in the fresh feed flow and the hydrofiner recycle flows. This value is computed based on the stoichiometric conversion of the various poisons to propylene and butylene using hydrogen. This value can be dynamically compensated using a lead/lag algorithm. In the existing feedforward control strategy, no dynamic compensation was performed. Similarly, the feedback strategy uses a PID controller with no time delay compensation to compute the required hydrogen. The lb-moles of hydrogen and poisons are then passed to a ratio control tag. The ratio tag computes and controls the ratio of lb-moles of hydrogen to lb-moles of poisons by adjusting the hydrogen controller setpoint. The PID tuning constants were :

K_o =	30 min	Reset Constant
K_1 =	0.0016	Linear Gain Constant
K_2 =	0 min	Derivative Constant
T_s =	6 min	Sample and Control Time

The value of the linear gain constant reveals that in order for the PID control strategy to function properly it must be grossly detuned. This is due to the long time delay of 18 minutes associated with the inlet and outlet poisons analysis. Since the process was not modelled in this case, it was very easy for the control strategy to over control the total outlet poisons by excessively varying the hydrogen flow controller. The long reset time also reveals that the strategy was tuned to be cautious in over controlling the hydrogen flow controller.

Figure 4.3.14 illustrates typical behaviour of the existing PID control strategy over a 3 day period. The strategy is capable of slowly tracking changes in process conditions with the changes in fresh feed and poisons occurring. However, because it remains very much detuned in order to prevent uncontrollable oscillations it allows the total outlet poisons to deviate as much as 850 ppm from the target of 350 ppm. Although similar deviations were observed with the MAP controller there were experiments which clearly illustrated that it could move the hydrogen flow rapidly enough to bring the total outlet poisons back to target quickly and with a minimum of overshoot. Figure 4.3.9 illustrates the MAP controller quickness to respond to a large feed disturbance. This type of response is not presently possible with the PID control strategy. It could be made possible if the time delay associated with the analyzer was compensated for. This was not done for this series of experiments.

Figure 4.3.2 Open Loop Hydrofiner Step Tests
1 December 1988

(a) Total Outlet Poisons

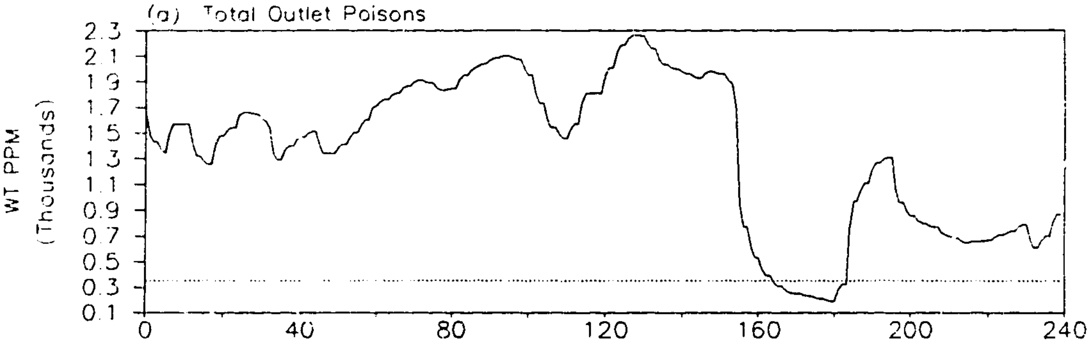

(b) Hydrogen Flow

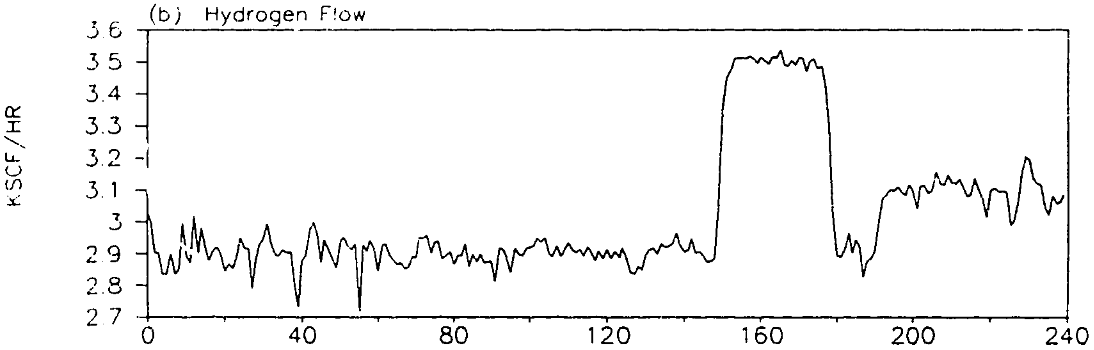

(c) Total Inlet Poisons

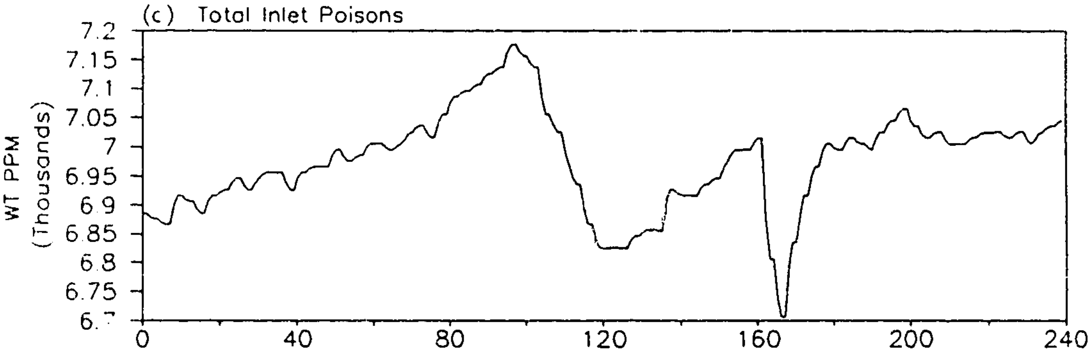

(d) Fresh Feed Flow

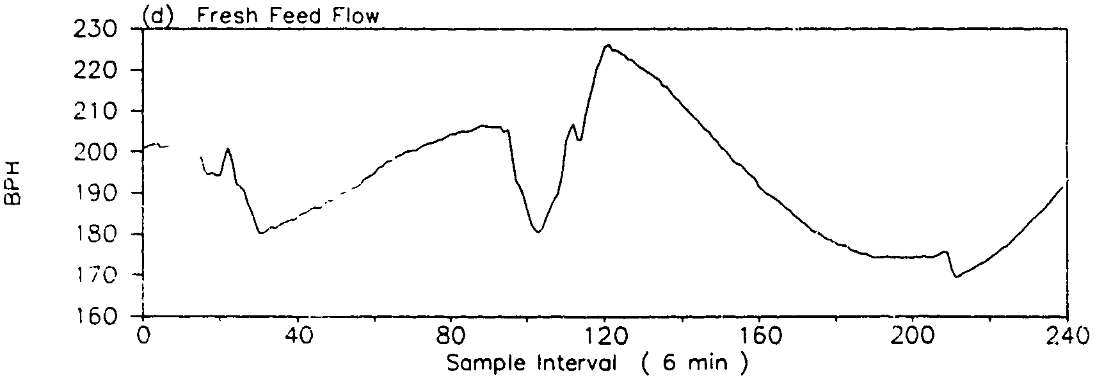

Figure 4.3.3 Open Loop Hydrofiner PRBS Test
2 December 1988

(a) Total Outlet Poisons

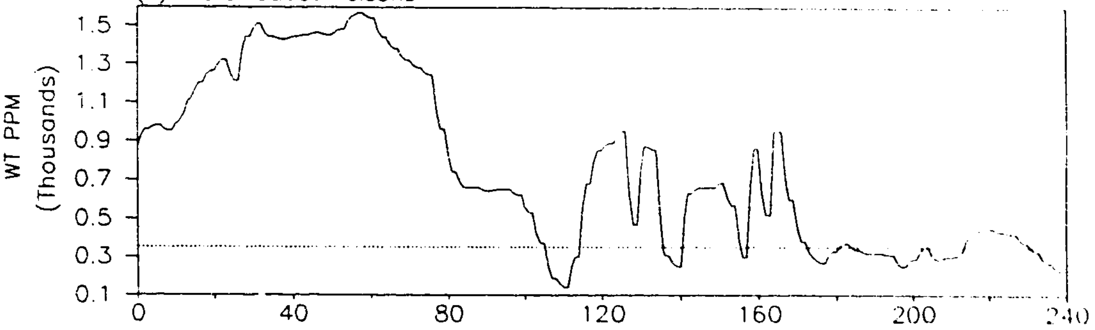

(b) Hydrogen Flow

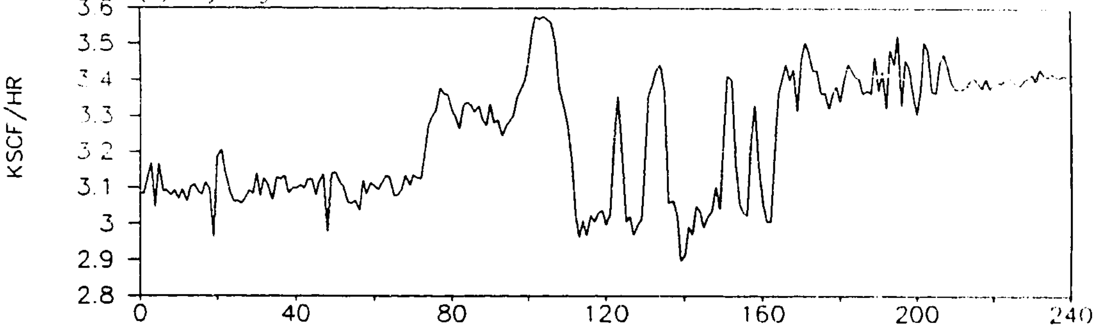

(c) Total Inlet Poisons

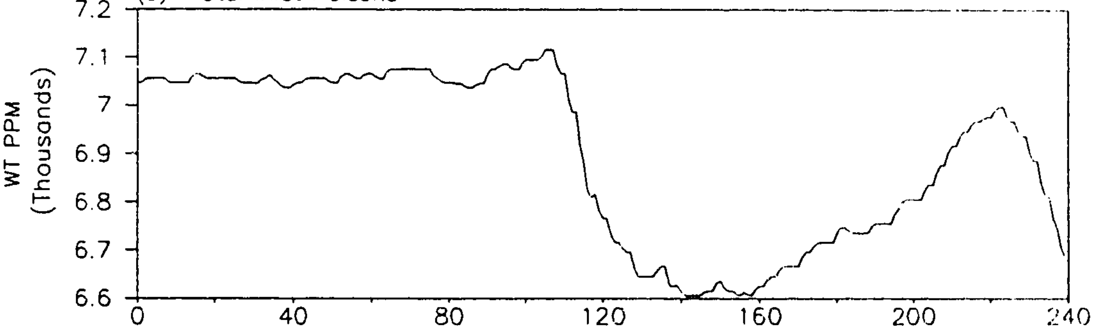

(d) Fresh Feed Flow

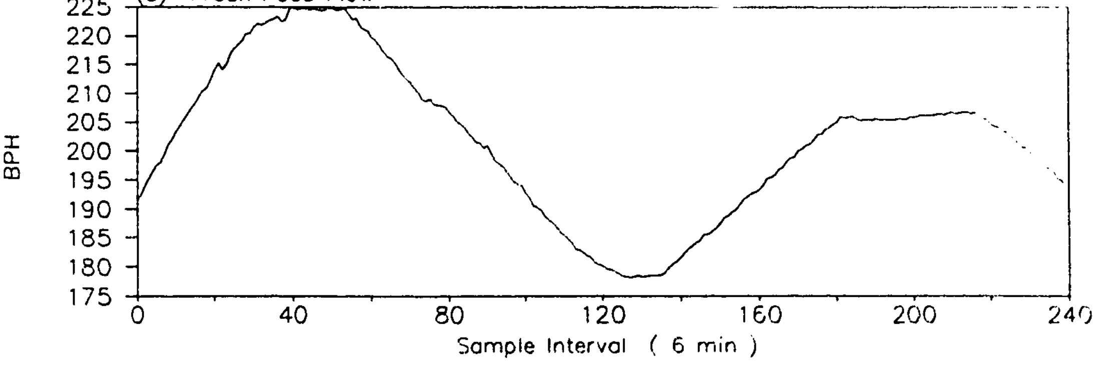

Figure 4.3.4 Hydrofiner Step Test On-line Identification
3 December 1988
Deadzone=0, tr(P)=0.1, RLS=ON

(a) Total Outlet Poisons

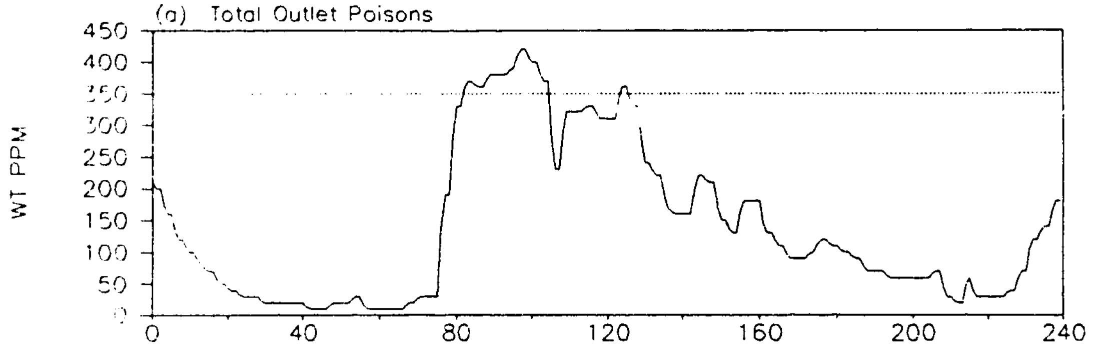

(b) Hydrogen Flow

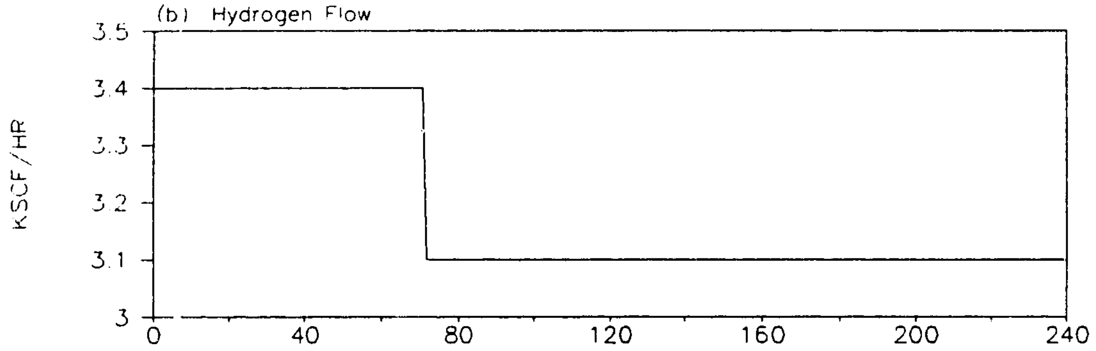

(c) Total Inlet Poisons

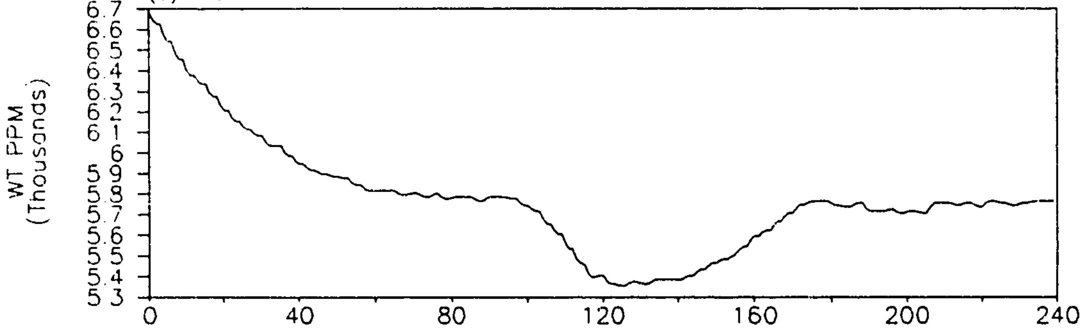

(d) Fresh Feed Flow

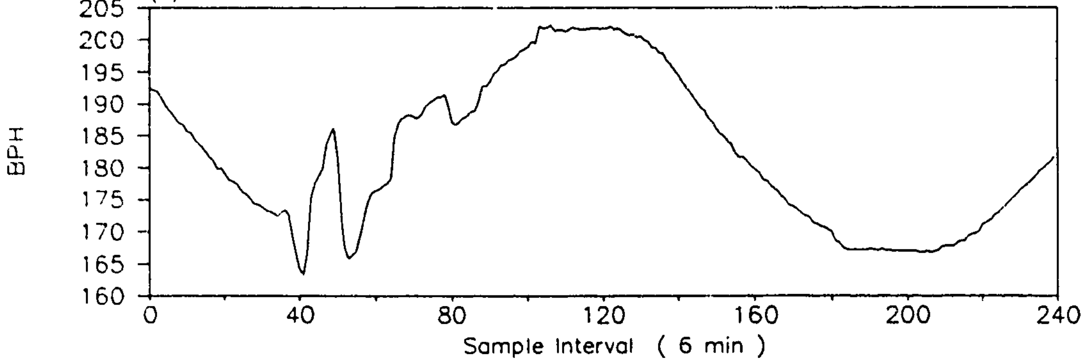

Figure 4.3.5 Hydrofiner Open Loop Step Test Identification
3 December 1988
Deadzone=0, tr(P)=0.1, RLS=ON

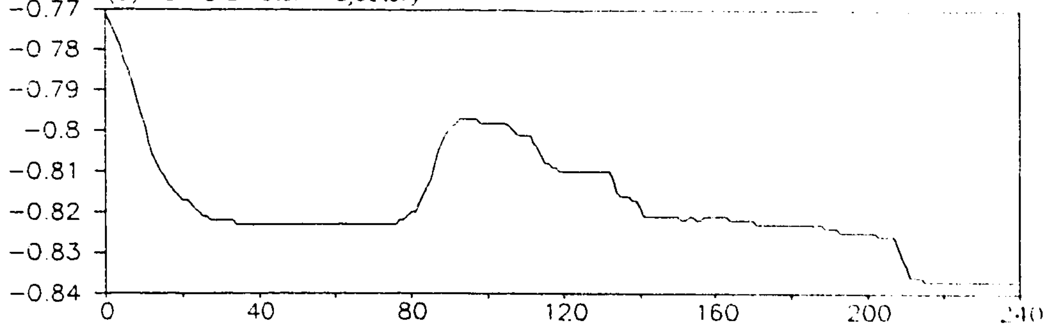
(a) a Parameter Trajectory

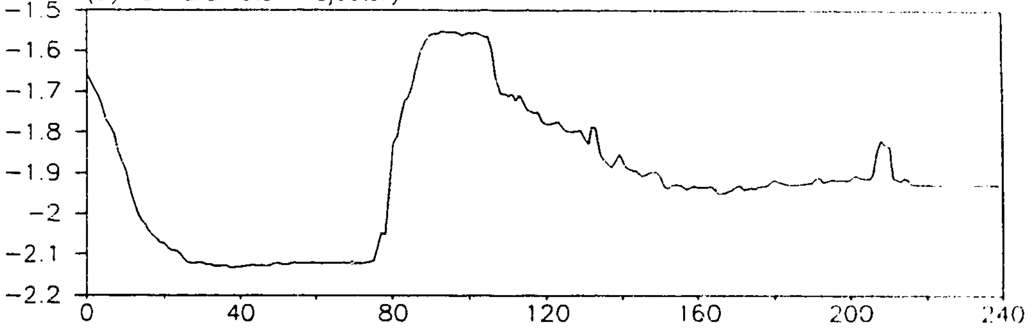
(b) b Parameter Trajectory

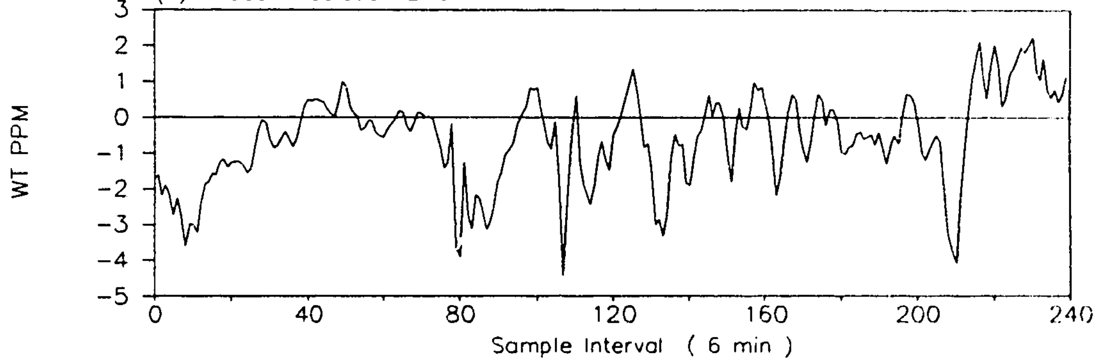
(c) Model Prediction Error

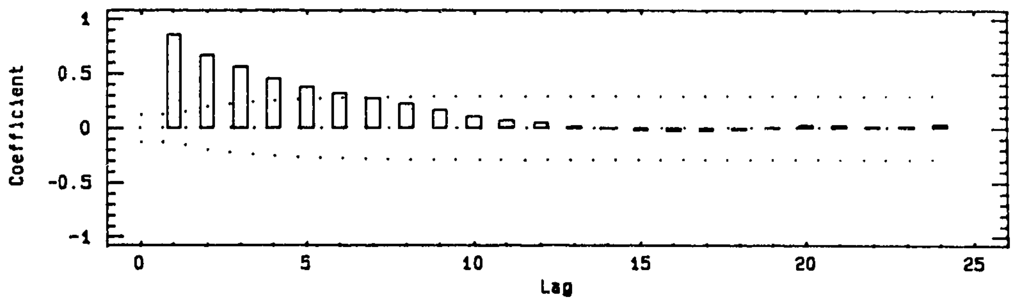
(d) Estimated Residual Auto-Correlation Sequence

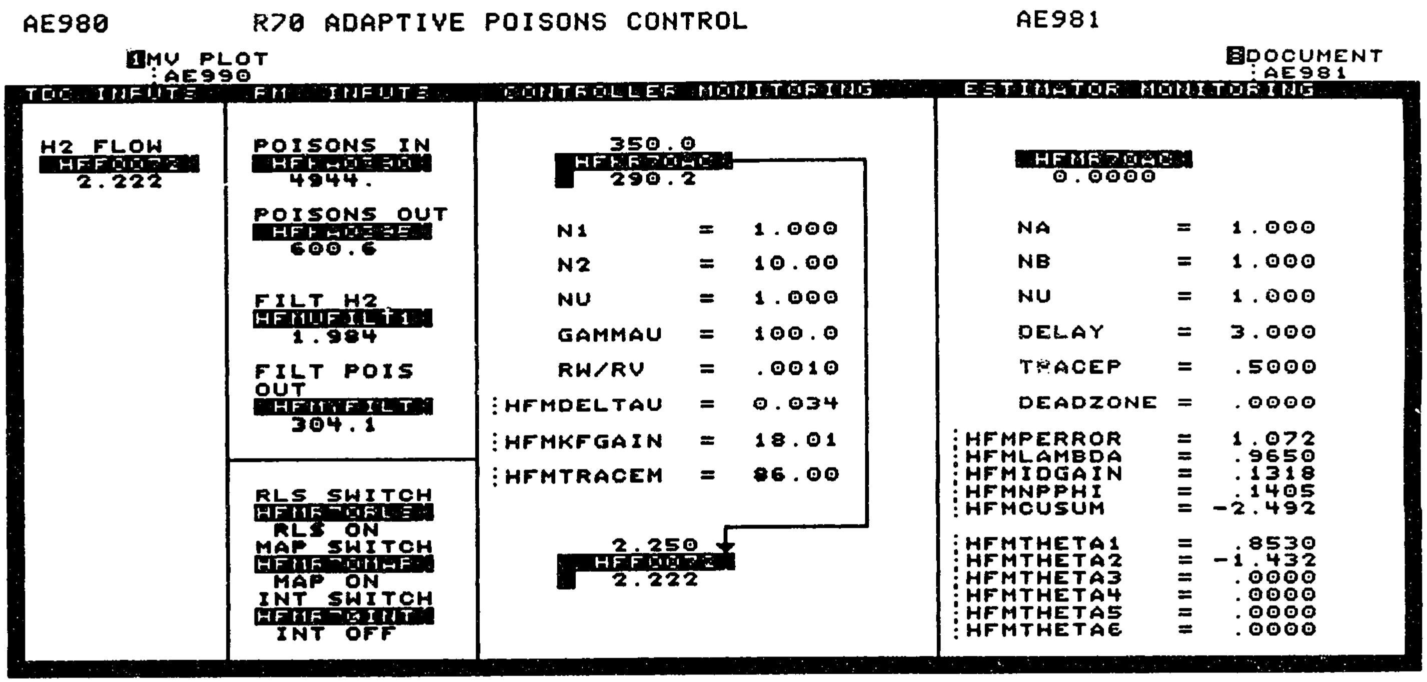

AE980 R70 ADAPTIVE POISONS CONTROL AE981

1 MV PLOT
:AE990

8 DOCUMENT
:AE981

H2 FLOW
HFF0072
2.222

POISONS IN
HFFA0330
4944.

POISONS OUT
HFFA0335
600.6

FILT H2
HFMUFILT1
1.984

FILT POIS
OUT
HFMYFILT
304.1

RLS SWITCH
HFMR70RLS
RLS ON
MAP SWITCH
HFMR70MAP
MAP ON
INT SWITCH
HFMR70INT
INT OFF

350.0
HFMR70AC
290.2

N1 = 1.000
N2 = 10.00
NU = 1.000
GAMMAU = 100.0
RW/RV = .0010
:HFMDELTAU = 0.034
:HFMKFGAIN = 18.01
:HFMTRACEM = 86.00

2.250
HFF0072
2.222

HFMR70AC
0.0000

NA = 1.000
NB = 1.000
NU = 1.000
DELAY = 3.000
TRACEP = .5000
DEADZONE = .0000
:HFMPERROR = 1.072
:HFMLAMBDA = .9650
:HFMIDGAIN = .1318
:HFMNPPHI = .1405
:HFMCUSUM = -2.492

:HFMTHETA1 = .8530
:HFMTHETA2 = -1.432
:HFMTHETA3 = .0000
:HFMTHETA4 = .0000
:HFMTHETA5 = .0000
:HFMTHETA6 = .0000

Figure 4.3.6 Honeywell PMXIII Multi-Step Adaptive Predictive Controller Operator/Engineer Interface

Figure 4.3.7 Hydrofiner Open Loop PRBS Test

6 December 1988
Deadzone=0, tr(P)=0.01, RLS=ON
N1=1, N2=10, Nu=1, Lambda=10000, Rw/Rv=0.05

(a) Total Outlet Poisons

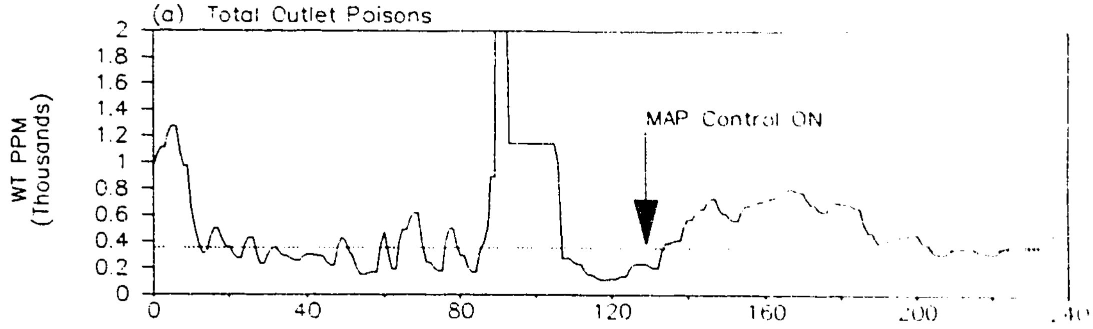

(b) Hydrogen Flow

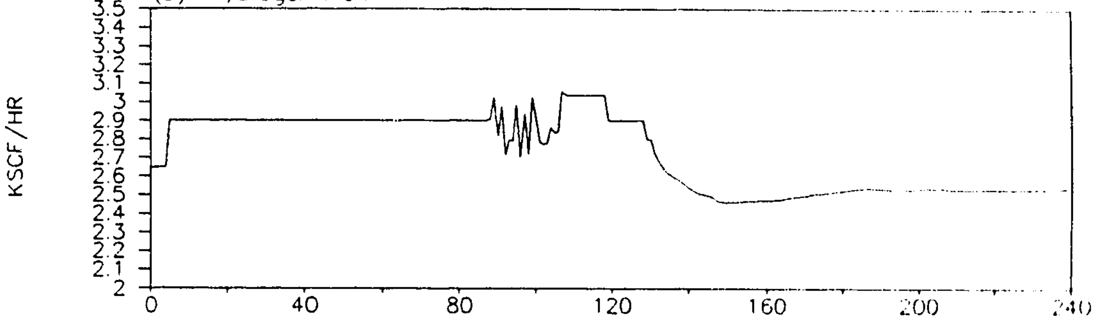

(c) Total Inlet Poisons

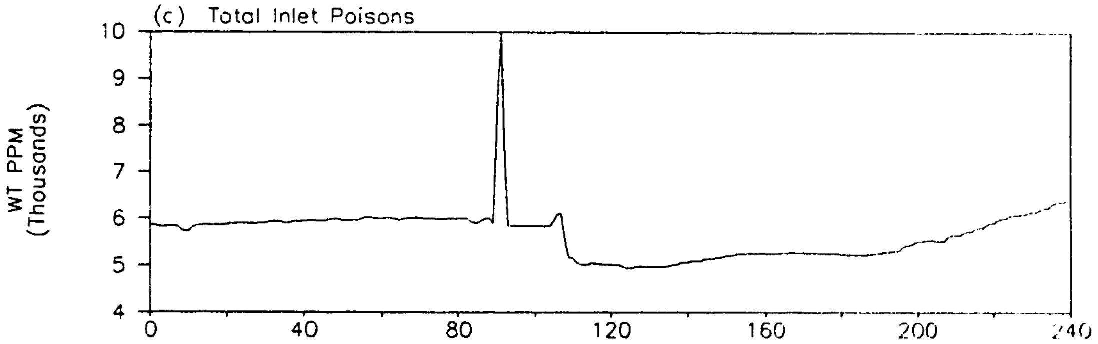

(d) Fresh Feed Flow

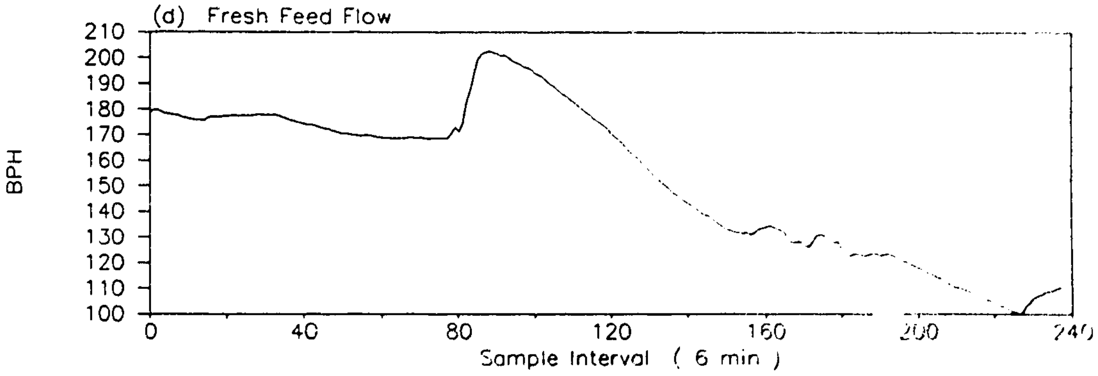

Figure 4.3.7 Hydrofiner Open Loop PRBS Test (... cont)

6 December 1988
Deadzone=0, tr(P)=0 01, RLS=ON
N1=1, N2=10, Nu=1, Lambda=10000, Rw/Rv=0 05

(e) a Paramter Trajectory

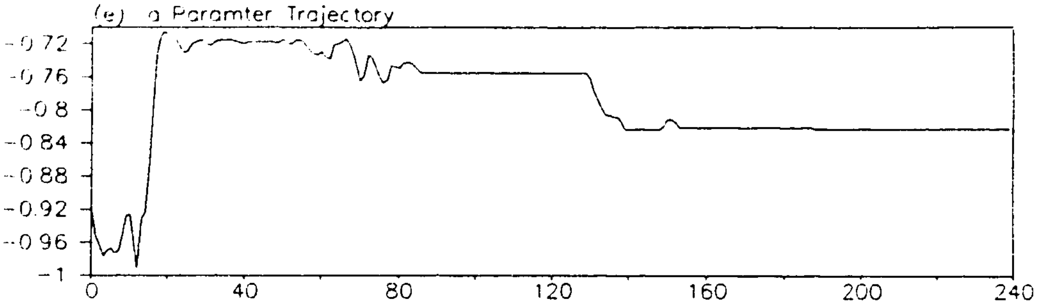

(f) b Parameter Trajectory

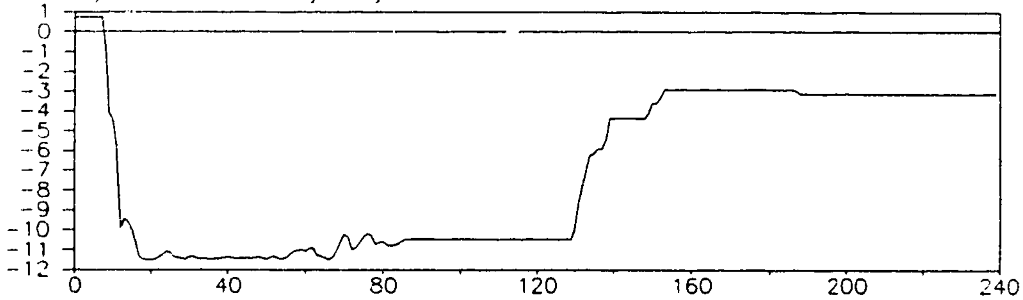

(g) Model Prediction Error

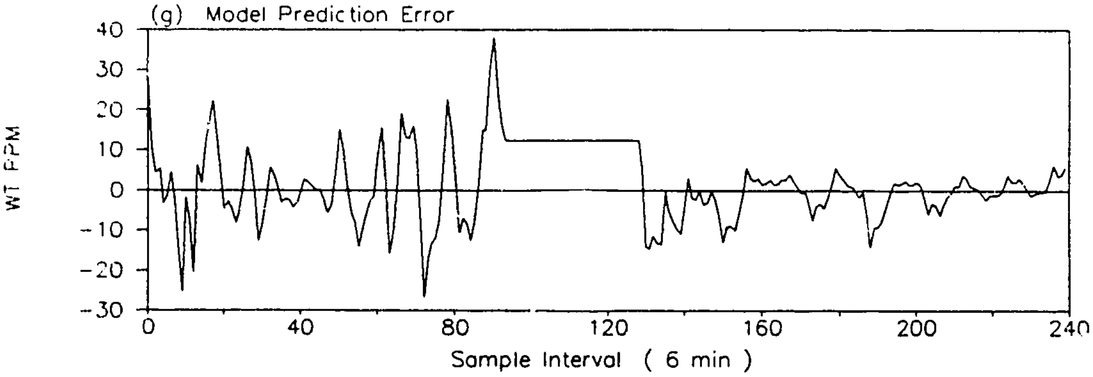

Figure 4.3.8 MAP Control of Hydrofiner
7 December 1988
N1=4, N2=10, Nu=2, Lambda=1200, tr(P)=0.01

(a) Total Outlet Poisons

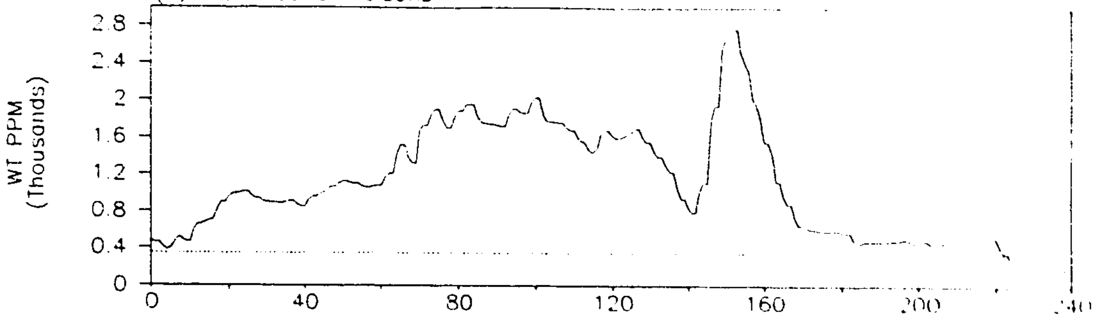

(b) Hydrogen Flow

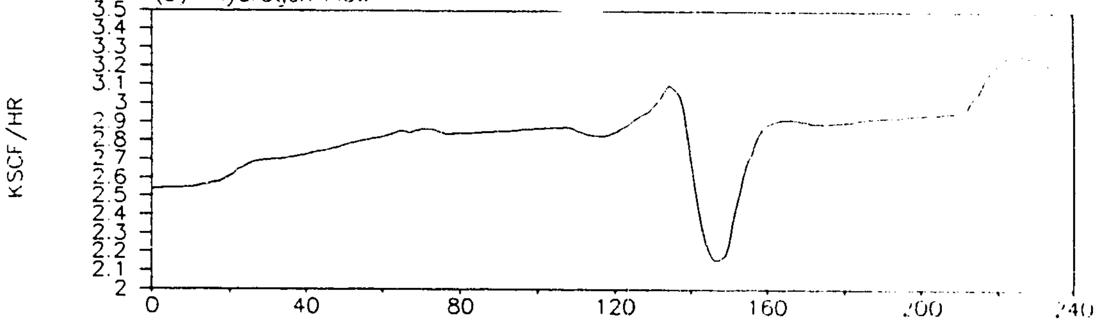

(c) Total Inlet Poisons

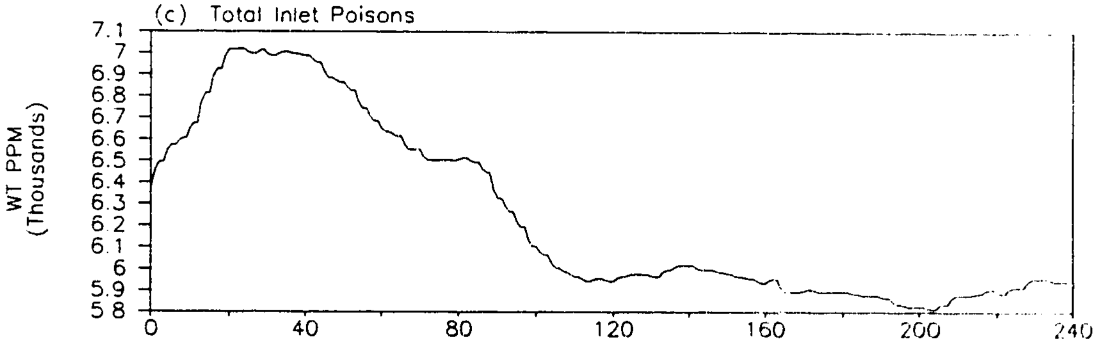

(d) Fresh Feed Flow

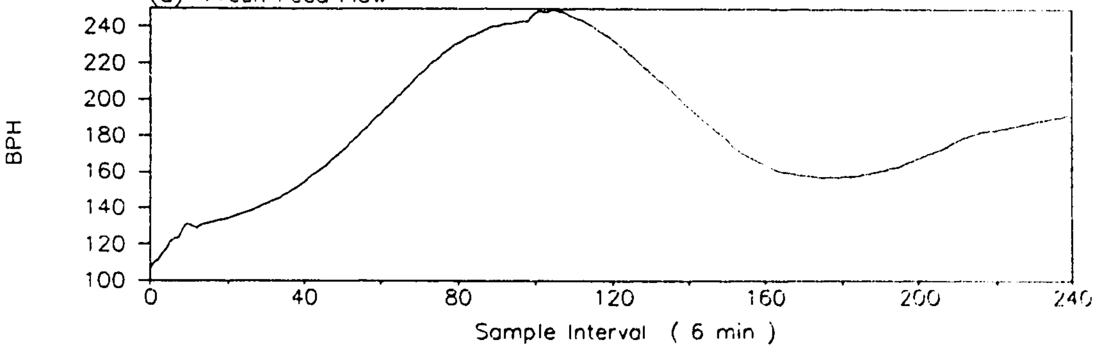

Figure 4.3.8 MAP Control of Hydrofiner (... cont)
7 December 1988
N1=4, N2=10, Nu=2, Lambda=1200, tr(P)=0.01

(e) a Parameter Trajectory

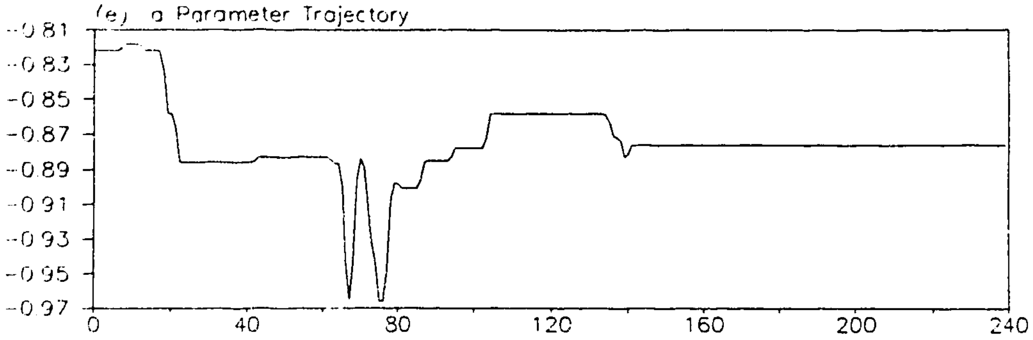

(f) b Parameter Trajectory

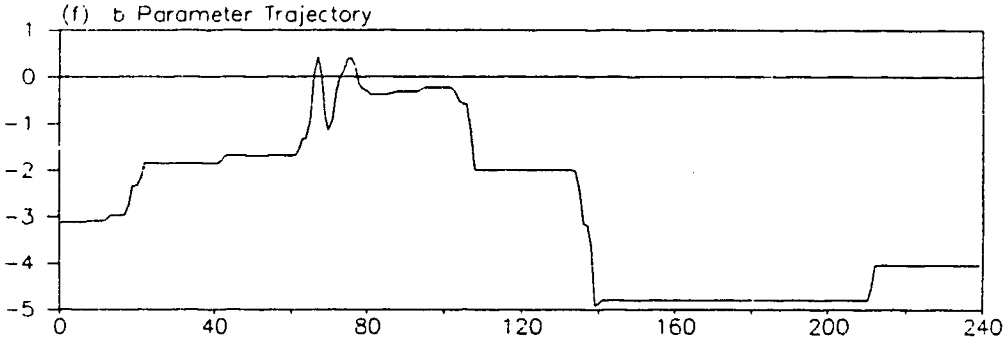

(g) Model Prediction Error

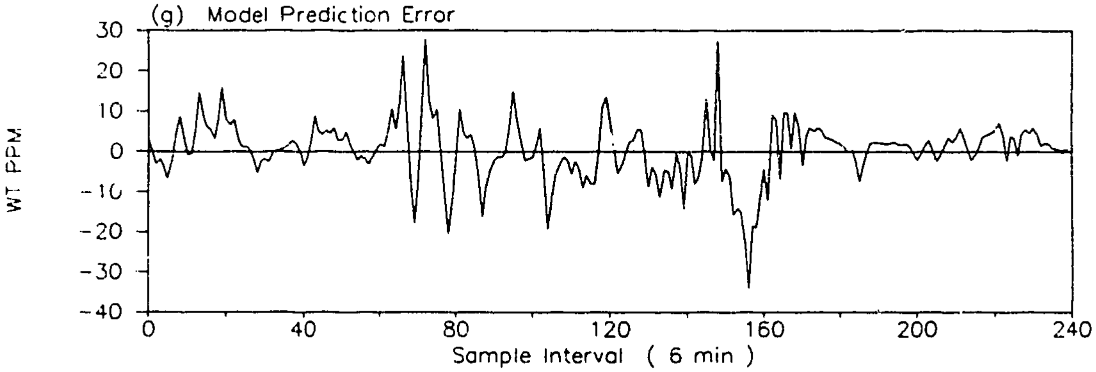

(h) Residual Estimated Auto-Correlation Sequence

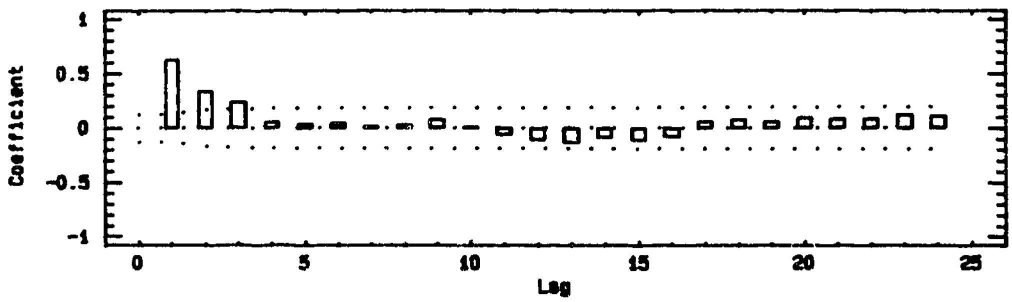

Figure 4.3.9 MAP Control of Hydrofiner
10 December 1988
N1=4, N2=10, Nu=2, Lambda=400, Rw, Rv=0.001

(a) Total Outlet Poisons

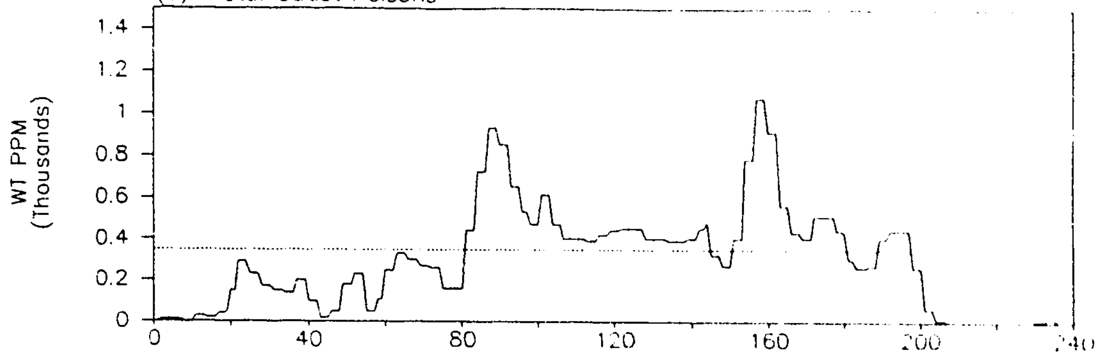

(b) Hydrogen Flow

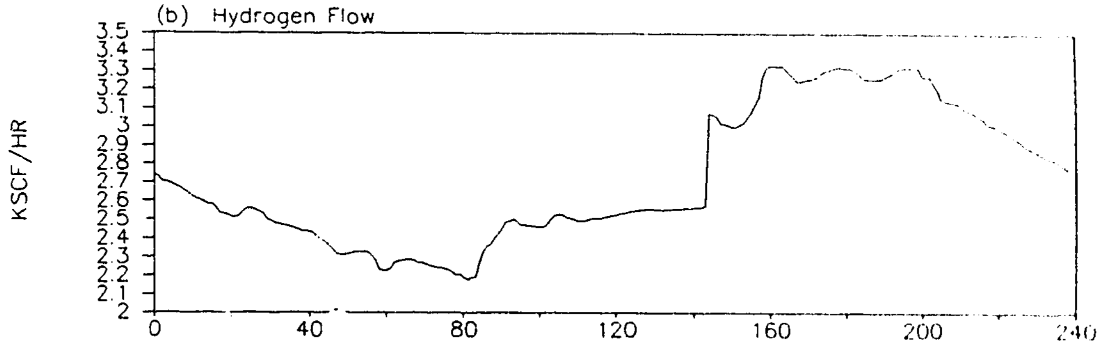

(c) Total Inlet Poisons

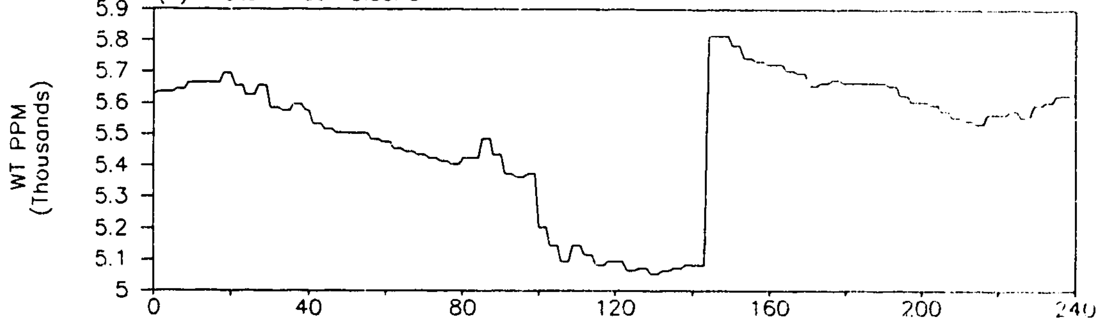

(d) Fresh Feed Flow

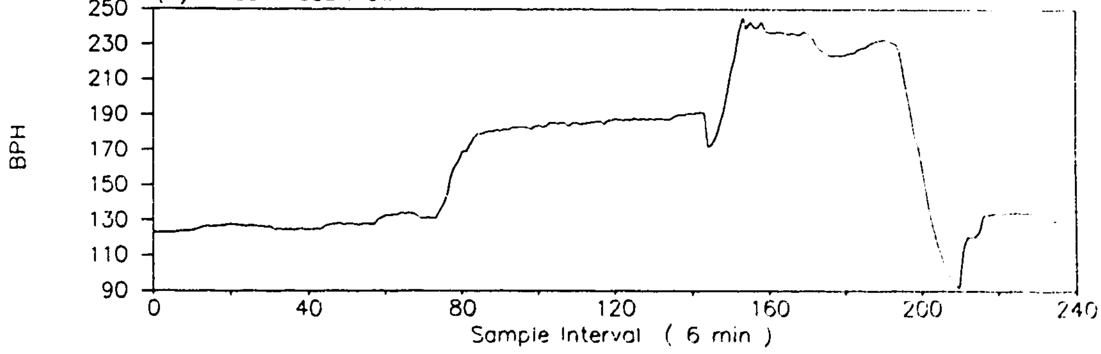

Figure 4.3.9 MAP Control of Hydrofiner (... cont)
10 December 1988
N1=4, N2=10, Nu=2, Lambda=400, Rw/Rv=0.001

(e) a Parameter Trajectory

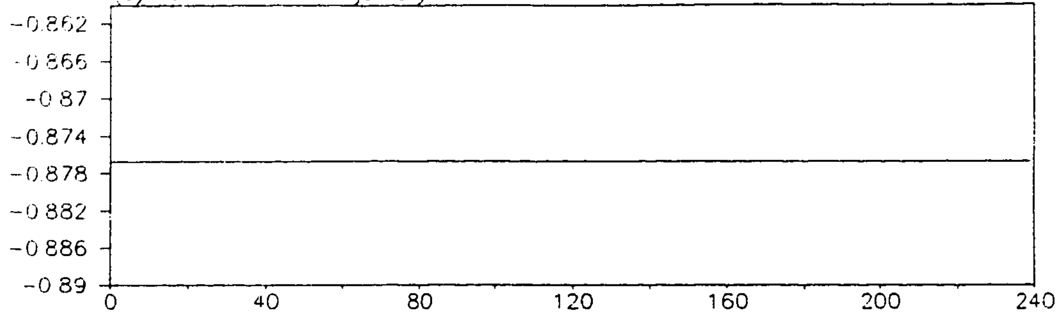

(f) b Parameter Trajectory

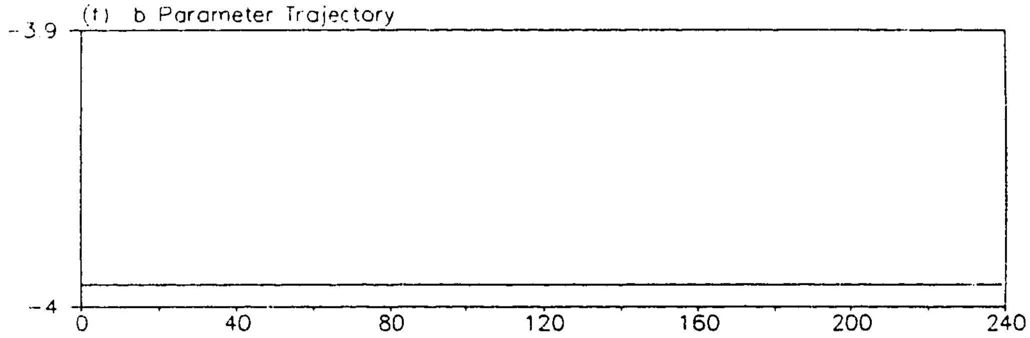

(g) Model Prediction Error

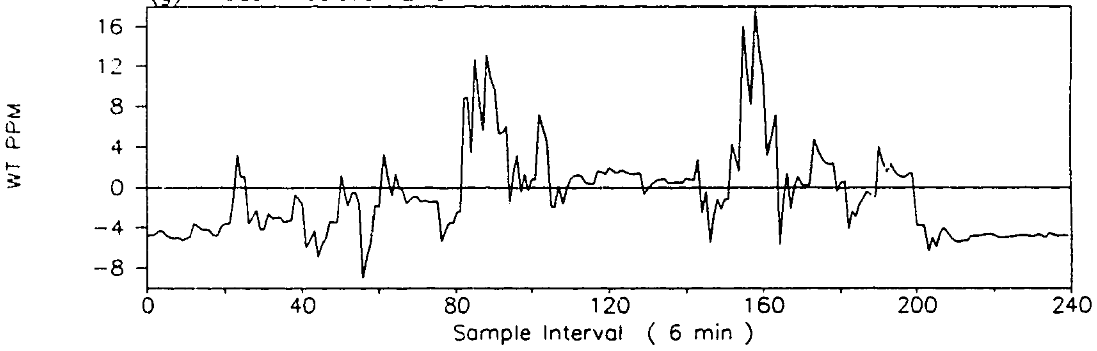

(h) Residual Estimated Auto-Correlation Sequence

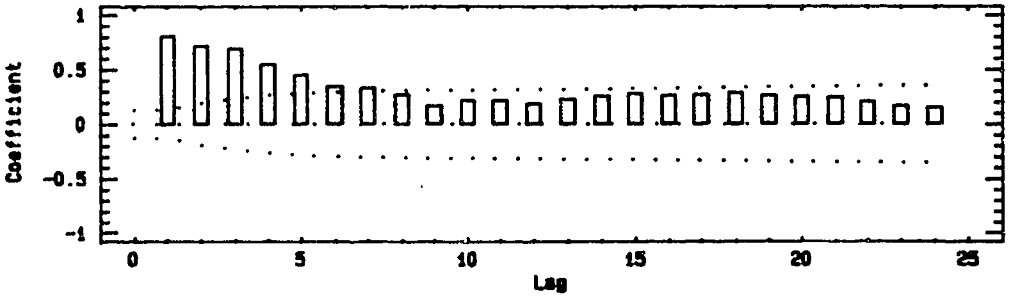

Figure 4.3.10 MAP Control of Hydrofiner
11 December 1988
N1=4, N2=10, Nu=2, Lambda=400, Rw/Rv=0.001, RLS=OFF

(a) Total Outlet Poisons

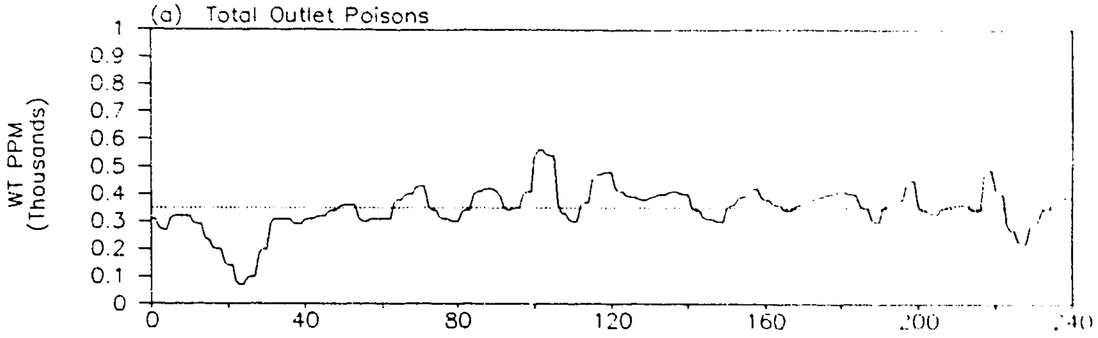

(b) Hydrogen Flow

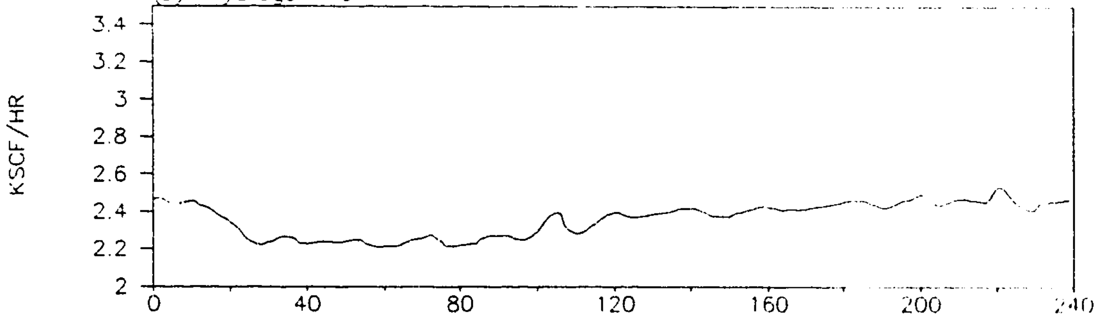

(c) Total Inlet Poisons

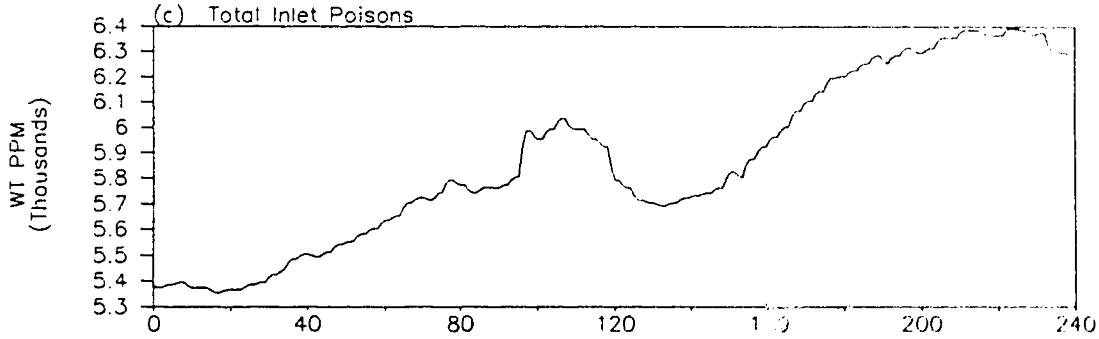

(d) Fresh Feed Flow

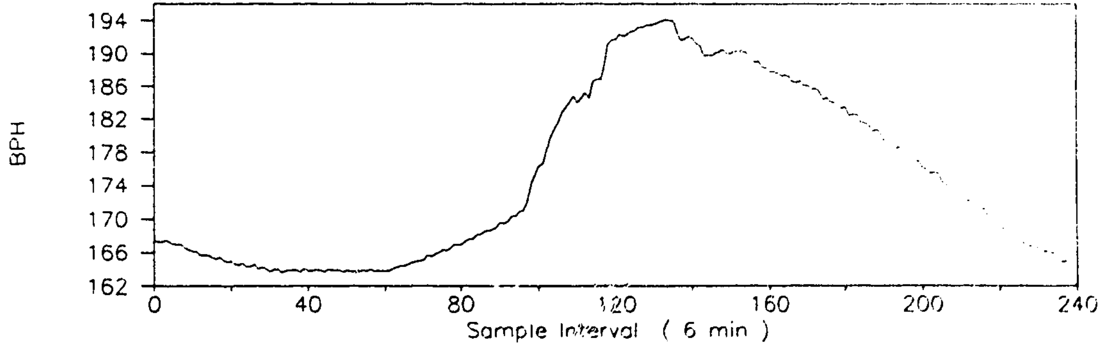

Figure 4.3.10 MAP Control of Hydrofiner (... cont)
11 December 1988
N1=4, N2=10, Nu=2, Lambda=400, Rw/Rv=0.001, RLS=OFF

(e) a Parameter Trajectory

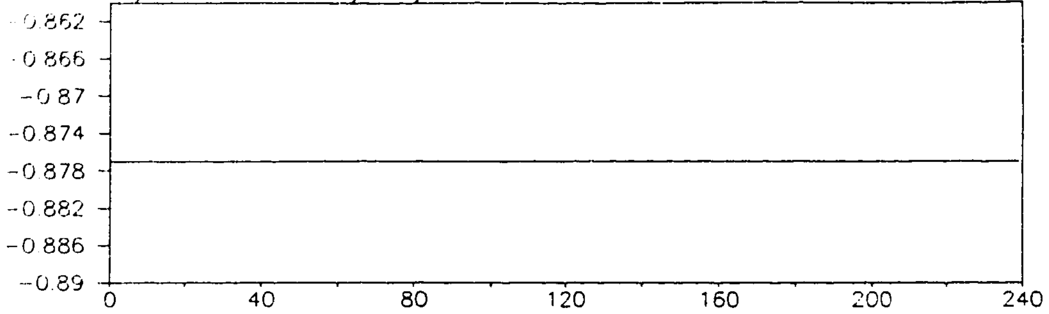

(f) b Parameter Trajectory

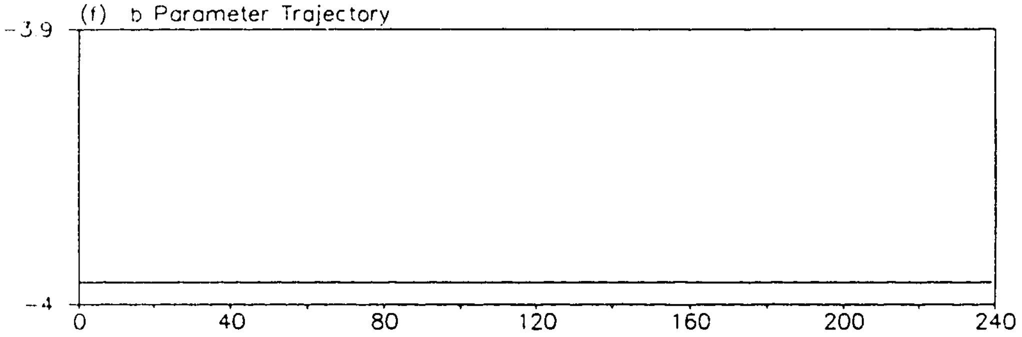

(g) Model Prediction Error

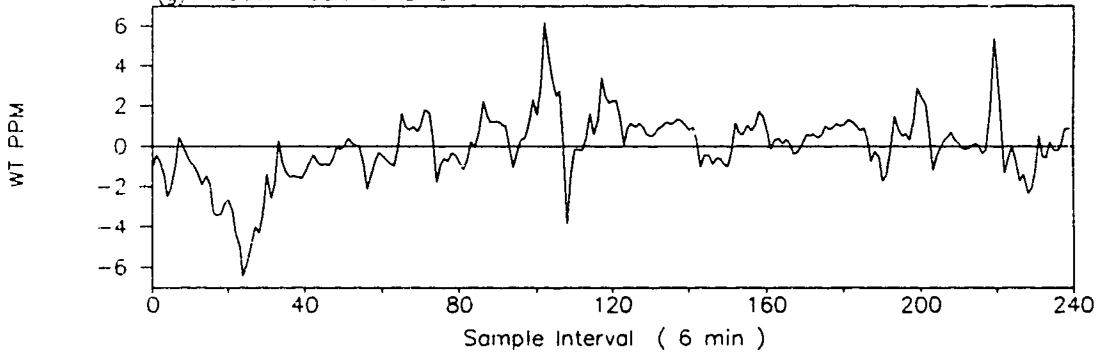

(h) Residual Estimated Auto-Correlation Sequence

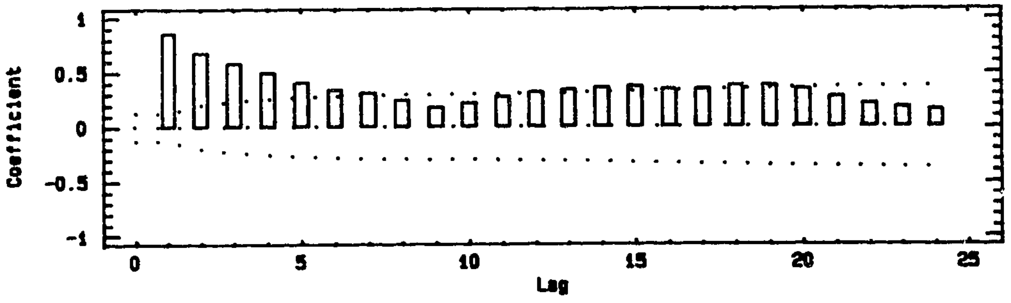

Figure 4.3.11 MAP Control of Hydrofiner
12 December 1988
N1=4, N2=10, Nu=2, Lambda=400, Rw/Rv=0.005, RLS=ON

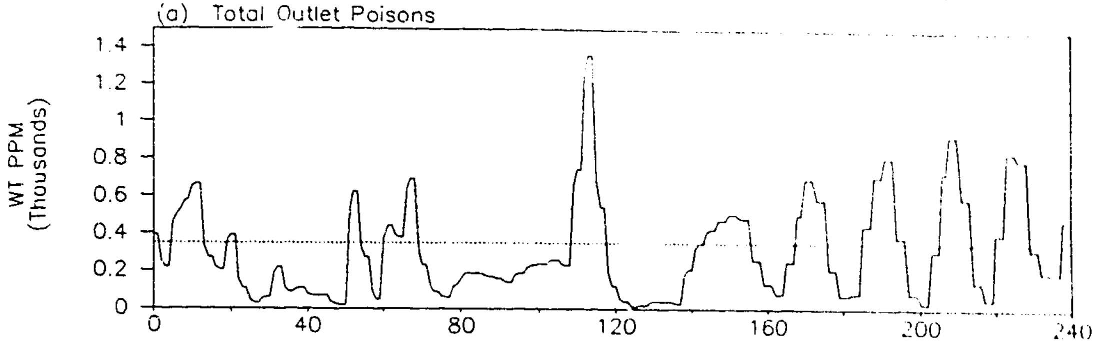
(a) Total Outlet Poisons

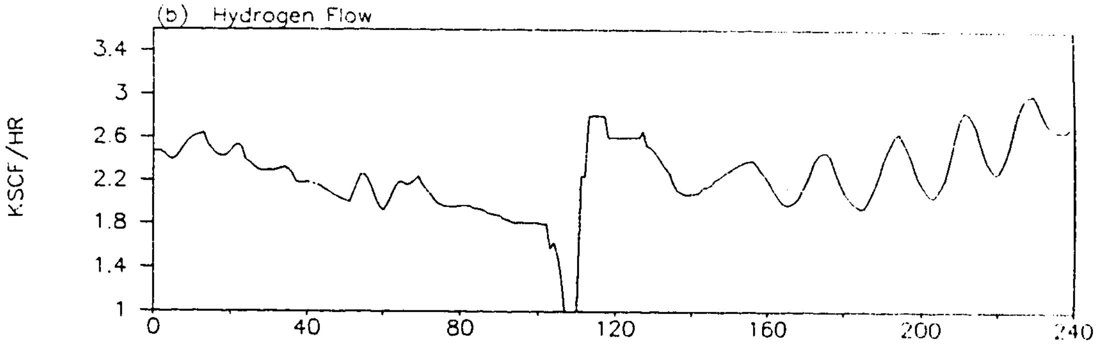
(b) Hydrogen Flow

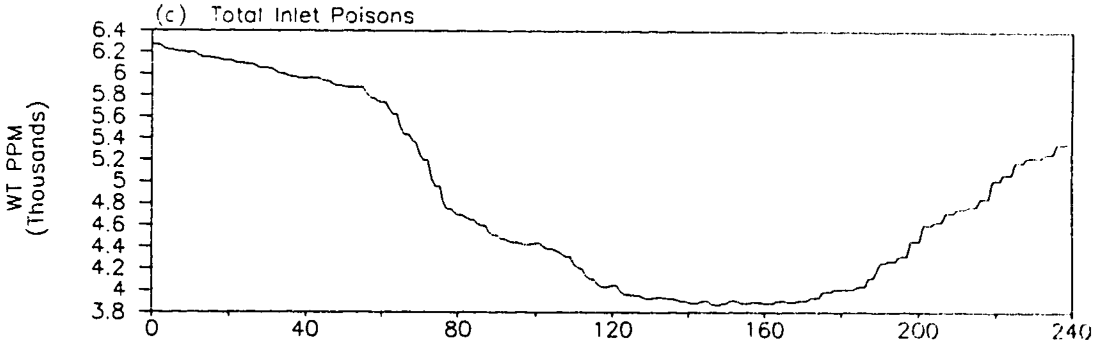
(c) Total Inlet Poisons

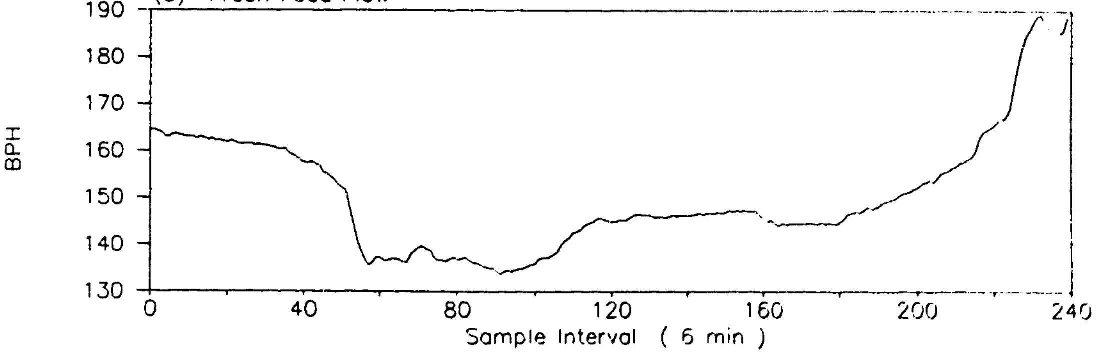
(d) Fresh Feed Flow

Figure 4.3.11 MAP Control of Hydrofiner (... cont)
12 December 1988
N1=4, N2=10, Nu=2, Lambda=400, Rw/Rv=0.005, RLS=ON

(e) a Parameter Trajectory

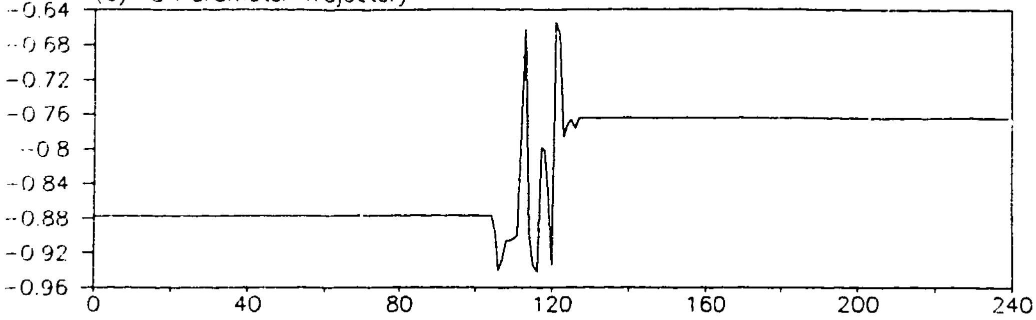

(f) b Parameter Trajectory

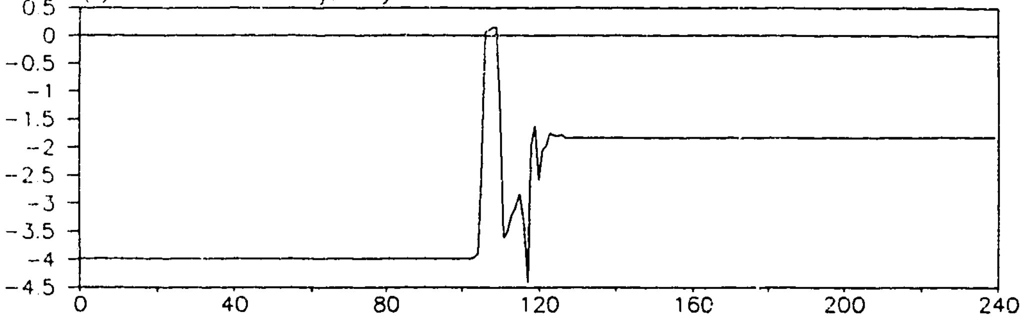

(g) Model Prediction Error

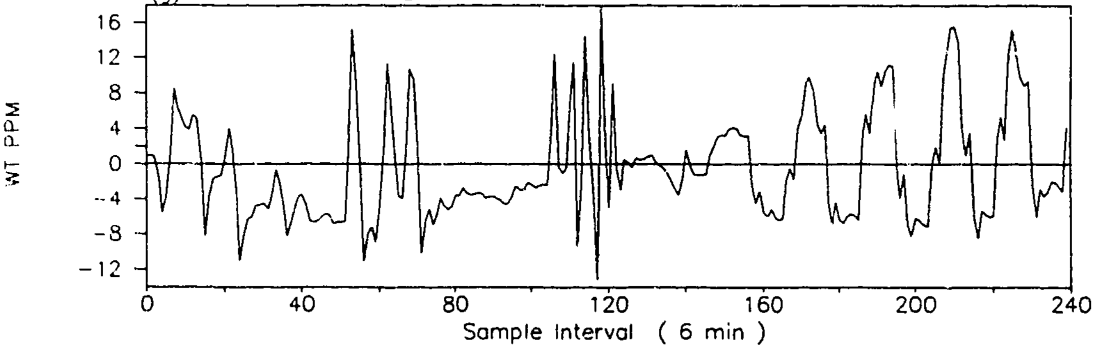

(h) Residual Estimated Auto-Correlation Sequence

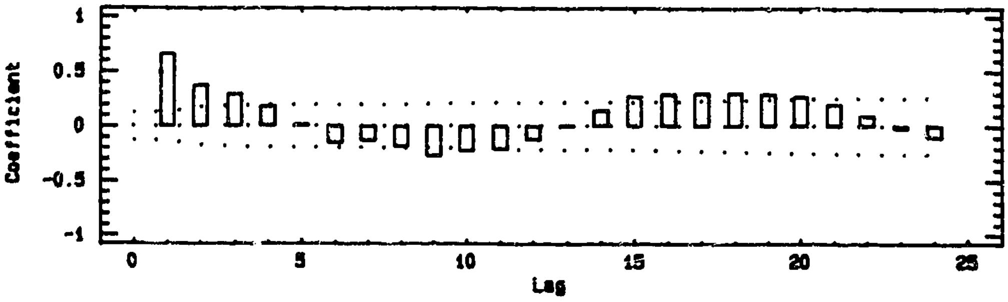

Figure 4.3.12 MAP Control of Hydrofiner
17 December 1988
N1=4, N2=10, Nu=2, Lambda=400, Rw/Rv=0.005

(a) Total Outlet Poisons

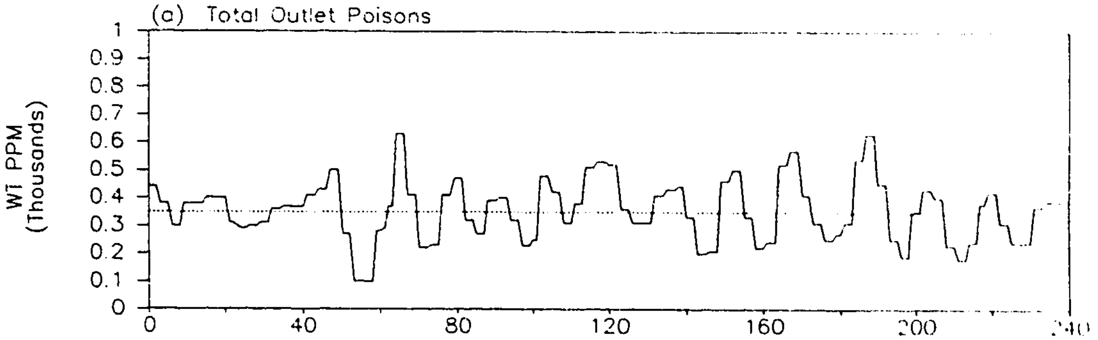

(b) Hydrogen Flow

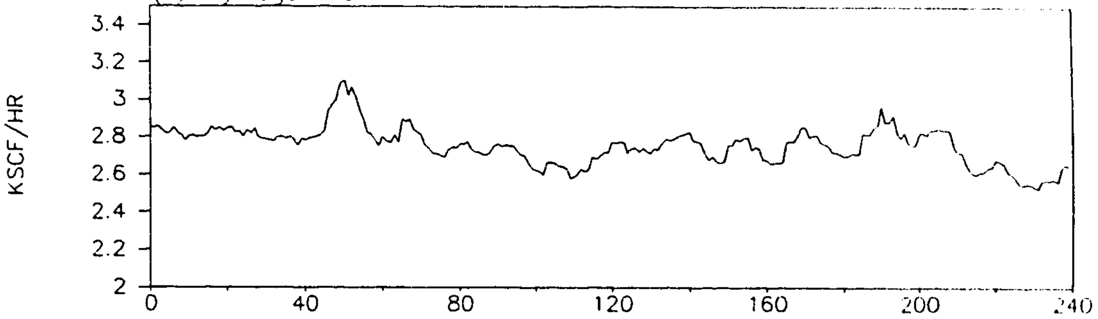

(c) Total Inlet Poisons

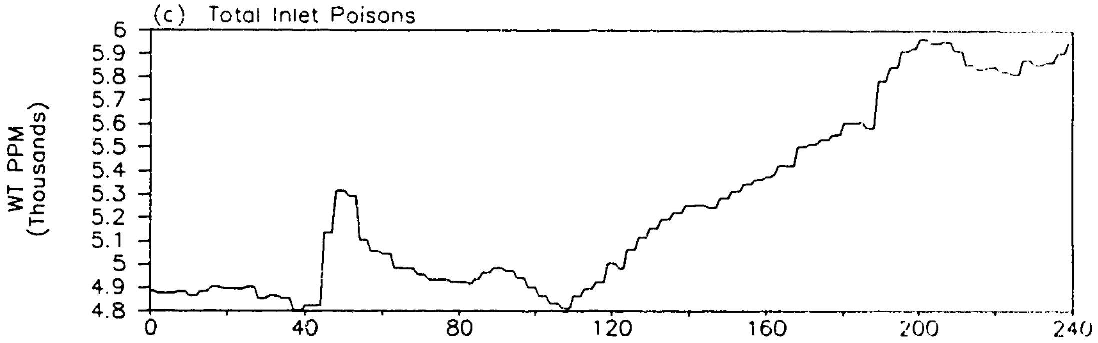

(d) Fresh Feed Flow

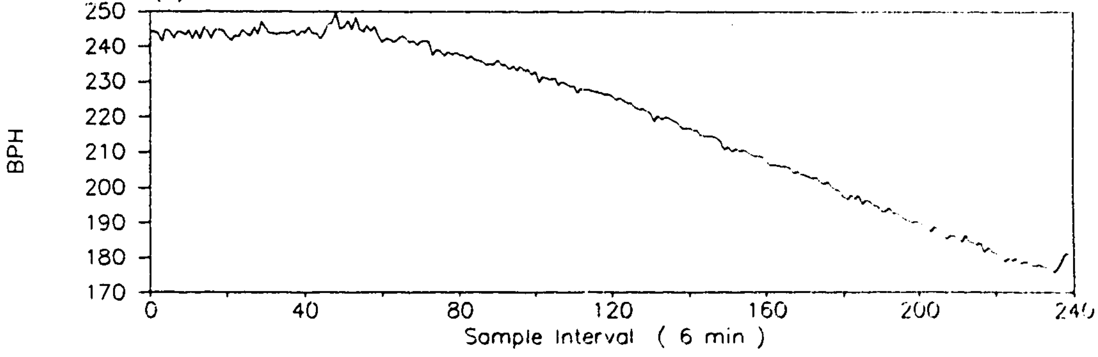

Figure 4.3.12 MAP Control of Hydrofiner (... cont)
17 December 1988
N1=4, N2=10, Nu=2, Lambda=400, Rw/Rv=0.005

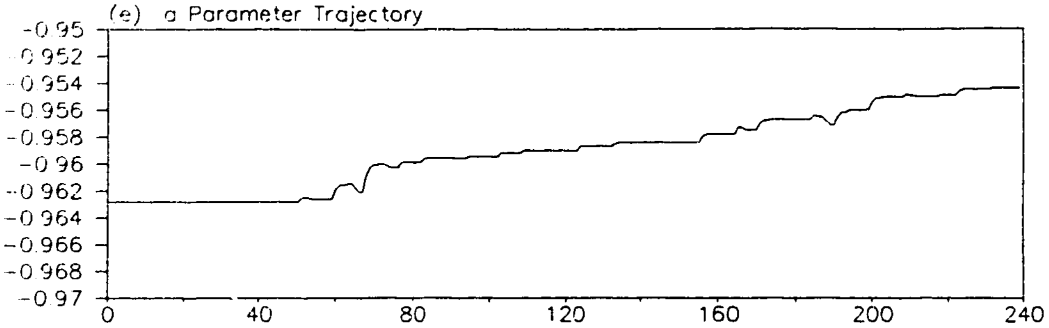
(e) a Parameter Trajectory

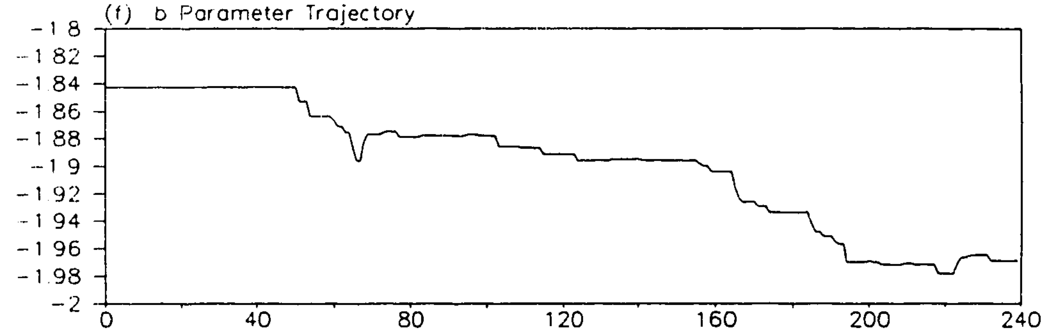
(f) b Parameter Trajectory

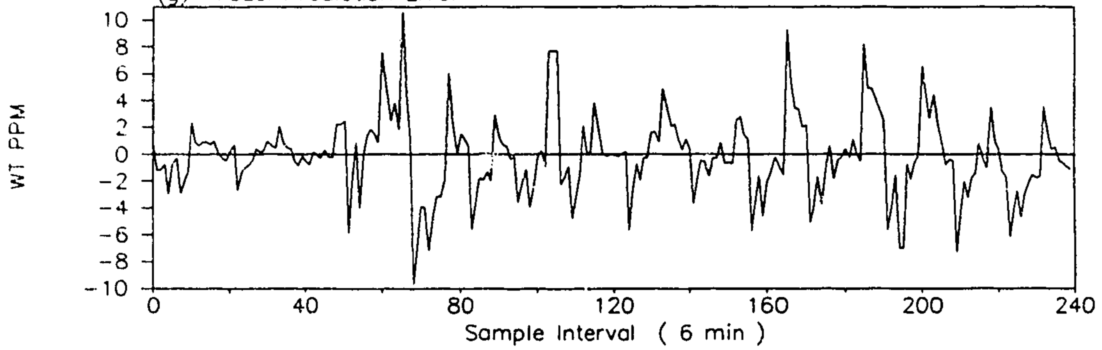
(g) Model Prediction Error

(h) Residual Estimated Auto-Correlation Sequence

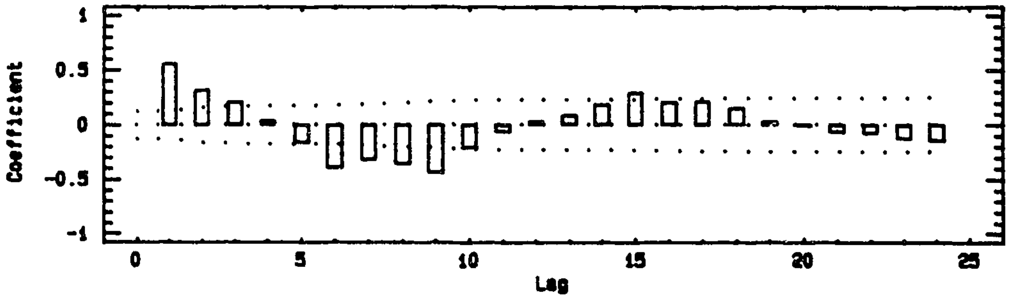

Figure 4.3.13 MAP Control of Hydrofiner
19 December 1988
N1=4, N2=10, Nu=2, Lambda=400, Rw/Rv=0.005

(a) Total Outlet Poisons

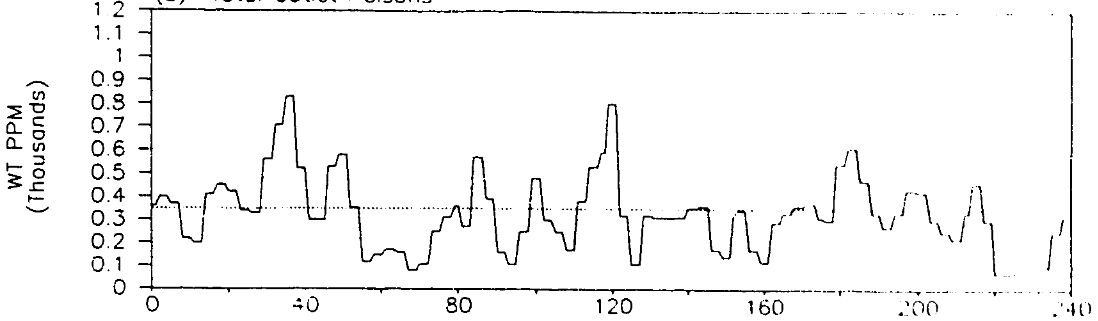

(b) Hydrogen Flow

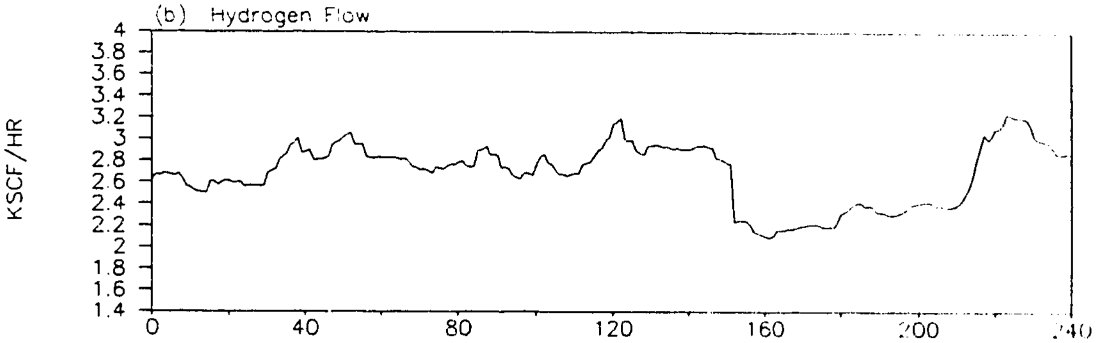

(c) Total Inlet Poisons

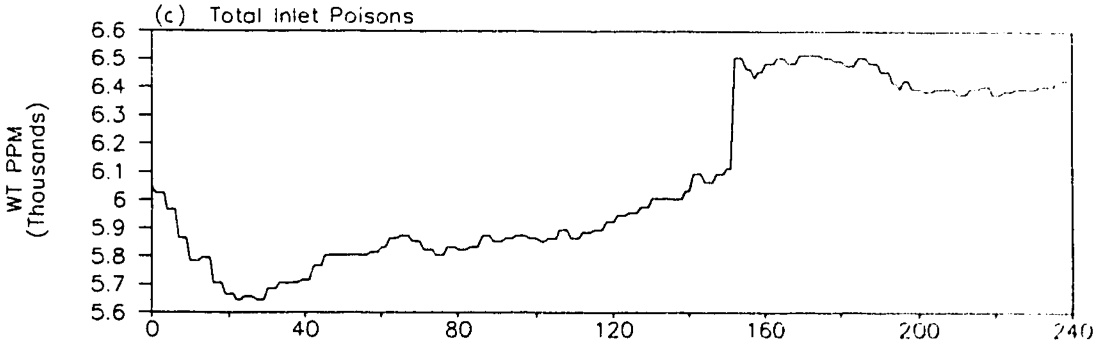

(d) Fresh Feed Flow

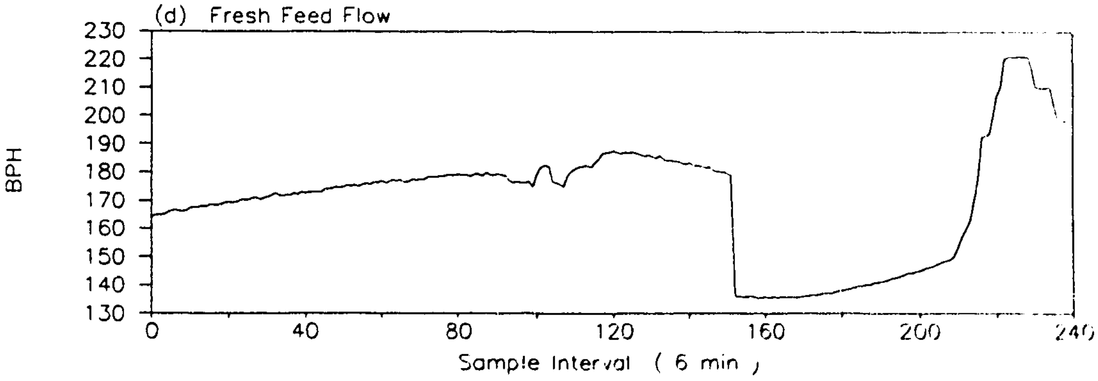

Figure 4.3.13 MAP Control of Hydrofiner (... cont)
19 December 1988
N1=4, N2=10, Nu=2, Lambda=400, Rw/Rv=0.005

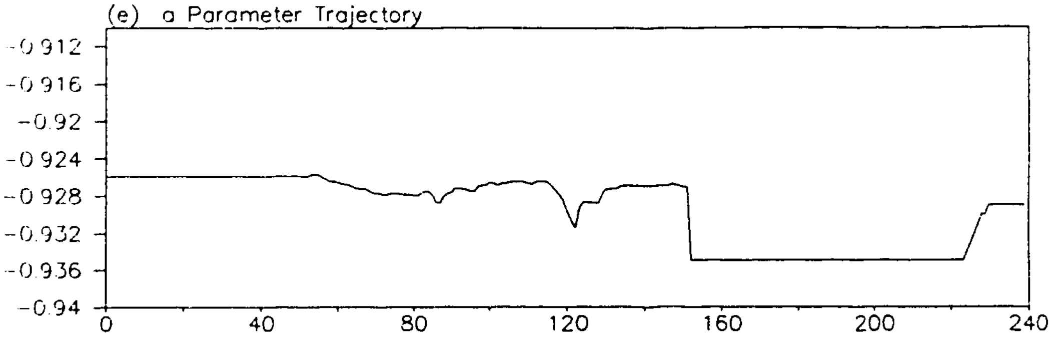
(e) a Parameter Trajectory

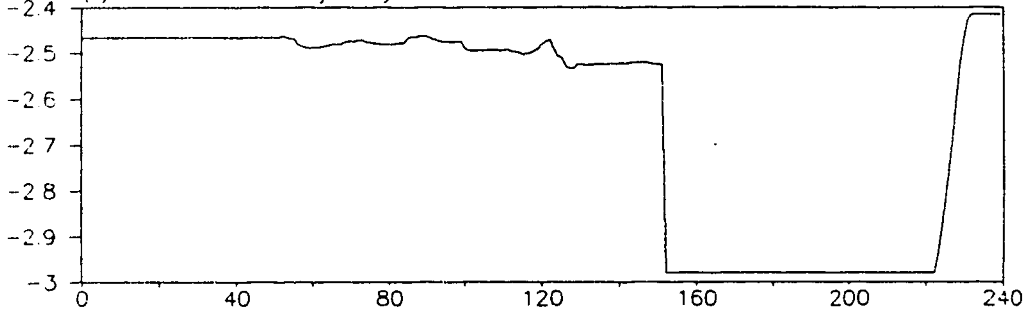
(f) b Parameter Trajectory

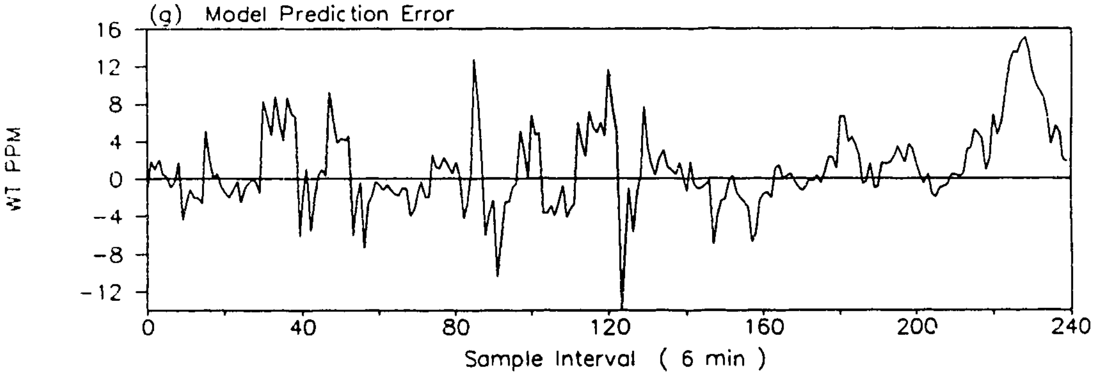
(g) Model Prediction Error

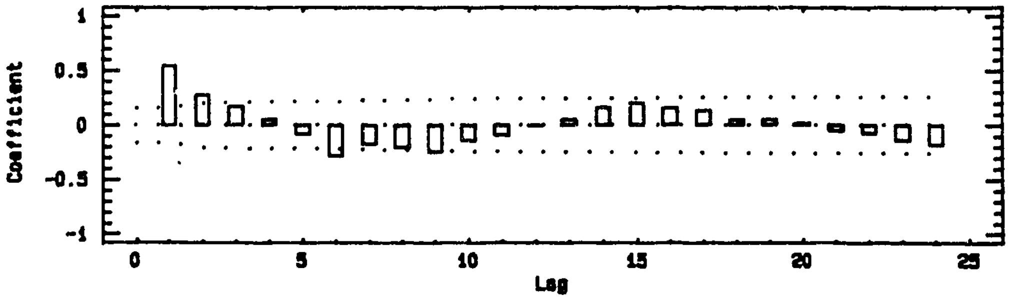
(h) Residual Estimated Auto-Correlation Sequence

Figure 4.3.14 PID Control of Hydrofiner
10–13 March 1989
Ko=30, K1=0.0016, K2=0.0

(a) Total Outlet Poisons

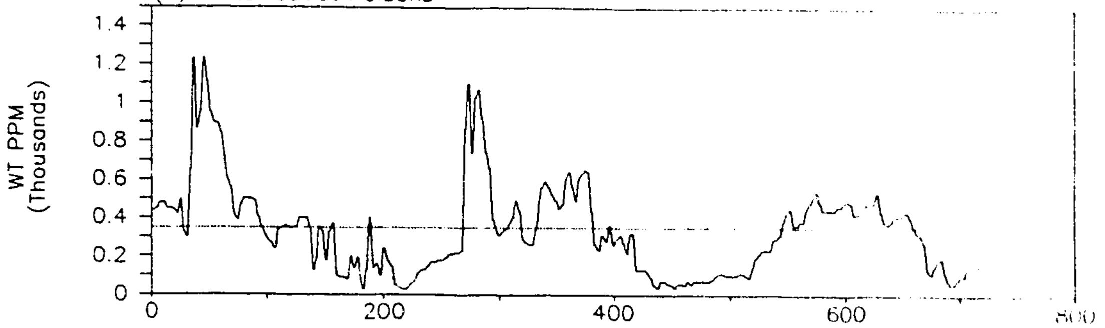

(b) Hydrogen Flow

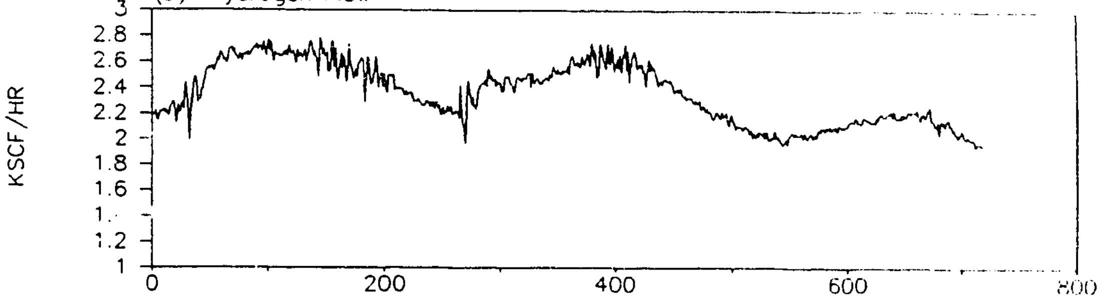

(c) Total Inlet Poisons

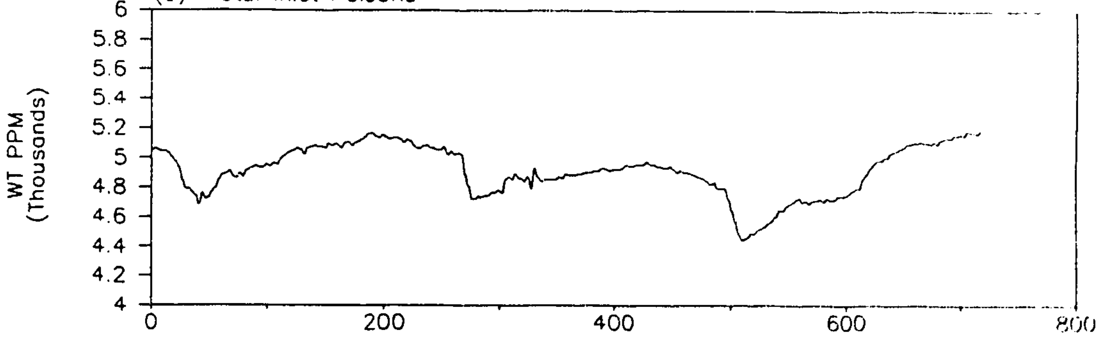

(d) Fresh Feed Flow

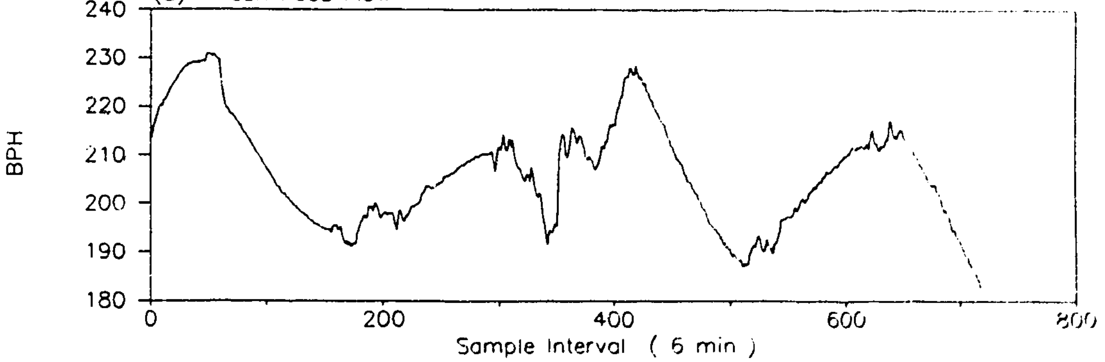

5.0 CONCLUSIONS AND FUTURE WORK

The main contribution of this thesis is the evaluation and implementation of the Multi-Step Adaptive Predictive Controller (MAPC) in an industrial environment. MAPC, developed and analyzed by Sripada,(1988) and Foley,(1988), was successfully applied to two industrial chemical processes at Esso Chemical Canada in Sarnia at the higher olefins plant in the fall of 1988.

The conclusions from both the university and industrial applications are summarized in two parts. The first part deals with the on-line recursive least squares estimator. The second part with the multi-step adaptive predictive controller.

5.1 Recursive Least Squares Estimator Conclusions

1. Using a Pseudo Random Binary Sequence to provide broadband frequency excitation to the process works extremely well in both the open and closed loop cases. The polychamber reactor used a closed loop test and the Hydrofiner used an open loop test. Both were well accepted by the process operators. It was shown that PRBS testing increases the overall output variation of the process by a relatively small, acceptable amount.

2. Regressor filtering is critical for good, robust parameter estimation. For the university results, it was imperative

that a second order $\Delta/T(z^{-1})$ filter be used for the first order plant model. A successful choice for the filter pole location was demonstrated to be 0.7 to 0.8. This discrete filter pole location generally corresponds to the corner frequency location of the continuous time plant frequency response. It is important in chemical process control that a good low frequency model is estimated. This low frequency range extends from the low frequencies to the plant crossover frequency.

3. Off-line analysis of PRBS test data prior to on-line parameter estimation is very helpful in determining initial model parameter estimates. Software analysis packages such as *IDSA* (MacGregor and Taylor, 1987), *MATLAB-386* (Matlab Corporation, 1987) and *STATGRAPHICS* (Statgraphics Corporation, 1987) provide a control engineer with a means to analyze and simulate the process off-line. Off-line simulation allows initial "tuning" parameters to be established. This leads to easy and confident on-line implementation of the estimator.

4. The use of the constant trace forgetting factor posed no problems. It was very convenient to change the trace specification in order to provide additional parameter filtering. Low trace specifications made the model parameters converge slowly, thus minimizing the risk of process upsets. It must be emphasized that this is a must in

the chemical process area. Internal plant recycles can cause major incidents if a control strategy responds too rapidly to process disturbances.

5. Using a deadzone on the model prediction error is not an effective means for turning the RLS estimator on and off. Selecting a deadzone too large keeps the estimator turned off all the time. Process dynamics may change, and the deadzone does not allow the estimator to identify the new parameter set. Selecting a deadzone which is to small may cause model parameters to drift or to oscillate. Further, a deadzone specification does not address structured dynamics which may be resident in the model prediction errors. It is possible to have model prediction errors which are normally distributed about zero with a certain standard deviation but still contain structured dynamics. Off-line analysis of the residual auto-correlation sequence provided an effective means for showing structured unmodelled dynamics in the residual series. An effective on/off RLS estimator criterion would look at both time and frequency characteristics of the model prediction errors.

5.2 Multi-Step Adaptive Predictive Control Conclusions

1. The most important property of a controller which is to function in a chemical industry is its ability to provide good, robust regulatory response. The majority of industrial PID controllers are tuned for such a response. In implementing the MAP controller, it was the regulatory characteristics that were emphasized. It was found that the MAP controller was able to provide good regulatory response in both the polychamber bed temperature control and hydrofiner total outlet poisons control applications.

2. In tuning the MAP controller, the most convenient approach was to fix the control, maximum and minimum prediction horizons (*i.e.* N_u, N_1 and N_2) and manipulate the control weighting and ratio of noise covariances (*i.e.* λ and R_w/R_v). Theoretically, if no model-plant mismatch exists the control weighting factor does not affect regulatory response. In all the experiments performed, the control weighting had to be carefully selected in order to provide good process regulation. It was found that using the guideline established by McIntosh, (1988) of using $\lambda=tr(A^TA)/N_u$ was very successful in estimating the amount of control weighting to be used.

3. During the university CSTH experiments it was discovered that the performance of the MAP controller was very peculiar

during fast parameter transients. Fast parameter estimation caused a non-linear interaction with the Kalman filter predictor. This non-linear interaction could cause uncontrollable oscillations and instability if the RLS estimator and R_w/R_v tuning parameters were not chosen correctly. In the experiments, decoupling of the two was achieved by detuning the model parameter estimator and/or the Kalman filter predictor. An alternative to detuning would be to fix the Kalman gain vector during estimation. Once the estimation was complete, the Kalman gain vector could be allowed to update. Any future work would have to investigate the process response to updating the Kalman gain vector after parameter estimation with a range of R_w/R_v values. This would be to ascertain whether this technique of decoupling had any adverse effects on the process output.

4. Operator acceptance of the MAP controller was enthusiastic. Every effort was made to design the MAP software and operator interface to be consistent with the existing control software at the Higher Olefins Plant. This consistency of the operator interface resulted in a minimum of training being required. The industrial experiments were left on for several weeks with the RLS estimator being both attended and unattended. The hydrofiner application showed many periods where the RLS estimator was left on for several days, with plenty of movement in the parameter trajectories. The ability of an adaptive controller to function in this manner

is proof that the board operators were confident of the integrity of the technology.

The software implementation of the MAP controller on the Honeywell PMX computer using the ANSI-66 Fortran programming language posed no special computing problems. However, the software did take a considerable amount of time to write, implement and verify. Complexities arose in programming the state space model, non-linear modified Kalman filter predictor and the horizon of future output predictions. In order to take advantage of the sparse nature of the state-space model matrices a significant programming effort is required to sort out the complex indexing operations that are required for a MAP controller which can handle all the possible combinations and permutations of plant models.

5.3 Future Work

The work performed in this thesis focused on Single-Input, Single Output (*SISO*) control applications with overdamped responses. Although these comprise the majority of applications in chemical process control, recently there has been a significant interest in multi-variable process control. A good example of this is Shell Corporation's use of Quadratic Dynamic Matrix Control (*QDMC*) and Exxon Chemical's use of Linear Programmed Dynamic Matrix Control (*LPDMC*). Both these control strategies provide robust multi-variable control with constraint handling capabilities. Since computer computational time and memory storage is no longer an issue with modern control computers, extending the capabilities of MAPC to handle constraints is a must. Constraint handling (Muhta, 1990) enables control engineers and process operators to tune an application to the day to day requirements of the plant. Multi-variable control on the other hand allows several interacting control objectives to be met in an optimal fashion.

To improve the robustness of MAPC, the RLS estimator and Kalman filter predictor must be decoupled in a more sensible way than simply detuning the two components to provide a linear process response. This was found to be a nuisance with the MAP controller as care always had to be exercised to prevent the control application from becoming oscillatory or unstable.

A third item which should be considered is estimation and control of higher order systems with time delay. It was found that two model parameters are relatively simple to estimate. Unfortunately, the use of higher order models increases the time required for the parameters to converge.

6 REFERENCES

ASTROM, K.J. (1970). *Introduction to Stochastic Control Theory.* Academic Press, New York.

BENDAT, J.S. (1980). *Engineering Applications of correlation and spectral analysis.* John Wiley & Sons.

BENDAT, J.S. and A.G. PIERSOL (1971). *Random Data Analysis and Measurement Procedures.* John Wiley & Sons, New York.

BIERMAN, G.J. (1977). *Factorization Methods For Discrete Sequential Estimation.* Academic Press, New York.

BLACKMAN, R.B. and J.W. TUKEY (1958). *The Measurement of Power Spectra. From the Point of View of Communications Engineering.* Dover Publications, New York.

BOX, G.E.P. and G.M. JENKINS (1976). *Time Series Analysis: forecasting and control*. Holden-Day, Oakland, California.

BROWN, R.G. (1983). *Introduction to Random Signal Analysis and Kalman Filtering.* John Wiley & Sons, New York.

BURDEN, R.L., J.D. FAIRES and A.C. REYNOLDS, (1981). *Numerical Analysis Second Edition.* Prindle, Weber and Schmidt, Boston, Massachusetts.

CLARKE, D.W. and P.J. GAWTHROP (1979). Self-tuning control. *Proc. IEE, 122,* 929-934.

CLARKE, D.W., C. MOHTADI and P.S. TUFFS (1987a). Generalized Predictive Control - Part I. The basic algorithm. *Automatica*, 23, 137-148.

CLARKE, D.W., C. MOHTADI and P.S. TUFFS (1987b). Generalized Predictive Control - Part II. Extensions and interpretations. *Automatica*, 23, 149-160.

CUTLER, C.R. and B.L. RAMAKER (1980). Dynamic Matrix Control - A Computer Control Algorithm. *JACC, 1,* San Francisco, USA, Paper WP5-B.

DAVIES, W.D.T. (1970). *System Identification for Self-Adapative Control.* John Wiley & Sons, London.

DORF, R.C. (1980). *Modern Control Systems.* University of California. Addison-Wesley, Massachusetts.

FOLEY, M.W. (1988). *Adaptive Control Using A Kalman Filter.* M.Sc. Thesis. University of Alberta, Dept. of Chemical Engineering.

GOODWIN, G.C. and M.E. SALGADO (1988). Information and Intelligent Control. *Workshop on Adaptive Control Strategies for Industrial Use.* 153-165.

GOODWIN, G.C. and K.S. SIN (1984). *Adaptive Filtering, Prediction and Control.* Prentice-Hall, Englewood Cliffs.

HAYKIN, S. (1978). *Communication Systems, Second Edition.* John Wiley & Sons, New York.

JENKINS, G.M. and D.G. WATTS (1968). *Spectral Analysis and its applications.* Holden-Day, San Francisco.

KAILATH, T. (1980). *Linear Systems.* Prentice-Hall, Englewood Cliffs.

KALMAN R.E. and R.S. BUCY (1961). New results in linear filtering and Prediction Theory. *J. Basic Eng., Trans., ASME Ser.D.,* Vol. 83, No. 3, 95-108.

LJUNG, L. and T. SODERSTROM (1983). *Theory and Practice of Recursive Identification.* MIT Press, Cambridge.

MACGREGOR, J.F. (1987). *Discrete Time Process Identification: Theory and Applications.* Prepared for : An Intensive Short Course on Digital Computer Techniques for Process Identification and Control. McMaster University, Dept. of Chemical Engineering.

MACGREGOR, J.F. and P.A. TAYLOR (1987). *IDSA VERSION 3.0.* McMaster Process Control Laboratory. Dept. of Chemical Eng. McMaster University, Hamilton, Ont.

MAN, D. (1984). *Process Control using Single Series Forecasting.* M.Sc. Thesis, University of Alberta, Dept. of Chemical Engineering.

MATHWORKS, INC (1987). *Matlab-386 Version 3.25.*

MCINTOSH, A.R. (1988). *Performance and Tuning of Adaptive Generalized Predictive Control.* M.Sc. Thesis. University of Alberta, Dept. of Chemical Engineering.

MOHTADI, C. (1986). *Studies in Advanced Self-Tuning Algorithms.* D. Phil. Thesis, Oxford University.

MOHTADI, C. (1988). On the Role of Prefiltering in Parameter Estimation and Control. *Workshop on Adaptive Control Strategies for Industrial Use.* 261-282.

MUHTA, R. (1990). Constrained GPC. M.Sc. Thesis. University of Alberta, Dept. of Chemical Engineering.

OPPENHEIM, A.V. and R.W. SCHAFER (1975). Digital Signal Processing. Prentice-Hall, Inc., Englewood Cliffs, New Jersey.

SRIPADA, N.R. (1988). Multistep Adaptive Predictive Control. Ph.D. Thesis, University of Alberta, Dept. of Chemical Engineering.

SHAH, S.L. (1986). Parameter Estimation Techniques For Self-Tuning Control. Research Report 861201, University of Alberta, Dept. of Chemical Engineering.

GRAPHIC SOFTWARE SYSTEMS (1987). Statgraphics Version 4.0. Graphic Software Systems, Inc.

TUFFS, P.S. and D.W. CLARKE (1985). Self-Tuning Control of Offset: a unified approach. IEE Proc. D, 132, 100-110.

WALGAMA, K.S. (1986). Multivariable Adaptive Predictive Control for Stochastic Systems with Time Delays. M.Sc. Thesis, University of Alberta, Dept. of Chemical Engineering.

WITTENMARK, B. (1988). Adaptive Control : Implementation and Application Issues. Lund Institute of Technology, Sweden. Workshop on Adaptive Control Strategies for Industrial Use. 245-260.